Contract No.:

This manuscript has been authored by Savannah River Nuclear Solutions (SRNS), LLC under Contract No. DE-AC09-08SR22470 with the U.S. Department of Energy (DOE) Office of Environmental Management (EM).

SRNL-L4500-2018-00011

Remediation of Spent Oxalic Acid Nuclear Decontamination Solutions using Ozone

By Edward Ketusky,
B.S., Nuclear Engineering; M.Tech, Chemical Engineering; MBA
March 2017

Submitted in accordance with the requirements of Lancaster University for the degree of

Doctor of Philosophy in the Faculty of Science and Engineering

Department of Engineering
Lancaster University
Lancaster UK

ABSTRACT

The Savannah River Site (SRS) has forty-three remaining very large underground tanks containing significant quantities of nuclear waste generated primarily from cold-war radiochemical separations. All of the tanks eventually must be closed. As part of decommissioning/closing the nuclear waste tanks, even residual quantities of the waste must be removed. Although most sludge can be removed mechanically, chemically cleaning (i.e. decontamination) with oxalic acid is used to aid in the removal of residual quantities.

Although oxalic acid works for cleaning the tanks, its downstream impacts are considered detrimental. To better understand and quantify the impacts, detailed models were developed to account for different potential processing strategies for handling the spent oxalic acid nuclear decontamination slurries. Although the results vary, the models show that regardless of the oxalate handling strategies: 1) significant washing to decrease sodium concentration/solids concentration in vitrification feed will be required, and 2) the creation of copious future additions of feed for salt processing will be unavoidable.

Using a Theory of Inventive Problem Solving (TRIZ) approach, a modified form of the Chemical Oxidation Reduction Decontamination (CORD) ultraviolet (UV) light was identified as being used with an analogous but already resolved problem that could be adapted to SRS HLW tank cleaning. A novel preliminary process called Enhanced Chemical Cleaning (ECC) was envisioned.

As part of maturing the technology, the literature review identified three possible oxalate decomposition mechanisms associated with ECC. They are:

1) A heterogeneous non-Advanced Oxidation Process (AOP) mechanism where the target organic adsorbs onto the surface of a solid, often particulate, metal oxide at a so-called active site, followed by ozone attack on the sorbed organic;

2) A homogeneous non-AOP mechanism that operates under low pH acidic conditions and which involves complexation of the catalysing metal ion with the oxalate followed by ozone attack on the complex; and,

3) A homogeneous AOP mechanism that operates at a high basic pH and which involves metal ions catalysing the formation of hydroxyl radicals from ozone, with the said hydroxyl radicals then driving the oxalate decomposition.

Process testing was conducted using slurries made from simulants designed to be chemically similar to real High-Level Waste (HLW) sludge types. Testing using slurries made from real HLW sludge was also performed, but because of safety limitations associated with handling HLW, only a much smaller scale test apparatus could be used. With the much smaller scale test apparatus, the purpose of the real HLW based testing was confirmatory. Each of the simulant decomposition test slurry was created using an Fe-rich or an Al/Mn-rich sludge simulant using either 1 wt% or 2.5 wt% oxalic acid. The real HLW based slurries were formed using 2 wt% oxalic acid.

As part of the main postulate of this effort, both the simulant decomposition test slurries and real HLW based slurries demonstrate that UV light increased the decomposition rate. Even without UV, by adding only ozone, the oxalate decomposition was completed on an industrially relevant timescale.

Also using simulant based testing, the overall oxalate decomposition exhibited four distinct stages related to the metal catalysts:

Stage One – At short ozonation times, ozone decomposes Fe oxalates and solubilise Fe from ozone action on the metal oxide constituents of the sludge.

Stage Two – At intermediate ozonation times, as a result of the loss of the solution capacity to complex (and so solubilise) Fe, Mn, and Ni ions due to O_3 driven oxalate decomposition, as well as the pH increase that accompanies that decomposition, Fe begins to precipitate. Oxalate decomposition is still primarily catalysed by Fe ions during this stage.

Stage Three – At intermediate ozonation times, Fe precipitation is near complete, and oxalate decomposition is now driven by ozone and Mn catalysis – Mn playing a major role in determining the final time to process endpoint of 1.1×10^{-3} M oxalate in solution.

Stage Four – At long ozonation times**,** the process endpoint with Mn precipitation now near completion with Ni being the dominant metal ion in solution.

Constructed plots compare the pH and remaining oxalate concentration, both as a function of time, suggesting some relationship. Regression analysis of the negative log of the oxalate concentration shows the R^2 values are all greater than 0.80, confirming correlation. Thus, pH can be used as a field measure for confirming when oxalate decomposition is complete.

As a principal hypothesis of this effort, using simulant based testing, both the scavenging effects of "all-ready present" nitrite (a soluble component of the sludge simulants) and oxalate mineralisation-derived carbonate are advantageously used in lieu of introducing hydroxyl radical probe compounds to the process. Specifically, differing nitrite concentrations between slurries showing no impact on the decomposition rates, and the build-up of carbonate not inhibiting the decomposition process strongly suggest that the decomposition is not the result

of radicals. Instead, the oxalate decomposition is likely the result of a direct reaction of ozone with metal complexed oxalate (i.e. mechanism 2 discussed above).

Statement of Authorship

I, Edward Ketusky, confirm that the work presented in this thesis was designed interpreted, and written by myself, except where otherwise stated, and has not been submitted in any previous application for a higher degree.

The source data presented in this thesis was produced by tests both designed and conducted by Edward Ketusky, while working for Savannah River Remediation and Savannah River National Laboratory [2009-2016], with testing also performed at AREVA NP (Lynchburg). The data was reviewed and interpreted by Edward Ketusky whilst registered to study for the degree of Doctor of Philosophy at Lancaster University between 2010 and 2016.

Date..5th March 2017..Signature of Candidate Signature on File

Director of Studies Declaration

I hereby certify that the candidate has fulfilled the conditions of the resolution and regulations appropriate for the degree of Doctor of Philosophy at Lancaster University and that the candidate is qualified to submit this thesis in application for that degree.

Date..5th March 2017..Signature of Supervisor Signature on File

Dedication

This thesis is dedicated to my family for their unconditional support, especially my loving wife, Kim, and my two sons, Jonathan and Matthew, who all encouraged me throughout this effort.

Acknowledgements

Many people have aided me in this research and made this thesis possible. Naming all key people would likely be impossible; therefore, I will probably leave someone out. In advance, please accept my apologies.

From my time at High-Level Waste Engineering, I would like to thank Renee Spires, Tommy Caldwell, Mark Mahoney, and Neil Davis. They were the first people to honestly trust my novel TRIZ determination that using oxalic acid to clean the High-Level Waste tanks, tied closely to decomposing the resultant spent acid solution represented the "ideal solution." At Savanah River National Laboratory, Chris Martino and Bill King, who spent considerable time helping me understand much of the oxidation chemistry. At AREVA NP (Lynchburg) Dennis Jones, John Remark, Ray Beatty, and Sarah Evans, all who helped me gain valuable insights. My supervisor Professor Colin Boxall who encouraged me throughout the process. And finally, to my many friends and colleagues that supported me during this research.

TABLE OF CONTENTS

List of Tables

List of Figures

ACRONYMS, ABBREVIATIONS AND SYMBOLS

·X	-	A radical, (other than hydroxyl radical) with X representing the chemical species
$	-	(U.S.) dollar
[ ]	-	concentration
2,4-D	-	2,4-dichlorophenoxyacetic acid
ε	-	Molar absorption coefficient (also called the extinction
ε 254 nm	-	The extinction coefficient of UV at 254 nm wavelength
λ	-	wavelength
hv	-	Application of UV light
A	-	Absorbance of a substance at a specified wavelength
$[A^-]$	-	Concentration of conjugate base of an acid
AA	-	Atomic Absorption
adds	-	additions
Am/Cm	-	Americium/Curium (separation and measurement method)
AOP	-	Advanced Oxidation Process
Approx.	-	Approximate
aq.	-	aqueous
ATR-FTIR	-	Attenuated Total Reflection – Fourier Transform Infrared
b	-	Length of the light path through the sample
BOD	-	Biological Oxygen Demand
c	-	concentration
CAN-	-	Canadian Depleted Uranium Decontamination
CAT	-	Catalyst

COD	-	Chemical Oxygen Demand
CITROX	-	(a mixture of) Citric acid and Oxalic Acid
CORD	-	Chemical Oxidation Reduction Decontamination
cm	-	centimetre
CV	-	Cold Vapour
DfD	-	Decontamination for Decommissioning
DfDx	-	Decontamination for Decommissioning-Improved
dia	-	diameter
DOE	-	(United States) Department of Energy
dpm	-	Disintegration per minute
DRT	-	Decontamination Regenerative Technology
ECC	-	Enhanced Chemical Cleaning
ECR	-	Effective Cleaning Radius
EDTA	-	ethylene diaminetetracetic acid
E_h	-	Electrode potential
E_h-pH	-	Alternate name for Pourbaix diagram
EPRI	-	Electric Power Research Institute
Evap	-	Evaporator
eq	-	equivalent
eq.	-	equation
f	-	average fraction of initially available radiation
g	-	gram
GAO	-	(U.S.) Government Accounting Office
g-value	-	The rate of hydroxide radical production

$[H^+]$ - hydrogen ion concentration

[HA] - Acid concentration

HA - Highly Active

HIC - High Integrity Container

HA - Highly Active

HLW - High-Level Waste

HM - H-Area Modified Purex

hp - Horsepower

HO_2- - Hydroperoxide ion

$\cdot HO_2$ - Hydroperoxide radical

$\cdot HO_3$ - Hydrotrioxy radical

I - Intensity of the transmitted light

I_o - Intensity of the incident light

ICP-ES - Inductively Coupled Plasma Emission Spectroscopy

ICP-MS - Inductively Coupled Plasma Mass Spectroscopy

i.d. - The inner diameter

IX - Ion Exchange

k - The reaction rate constant

- $k_{OH\cdot}$ - Rate constant specific to the reactant with hydroxyl radicals
- k_{H2O2} - Rate constant specific to the reactant with peroxide
- k_{O3} - Rate constant specific to the reactant with ozone

K_a - Acid dissociation constant

kg - kilogram

kl - kilolitre

kW	-	kilowatt
LOD	-	Level of Detection
LOMI	-	Low Oxidation Metal Ion
LP	-	Low Pressure
LS	-	Liquid scintillation
LTD	-	Less Than Detectable
M	-	moles/litre
mm	-	millimetre
MP	-	Medium Pressure
mW	-	milliwatt
NA	-	Not Applicable
nm	-	nanometre
NOM	-	Natural organic matter
NHE	-	Normal Hydrogen Electrode
nm	-	nanometre
NP	-	Nuclear Power
NR	-	Not Recorded
O(1D)	-	first excited stage of oxygen
$\cdot O_3^-$	-	ozonide radical
o.d.	-	outer diameter
OH·	-	Hydroxyl radical
OX	-	Oxalate
pCBA	-	p-chlorobenzoic acid
pK_a	-	negative base-10 logarithm of the acid dissociation constant, K_a

ppm	-	parts per million
PUREX	-	Plutonium Uranium Redox Extraction
PuTTA	-	Plutonium triphenoyltrifluoroacetone extraction analysis
PZC	-	Point of Zero Charge
q	-	Irradiation contact time
r	-	reaction rate
r_{ox}	-	oxalate decomposition rate
R	-	Other compounds
R^2	-	Coefficient of Determination, also commonly called R^2 values
RCRA	-	U.S. Resource Conservation and Recovery Act
R_{O3}	-	Rate at which ozone crosses the gas/liquid interface during sparging
ROS	-	Refractory Organic Substances
rpm	-	revolutions per minute
SRNL	-	Savannah River National Laboratory
SRS	-	Savannah River Site
ss	-	stainless steel
SS	-	Steady State
T	-	Transmittance
TOC	-	Total Organic Carbon
TRIZ	-	Teoriya Resheniya Izobretatelskikh Zadatch
TTP	-	Telescoping transfer pump
U.S.	-	United States
USA	-	United States of America

UV	-	Ultra Violet (light)
UVA	-	Ultra Violet absorption
UVT	-	Ultra Violet (light) transmissivity
V	-	Volts
vol%	-	percent volume
W	-	Watt
wt%	-	Weight percent
WW	-	Wash water
x	-	Acid digestion sequence
y	-	For the slurry nomenclature used herein (e.g. 1.Fe-2.y), the *y* term is used to denote one of the three UV light protocols.

1. INTRODUCTION

1.1 The Need to Chemically Clean SRS High-Level Waste Tanks

The Savannah River Site (SRS) is an 800 km^2 nuclear reservation located in South Carolina, USA. It was constructed during the 1950s to produce the primary materials used in the fabrication of nuclear weapons, primarily tritium and plutonium-239, in support of the USA's national defence programs. Five reactors were built at SRS to produce these materials. Also constructed were support facilities including two radiochemical separation plants, a heavy-water extraction plant, a nuclear fuel and target facility, a tritium extraction facility and waste management facilities.

Being 800 km^2, groups of buildings and processes (called areas), were envisioned similar to towns, with each named a letter of the alphabet. H-Area contained one of the radiochemical separation plants, while F-Area housed the other. Because of the large outer concrete size of the radiochemical separation and recovery plants, they were referred to as canyons, therefore resulting in the names H-canyon and F-canyon. F-canyon used the PUREX process, while H-canyon used a modified PUREX process, called the HM process. Fifty-one very large underground High-Level Waste (HLW) tanks were built near the canyons to support both the chemical separation and recovery plants. When referring to characterisations of tank waste, there is an F-Area tank waste, associated with waste generated from the PUREX radiochemical separation process. The F-Area sludge is iron-rich. The HM radiochemical separation process created the H-Area tank waste. It is Al/Mn-rich.

Various tank closure efforts have been initiated and underway since the 1980s, but only eight tanks are closed. As a legacy of the cold war, SRS remains home to more than 43 very large, underground, carbon steel tanks. The tanks store a combined total of approximately 1.2×10^8

litres of liquid radioactive HLW[1]. To inhibit corrosion of tank fabric, even before the liquid waste is transferred into the HLW tanks from the radiochemical separation facilities, it is first rendered heavily alkaline by adding sodium hydroxide (NaOH). This addition of NaOH resulted in a hydroxide concentration typically $\geq$ 1 M. However, with the resultant pH of ~14, metal ions precipitated out of the HLW liquid. The metal ion precipitation resulted in forming a sludge that is comprised of the oxides and hydroxides of iron, aluminium, manganese, other common metals (including actinides), as well as some interstitial liquid.

Figure 1 summarises the mass dominant solids (e.g. > 1% of the sludge solids mass) in representative F-Area sludge, while Figure 2 summarises the mass dominant solids in representative H-Area sludge[2].

[1] HLW is defined as radioactive waste with levels of activity in concentrations high enough to generate significant quantities of heat by the radioactive decay process or waste with large amounts of long-lived radionuclides that need to be considered in the design of a disposal facility for such waste. Disposal in deep, stable geological formations usually several hundred metres or more below the surface is the recognised option for disposal of HLW [IAEA Safety Standards Classification of Radioactive Waste General Safety Guide, No. GSG-1, International Atomic Energy Agency, Vienna, 2009].

[2] A detailed characterisation of the sludge solids in representative F-Area sludge is contained in Column A of Table 24, while for representative H-Area sludge, the characterization I contained in Table 25, with both tables contained in Appendix 1.

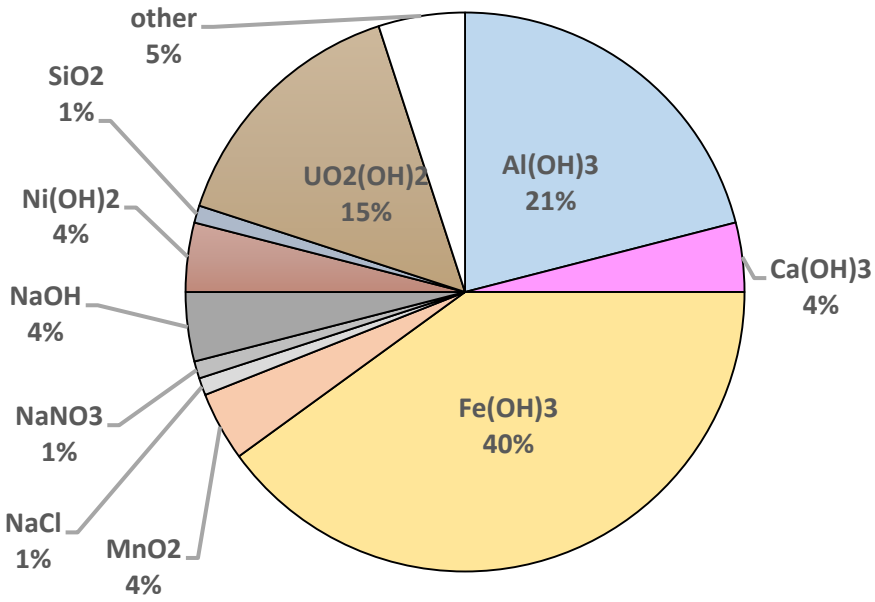

Figure 1. Representative mass predominate F-Area sludge solids constituents.

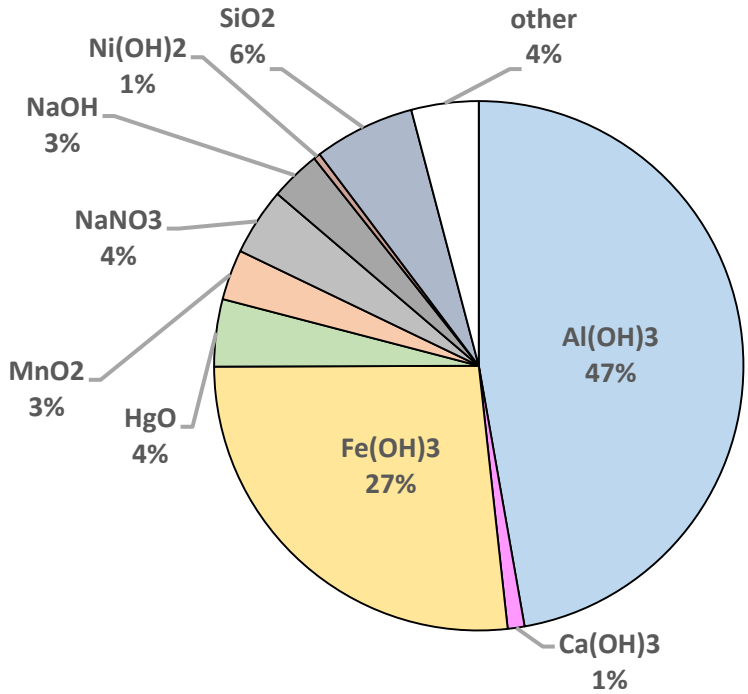

Figure 2. Representative mass predominate H-Area sludge solids constituents.

Over-time this sludge has even been shown to become compacted into a mostly solid mass as shown in Figure 3. As part of the eventual closing/decommissioning each of the HLW tanks, almost all of the sludge must first be removed.

Figure 3. Example of compacted sludge sample taken from HLW tank.

Approximately half of the HLW tanks were constructed from commercial grade carbon steel in the mid-1950s to the early 1960s and are single shelled, while the others, also made of carbon steel were built in the 1970s (Davis *et al.*, 2009; Ketusky *et al.*, 2011).

Figure 4 shows an example of the 1950s construction of a tank.

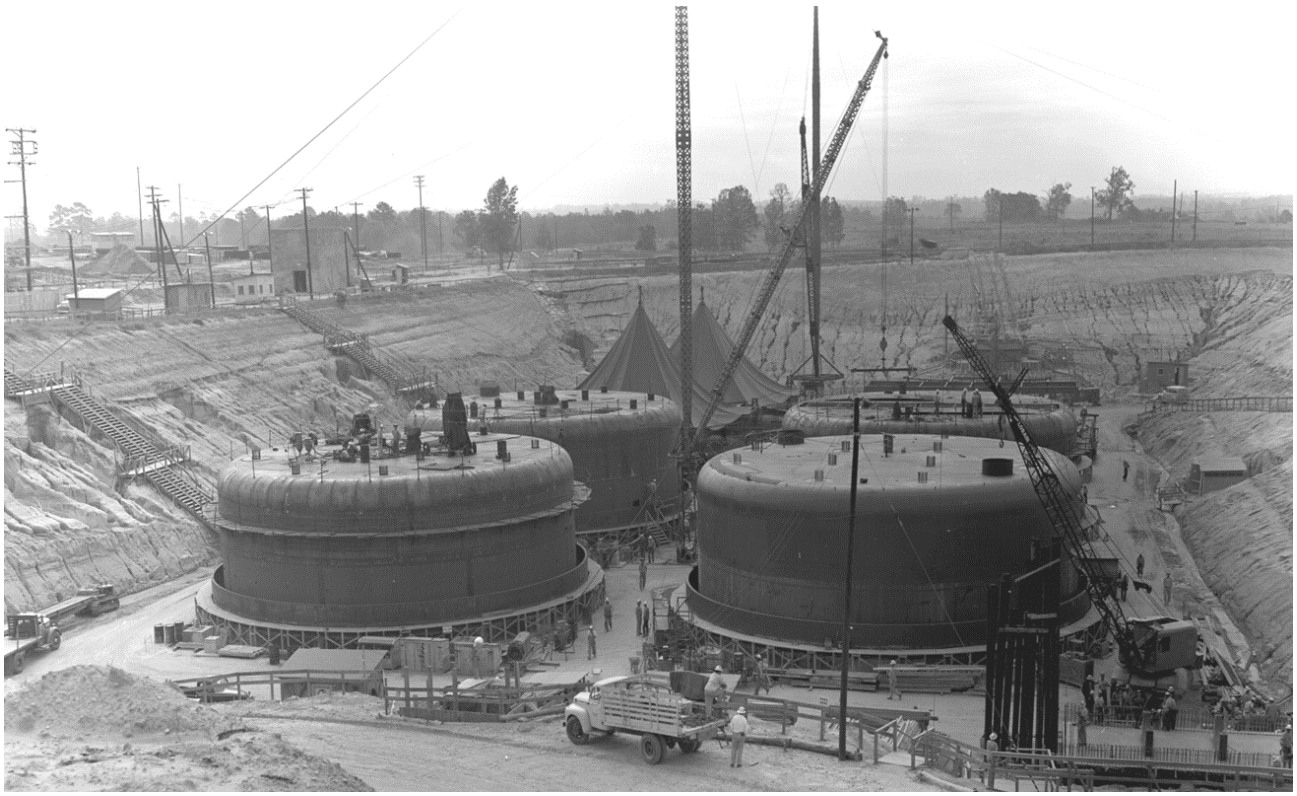

Figure 4. 1950s construction of an SRS HLW tank.

All of the HLW tanks are flat-bottomed, with their dimensions ranging from 23 to 26-metres in diameter, 7 to 10 metres high, with the volumetric capacity ranging from 2.8×10^6 to 4.9×10^6 litres (Davis *et al.*, 2009; Ketusky *et al.*, 2011). Many of the tanks contain an internal labyrinth, containing kilometres of carbon steel cooling coils, which further complicate waste removal, cleaning, and closure (Davis *et al.*, 2009; Ketusky *et al.*, 2011). Figure 5 shows an example of the vertical and horizontal cooling coils.

Figure 5. Example of the vertical and horizontal cooling coils in an SRS HLW tank.

Since the HLW tanks are subsurface (i.e. underground) access to the tank inside is limited through the typical 30 to 65 cm diameter riser openings (Davis *et al.*, 2009). The sludge in each of the tanks must eventually be removed to the maximum extent practical and closed, as required by the United States Federal Facilities Agreement (National Academy of Science, 2006). The Savannah River Site utilises both mechanical and chemical methods for removing HLW sludge from tanks. The mechanical means, predominantly consisting of mixing/slurring with long-shafted slurry pumps, with ensuing transfers using centrifugal transfer pumps, are used to remove the bulk of the waste[3].

[3]Appendix 2 contains a brief description and characteristics of different pumps used in SRS HLW, as well as some pictures and diagrams (i.e. Table 40, Figures 48 through 52).

Although the bulk volume of sludge in most tanks has been shown to be removable using hydraulic slurrying techniques, use of chemically aided techniques to partially digest the HLW sludge is also used. That is, only after hydraulic slurrying is no-longer continuing to be successful, is chemically cleaning performed. Chemically cleaning the tank renders the sludge more amenable to suspension with subsequent removal via slurrying. Chemical cleaning is employed only when residual quantities of solids remain (e.g., less than about 5,000 kg of sludge solids stay in the tank) and mechanical methods are no-longer effective (Ketusky *et al.*, 2011). Chemical cleaning is necessary to support the requirements for HLW tank decommissioning/closure (Davis *et al.*, 2009). Upon tank decommissioning, the residual volume of waste solids allowed to remain ranges from about 50 to 500 kg. Hypothetically, if the solids were spread out evenly on the bottom of the tank, the solids would only be roughly 0.025 to 0.25 cm thick (Davis *et al.*, 2009, Ketusky *et al.*, 2011). The closure requirement for each of the different tanks is primarily driven by the high specific activity of the waste in conjunction with their proximity to their respective water table (Davis *et al*., 2009). In fact, based on a United States Department of Energy-Savannah River Operations Office (DOE-SR) report about 20% of the bottom of the tanks are either within their respective water table, seasonable high water table, or within a perched water table caused the original construction of the tank areas (DOE-SR, 2000).

Although chemically cleaning the HLW tanks represent a specific need, the very similar decontamination of nuclear reactor processes and installations is essential for reducing occupational exposures, permitting reuse of components, facilitating waste management, and decommissioning facilities. Steels and aluminium based alloys are ubiquitous on nuclear sites, with many approaches used for their decontamination.

1.2 Preference for Using Oxalic Acid as the Chemical Cleaning Solution

Oxalic acid remains the agent for cleaning the metal surfaces inside HLW tanks before closure because of its combined digestion and complexing abilities (Ketusky *et al.*, 2011), as well as its controllable corrosion control characteristics (Wiersma *et al.*, 2012). Other common acids considered for cleaning the inside of HLW tanks include nitric acid and oxalic/citric acid blends (Ketusky *et al.*, 2011; Nuclear Energy Agency, 2008). While both pure oxalic acid and oxalic /citric acid mixtures have been shown to be potentially equally effective in cleaning the SRS HLW tanks, there are undesirable downstream impacts on salt processing and vitrification associated with introducing citric acid into the HLW system (Ketusky *et al.*, 2011, Adu-Wusu, 2003). One of the primary impacts of using citric acid includes flammability concerns in the vitrification process (Adu-Wusu, 2003).

Oxalic acid has system-specific advantages (Davis *et al.*, 2009; Ketusky *et al.*, 2011; National Academy of Science, 2006; Ketusky, 2016; Bradbury, 2001; Wiersma *et al.*, 2012):

- Oxalic acid is known to aggressively solubilise iron oxide (Wile *et al.*, 1997; Nuclear Energy Agency, 2008; Calderon *et al.*, 2000; Taxiarchou *et al.*, 1999). It is a complexing agent commonly used for rust removal (Zhang *et al.*, 1985) and thus is useful for the decontaminating highly corroded surfaces; and,

- Oxalic acid can act as a corrosion inhibitor for carbon steels (Wiersma *et al.*, 2012), thus preventing the over-aggressive digestion during decontamination of structures comprised of such steel, so protecting their structural integrity.

Oxalic acid is a commonly used nuclear decontamination agent (Nuclear Energy Agency, 2008). Oxalic acid's twin propensities to solubilise iron oxides and inhibit carbon steel

corrosion, making it particularly appealing for use in chemically cleaning the SRS HLW tanks (Davis *et al.*, 2009; Wilde and Berger, 1984), which includes digestion of HLW sludge.

Consequently, when hydraulic slurrying alone has become unsuccessful in removing more sludge, concentrated oxalic acid solution has been added to the HLW tank to digest the sludge and aid in its removal. After digesting[4] the sludge, the solubilised sludge plus a fraction of remaining solids suspended via hydraulic slurrying, are transferred out of the HLW tank as a *spent acid slurry*[5].

1.3 Overview of the HLW Baseline Cleaning Process

A simplified diagram of the *Historical Baseline Chemical Cleaning Process* for cleaning of the SRS HLW tanks is summarised in Figure 6.

[4] Digestion of the HLW sludge is also commonly called dissolution. Therefore, both terms are used.

[5] Key process locations and streams identified in italics within this chapter, are defined as part of the Historical Baseline Chemical Cleaning Process of the SRS HLW tanks contained as Figure 6.

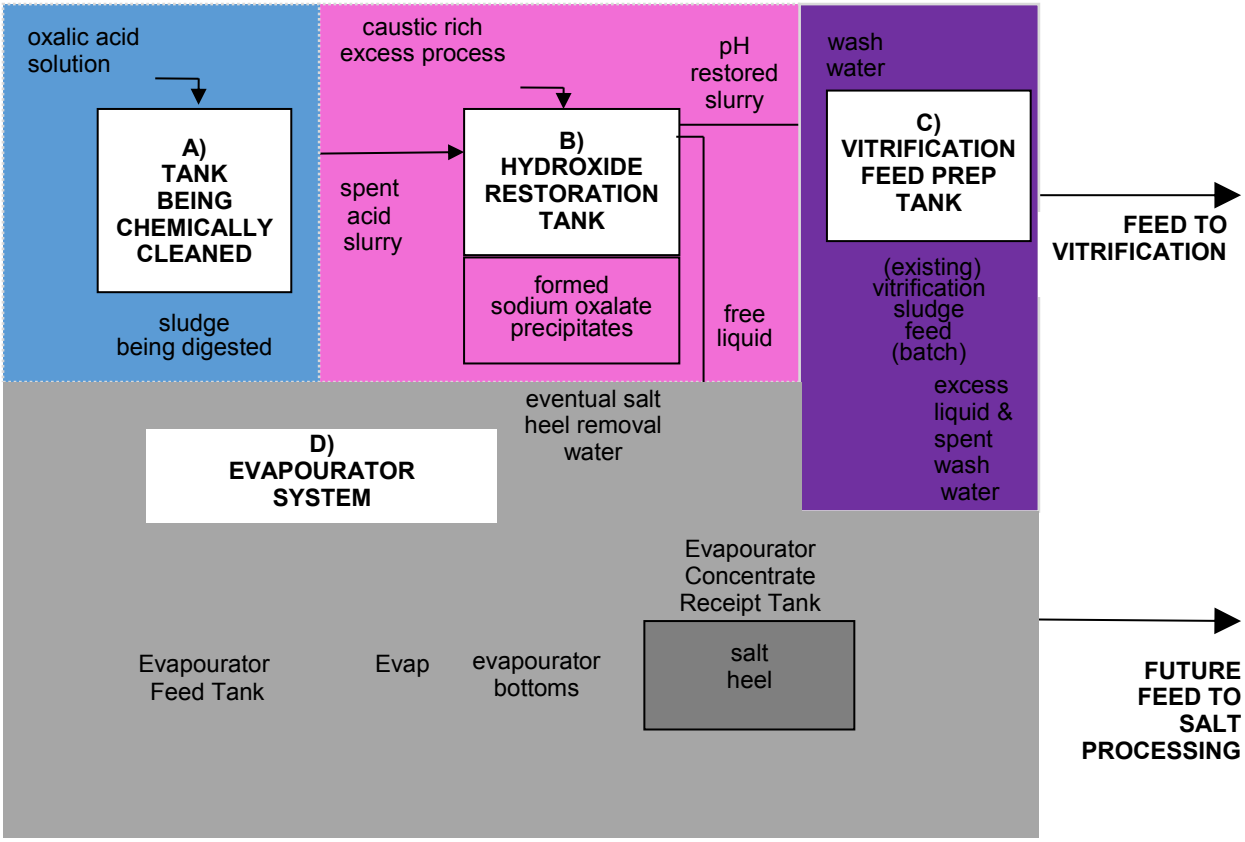

Note: Multiple Evaporator Feed Tanks, Evapourators, and Evapourator Concentrate Receipt Tanks exist at SRS, with only one overall D) Evapourator System shown to maintain clarity.

Figure 6. Summary of SRS *Historical Baseline Chemical Cleaning Process* for cleaning HLW tanks.

Starting at the top left of Figure 6, a description of the *Historical Baseline Chemical Cleaning Process* for cleaning HLW tanks is provided as follows.

A) *Tank Being Chemically Cleaned*

An 8 wt% o*xalic acid solution* is added to the *Tank Being Chemically Cleaned*. The tank is then mixed using slurry pumps (with a brief description of the types of slurry and transfer pumps, as well as pictures and diagrams are provided as Appendix 2). After slurrying for a minimum of 72 hours, with the acid *digesting the sludge*, the slurrying is stopped. The *spent acid slurry* is then transferred out of the HLW tank being cleaned using a transfer pump. The *spent acid slurry* is pumped into the *Hydroxide Restoration Tank*.

B) *Hydroxide Restoration Tank*

Before receiving the *spent acid slurry,* this tank was pre-staged with available c*austic rich excess process supernatant to* restore the mix to within the standard HLW system corrosion control parameters, i.e. a free hydroxide concentration of > 1 M. The available c*austic rich excess process supernatant would* be from other HLW tanks in the process, such as from an *Evaporator Concentrate Receipt Tank*. Since the sodium concentration of the *caustic rich excess process supernatant* is >> than 6 M, large quantities of a *sodium oxalate precipitate form* (Ketusky *et al.*, 2011). The solids including the formed *sodium oxalate preci*pitates in the *Hydroxide Restoration Tank* are sent as part of the alkali-treated *caustic restored slurry,* which itself will be rich in precipitated sodium oxalate, to the *Vitrification Feed Preparation Washing Tank.*

C) *Vitrification Feed Preparation Tank*

In the *Vitrification Feed Preparation Tank,* the *hydroxide restored slurry* is combined with an *existing vitrification sludge feed batch.*

The *existing vitrification sludge feed batch*, for example, could be derived from the initial mechanical tank cleaning step. The w*ash wate*r (WW) is added to the tank, and then washing is performed[6]. Washing reduces both the sodium concentration (Pike *et al.*, 2004; Shafer, 2010) and the weight percent loading of solid sodium oxalate (Pike *et al.*, 2004)*,*

[6] Even without using the *Historical Baseline Chemical Cleaning Process*, the vitrification feed must be washed to reduce the [Na] from about 3.7 M to < 1 M, as well as to decrease the sodium oxalate solids loading to ≤ 14 wt%.

Use of the Historical Baseline Chemical Cleaning Process only further exacerbates the required number of wash cycles - where a "wash-cycle" refers to a single filling, slurrying, and subsequent pump-down of the *Vitrification Feed Preparation Washing Tank.*

D) Evaporator System

As part of the general process of transferring liquids to D) *Evaporator System, excess fluid* and *spent wash water* from the Vitrification Feed Preparation Tank, saturated with dissolved sodium oxalate, are transferred to the *Evaporator Concentrate Receipt Tank.* Then the *excess liquid and spent wash water,* as part of evaporator recycle are transferred back to the *Evaporator Feed Tank* and then fed to the *Evaporator (Evap).* Evaporation is required to remove water from the supernatant, thus maintaining the needed operating volume necessary to continue operating the HLW process. With the sodium concentration in the *Evaporator Concentrate Receipt Tank* > 6 M, sodium oxalate again precipitates and ultimately ends as part of the sparingly-soluble *salt heel* within the Evaporator *Concentrate Receipt Tank*.

In the future, as part of removing waste to support closure, the *salt heel,* which now includes the sodium oxalate precipitate from chemical cleaning, will need to be dissolved, requiring significant amounts of *future salt heel removal water*, thus creating a copious additional *Future Feed for Salt Processing*.

Downstream (i.e. outside) of the HLW process shown in Figure 6, the *Future Feed for salt Processing* will be mixed with grout and immobilised (i.e. turned into saltstone). With salt processing having a typical feed-to-grout ratio of 10 vol%, even further "dilution" will occur creating significant additional volumes of saltstone, therefore requiring the misappropriation of considerable amounts of saltstone vault volume.

1.4 Comparative Cost of Vitrification to Saltstone

With only two waste removal paths from HLW as shown in Figure 6, a rough cost comparison is provided to in aid understanding the significance of process impacts based on chosen oxalate disposal strategy.

A recent United States Government Accounting Office (GAO) report roughly estimated the cost of treating liquid SRS radioactive waste sent to saltstone as $40.50/litre (GAO, 2017). A cost comparison between vitrification and grouting at West Valley (where grouting, as a process, is similar to SRS salt processing), as stated in the report, determined the vitrification cost for a gallon of waste to be a factor of 57 times larger than using saltstone (GAO, 2017). Thus, the cost estimated for SRS vitrification is $2,307/litre (2017 U.S dollars).

1.5 Negative Impacts from Using Oxalic Waste to Clean HLW Tanks

Historically, there are four documented impacts associated with using oxalic acid to clean the SRS HLW tank. They are:

1) The "necessary free operating volume," refers to the volume that must be maintained in the HLW system to continue operations, transferring, and preparing of waste for disposal. Without maintaining the "necessary free operating volume," the current level of HLW operations could not continue. The additional liquid added as part of the tank cleaning would likely consume all of the currently available storage capacity. Without significant evaporative capacity, the liquid added from tank cleaning would quickly consume the very limited "currently available storage volume." and compete for "necessary free operating volume." With any usage of the "necessary free operating volume," the current level of HLW operation would become further restricted/limited.

2) The observed mal-operation of the HLW *evaporators* when evaporating oxalate-rich solutions, leading to oxalate "clogging" of the evaporators (Ketusky, 2012).

3) Because of the *Evaporator Concentrate Receipt Tank* chemistry, significant quantities of sodium oxalate from the *Historical Baseline Chemical Cleaning Process* would precipitate in the *Evaporator Concentrate Receipt Tank* (Weber, 2011; Wiley, 2012). This precipitation would consume significant operating volume needed for *evaporator bottoms.* The bottoms would eventually require substantial quantities of *salt heel removal water* to dissolve the *salt heel*. The considerable amounts of *eventual salt heel removal water* added, would result in copious volumes of additional *Future Feed for Salt Processing.* Because of the feed-to-grout ratio associated with making saltstone, further dilution occurs, resulting in excessive vault space required to dispose of the sodium oxalate addition to the sparingly-soluble *salt heel*.

4) The resultant sodium oxalate *Hydroxide restored slurry* would be sent to the *Vitrification Feed Preparation Tank* and combined with an *existing vitrification sludge feed batch*. Increased washing will be required to decrease both the: 1) soluble sodium concentration; and, 2) the weight percent loading of solid sodium oxalate in the *feed to vitrification,* both to support glass quality requirements (Pike *et al.*, 2004). Conforming to the vitrification feed criteria, both the sodium concentration must be $\leq$ 1 M, while the weight percent of sodium oxalate solids must be less than 14 wt% (Pike *et al.*, 2004; Chew and Hamm, 2010).

The last two issues, i.e. 3) and 4), are directly associated with the solubility of sodium oxalate. Appendix 1 contains the detailed models that calculate the fate of the oxalate through each part of the process, as well as the implications to 1) Vitrification, expressed in terms of required

additional vitrification feed batch preparation washing; and 2) Salt processing/Saltstone, conveyed in terms of additional feed for salt processing and required additional vault volume.

As previously discussed, there are only two current possible paths for waste to be removed from the SRS HLW process. That is 1) as *Feed to Vitrification*; or, 2) as *Future Feed for salt Processing* which eventually is solidified with grout[7] and sent to a disposal vault[8] . The role of two possible paths is summarised by Equation 1-1.

sodium oxalate removed through salt processing	=	*sodium oxalate added from the chemical cleaning*	-	*sodium oxalate sent to vitrification*	(eq. 1-1)

The models used to estimate the impacts of the *Historical Baseline Chemical Cleaning Process* on vitrification and salt processing is provided in Appendix 1. The results are summarised in Table 1.

[7]The future feed for salt processing must be added to grout, using a 100 vol parts grout to 10 vol parts feed, before being placed in a vault.

[8]The number of additional vaults required based are based on the current-design-vault which has a capacity of approximately 2.0×10^7 litres.

Table 1. Vitrification and salt processing impacts.

Case	Tanks cleaned	Formed $Na_2C_2O_4$ (kg)	Vitrification feed preparation handling		Impacts to vitrification		Impacts to salt processing		
			Blending / washing	Max wt% $Na_2C_2O_4$ allowed (wt%)	Additional required wash cycles	Fraction of $Na_2C_2O_4$ to vitrification	Fraction of $Na_2C_2O_4$ to salt processing	Future *feed for salt* processing (litres)	Number of Additional vaults
#1	2	102,000	Add to unwashed then wash	14	9	0.25	0.75	2,900,000	1.44
	3	153,000			12	0.18	0.82	4,800,000	1.58
#2	2	102,000	Add to pre-washed with minimal additional washing	14	9 pre, 5 post	0.25	0.75	2,900,000	1.44
	3	153,000			9 pre, 7 post	0.17	0.83	4,800,000	1.60
#3	2	102,000	Add to unwashed then wash	20	8	0.29	0.61	2,400,000	1.18
	3	153,000			12	0.25	0.75	4,300,000	1.44
#4	2	102,000	Add to pre-washed with minimal additional washing	20	9 pre, 5 post	0.35	0.65	2,500,000	1.26
	3	153,000			9 pre, 7 post	0.25	0.75	4,300,000	1.44

As can be seen in Table 1, column entitled "Impacts to vitrification - Additional required wash cycles," increasing the sodium oxalate added to an *existing vitrification sludge feed batch* from chemically cleaning either two or three tanks, results in additional wash cycles. Specifically, an increase in a minimum of two additional wash cycles if added to a prewashed *vitrification sludge feed batch*, or four additional wash cycles if added to an unwashed *vitrification sludge feed batch*. The sub-column entitled "Fraction of total $Na_2C_2O_4$ to vitrification" shows a decrease in the fraction of oxalate being removed from the process through *vitrification,* when cleaning three tanks vs two. This behaviour is because more "Additional required wash cycles' are required to reduce both the sodium concentration and the solids sodium oxalate loading, as an *existing vitrification sludge feed batch* is fed new solid $Na_2C_2O_4$.

As previously summarised by Equation 1-1, since there are only two current disposal paths to remove waste from the HLW process. Decreasing the amount of oxalate being *vitrified*, result in the same amount of oxalate precipitating and becoming part of the sparingly-soluble salt heel, but ultimately requiring significant volumes of additional water to solubilise and remove the salt heel from the HLW process, creating a copious additional *Future Feed for salt*

Processing. The column entitled, "Impacts to vitrification - Additional required wash cycles," also shows that regardless of the amount of pre-washing, for the chemical cleaning of two tanks, at least five post loading wash cycles will be required.

Using Equation 1-1, Appendix 1 quantifies the copious additional *future feed for salt processing*. For every two tanks cleaned, approximately 2.4 to 2.9×10^6 litres of *future feed for salt processing* results. For every three tanks cleaned about 4.3 to 4.8×10^6 litres of *future feed for salt processing* are created. Additionally, the feed-to-grout volume ratio used for immobilisation of the salt waste results in further dilution. The radioactive grout as the result of chemically cleaning two tanks will require the equivalent of 1.18 to 1.44 current vaults for immobilisation of the additional salt waste, with each current design vault capacity being 2.0×10^7 litres. Similarly, the impact from chemically cleaning three tanks will require the equivalent of 1.44 to 1.60 current design vaults for the immobilisation.

2. ARRIVING AT A CONCEPT TO TEST

2.1 Search for a Solution to Problem

Decontamination of nuclear reactors, plants and installations are essential for reducing occupational exposures, permitting reuse of components and facilitating waste management and facility decommissioning (EPRI, 1989; Dow Chemical, 1977). Steels and aluminium-based alloys are ubiquitous in United States Department of Energy nuclear sites with several approaches used for their decontamination. In this context, oxalic acid plays two roles. It plays the role of the reductant for excess oxidant that remains after an initial surface oxidation step (to solubilise the metal substrate). It also plays the part of the complexing agent for metal ions released during the decontamination step, i.e. Fe^{2+}, Mn^{2+}, Ni^{2+} etc. (Reiss *et al.*, 2009; Nuclear Energy Agency, 2008; Wille and Berthaldt, 2000; Wilde *et al.*, 1984; Remark, 1989). An example of an oxidant that is deployed in the former step is permanganic acid, HM_nO_4, where the excess remaining after the initial surface oxidation step is reduced from Mn^{+7} to Mn^{+2} by oxalic acid (Bradbury, 2001; Wille and Berthaldt, 2000; Remark, 1989).

So as not to replicate various previous searches for alternative processes to replace the Historical Baseline Chemical Cleaning Process to clean SRS HLW tanks (Adu-Wusu *et al.*, 2003), the search for an alternative deployed a modified TRIZ approach. TRIZ is a Russian acronym for "Teoriya Resheniya Izobretatelskikh Zadatch," which roughly translates as the Theory of Solving Inventive Problems. TRIZ is different from most other approaches in that it is based on the underlying principle that “Inventing is the removal of technical contradictions (Davis *et al.*, 2009).” A unique attribute associated with TRIZ is that it looks similar but already resolved problems, then adapts the resolutions (Davis *et al.*, 2009). Using the TRIZ approach, the need for an alternative was restated as follows:

Remove 90% of 18,900 litres of metal hydroxide sludge from a HLW tank within an approximate six-month duration, while minimising (Davis *et al.*, 2009):

1) Creation of additional waste
2) Creation of new waste streams
3) Consumption of available operating volume within the HLW process;
4) Introducing new chemicals into the HLW process
5) Changing the process chemistry beyond that currently analysed for impacts to downstream facilities.

The stated minimum cleaning effectiveness was chosen based on the maintaining the same overall cleaning effectiveness as the Historical Baseline Chemical Cleaning Process as documented by SRNL and described in detail in Chapter 1 (Stallings *et al.*, 2004; Adu-Wusu *et al.*, 2003).

A review of current industrial practices was undertaken to find an analogous but recently solved problem, where the determined solution could likely be readily adapted for HLW tank cleaning. Using the TRIZ approach, the scale/crud removal from the secondary side of heat exchangers in nuclear power plants was identified to be a partially analogous, but an already solved problem.

Five primary state-of-the-art dilute Decontamination Regenerative Technologies (DRTs) that are commercially used in cleaning the secondary loop in nuclear power plant steam generators were identified being worthy of further evaluation. A sixth DRT that has only undergone limited testing was also reviewed. Assessments for each of the DRTs were primarily based on Bradbury, 2000, and Bushart *et al.*, 2003.

2.1.1 Low Oxidation Metal Ion

Low Oxidation Metal Ion (LOMI) technology was developed in the 1970s. The process uses the vanadous ion, V^{2+} in the form of vanadium picolinate, $C_{18}H_{12}N_3O_6V$, to reduce Fe^{3+} ions in nuclear power plant scale to the more soluble Fe^{2+}. At the same time, V^{2+} is summarised to V^{3+}. Formic acid, CH_2O_2, is then added to the reagent to scavenge oxidising radicals (Bradbury, 2000).

The LOMI process is applied similar to the CAN-DECON process (see Section 2.1.2 below). The reactor coolant is first adjusted to a pH=7, then heated above 80ºC. The chemical decontamination solution is injected, with a side stream of circulated coolant passed through a filter and cation exchange resin column to regenerate the solution online (Cacuci, 2010). A second generation LOMI process uses less formate and NaOH resulting in the use of significantly less ion exchange resin for waste clean-up (Remark, 1989).

Since the LOMI technology cannot be used in open-air systems, such as in the SRS HLW tanks[9], the technology was quickly discounted from further consideration (Davis *et al.*, 2009).

According to Remark (Remark, 1989), the leading oxide removal method for LOMI process is an oxidation-reduction mechanism, where the vanadous ion transfers an electron to the ferric ion, Fe^{3+}, in the scale reducing the ferric ion to ferrous ion, Fe^{2+}. The reduction of the ferric ion to ferrous destabilises the corrosion film structure, allowing the complexing agent, picolinic acid, $C_6H_5NO_2$ to chemically bond with the metallic species in the corrosion film.

[9]The SRS HLW tanks must remain vented to minimise H_2 build-up from radiolysis of water.

2.1.2 Canadian Depleted Uranium Decontamination

Similar to LOMI, the Canadian Depleted Uranium Decontamination (CAN-DECON) technology uses oxalic acid, $H_2C_2O_4$, as both the reducing and chelating agent, and ethylene diaminetetracetic acid (i.e. EDTA), $C_{10}H_{16}N_2O_8$, as a complexation agent (Bradbury, 2000). Citric acid, $C_6H_8O_7$, may also be used as a chelating agent (Davis *et al.,* 2009). The primary mechanism for the oxide film removal is acid-digestion (Remark, 1989). With this technology, mixed bed ion exchange resins are utilised to remove the metals and regenerate the acid (Bradbury, 2000).

2.1.3 Citric Acid/Oxalic Acid

According to Bradbury (Bradbury, 2000), citric acid/oxalic acid (CITROX) technology uses oxalic acid, $H_2C_2O_4$, as the reducing agent and citric acid, $C_6H_8O_7$, as a chelating agent. The CITROX blend was developed primarily to minimise iron oxalate precipitation when using oxalic acid to remove scale. The cleaning solution is made using anhydrous (i.e. dry) organic acid, added in a powder form. Typically, the acid is dissolved in a mixing tank, heated, and injected into the preheated system to be decontaminated. The digestion occurs rapidly even at room temperature. As the chelating agent, citric acid, $C_6H_8O_7$, helps keep the metal from precipitating out, until the metals are removed from the spent cleaning solution via cation exchange. The primary mechanism for the oxide film removal is acid-digestion (Remark, 1989). Being a regenerative process, the solvent is continuously circulated through the resin bed, removing the dissolved metals, including radionuclides, hence, restoring/regenerating the acid.

The use of CITROX technology to clean HLW tanks creates a significant quantity of secondary waste, because of spent ion exchange resin. The use of citric acid/oxalic acid blends have been

shown to work well for scale removal in nuclear power plants. The use of the oxalic acid solution, however, has been shown to be as equally effective as the CITROX blend in dissolving HLW sludge (Stallings *et al.*, 2004; Adu-Wusu *et al.*, 2003).

2.1.4 Decontamination for Decommissioning

According to Bradbury (Bradbury, 2000), the Decontamination for Decommissioning (DfD) technology uses fluoroboric acid, HBF_4, as both a reducing and chelating agent. The DfD process has been applied to a wide range of decontamination efforts, ranging in size from a primary loop in a nuclear power plant to a small positive displacement pump. With DfD being a regenerative process, as the solvent is regenerated by passing it through a cation exchange resin. Eventually, when the cleaning is complete, the HBF_4 is neutralised and prepared for disposal (Bradbury, 2000).

Use of fluoroboric acid has been strictly prohibited within the processes that generate HLW. Thus, in addition to the secondary waste created as spent ion exchange resin, use of fluoroboric acid would negatively introduce new chemicals to the HLW process, resulting in changes to the process chemistry beyond that currently analysed, concerning potential impacts on downstream facilities. Therefore, during the TRIZ search for an alternative, the DFD process was eliminated from further consideration for application in cleaning the HLW tanks (Davis *et al*., 2009).

2.1.5 Decontamination for Decommissioning-Improved

DfD uses ion exchange resin creating secondary waste. An enhancement to DfD, DfDx, involves replacing the ion exchange column with an electrochemical cell so minimising secondary waste. However, as a successor to DfD, the primary chemical used within DfDx is also fluoroboric acid, HBF_4 (Bushart *et al*., 2003). As previously stated, since the use of fluoroboric acid has

been prohibited within the precursor processes that give rise to HLW. Thus, use of fluoroboric acid would negatively introduce new chemicals to the HLW process, thus changing process chemistry beyond that currently analysed, concerning impacts on downstream facilities.

Additionally, because of the use of an electrochemical cell (Bradbury, 2001; Bushart *et al*., 2003), use of the DfDx technology has been considered restricted to the decontamination of small components, such as the decontamination of a single pump. The DfDx technology, therefore, was also eliminated from further consideration since it was not considered to have a proven capability of removing 90% of 18,900 litres of sludge from HLW tank within six months (Davis, 2009).

2.1.6 Chemical Oxidation Reduction Decontamination with Ultraviolet Light

According to Wille and Berthaldt (Wille and Berthaldt, 2000), the Chemical Oxidation Reduction Decontamination (CORD) with ultraviolet light (UV) (i.e. CORD UV) technology uses oxalic acid as the reducing agent. The CORD UV treatment steps typically include (Wille and Berthaldt, 2000):

- A series of customised chemical oxidation and reduction steps optimised for the unique surface from which the contaminant is to be removed, and
- Decomposition of the solvent (in this case, oxalic acid) to carbon dioxide and water utilising a patented photo-oxidation treatment process, which uses ozone/UV, such that the oxalate is removed.

According to Wille and Berthaldt, the whole cleaning effort can normally be performed within a reactor using only one full system of demineralised water. Exposure to oxalic acid results in

digestion of metal hydroxides and oxides to give soluble metal oxalates. The oxalates are then decomposed via photo-oxidation with the solution reused.

An envisioned adaptation of the CORD UV process for HLW tank cleaning would minimise the volume of liquid added to the HLW process by delivering the removed sludge as a precipitate slurry, with the potential to continually regenerate/refresh and reuse the solvent. The regeneration of the acid would minimise the amount of total liquid added to the process (Davis *et al.,* 2009). Another advantage of such a CORD UV based process is that no new chemicals would need to be introduced to the HLW. As for flammability concerns, no volatile organics are used since oxalate is decomposed to CO_2 (Davis *et al.,* 2009).

2.2 Technology Down Select

With all six of the technologies being Decontamination Regenerative Technologies (DRTs), all were considered to add only minimal amounts of liquid to the HLW process (i.e. consume minimum available operating volume within the HLW process) (Davis *et al.,* 2009). When performing the TRIZ operation of "trading the contradictions," LOMI could not be applied in the air atmosphere and was, therefore, was considered the only technology that could not obtain the stated goal of 90% removed. With most DRTs, the use of ion exchange technology is fundamental to its dilute regenerative nature, with DfDx being the primary exception and CORD UV also being a possible exception if operated as a destructive regenerative process without ion exchange (Wille and Berthaldt, 2000; Davis *et al.*, 2009). All of the DRTs were considered to have a well-proven throughput except for DfDx. Except for CORD UV, each of the DRTs would either negatively introduced new chemicals to the HLW process, or change the process chemistry beyond that currently analysed concerning impacts on downstream facilities. Table 2 summarises the TRIZ contradiction table.

Table 2. TRIZ contradiction table for the six identified dilute decontamination regenerative technologies.

Technology	Sludge digestion (i.e. about 90%)	Secondary waste	Downstream impacts	Throughput capability demonstrated?
LOMI	Will not work in air	Contradiction - creates used ion exchange resin	Not evaluated	Proven
CAN-DECON	Proven	Contradiction- creates used ion exchange resin	Potential contradiction - uses EDTA; downstream impacts on vitrification process are not well understood	Proven
CITROX	Proven	Contradiction- creates used ion exchange resin	Potential contradiction - uses citric acid; downstream impacts on vitrification process are not well understood	Proven
DfD	Proven	Contradiction- creates used ion exchange resin	Potential contradiction – adds fluoroboric acid; downstream impacts are not fully understood	Proven
DfDx	Proven	Contradiction– does not use resin, smaller volume of carbon media used to collect metals	Potential contradiction – adds fluoroboric acid; downstream impacts are not fully understood	Potential contradiction – not proven
CORD UV	Proven	Can be operated as a destructive regenerative process without using ion exchange	Uses oxalic acid	Proven

As previously stated, although the CORD UV process in nuclear power plant applications commonly uses ion exchange (IX), use of IX is not fundamental to the base technology (Wille and Berthaldt, 2000). The CORD UV technology can be operated using ozone and UV as a photo-oxidation destructive dilute regenerative method (Wille and Berthaldt, 2000;

Davis *et al.*, 2009). Ultimately, the CORD UV technology was the only DRT which did not have contradictions (Davis *et al.*, 2009). Therefore, with no contradiction trading required, the (destructive regenerative adaptation of the) CORD UV[10] process became the TRIZ identified resolution.

2.3 Conceptual Process Flow Diagram and Technology Gaps

To show continuity with the Historical Baseline Chemical Cleaning Process, but also to recognise the changes suggested by the TRIZ exercise, the resolution identified by the TRIZ process to clean the HLW tanks is termed Enhanced Chemical Cleaning (ECC*)*. A conceptual process flow diagram is drafted for the ECC process as shown in Figure 7.

Similar to Chapter 1, where locations and streams shown of Figure 6 as part of the Historical Baseline Chemical Cleaning Process, within Chapters 2 and 3, locations and streams associated with the *Conceptual ECC Process*, shown by Figure 7, are italicized within this chapter.

[10] For simplicity within this thesis, the destructive regenerative adaptation of the CORD UV for oxalate decomposition of spent oxalate cleaning solutions, is also referred to as the CORD UV process.

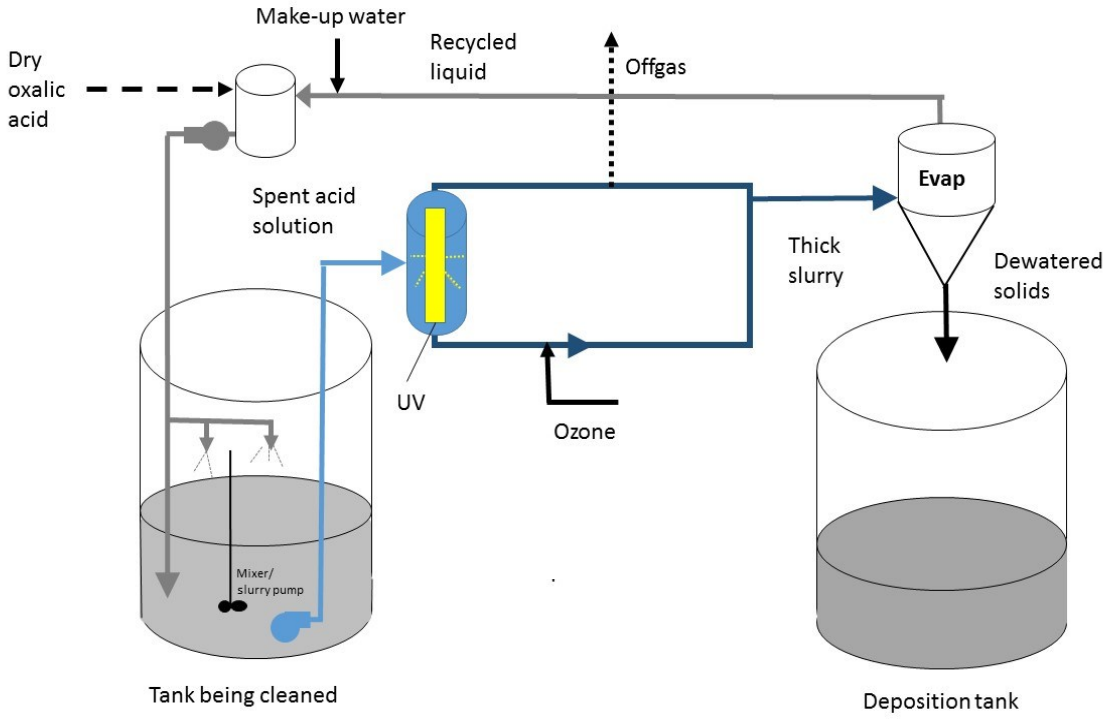

Figure 7. Conceptual process flowsheet for proposed *Enhanced Chemical Cleaning (ECC)* process.

The conceptual process was envisioned to run as follows.

Starting at the upper left side of Figure 7, dry oxalic acid and make-up water are combined in a small tank (i.e. called the make-up tank) to make a *dilute oxalic acid solution*. The oxalic acid solution is transferred to the *HLW Tank Being Cleaned*, lowering the pH and digesting the sludge. Immediately prior to chemical cleaning the pH is approximately 10.5. After the acid is added, the goal would be for the pH in the Tank to be maintained at around 2.

After the sludge solids are digested, they are suspended through use of slurry (i.e. mixer) pumps and moved out of the *HLW Tank Being Cleaned*. That is, the sludge solids as part of the *spent acid solution* are transferred out of the *HLW Tank Being Cleaned*. The *spent acid slurry* is then treated with ozone and UV, where the oxalate decomposes into CO_2 and off-gas. The oxalate decomposition process increases the pH to approximately 7 to 7.5, causing sludge

oxide solids to reform as a result of hydroxide-promoted precipitation. The *thick slurry* containing sludge oxide solids will be transferred out of the *oxalate decomposition process.* Using an *Evaporator*, a significant fraction of the liquid is separated/removed from the *thick slurry*. The resultant *dewatered solids* are transferred to the *Deposition Tank* (an existing HLW tank where the solids are combined with other HLW sludge to become future feed to vitrification), while the evaporator overheads (at a pH of around 7) are transferred back towards the *Tank Being Cleaned* as *recycled-fluid*. The pH in the *Deposition Tank* would be significantly greater than 12.

Before the *recycled-fluid* is added to the *HLW Tank Being Cleaned*, anhydrous oxalic acid is added to the *recycled-fluid* to refresh/renew the acid. The now *refreshed/restored oxalic acid* cleaning solution is added back into the *HLW Tank Being Cleaned* (maintaining the HLW tank pH at around 2), for further digestion of the sludge.

Key to the operation of ECC process is the regenerative dilute oxalic acid, oxalate decomposition either directly or indirectly via ozone[11,12], and the de-watering of the solids.

---

[11] Ozone and hydrogen peroxide are commonly used in AOPS. A decision was made early in the development of the ECC process to use ozone instead of hydrogen peroxide because of the potential safety concerns associated with using hydrogen peroxide, as well as process-upset corrosion concerns if hydrogen peroxide was inadvertently released to a HLW tank. Use of both ozone and hydrogen peroxide, however, were investigated as part of the literature review, with only the ozone-based oxalate decomposition tested as part of this thesis.

[12] As a somewhat related point, the normal oxidant in the CORD UV used for decomposing oxalate is hydrogen peroxide. However, using a similar setup at a commercial nuclear power plant, ozone has been used in place of hydrogen peroxide by AREVA, with the process also loosely referred to as CORD UV. Therefore, for simplicity when referring to CORD UV as part of this thesis, the oxidant for CORD UV not considered limited to hydrogen peroxide, but may instead be ozone.

2.4 Thesis Statement

The main postulate of this thesis, in the context of the ECC process, is that ozonation alone can efficiently be used to decompose spent oxalic acid in HLW tank nuclear decontaminations solutions in an industrially relevant time frame. As part of exploring this postulate, two hypotheses relating to CORD UV decomposition of spent oxalic acid solutions are investigated– both regarding its application to cleaning HLW tanks at SRS, and in a more general sense, the decomposition mechanisms associated with the ozonation of heavily metal loaded spent oxalic acid waste solutions. Those two hypotheses are:

1) That dark ozonation (i.e. ozonation without UV) is fully capable of decomposing the heavily weighted spent oxalic acid cleaning solutions within industrial relevant time frames; and

2) That the minimal impacts on oxalate decomposition rates observed as a result of already present hydroxyl radical scavengers during the oxalate decomposition testing, demonstrate that, at least under acid conditions, the decomposition of oxalate is not hydroxyl radical driven.

Demonstration of hypothesis 2) would indicate that the envisioned *ECC Process* under acid conditions would not an advanced oxidation process (AOP) based on the associated definitions (see Section 3.4 below). Based on the review of reaction mechanisms contained in Chapter 3, it may be possible that the rate-limiting step in oxalate decomposition during metal-catalysed ozonation of oxalic acid under acidic conditions is a direct O_3 attack on metal oxalate complexes or on oxalates that are sorbed onto the surface of metal oxide particles in the sludge.

Also investigated, as part of this thesis, are: 3) understanding the different roles that the Fe, Mn, and Ni play throughout the decomposition process, and 4) using pH as a field measurement to determine when oxalate decomposition can be considered complete.

Points 1) through 4) are explored in more detail in Chapters 4 and 5.

3. APPLICABLE CONCEPTS AND TECHNOLOGIES

In Chapter 2, the conceptual *ECC Process* was proposed wherein; *the spent acid slurry* is transferred out of the *HLW Tank Being Cleaned* to an above ground *Oxalate Decomposition Process*. This adapted process was identified using TRIZ methodology as a viable alternative to the Historical Baseline Chemical Cleaning Process.

The *ECC Process* has two unique aspects associated with oxalate compared to the SRS Historical Baseline Chemical Cleaning Process for cleaning HLW tanks with oxalic acid (Davis et *al.*, 2009):

1) The *ECC Process* would use significantly more dilute oxalic acid solutions vs the concentrated acid solutions used in the baseline (i.e. currently 1 to 2.5 wt% oxalic acid solution is used in CORD UV, compared to a concentrated 8 wt% oxalic acid solution used in the chemical cleaning baseline); and,

2) The conceptual *ECC Process* decomposes oxalate into CO_2, which can be off-gassed[13] achieving the goal stated in Chapter 2 of minimising the creation of additional waste.

[13] Although the *ECC Process off-gas* would be required to be filtered and monitored before being released to ensure no unacceptable discharges, purge exhaust filtering and monitoring requirements are universally used within HLW to ensure flammable gas concentrations are not approached and hence are not considered to represent a new technology.

3.1 Overview of the Sludge Digestions Concepts

Previous studies of HLW sludge digestion (Adu-Wusu *et al.*, 2003; Stallings *et al.*, 2004; Ketusky *et al.*, 2011; Martino *et al.*, 2012) and, more specifically, iron oxide digestion (Cornell and Schindler, 1987; Panias *et al.*,1996; Lee, 2005), indicate that at a pH of around 2 the most effective digestion of iron oxides occurs, as well as SRS HLW sludge types, when using oxalic acid. However, as described in Chapter 1, SRS HLW cleaning histories show that a pH ~10.5 is usually encountered immediately before initiating chemical cleaning (Adu-Wusu *et al.*, 2003; Stallings *et al.*, 2004, Ketusky *et al.*, 2011; Martino *et al.*, 2012).

Preliminary laboratory scale titrations conducted by this author (*inter alia*) using 1 wt% to 2.5 wt% oxalic acid have confirmed that a pH of ~2 can be obtained by simple oxalic acid addition to both simulant and real waste (Ketusky *et al.*, 2011; Martino *et al.*, 2012). Thus, with the possibility that such dilute oxalic acids may be a more effective cleaning solution compared to concentrated oxalic acids (Ketusky, 2008; Lee, 2005), the majority of the research discussed herein focuses on oxalate decomposition.

3.2 History of the CORD UV Process

Arriving at the TRIZ determined alternative as discussed in Chapter 2, the CORD UV process was studied for a more detailed understanding of its mode of action.

Bradbury states that in the 1980s workers at Siemens started to consider new developments in nuclear power plant secondary side decontamination specifically for the European market (Bradbury, 2000). The characteristics of the European market included a significant restriction on the creation and disposal of secondary waste. At that time in the U.S., spent ion exchange resin could be de-watered and economically disposed of using a High Integrity Container (HIC) for first dewatering then burial of the ion exchange resin.

However, with European countries having significant restrictions associated with waste, especially those with chelating agents and ion exchange capabilities, an alternate process for minimising secondary waste and spent ion exchange resins was required. In the Siemens developed process, Mn(VII) in the form of permanganic acid, HM_nO_4, is first applied as the primary oxidative decontamination agent; this is followed by application of oxalic acid, $H_2C_2O_4$, to reduce any unspent Mn(VII). According to Riess *et al.* (Riess *et al.*, 2007), the dissolved contamination metal substrate corrosion products (Cr, Fe, Ni), as well as the reduced manganese (Mn(II)), are then removed using ion exchange resins during each acid addition "strike." By the end of each strike, the decontamination chemicals have been decomposed into water and CO_2 using the oxidant and UV. The result is an incredibly low-volume secondary waste stream, free of both chelating agents and decontamination chemicals (Willie *et al.*, 1997; Willie and Berthaldt, 2000).

3.3 Oxidation Overview

In terms of electron transfer, oxidation is the loss of electrons, while reduction is the gain of electrons. These electron transfers result in the chemical transformation of both the oxidant and the reductant, in some cases producing chemical species with an odd number of valence electrons (i.e. generate radicals) (Nagargoje *et al.,* 2014; Kommineni *et al.,* 2001). These radicals are highly unstable and, therefore, highly reactive because of the unpaired electrons. Oxidation reactions that produce the radicals are followed by additional oxidation reactions between the radical oxidants and other reactants until thermodynamically stable oxidation products are formed.

The oxidation potential measures the ability of an oxidant to initiate a chemical reaction.

According to Dorfman and Adams, some of the most potent oxidants are hydroxyl radicals, ozone, and chlorine (Dorfman and Adams, 1973). In this context, the two general types of oxidation reactions are considered as follows:

1) Direct, where substrates participate in non-radical based reactions with oxidants such as ozone, hydrogen peroxide, and chlorine; or

2) Indirect where substrates react in an AOP, e.g. hydroxyl radicals created indirectly from ozone or hydrogen peroxide.

With the oxalate decomposition in the CORD UV process historically identified as an AOP (Bradbury, 2003), Section 3.4 documents the literature review primarily associated with AOPs and the generation of hydroxyl radicals, while Section 3.5 documents the literature review associated with advanced non-hydroxyl-based reactions.

To provide a comparison of the oxidative power of common oxidants, Table 3 shows the oxidative potential at a pH of 7 for hydroxyl radicals. Also included are advanced non-hydroxyl based oxidants (e.g. the positively charged hole on TiO_2). The listed oxidants considerably exceed those associated with so-called tertiary processes (i.e. those involving the use of non-advanced oxidants), such as permanganate (MnO_4^-), hypochlorous acid (HClO), and chlorine (Cl_2).

Table 3. The oxidation potential of select oxidising species (Techcommentary, 2006; Carey, 1992; Munter, 2001).

Oxidation species	Oxidation potential (V)
Positively charged hole on TiO_2^+	3.21
Hydroxyl radical[14]	2.80
Atomic oxygen	2.42
Ozone	2.07
Hydrogen peroxide	1.78
Permanganate	1.68
Hypochlorous acid	1.49
Chlorine	1.36

3.4 Definition of an AOP and Hydroxyl Radical Processes

Oxalate ions are among the most widely used complexing agents (Lagunova *et al.*, 2012). Although oxalate is commonly formed as an intermediate during the decomposition of organics (Huang *et al.*, 2007; Yoo and Kim, 2002; Pleigo *et al.*, 2014), the ability of hydroxyl radicals to decompose oxalate can be considered to be well demonstrated (Pleigo *et al.*, 2014; Mazellier and Sulzberger, 2001; Trapido, 2007; Goroma and Gurol, 2005). In fact, the efficacy of CORD UV process for oxalate destruction is commonly explained as being a hydroxyl radical based AOP (Davis *et al.*, 2009; Bradbury, 2000).

The exact definition of an AOP, differs amongst authors, mainly based on their expertise. For instance:

1) Munter, 2001, states that AOPs have proceeded along one of the two routes:

[14] For uniformity within this thesis, hydroxyl radicals are given the standard notation where the radical symbol is shown to the right of "OH, "as "OH·," while for all other radicals discussed in this thesis, the radical symbol is shown to the left.

- Oxidation with O_2 in temperature ranges intermediate between ambient conditions and those found in incinerators. For example, Wet Air Oxidation processes in the region of 1 to 2×10^4 Pa and 200 to 300ºC; or

- Use of high energy oxidants such as ozone and H_2O_2 or photons that generate highly reactive intermediates (i.e. OH· created by photolysis of a suitable precursor).

2) Focusing less on the chemical process, but more on familiarity, Kasprzyk-Hordern *et al.*, 2003, defines an AOP as being "an oxidation process which generates OH· in sufficient quantities to benefit water treatment."

3) Concentrating on potential use, Ollis, 1993, states that AOPs are aqueous phase processes which are based primarily on the intermediacy of the OH·, in the mechanism(s) that destroy the target pollutant, xenobiotic, or contaminant compound.

4) Being recognised experts in AOP water treatment, Vogelpohl and Kim, 2004, define AOPs as near ambient temperature and pressure water treatment processes which are based on the generation of OH· to initiate oxidative destruction of organics.

Regardless of the nuances in definitions used between researchers, the term AOP originally and meant a process in which oxidation occurs primarily through reactions with hydroxyl radicals (Glaze and Kang, 1989; Esplugas *et al.,* 2002). AOPs are centered on adding ozone or hydrogen peroxide to force oxidation (Trapido, 2007). Central to this section's review is the fact that in the nuclear industry hydroxyl radicals have historically been considered essential in destroying oxalate (Davis *et al.*, 2009; Bradbury, 2001). Thus, Fenton, Fenton type, and Fenton like reactions which occur "only" under acidic conditions are also investigated (Lui *et al.,* 2007; Bossman *et al.*, 1998; Benitez *et al.*, 1999; Perez *et al.*, 2002; Teel *et al.*, 2002; Pouran *et al.*, 2014; Palanivelu and Kavitha, 2004). Iron oxalate bearing

processes, such as ferrous oxalate, $Fe(C_2O_4)_2^{2-}$, and ferrioxalate, $Fe(C_2O_4)_3^{3-}$ which further expand the pH range of Fenton type reactions are investigated (Hislop and Bolton, 1999; Yoon and Jeong, 2005; Safarzadeh-Amiri *et al.*, 199; Trapido, 2007).

Munter, 2001; Kommineni *et al.,* 2001, Grosse *et al.*, 1998; Vogelpohl and Kim, 2004; Gottschalk *et al.*, 2000, summarises several different AOP-type processes and combinations available for generating hydroxyl radicals. Methods commonly considered include both dark (non-UV) and photochemical (use of UV) methods. For this literature review, these methods are grouped and discussed as follows:

- Non-UV Methods
    - Ozone
        - Ozonation at elevated pH (> 8.5)
        - Ozone plus hydrogen peroxide (O_3/H_2O_2), also called peroxone
        - Ozone plus catalyst(s) (i.e. O_3/CAT), including homogeneous (e.g. metal ions) and heterogeneous (e.g. metal oxide surfaces) catalysts
    - Hydrogen peroxide plus catalysts
        - Fenton's (H_2O_2/Fe^{2+}); non-iron Fenton's, also commonly called Fenton's like (i.e. using specific other transitions metal that catalytically behave like iron), and Fenton type (H_2O_2/Fe other than Fe^{2+})[15].

[15] Metal ions considered to be part of a Fenton's type process may also be part of a complex/ligand.

  - Other possible methods include hydrodynamic cavitation (Benito *et al.,* 200; Raut-Jadhav *et al.*, 2013), ultrasound/acoustic cavitation (Son, 2016), and generation by electron beam (Gehringer *et al.*, 1996).

- Photochemical (UV) based methods

  - UV plus ozone; may also include catalysts

  - UV plus hydrogen peroxide; may also include other catalysts

  - UV plus ozone with hydrogen peroxide

  - UV Fenton's, UV non-iron Fenton's, or UV Fenton's type. Again, the metallic ions may be part of a complex/ligands such as ferrioxalate, which would effectively extend the pH range of the process.

  - Photocatalytic oxidation, such as UV with the semiconductor TiO_2

According to Ince and Apikyan, 2000, AOPs have recently become essential counterparts of effluent treatment plants due to increasing public concerns for health-related environmental problems and the consequent revision of discharge standards. Despite the fact that AOPs are expensive to install and operate, they are nevertheless becoming unavoidable in the treatment of industrial effluents. This unavoidable use includes the removal/detoxification of Refractory Organic Substances (ROS[16]) (Munter, 2001).

[16] ROS refers to organics that are poorly biodegraded and exhibit a low value for the ratio of Biological Oxygen Demand (BOD) to Chemical Oxygen Demand (COD) (Matavos-Aramyan and Moussavi, 2017).

Ince and Apikyan, 2000, note that the last decade has seen AOPs emerging as promising alternatives to tertiary treatments (i.e. those involving the use of non-advanced oxidants such as permanganate), owing to their potency to render partial and complete destruction of many refractory compounds. Such refractory compounds include dyestuffs and halogenated and aromatic organics (Bauman and Stenstrom, 1990; Kusakabe *et al.*, 1991; Ince *et al.*, 1997; Ince, 1998; Ince and Tezcanli, 1999). Typical aromatic compounds include benzene, C_6H_6, and toluene, C_6H_5-CH_3.

The hydroxyl radical is a powerful, extremely reactive, non-selective chemical oxidant which attacks most organic molecules with rate constants, $k_{OH\cdot}$ in the order of 10^6 to 10^9 $M^{-1}sec^{-1}$ (Canton *et al.*, 2003). Its reaction rate with organic compounds can occur so quickly that the reaction appears to be nearly diffusion controlled (Von Gunten, 2003). Also, AOPs have the potential to summarise completely (i.e. mineralise) organic contaminants to CO_2, H_2O and mineral salts (Canton *et al.*, 2003; Li *et al.*, 1999). As described above, AOPs are suited for destroying dissolved organic contaminants such as halogenated hydrocarbons[17]; aromatic compounds[18]; phenols, C_6H_6O; and pesticides[19]. Also, AOPs can also be used to summarise

[17] Halogenated hydrocarbons are organic compounds consisting of C-C, C-H and C-X bonds, where X is a halogen atom (i.e. F, Cl, Br, I). (Minaata *et al.*, 2011), including trichloroethylene, C_2HCl_3, vinyl chloride, C_2H_3Cl (Glaze and Kang, 1989), pesticides, such as trisodium hexafluoroaluminate, Na_3AlF_6. (Marin *et al.*, 2012).

[18] Common aromatic compounds include: benzene, C_6H_6; toluene, C_6H_5-CH_3; and, ethylbenzene, C_8H_{10} (Mokrini *et al.*, 1997; Ledakowicz *et al.*, 2001; Von Gunten, 2003, Safarzadeh-Amiri *et al.*, 1997).

[19] Trisodium hexafluoroaluminate, Na_3AlF_6 is an example of a pesticide (Marin *et al.*, 2012).

inorganic contaminants such as cyanide, CN^-, sulfide, S^{2-} and nitrite, NO_2^- (Portjanskaja, 2012).

Many AOPs exhibit considerable similarities to each other due to the participation of hydroxyl radicals in most mechanisms that are operative during the reactions (Glaze and Kang, 1989; Esplugas *et al.,* 2002). The kinetics of hydroxyl radicals can be approximated as first order with respect to OH· concentration and to the reactant (Munter, 2001; Kasprzyk-Hordern *et al.*, 2003). The rate constants, $k_{OH\cdot}$ are in the range from 10^8 to 10^{10} $M^{-1}sec^{-1}$, whereas the OH· concentration in many of the AOPs is only between 10^{-10} and 10^{-12} M, meaning that a pseudo first order constant would be in the range of 1 to 10^{-4} sec^{-1} (Chamarro *et al.*, 1996). Since the OH· radicals, as well as other potential radicals, are so reactive, they are usually generated ‘‘in-situ’’ (Esplugas *et al.*, 2002).

3.4.1 Non-Photochemical Methods

Under acid conditions, there are three common methods for generating OH· without applying UV light (Munter, 2001; Vogelpohl and Kim, 2004; Kasprzyk-Hordern *et al.*, 2003; Esplugas *et al.*, 2002).

Common non-photochemical methods are:

- O_3 with H_2O_2 (commonly referred to as peroxone);
- Hydrogen peroxide plus catalysts [includes Fenton, Fenton-type (i.e. Fe^{3+} based), or Fenton-like systems (i.e. H_2O_2 with transition element catalyst); and,
- O_3 plus catalysts.

3.4.1.1 Direct and Indirect Ozonation

Due to its structure, molecular ozone can react as a dipolar, electrophilic or nucleophilic reagent. As a result of its high reactivity, ozone is very unstable in water (Kasprzyk-Hordern *et al.*, 2003).

As summarised in Section 3.3, two possible substrate oxidation routes can obtain in an ozonation process (Von Gunten, 2003; Ledakowicz *et al.*, 2001; Chiang *et al.*, 2006; Hoigné and Bader, 1977; Arslan *et al.*, 1999; Baig and Liechti, 2001; Li *et al.*, 2010):

1) Directly, reacting with ozone (Lagunova *et al.*, 2012), especially under non-acidic conditions (Tomiyasu *et al.*, 1985),

2) Indirectly, by reacting with OH· created from reactions between the O_3 and the catalysts (Esplugas *et al.*, 2002, Hoigné *et al.*, 1976; Silva and Jardim, 2006; Asano *et al.*, 2008; Garoma *et al.*, 2008; Logager *et al.*, 1992).

Figure 8 shows these routes, schematically.

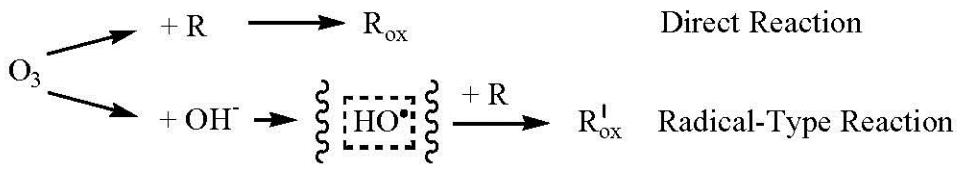

Figure 8. How ozone can act toward other compounds (R) in aqueous solution.

Detailed kinetic models for the direct reaction of ozone with a range of organic and inorganic compounds were first established by Hoigné and Bader, 1983. As part of their models, it was shown that the pH value of the solution significantly influences ozone decomposition in water. The half-life of ozone in industrial wastewater can vary from less than a minute to up to 30 minutes, depending on the types and ozone-reactivity of the pollutants as well as upon pH

(Vogelpohl and Kim, 2004). As the pH increases, the decomposition rate of O_3 in water to form hydroxyl radicals increase (Munter, 2001, Ershow and Morozov, 2009). This relationship between pH and the decomposition of O_3 in water is because the reaction is catalysed by the hydroxide ion (Gural and Singer, 1982). For example, at pH < 3, the hydroxide ion does not influence the decomposition of O_3, while pH > 7, the typical half-life time of O_3 ranges from 15 to 25 minutes (Nawrocki *et al.*, 2000; Masschelein, 1990). Thus, depending on solution pH, ozone can promote both direct and indirect oxidation of organic species pollutants.

3.4.1.2 Ozone Plus Hydrogen Peroxide (also called Peroxone)

A recent interpretation of the mechanism that accounts for OH· production is shown by Reactions 3-1 through 3-6 (Merényi *et al.*, 2010),

$$H_2O_2 \rightarrow HO_2^- + H^+ \quad (3\text{-}1)$$

$$HO_2^- + O_3 \rightarrow \cdot HO_2 + \cdot O_3^- \quad (3\text{-}2)$$

$$\cdot O_3^- + H^+ \rightarrow \cdot HO_3 \quad (3\text{-}3)$$

$$\cdot HO_3 \rightarrow O_2 + OH\cdot \quad (3\text{-}4)$$

$$\cdot HO_2 \rightleftarrows \cdot O_2^- + H^+ \quad (3\text{-}5)$$

$$\cdot O_2^- + O_3 \rightarrow O_2 + \cdot O_3\text{-} \quad (3\text{-}6)$$

In Reactions 3-1 through 3-4, H_2O_2 first dissociates forming the hydroperoxide ion, HO_2^-, and hydrogen ion, H^+. The hydroperoxide ion, HO_2^-, reacts with O_3 creating a hydroperoxide radical, $\cdot HO_2$, and an ozonide radical ion, $\cdot O_3^-$. The $\cdot O_3^-$ protonates creating the hydrogen trioxy radical, $\cdot HO_3$, which subsequently decomposes into O_2, plus hydroxyl radial, OH· (representing one of two reaction paths for producing OH· from peroxone).

In the other reaction path, the hydroperoxide radical, $\cdot HO_2$ created in Reaction 3-2, is in equilibrium with a superoxide radical ion, $\cdot O_2^-$ and the hydrogen ion, H^+, as shown by Reaction 3-5. The superoxide radical ion, $\cdot O_2^-$ reacts with O_3 forming an ozonide radical ion, $\cdot O_3$ as demonstrated by Reaction 3-6, thereby forming another $OH\cdot$ pathway via $\cdot O_3^-$ (repeating Reactions 3-3, and 3-4).

As a result, two moles of $OH\cdot$ are formed per one mole of H_2O_2 and two moles of ozone, as summarised in Reaction 3-7 (Merényi *et al.*, 2010; Hoigné *et al.*, 1982; Munter, 2001):

$$2O_3 + H_2O_2 \rightarrow 2OH\cdot + 3O_2 \qquad (3\text{-}7)$$

Documented organic decompositions using O_3/H_2O_2 include that of atrazine, $C_8H_{14}ClN_5$, using O_3/H_2O_2, in water (Paillard *et al.*, 1988). Comparison of the results of decomposition tests revealed closer-to-complete-decomposition with O_3/H_2O_2 as compared to O_3 alone, and that this degradation depended upon the O_3 dose, contact time, and alkalinity of the water (Munter, 2001).

Duguet *et al.* (Duguet *et al.*, 1985) developed the concept of the H_2O_2 introduction point for peroxone. It was based on tests showing that best overall decomposition occurred when H_2O_2 was added only after first oxidising the highly reactive substances with O_3. This behaviour was explained as the first stage allowing for the full advantage of selective molecular O_3 reactions before converting the process to non-selective free radical attack making oxidation of the more refractory molecules possible (Munter, 2001). Vogelpohl and Kim (Vogelpohl and Kim, 2004) showed that at lower pH values, the addition of H_2O_2 in a 1:2 ratios of H_2O_2/O_3 accelerates the decomposition of O_3 resulting in the increased formation of hydroxyl radicals. They concluded, similarly to Gottschalk (Gottschalk *et al.*, 2000), that at an H_2O_2 concentration $> 10^{-7}$ M with a pH < 7, H_2O_2 in the form of the HO_2^- anion will react with two O_3 reactants producing two $OH\cdot$, as per the stoichiometry of Reaction 3-7 above.

Although H_2O_2 is a relatively inexpensive, highly soluble and readily available chemical, it is hardly used as a direct oxidant because of its low reaction rate constant with organics and other pollutants vs that for OH· (i.e. $k_{O3} << k_{OH\cdot}$). Instead, O_3 is used in combination with UV light, other catalysts, or other oxidising agents (Munter, 2001). Indeed, the efficiency of a peroxone process can be improved significantly by adding UV (Esplugas *et al.*, 2002), as discussed in Section 3.4.2.3.

3.4.1.3 Fenton, Fenton-Type and Fenton-Like Systems

The Fenton process was first reported by Fenton in 1884 for maleic acid oxidation. Reaction 3-8 shows the generation of OH· in the Fenton process.

$$Fe^{2+} + H_2O_2 \rightarrow Fe^{3+} + OH^- + OH\cdot \quad (3\text{-}8)$$

The rate constant, k_{H2O2}, for the reaction of Fe^{2+} with H_2O_2 is approximately 63 $M^{-1}sec^{-1}$ at 25ºC at an assumed pH ~7 (Laat and Gallard, 1999). Under these conditions, Fe^{2+} summarises to Fe^{3+} in a range of a few seconds to minutes, based on exact solution conditions (Munter, 2001). The H_2O_2 is then decomposed catalytically by the so-generated Fe^{3+}, generating further OH· according to the Reactions 3-9 through 3-11:

$$Fe^{3+} + H_2O_2 \leftrightarrow H^+ + Fe\text{-}OOH^{2+} \quad (3\text{-}9)$$

$$Fe—OOH^{2+} \rightarrow \cdot HO_2 + Fe^{2+} \quad (3\text{-}10)$$

$$Fe^{2+} + H_2O_2 \rightarrow Fe^{3+} + OH^- + OH\cdot \quad (3\text{-}11)$$

For this reason, most waste destruction catalysed by Fenton's reagent, Fe^{2+}/H_2O_2, is simply considered an Fe^{3+}-H_2O_2 catalysed destruction process, i.e. an Fe^{3+}-H_2O_2 Fenton-like process. In light of the mechanism described above, it is possible for the ferrous ion in Fenton's reagent to be replaced with a ferric ion (Gottschalk *et al.*, 2000; Munter, 2001).

All transition metals will catalyse the decomposition of H_2O_2 (Bowers *et al.*, 1989; Ravikumar and Gurol, 1994; Miller and Valentine, 1999; Teel *et al.*, 2001). Iron has been the most commonly used catalyst in the application of Fenton's reagent for industrial waste treatment and soil and groundwater remediation (Bowers *et al.*, 1989; Ravikumar and Gurol, 1994; Miller and Valentine, 1999; Teel *et al.*, 2001).

Use of Fe^{2+}-H_2O_2 as an oxidant for wastewater treatment is attractive because (Munter, 2001):

- Iron is a highly abundant and a nontoxic element
- H_2O_2 is easy to handle and relatively environmentally benign

Overall, the Fenton process is very effective for OH· generation; however, it involves consumption of one Fe^{2+} ion for each OH· produced, hence requiring a high concentration of Fe^{2+} (Munter, 2001). According to Barbusiński, 1999 and Prousek, 1995, the Fenton reaction can also involve several other transition cations of metals (M^{n+}), commonly called Fenton-like (or non-iron Fenton) reactions, can be shown as Reaction 3-12:

$$(M^{n+}) + H_2O_2 \rightarrow (M^{n+1}) + OH^- + OH\cdot \quad (3\text{-}12)$$

Alternative non-iron Fenton catalysts and their reactivity towards hydrogen peroxide activation were studied by Bokare and Choi, 2014, concluding that elements with multiple redox states (like chromium, cerium, copper, cobalt, manganese and ruthenium) would directly decompose H_2O_2 into OH· through conventional Fenton-like pathways. However, the H_2O_2 activation mechanism is specific to the nature of the catalyst; it is effectively controlled by solution pH and metal-ligand complexation (Bokare and Choi, 2014).

There is evidenced by the conclusions of El-Raady and Nakajima, 2006, whereas part of a more extensive study, to understand the impact of different metals, the results of Fenton-like to a "true"

Fenton process, with both maintained at a pH of 2, were compared. For the degradation of formic acid, the Fe^{2+} catalysts resulted in closer-to-complete-decomposition than the Cu^{2+}, while oxalic acid was not effectively decomposed using metallic ions and H_2O_2 (El-Raady and Nakajima, 2006). The ineffectiveness of a Fenton process in decomposing oxalate was also noted by Pliego *et al.,* 2014, stating that it is relatively resistant to decomposition under operating conditions in a conventional Fenton process. Similarly, Kavitha and Palanivelu, 2004, when talking about the ineffectiveness of oxalate decomposition in a Fenton process, states that oxidation did not proceed to complete decomposition of oxalate to CO_2, but instead formed potentially stable complexes like ferric oxalate, precluding OH· production. In addition, the refractory nature of oxalic acid to Fenton's reaction is also well documented (Gogate and Pandit, 2003). Gogate and Pandit, 2003, further state that Fenton's chemistry is not a universal solution as there are many chemicals, which are refractory towards Fenton's reagent such as oxalic acid.

Pham *et al.*, 2013, studied copper as the catalysts. Although a Fenton-like mechanism has commonly been proposed to describe the reaction of Cu(I) with H_2O_2, with evidence presented for the formation of OH·, the results of other studies suggest that, at least under some conditions, a higher oxidation state of copper (i.e. Cu(III)) rather than free OH· may be the true active intermediate (Pham *et al.*, 2013).

Similarly, Watts *et al.*, 2005, investigated the occurrence of chemical oxidation and reduction reactions with soluble manganese and manganese oxide-catalysed Fenton-like reactions. Based on decomposition rates for those tests, the data at a pH of 3 to 6 demonstrate that soluble manganese promotes hydroxyl radical production in acidic pH regimes; however, significant concentrations of catalyst are required compared to iron-catalysed reactions.

3.4.1.4 Ozone Plus Catalyst

According to Kasprzyk-Hordern *et al.*, 2003, catalytic ozonation is one of the most recently developed means of removing contaminants from drinking and wastewater. Several studies show that catalytic ozonation is very useful in the removal of several organic compounds.

A range of homogeneous metal ion and heterogeneous metal oxide catalysts (Fe_2O_3, Al_2O_3–Me, MnO_2, Ru/CeO_2, TiO_2–Me, Fe^{2+}, Fe^{3+}, Mn^{2+}, etc.) have been studied, some exhibiting significant acceleration in target compound decomposition (Munter, 2001), although the mechanism in most cases remains unclear. Reflecting this, Kasprzyk-Hordern *et al.*, 2003, notes that catalytic ozonation has been essentially limited to laboratory investigation. The heterogeneous routes are discussed first.

Heterogeneous Catalytic Ozonation

There are at least two basic types of heterogeneous catalysis:

1) Radical creating processes, including the use of hole based methods on semiconductor photocatalysts such as titanium oxide; and,

2) Non-radical based processes including:
    a) Complexation of the target organic with transition metals and other multi-valent metals (strictly speaking a homogeneous process), especially in the case of carboxylic acid-based pollutants
    b) Adsorption of the organic at active sites on the surface of a solid (often particulate) metal oxides followed by ozone attack on the complex or sorbed organic.

In the case of the oxalate carboxylic acid system under study, this includes complexes such as ferrioxalate and cobalt-metal/oxalate catalysts.

The decomposition of the organic in both of these mechanisms (metal complexed and metal oxide adsorbed organic) is believed to proceed by a non-radical decomposition mechanism. Thus, radicals are not the primary driving mechanism in these decomposition processes, and the processes do not meet the definition of AOPs employed in the discussion of this section and therefore are discussed in Section 3.5.

Homogeneous Catalytic Ozonation

Homogeneous catalytic ozonation proceeds by:

1) Ozone decomposition, catalysed by soluble metal ions, to generate (hydroxyl) radicals which then attack the target organic (oxalate) (Gracia *et al.*, 1996; Piera *et al.*, 2000; Sauleda and Brillas, 2001); or,

2) Complexation of the target organic with a transition metal or other multi-valent metal ion followed by direct ozone attack on that complex.

The latter homogeneous type (2) reaction, is a non-radical based process and was described immediately above. As it doesn't meet the definition of an AOP employed in this section, it is also discussed in detail in Section 3.5. The focus of this section is limited to homogeneous reaction type (1).

Due to the homogeneous nature of this process, its efficiency and mechanism can be influenced by solution factors such as pH and reactant concentration. From the perspective of oxalate decomposition, the use of oxidative decomposition of oxalate in neutral and alkaline solutions with simple un-catalysed (i.e. in the absence of metal catalysts) ozone sparging has been widely studied. Of particular relevance to this work is a recent paper by Lagunova *et al.*, (Lagunova *et al.*, 2012) that investigates the pH and temperature dependence of the process – identifying optimum conditions for oxalate destruction as a pH of 10 and a temperature of 50 to 60^{o}C.

Lagunova also noted that, due to the need for initiation by hydroxide ions, decomposition of ozone to form hydroxyl radicals occurs very slowly at a pH of 2. This agrees with an earlier observation by Beltrán *et al.*, (Beltrán *et al.*, 2003a). The significance of the observation is that it recognised that ozone barely reacts with the oxalic acid in acidic solution. The only way that oxalic acid ozonation can occur homogeneously at low pH is by a direct pathway such as reactions involving ozone and Co(II)-oxalic acid complexes (Pines and Reckow, 2002).

The catalysts for these homogeneous catalytic ozonation routes are typically transition metals such as Fe, Mn, Ni, Co, Cd, Cu, Ag, Cr, and Zn. For example, Legube *et al.*, 1996 as part of wastewater treatment, investigated catalytic ozonation with the objective to evaluate the efficiency vs ozonation alone of different organic compounds. Numerous metals (Fe, Mn, Ni, Co, Zn, Ag, Cr) under various forms including metal, solid oxide, deposited metal on supports, were reported to enhance the efficiency of ozone towards the decomposition of the organics.

According to Kasprzyk-Hordern *et al.*, 2003 the nature of the transition metal determines not only the reaction rate, but also selectivity, and ozone consumption. The mechanism of the first catalytic ozonation route described above is based on ozone decomposition followed by the generation of OH·. The transition metal ions present in the solution initiate the ozone decomposition reaction by the production of the radical $\cdot O_2^-$. The transfer of an electron from an $\cdot O_2^-$ ion to O_3 causes the formation of $\cdot O_3^-$, and subsequently OH· (Gracia *et al.*, 1995).

Gracia *et al.*, 1996 and Cortés, 1998 examined the catalytic activity of Mn^{2+}, Fe^{2+}, $Fe^{3+,}$ Cr^{3+}, Ag^+, Cu^{2+}, Zn^{2+}, Co^{2+} and Cd^{2+} sulfate in the process of humic substances ozonation in water. Kasprzyk-Hordern *et al.*, 2003, states that O_3 reacts quickly with humic substances producing low-molecular-weight oxygenated by-products that are more easily biodegradable, polar and hydrophilic than their precursors. According to Kasprzyk-Hordern *et al.*, 2003, ozone decomposition catalysed by soluble metal ions to generate hydroxyl radicals did not remove

the organic matter to any significant extent. The level of complete oxidation to carbon dioxide and water, which is the only way to eliminate organic matter, was minimal in water treatment (i.e. with only insignificant reductions in organic carbon quantities observed).

Gracia *et al.*, 1996, observed that for very high ozone dosages (4.5 gram O_3/ gram Total Organic Carbon (TOC)), which are not used at water treatment plants, ozonation alone provides 33% TOC reduction in water. As stated in Kasprzyk-Hordern *et al.,* 2003, the application of catalytic ozonation with transition ions significantly improved the efficiency of humic substances removal from water under the same experimental conditions. The best results were obtained for Mn^{2+} (62% TOC) and Ag^{+} (61% TOC). Ozonation in the presence of the other transition metals was Fe^{2+}, $Fe^{3+,}$ Cr^{2+}, Cu^{2+}, Zn^{2+}, Co^{2+} and Cd^{2+} were slightly less efficient. The application of catalytic ozonation resulted in a significant decrease in the required ozone consumption. In summary, ozone dosages, which are usually applied in water treatment plants, do not cause the mineralisation of humic substances. Higher TOC removal was observed in the case of very high ozone dosages; however, here again, total mineralisation was not obtained. The application of catalytic ozonation, however, is a possible means of achieving a significant increase of humic substances removal as reported by Gracia *et al.,* 1996; Cortés *et al.,* 1998. Mn^{2+} and Fe^{2+} ions introduced to the reaction system at the concentration of 6×10^{-5} M were found to be useful catalysts for the ozonation of chlorinated benzene derivatives carried out under neutral pH and at an ozone dose of 1.5 grams O_3 per gram of TOC. After 20 minutes of contact time, the percentage of COD reduction in the case of model water was 18% for ozonation alone, 55% for catalytic ozonation in the presence of Fe^{2+}, 66% in the case of the O_3/Mn^{2+} system, and only 12% for O_3/Fe^{3+}. Ozonation with Fe^{3+} as well as ozonation alone at a high pH value of 8.4 caused only 5% of TOC reduction. However, ozonation with Fe^{2+} or Mn^{2+} resulted in 40% of TOC reduction. Catalytic ozonation produced mainly formaldehyde, CH_2O, and glyoxal, $C_2H_2O_2$ in the case of Fe^{2+}/O_3 and glyoxal for

Mn^{2+}/O_3 (Cortés *et al.*, 1998). For wastewater from the production of the organochloride pesticides dicofol, $C_{14}H_9Cl_5O$, and tetradifon, $C_{12}H_6Cl_4O_2S$, containing chlorinated benzene derivatives, the percentage of COD reduction was as follows: 38 and 35% for O_3/Fe^{2+} and O_3/Mn^{2+}, respectively (Cortés *et al.*, 2000).

At the neutral to basic pH values of the systems discussed above, the mechanism of catalytic ozonation with the usage of transition metal ions as catalysts is based on an ozone decomposition reaction followed by the generation of hydroxyl radicals. The ions present in the solution initiate the ozone decomposition reaction by the production of the radical $\cdot O_2^-$. As previously discussed in Reaction 3-6, the transfer of an electron from $\cdot O_2^-$ ion to O_3 causes the formation of $\cdot O_3^-$, and subsequently OH· (Gracia *et al.*, 1995). The mechanism of the Fe^{2+}/O_3, is based on the generation of hydroxyl radicals, (Piera *et al.*, 2000; Sauleda and Brillas, 2001) and can be expressed using the following reactions (Logager *et al.*, 1991). The Fe^{2+}/O_3 system involves the direct reaction of Fe^{2+} with ozone resulting in the production of OH· as shown in Reactions 3-13 through 3-14:

$$Fe^{2+} + O_3 \rightarrow FeO^{2+} + O_2 \quad (3\text{-}13)$$

$$FeO^{2+} + H_2O \rightarrow Fe^{3+} + OH\cdot + OH^- \quad (3\text{-}14)$$

FeO^{2+} is also able to oxidise Fe^{2+} to Fe^{3+} (at a slower rate) with the termination of the chain reaction as shown by Reaction 3-15:

$$FeO^{2+} + Fe^{2+} + 2H^+ \rightarrow 2Fe^{3+} + H_2O \quad (3\text{-}15)$$

Processes such as the above, as well as the related Fenton reaction, can be accelerated by the application of UV light. Photochemical methods are discussed in Section 3.4.2.

3.4.2 Photochemical Methods

In many cases, conventional ozone or hydrogen peroxide oxidation does not wholly oxidise organics to CO_2 and H_2O (EPRI, 1996). Intermediate oxidation products may be toxic (Vogelpohl and Kim, 2004). Completion of oxidation reactions, as well as the oxidative destruction of compounds immune to unassisted ozone or H_2O_2 oxidation, are commonly achieved by supplementing the reaction with UV light (Munter, 2001; Vogelpohl and Kim, 2004).

Regarding the photolysis of ozone to create hydroxyl radicals, UV lamps should have a maximum radiation output at 254 nm for efficient conversion. However, many organic contaminants also absorb UV energy in the range of 200 to 300 nm (Munter, 2001). The UV adsorption by the contaminants limits the ability of the UV to react with the ozone. Based on this, a discussion of the influence of UV on the AOP systems presented in Section 3.4.2.1 follows.

3.4.2.1 Ozone–UV (O_3/UV)

Homogeneous Ozone-UV Ozonation

Ozone readily absorbs UV at 254 nm wavelength (the extinction coefficient ε254 nm = 3300 $M^{-1}cm^{-1}$) producing H_2O_2 as an intermediate, which then decomposes to OH· (Gottschalk *et al.*, 2000), as shown by Reactions 3-16 and 3-17:

$$O_3 + h\nu \rightarrow O_2 + O(1D) \quad (3\text{-}16)$$

$$O(1D) + H_2O \rightarrow H_2O_2 \rightarrow 2OH\cdot \quad (3\text{-}17)$$

Munter, 2001, states that photolysis of ozone may be an expensive way to make hydrogen peroxide, that is subsequently photolysed to OH·. Although photochemical cleavage of H_2O_2

is conceptually the simplest method to produce hydroxyl radicals, the exceptionally low molecular absorptivity of H_2O_2 at 254 nm (ε_{254nm} = 18.6 $M^{-1}cm^{-1}$) limits the OH· yield in the solution.

Table 4 shows that photolysis of ozone yields more radicals per incident photon at 254 nm than the UV/H_2O_2 process – although the absorptivity of H_2O_2 can be increased by using UV lamps with output at lower wavelengths. However, this raises the power requirement of the UV lamps.

Table 4. Formation of hydroxyl radicals from photolysis of ozone and hydrogen peroxide (EPRI, 1996).

Oxidant	ε 254 nm, (M^{-1} cm^{-1})	Stoichiometry	OH· formed per incident photon
H_2O_2	20	$H_2O_2 \rightarrow 2OH\cdot$	0.09
O_3	3300	$3O_3 \rightarrow 2OH\cdot$	2.00

In practice, the power requirement for UV lamps in ozone photolysis is in the watts (W) range vs kilowatts for hydrogen peroxide photolysis (Munter, 2001).

If water solutions contain organic compounds strongly absorbing UV light, then UV radiation usually does not give any additional effect to ozone because of the screening of ozone from the UV by optically active compounds (Munter, 2001; Trapido, 2007). Although phenolic compounds (e.g., phenol, p-cresol, 2,3-xylenol, 3,4-xylenol) are readily oxidizable by ozone, complete decomposition is uncommon (Benitez *et al.*, 1999; Esplugas *et al.,* 2002).

As early as 1987, it was demonstrated that the O_3/UV system could completely mineralise organic compounds with a short molecular chain, e.g. glyoxylic acid, oxalic acid, formic acid, as reported by Gurol and Vatistas, 1987, with Takahashi, 1990, later confirming.

Heterogeneous Ozone-UV Ozonation

In addition to the above photochemical homogeneous reaction described immediately above, Section 3.4.1.4 briefly mentions heterogeneous hole-based reactions arising, where the use of UV light is normally used to promote the formation of electron-hole pairs on semiconductor materials which then subsequently react to form radicals (Hernandez-Alonso *et al.*, 2002). Since UV is used, it is discussed here as part of Section 3.4.2.1.

Studies of the decomposition of acetic acid in O_3/H_2O_2 solutions in the presence and absence of TiO_2 reveal a significant increase in hydroxyl radical yield in the presence of TiO_2 compared to its absence (Tong *et al.*, 2011).

When TiO_2, a solid metal catalyst, is illuminated with UV light of wavelength less than 380 nm, valence band electrons are excited to the conduction band, creating vacancies or "holes" in the valence band (Crittenden *et al.*, 1996, Kommineni *et al.,* 2001). The excited-state electrons can initiate a wide range of mostly reductive chemical reactions; however, organic destruction in such systems is primarily due to hydroxyl radical generation. These radicals can be produced either as a result of oxidation of water by valence band holes, or the reduction of molecular oxygen by conduction band electrons (Crittenden *et al.*, 1996).

3.4.2.2 Hydrogen Peroxide-UV (H_2O_2/UV)

The direct photolysis of hydrogen peroxide leads to the formation of OH· as shown by Reaction 3-18.

$$H_2O_2 + h\nu \rightarrow 2OH\cdot \qquad (3\text{-}18)$$

Also, HO_2^-, which is in an acid–base equilibrium with H_2O_2, absorbs the UV radiation of the wavelength 254 nm. The equilibrium and absorption are shown by Reactions 3-19 and 3-20:

$$H_2O_2 \leftrightarrow HO_2^- + H^+ \quad (3\text{-}19)$$

$$HO_2^- + h\nu \rightarrow OH\cdot + \cdot O^- \quad (3\text{-}20)$$

The H_2O_2/UV process has been successfully used for the destruction of chlorophenols (i.e. molecules having one or more covalently bonded chlorine atoms) (Trapido *et al.*, 1997) and other chlorinated compounds (Nicole *et al.*, 1991; Hirvonren *et al.*, 1996). Bischof *et al.*, 1996, reported that molecules of atrazine, $C_8H_{14}ClN_5$, desethylatrazine, $C_6H_{10}ClN_5$, and simazine, $C_7H_{12}ClN_5$, could be mineralised eventually to carbon dioxide within industrially relevant decomposition times using hydrogen peroxide/UV.

3.4.2.3 Ozone Hydrogen Peroxide UV (O_3 H_2O_2 UV)

The addition of H_2O_2 to the O_3/UV process is identified as accelerating the decomposition of ozone, which results in an increased rate of OH· generation (EPRI, 1996). Mokrini *et al.*, (Mokrini *et al.*, 1997), investigated the oxidation of phenol, and benzoic acid. Experimental results indicated that both phenol and benzoic acid are destroyed more rapidly when H_2O_2 was added to the decomposition process. Trapido and Kallas, (Trapido and Kallas, 2000) also reported that the UV plus peroxone (i.e. peroxide/ozone mixtures) was more effective for the degradation of nitrophenols than ozonation or binary combinations of UV ozone, UV peroxide or peroxone.

3.4.2.4 Photo Fenton and Fenton like Systems

According to Munter, 2001, when Fe^{3+} ions are added to the H_2O_2/UV process, the process is commonly called Photo-Fenton-type oxidation. At pH of 3, the $Fe(OH)^{2+}$ complex forms, as shown by Reactions 3-21 and 3-22:

$$Fe^{3+} + H_2O \rightarrow Fe(OH)^{2+} + H^+ \quad (3\text{-}21)$$

$$Fe(OH)^{2+} \leftrightarrow Fe^{3+} + OH^- \quad (3\text{-}22)$$

When exposed to UV, the complex is further subjected to decomposition and will produce OH· radicals and Fe^{2+} ions, as shown by Reaction 3-23 (Munter, 2001):

$$Fe(OH)^{2+} + h\nu \rightarrow Fe^{2+} + OH\cdot \quad (3\text{-}23)$$

The Photo-Fenton-type reaction relies heavily on the UV irradiation to initiate the generation of OH· (Munter, 2001). Sun and Pignatello, 1993, demonstrated that many herbicides and pesticides could be completely mineralised using $h\nu$−Fe(III)/H_2O_2 process. Ruppert *et al.*, 1993, Huang *et al.,* 2001, demonstrated the mineralisation of chlorophenol (i.e. organochloride of phenol that contains one or more covalently bonded chlorine atom) with Photo-Fenton. Per Munter, 2001, the increased efficiency of Fenton/Fenton-like reagents with UV/visible irradiation is attributed to the following:

1) Photo-reduction of ferric ion and ferric hydroxide produces ferrous ion, as shown by Reaction 3-23. The ferrous ion produced reacts with H_2O_2 generating a second hydroxyl radical and ferric ion, and the cycle continues;

2) The absorption spectrum of hydrogen peroxide does not extend beyond 300 nm and has a low extinction coefficient beyond 250 nm. On the other hand, the absorption

spectrum of ferric ion extends to the near-UV/visible region and has a large extinction coefficient, thus enabling photo-oxidation and mineralisation by visible light.

Ferrioxalate is a photo-active catalyst, first discovered in 1833 and it was later suggested as a chemical actinometer for light intensity measurements (Munter, 2001; Zuo and Deng, 1997; Zuo and Hoigné, 1992). It is commonly considered a modified form of Fenton's reagent (Waite *et al.*, 2000; Safarzadeh-Amiri *et al.*, 1997; Sun and Pignatello, 1993). The production of OH· and hence the degradation of organic contaminants is accelerated by the addition of UV and a chelating agent such as oxalate to the Fe/H_2O_2 system. Oxalate forms photo-active Fe^{3+} complexes and Fe^{2+} complexes. Both complexed and uncomplexed Fe^{2+} react with H_2O_2 to produce OH· radicals. Major reactions between iron, oxalate and H_2O_2 are as shown by Reactions 3-24 to 3-26 (Zuo and Hoigné, 1992; Faust and Zepp, 1993):

$$HC_2O_4^- + OH\cdot \rightarrow \cdot C_2O_4^- + H_2O \quad (3\text{-}24)$$

$$H_2O_2 + OH\cdot \rightarrow \cdot HO_2 + H_2O \quad (3\text{-}25)$$

$$Fe^{2+} + OH\cdot \rightarrow Fe^{3+}OH^{2+} \quad (3\text{-}26)$$

3.4.2.5 Photo-Catalytic

Munter, 2001; Kasprzyk-Hordern *et al.*, 2015 explain photocatalysis as the photo-excitation of a solid semiconductor as a result of the absorption of electromagnetic radiation often, but not exclusively, in the near UV spectrum. Under near UV irradiation, a suitable semiconductor material may be excited by photons possessing energies of sufficient magnitude to produce conduction band electrons and valence band holes. These charge carriers can induce reduction or oxidation reactions, respectively.

Titanium dioxide, both in the forms of anatase and rutile, is one of the most widely used metal oxides in industry. Its high refractive index in the visible range permits preparation of thin films, and thus its use as a pigment material. On the other hand, its use as a catalyst support or as a catalyst and photocatalyst itself, is well known. Titanium dioxide acts not only as a catalyst support but also interacts with the supported phase as a promoter (Martin and Martin, 1995).

Per Munter, 2001, titanium dioxide (anatase), i.e. one of the tetragonal forms of titanium oxide, has an energy bandgap of 3.2 eV and can be activated by UV illumination with a wavelength up to 387.5 nm. At the ground level, since solar irradiation starts at a wavelength of about 300 nm, only 4 to 5% of the solar energy reaching the surface of the earth could be used as direct and diffused components when TiO_2 is used as a photocatalyst (Zhang *et al.*, 1994; Bahnemann 1991).

Per Munter, 2001, many toxic chemicals are degradable by TiO_2-driven photocatalytic oxidation, including halogenated hydrocarbons[20], aromatics molecules[21], chlorinated phenols[22], even dioxins[23].

---

[20] Halogenated hydrocarbons are organic compounds consisting of C-C, C-H, and C-X bonds where X is a halogen atom (F, Cl, Br, I) which are readily mineralised.

[21] Aromatic molecule has a planar ring with 4n+2 Pi-electrons, where "n" is a non-negative integer.

[22] Chlorinate Phenol is a molecule composed of phenol with substituted chlorines, biphenols, e.g., $C_{12}H_{10}O_2$.

[23] Dioxin is a general name for a family of chlorinated hydrocarbons studied who are wholly summarised yielding CO_2 and HCl as final products.

Photocatalysts such as titanium dioxide are often used in a colloidal or particulate form to maximise the semiconductor surface area available for solid/liquid contacting. At the surface of such particles, the photogenerated electrons and holes may react with absorbed species (Matthews, 1986; Zhang and Croue, 2014; and Zhang, 2011; Kasprzyk-Hordern *et al.*, 2003), as shown by Reactions 3-27 through 3-32:

$$e^- + O_2 \rightarrow \cdot O_2^- \quad (3\text{-}27)$$

$$h^+ + A^- \rightarrow \cdot A \quad (3\text{-}28)$$

$$h^+ + OH^- \rightarrow OH\cdot \quad (3\text{-}29)$$

$$OH\cdot + RH \rightarrow \cdot RHOH \quad (3\text{-}30)$$

$$OH\cdot + RH \rightarrow \cdot R + H_2O \quad (3\text{-}31)$$

$$h^+ + RH \rightarrow \cdot RH^+ \quad (3\text{-}32)$$

The valence band holes of TiO_2 possess an extremely positive oxidation potential and are thus thermodynamically capable of oxidising almost all organics. As well, the one-electron oxidation of water resulting in the formation of hydroxyl radicals is energetically feasible, as shown by Reaction 3-33 (Matthews, 1986; Kasprzyk-Hordern *et al.*, 2003):

$$H_2O + h^+ \rightarrow OH\cdot + H^+ \quad (3\text{-}33)$$

In fact, based on 3-33 the photo-mineralisation of organic pollutants by TiO_2 photocatalysis are often explained by the intermediacy of $OH\cdot$ (Mills *et al.*, 2015). However, due to the short lifetime and high reactivity of this radical, experimental verification often remains difficult (Mills *et al.*, 2015).

The pH value has a significant effect on the photocatalytic reaction because many properties, such as the surface state, the flat-band potential, with the dissociation of organic contaminants being strongly pH dependent (Munter, 2001)

Having discussed both non-photochemical and photochemical AOPs in detail, factors that may impact on their effectiveness are discussed. For completeness, common impacts in terms of AOPs are briefly discussed, as well as their potential impacts on the ECC process.

3.5 Non-Radical Pathways

The hydroxyl radical has high reaction rate constants with almost all organics in water. However, hydroxyl radical oxidation is often not effective in the degradation of aliphatic hydrophilic compounds that contain the carbonyl or carboxylic groups, these being the main products formed during the ozonation of natural organic matter (Von Gunten, 2003). This is because the consumption of hydroxyl radical by bicarbonates/carbonates ($k_{OH\cdot}$= 8.5×10^6 to 3.9×10^8 $M^{-1}sec^{-1}$) and ozone (k_{O3} = 1×10^8 to 2×10^9 $M^{-1}sec^{-1}$) are faster than its reactions with the saturated compounds (Von Gunten, 2003)[24].

In addition, as discussed in Section 3.4.1.4, due to the need for initiation by hydroxide ions, decomposition of ozone to form hydroxyl radicals occurs extremely slow at low pH values, something that was recently revisited and confirmed by Lagunova *et al.* (Lagunova *et al.,* 2012). Indeed, Beltrán *et al.*, 2003a and 2003b, have reported that ozone barely reacts with oxalate in acidic solution either directly or indirectly. They also note that transition metals do catalyse and promote oxalate decomposition under acidic conditions, but that the only way that

[24] For consistency $k_{OH\cdot}$ is used throughout this thesis when referring to a reaction rate constant of the applicable reactant with hydroxyl radicals, while k_{O3} is used for the reaction rate constant of the applicable reactant with ozone.

this can occur homogeneously is by a direct, non-AOP pathway involving ozone attack on transition metal-oxalic acid complexes, such as the Co(II)-oxalic acid complex (Pines and Reckhow, 2002). Since the initial *simulant decomposition test slurries* have a pH of around 2, non-radical based decomposition mechanisms must be considered and are investigated.

Catalytic ozonation through just such a non-hydroxyl radical based complexation pathway for aliphatic carbonyl/carboxylate may be more efficient. An example would be the compound that is the focus of this thesis, oxalate, whose rate constant for degradation by hydroxyl radicals is relatively low at a pH of 6 ($k_{OH\cdot} = 7.7\times10^6\ M^{-1}sec^{-1}$) (Pines and Reckhow, 2002; Buxton *et al.*, 1995). Therefore, oxalate is commonly used as a probe compound to study metal-catalysed ozonation routes that follow either metal ion complexation (e.g. Fe^{3+} or Co^{2+}) or metal oxide surface adsorption (e.g. at MnO_2, Fe_2O_3, Co_3O_4, and NiO) pathways. All are potentially used as catalysts during ozonation of oxalate (Andreozzi *et al.*, 1997; Beltrán *et al.*, 2005; Beltrán *et al.*, 2003a; and Avramescu *et al.*, 2008).

Over the past 25 years, there has been growing research interest in such AOP that incorporate transition metal catalysts but which have been shown not to involve radicals. As discussed above and in Section 3.4.1.4 above, there are two general types of such processes, categorised as follows:

- Heterogeneous processes: wherein the target organic adsorbs onto the surface of a solid (often particulate) metal oxide at a so-called active site, a process that is then followed by ozone attack on the sorbed organic; and

- Homogeneous processes: wherein, especially in the case of carboxylic acid-based pollutants, the target organic complexes with transition metals and other multi-valent metals, a process that is followed by ozone attack on the complex. In the case of the

oxalate carboxylic acid system under study here, this would include complexes such as ferrioxalate discussed above.

Homogeneous Non-AOP Ozonation Process

Beltrán *et al.*, 2003a, studied ozone-enhanced oxidation of oxalic acid in water using homogeneous cobalt as a catalyst. In the study, oxalic acid in water was treated with ozone in the presence of a Co^{2+} salt at acidic pH. The influence of different variables, including the initial oxalic acid, Co^{2+}, and ozone gas concentrations and the temperature was investigated. The experimental stoichiometric ratio varied between 0.7 and 1.4 moles of ozone consumed per mole of oxalic acid consumed, while the ozone efficiency reached values as high as 25%. At any condition applied, nearly total mineralisation was achieved. Beltrán concluded that at the low pH values studied, the metal-catalysed process was proceeded by a non-AOP direct route, i.e. by ozone attack on oxalic acid complexed to the Co(II).

In a different study associated with carboxylic acids, El-Raady and Nakajima, 2006, determined that only Co^{2+} and Mn^{2+} ions demonstrated high efficiency for the ozonation of oxalic acid, but a minor effect for the removal of formic acid by O_3. In the same study, Cu^{2+} showed a significant impact on the mineralisation of maleic acid degradation products in the unbuffered solution. Pines and Reckhow also found that trace amounts of Co^{2+}, 2×10^{-6} M, can accelerate the ozonation of organic compounds such as oxalic acid at low pH, placing this in the context that oxalic acid is a compound which does not readily react with molecular ozone (k_{O3} = 0.04 $M^{-1}sec^{-1}$) (Pines and Reckhow, 2002). Piera *et al.*, 2000, reported that the application of the Fe^{2+}/O_3 system, in the process of 2,4-dichlorophenoxyacetic acid (2,4-D) degradation at pH = 3, resulted in significant degradation of the compound, however, only the application of the O_3/Fe^{2+}/UV system provided complete degradation of 2,4-D. The main oxidising species were O_3 for direct ozonation. Again, all the above indicate that at low pH multivalent transition

metal catalysts in the solution phase can catalyse the homogeneous direct non-AOP decomposition of oxalate via metal complexation with the oxalate followed by ozone attack on the complex.

Considering these general observations, the roles of a range of commonly used metal catalysts in non-AOP reactions of relevance to the (oxalate) system under study in this thesis are reviewed.

3.5.1 Carboxylic Acid System Copper Non-AOPs

According to Zhang *et al.*, 2009, oxalate is usually used as a refractory model compound as this cannot be effectively removed by ozone and hydroxyl radical oxidation alone in water. They determined that cerium supported CuO significantly improved oxalate degradation in reaction with ozone. The optimum CuO loading amount was 12%. The molar ratio of oxalate removed/ozone consumption reached 0.84. The catalytic ozonation was most effective in a neutral pH range of 6.7 to 7.9 and became ineffective when the water solution was acidic or alkaline. Moreover, bicarbonate, a ubiquitous hydroxyl radical scavenger in natural waters, significantly improved the catalytic degradation of oxalate. Therefore, it was deduced that the degradation relied on neither hydroxyl radical oxidation nor acid assistance, two pathways usually proposed for catalytic ozonation. These special characteristics of the catalyst make it suitable to be potentially used for practical degradation of refractory hydrophilic or organic matter and compounds in water and wastewater. In-situ characterisation methods determined that surface Cu^{2+}, formed from ozone-driven oxidation of trace Cu^{+} on the catalyst, was the active site in coordination with oxalate forming a multi-dentate surface complex. Zhang, 2009 proposed that the complex can be further oxidised by molecular ozone and then decomposes through intra-molecular electron transfer. A ceria support enhanced the activity of the surface Cu^{+}/Cu^{2+} in this process.

3.5.2 Cerium and Palladium Non-AOPs

In a later study, Zhang *et al.*, 2011 studied the cerium supported palladium oxide (PdO/CeO_2) at a low palladium loading and found it to be very effective in catalytic ozonation of oxalate. During the tests, the oxalate was degraded into CO_2 with catalytic ozonation. The molar ratio of oxalate degraded compared to ozone consumption increased with increasing catalytic dose and decreasing ozone dosage and pH under non-acid conditions. The maximum molar ratio reached ~1.0, meaning that the catalyst was highly active and selective for oxalate degradation in water. Based on the use of atrazine as a probe chemical, it was determined that the catalytic ozonation did not promote hydroxyl radical generation from ozone. Moreover, bicarbonate, a ubiquitous scavenger, significantly improved the catalytic decomposition of the oxalate – the opposite of what would be expected if the oxalate decomposition was hydroxyl radical driven. Analysis with attenuated total reflectance Fourier transform infrared spectroscopy (ATR-FTIR) and in situ Raman spectroscopy revealed that: 1) oxalate was adsorbed on CeO_2 of the catalyst forming surface complexes; and, 2) O_3 was adsorbed on PdO of the catalyst and further decomposed to surface atomic oxygen, surface peroxide, and O_2 gas in sequence. The results indicated that the high activity of the catalyst was related to the synergetic function of PdO and CeO_2 in that the surface atomic oxygen readily reacts with the surface cerium-oxalate complex.

3.5.3 Cobalt Non-AOPs

Co^{2+} was examined as an ozonation catalyst by Pines and Reckhow, 2002. Laboratory-scale batch ozonation experiments were run at near-neutral pH and 24°C. A hydroxyl radical probe compound, p-chlorobenzoic acid, $C_7H_5ClO_2$, was also included in the solution matrix. Batch experiments showed that trace amounts of Co^{2+} accelerated the ozonation of oxalate. The rate of oxalate removal increased with the pH decreasing from 6.7 to 5.3. The presence of Co^{2+} also increased the removal rate of p-chlorobenzoic acid, $C_7H_5ClO_2$, indicating that the

generation of hydroxyl radicals are byproducts of Co^{2+} catalysed ozonation of oxalate. As proposed by Pines and Reckhow, 2002, the process of oxalic acid ozonation with the Co^{2+}/O_3 system at a pH ~ 6 follows a two-step reaction. In the first step, a Co^{2+}–oxalate complex forms, which is subsequently oxidised by ozone to form Co^{3+}-oxalate. The metal centre is suspected to be the site of the attack. The partial donation of electron density from oxalate ion to Co^{2+} may increase the reactivity of Co^{2+}–oxalate when compared with free Co^{2+}. Subsequently, the decomposition of Co^{3+} complex occurs with the formation of an oxalate radical and Co^{2+}. The rate of both oxalate removal and ozone decomposition increase with decreasing pH from 6.7 to 5.3 is contradictory to the typical relationship between ozone decomposition and pH. This conflicting behaviour provides further evidence that the principal reaction pathway is not by hydroxyl radicals, but some other decomposition mechanism.

The proposed homogeneous reaction pathway for the ozonation of a cobalt (II) – mono oxalate complex was summarised by Guo (Guo *et al.,* 2012) as shown by Reactions 3-34 through 3-37.

$$Co^{2+} + C_2O_4^{2-} \leftrightarrow CoC_2O_4 \quad (3\text{-}34)$$

$$CoC_2O_4 + O_3 \rightarrow CoC_2O_4^{+} + O_3^{-} \quad (3\text{-}35)$$

$$CoC_2O_4^{+} \rightarrow Co^{2+} + \cdot C_2O_4^{-} \quad (3\text{-}36)$$

$$\cdot C_2O_4^{-} + O_3 \rightarrow 2CO_2 + O_3^{-} \quad (3\text{-}37)$$

3.5.4 Titanium Non-AOPs

Paillard *et al.*, 1991, studying ozonation without UV, showed that ozone selectively summarised carboxylic functional groups at the surface of a titanium dioxide-based catalyst and that the reaction pathway did not include the formation of hydroxyl radicals. Instead, the

mechanism was explained as a selective oxidation mechanism of carboxylic functional groups that occurs via a heterogeneous reaction route involving carboxylate group adsorption on the catalyst surface (carboxylate is known to have a high adsorption affinity for titanium surfaces) followed by subsequent oxidation of the so-adsorbed compound by ozone at the catalyst surface. Paillard's analyses compared the efficiency of catalytic ozonation O_3/TiO_2 with plain ozonation and a combination of O_3/H_2O_2 using oxalic acid as a model compound. The O_3/TiO_2 system was preferable over ozone (both without UV) in terms of process efficiency in TOC reduction.

3.5.5 Manganese Non-AOPs

Ma and Graham, 1999, proposed that formed in-situ hydrous Mn(VII) initiated the decomposition of ozone to form hydroxyl radicals. Andreozzi *et al.,* 1992, alternately proposed that organic radicals and hydroxyl radicals were reactive intermediates of Mn^{2+}-catalysed ozonation of oxalic acid at pH ~ 4.7. Both systems were homogeneous.

Manganese is also capable of catalysing oxalate by heterogeneous routes. For example, Andreozzi *et al.* 1996, using a solid-phase MnO_2 catalyst showed that the decomposition mechanism involved the formation of a surface Mn-oxalic acid complex (analogous to that generated in titanium oxide systems discussed above). In their study of the role of surface oxalate complexes in manganese oxide catalysed ozone-driven oxidation, Kasprzyk-Hordern *et al.*, 2003; Andreozzi *et al.*, 1996, assert that the oxidation of oxalic acid is only explained by the formation of a surface complex. After the complex forms, a 'one electron' exchange step occurs with subsequent detachment of the reduced surface metal centre. Reactions 3-38 through 3-40 summarize this.

$$Mn^{3+}OH_2^{+} + C_2O_4^{2-} \quad \leftrightarrow \quad Mn^{3+}C_2O_4^{-} + H_2O \qquad (3\text{-}38)$$

$$Mn^{3+}C_2O_4^- \leftrightarrow Mn^{2+} + \cdot CO_2^- + CO_2 \quad (3\text{-}39)$$

$$Mn^{2+} \rightarrow Mn^{2+}_{aq} \quad (3\text{-}40)$$

The adsorbed ozone can react with the surface $Mn^{3+}C_2O_4^-$ complex at a rate at least comparable with that of the intramolecular electron transfer (Andreozzi *et al.*, 1996), as shown by Reaction 3-41:

$$Mn^{3+}C_2O_4^- + O_3 + 2H^+ \rightarrow 2CO_2 + O_2 + Mn^{3+}OH_2^+ \quad (3\text{-}41)$$

Ozone can also oxidise reduced species Mn^{2+}_{aq} and Mn^{2+} (Andreozzi *et al.*, 1996), as shown by Reactions 3-42 and 3-43:

$$Mn^{2+}_{aq} \xrightarrow{O_3} Mn(III, IV)OH_2^+ \quad (3\text{-}42)$$

$$Mn^{2+} \xrightarrow[H_2O]{O_3} Mn(III, IV)OH_2^+ \quad (3\text{-}43)$$

Differing from most of the other observed reaction rates vs pH, Kasprzyk-Hordern *et al.*, 2003, determined that the efficiency of manganese-catalysed ozonation increases with decreasing pH of the solution. This observed dependence of the system reactivity upon pH can be related to the negative influence of this parameter on the concentration of the Mn–oxalic acid complex, with the charge of the oxide surface, strongly depending on pH. A decrease of reactivity in the pH range of 4.1 to 6.0 is consistent with the decline in the concentration of the surface sites $MnOH_2^+$ that can support the adsorption of oxalic acid (Andreozzi *et al.*, 1996). Moreover, the degree of dissociation of the carboxylic acid, which can be indicated by its pK_a value (where pK_a is the negative log to the base 10 of the acid dissociation constant, Ka) also influences the adsorption of the organic compound to the catalyst surface, as well as its susceptibility to oxidation. In the case of oxalic acid, the pK_a values are 1.2 and 4.2. The total ionisation of

this compound will, therefore, take place at a pH value above 4.2. As a result, the highest adsorption of oxalic acid to a positively charged manganese oxide surface (due to $MnOH_2^+$ groups) would take place at pH > 4.2. However, the concentration of the surface sites, $MnOH_2^+$, that can support the adsorption of oxalic acid decreases with an increase in pH. That is, the charge on the surface of the manganese oxide catalyst switches from positive below pH of 4.97 to negative above pH of 4.97. The pH of this reversal referred to as the Point of Zero Charge (PZC) (Miyattah *et al.*, 2016). Therefore, both PZC of the catalyst and pK_a of the dissociative organic compound should be taken into consideration when discussing the process of catalytic ozonation. The effect of temperature on the efficiency of manganese-catalysed ozonation of oxalic acid is also significant. An increase in temperature from 10ºC to 35ºC causes a substantial increase in ozonation efficiency.

3.5.6 Iron and Iron Oxalate Type Non-AOPs

Logager *et al.*, 1992, studied the oxidation of ferrous ions by ozone in acidic solutions, with a pH of near 0 to 2, using a stopped-flow spectrophotometer. The reaction can be characterised as an oxygen atom transfer from O_3 to Fe^{2+}.

Bossman *et al.*, 1998, notes that, although it is a widely accepted in the AOP arena that oxidations using the Fenton or the photochemically enhanced Fenton reactions are initiated by free hydroxyl radicals. The question arises whether OH· production is too slow to compete with the direct electron transfer between the target organic substrate and a hydrated higher-valent iron species (most likely Fe^{4+}_{aq}). The reduction potentials of the reactive intermediates (OH·, Fe^{4+}_{aq}), as well as Fe^{2+}_{aq}, Fe^{3+}_{aq}, and H_2O are listed in Table 5, allowing for the oxidising power of those entities to be easily compared.

Table 5. Reduction potentials of Fe^{2+}_{aq}, Fe^{3+}_{aq}, H_2O_2 and the reactive intermediates of OH· and Fe^{4+}_{aq}.

Redox couple	E^0 (V vs NHE)
$OH\cdot_{aq}/H_2O_{aq}$	2.59 (pH=0)
$OH\cdot_{aq}/HO^-_{aq}$	1.64 (pH=14)
$Fe^{3+}_{aq}/Fe{=}O^{2+}$ (porphyrine chelate)	~0.9 (pH=0)
$Fe^{3+}_{aq}/Fe{=}O^{2+}$ (porphyrine chelate)	~1.3 (pH=7)
$Fe^{3+}_{aq}/Fe^{4+}_{aq}$	~1.8 (pH=0)
$Fe^{3+}_{aq}/Fe^{4+}_{aq}$	~1.4 (pH=7)
$Fe^{2+}_{aq}/Fe^{3+}_{aq}$	0.771 (pH=0 to 3)
H_2O_2/H_2O	1.776 (pH=0)
H_2O_2/H_2O	0.878 (pH=14)
H_2O_2/O_2	0.682 (pH=0)
H_2O_2/O_2	-0.076 (pH=14)

Depending on the substrate, reactive intermediates other than hydroxyl radicals have been proposed for Fenton's reaction. In the case of compounds which may form highly stabilised Fe^{2+} complexes (e.g. Fe^{2+} complexes with EDTA), Bossman *et al.*, 1998 suggested that the base-induced nucleophilic addition of H_2O_2 to the electrophilic iron centre of these complexes yields the reactive intermediate of Fenton reagents.

Irradiation of ferrioxalate in an acidic solution generates carbon dioxide (Waite *et al.*, 2000; Safarzadeh-Amiri *et al.*, 1997; Sun and Pignatello, 1993), as shown by Reactions 3-44 through 3-46, with Reaction 3-46 producing superoxide.

$$[Fe(C_2O_4)_3]^{3-} + h\nu \rightarrow [Fe(C_2O_4)_2]^{2-} + \cdot C_2O_4^- \quad (3\text{-}44)$$

$$\cdot C_2O_4^- + [Fe(C_2O_4)_3]^{3-} \rightarrow [Fe(C_2O_4)_2]^{2-} + C_2O_4^{2-} + 2CO_2 \quad (3\text{-}45)$$

$$C_2O_4^- + O_2 \rightarrow \cdot O_2 + 2CO_2 \quad (3\text{-}46)$$

Photolysis of ferrioxalate produces ferrous (free or complexed with oxalate) ion, which in combination with hydrogen peroxide provides a constant source of Fenton's reagent and

hydroxyl radicals. Zepp *et al.*, 1992 and Safarzadeh-Amiri *et al.*, 1997, demonstrated the formation of hydroxyl radicals in the photolysis of ferrioxalate/H_2O_2 mixtures.

Balmer and Sulzberger, 1999, state that the ferrioxalate complex consists of a Fe^{3+} chelated by a varying number (n=1, 2, or 3) of oxalate ions, depending on the concentration of the reacting species and pH. The reaction is initiated by adsorption of light by the ferrioxalate complex, resulting in a ligand to metal charge-transfer transition occurring in the complex, which leads to the formation of a charge-transfer state, followed by decomposition of this excited complex, producing Fe^{2+} and an oxalate radical, Reaction 3-47:

$$Fe^{3+}(C_2O_4)_n^{(3-2n)} + h\nu \leftrightarrow Fe^{2+}(\cdot C_2O_4)_n^{(3-2n)\cdot} \quad (3\text{-}47)$$

Per Thomas *et al.*, 2016, this can include an iron oxalate under non-photolytic conditions reacting directly with the oxidant hydrogen peroxide as shown by Reaction 3-48.

$$FeC_2O_4 + H_2O_2 \rightarrow FeC_2O_4^+ + OH\cdot + OH^- \quad (3\text{-}48)$$

Per Balmer and Sulzberger, 1999, the oxalate radical decomposes into a carbon dioxide radical and carbon dioxide. This decomposition is shown by Reaction 3-49. Alternately, it can react with molecular oxygen to produce the superoxide radical ($\cdot O_2^-$), which is in equilibrium with its protonated form ($\cdot HO_2$), and carbon dioxide. This reaction with molecular oxygen which produces the superoxide radical is shown by Reaction 3-50.

$$\cdot C_2O_4^- \rightarrow \cdot CO_2- + CO_2 \quad (3\text{-}49)$$

$$\cdot C_2O_4^- + O_2 \leftrightarrow \cdot O_2^- + 2CO_2 \quad (3\text{-}50)$$

The superoxide produced by Reaction 3-50 can react to form H_2O_2 by two routes, Reactions 3-51 and 3-52 (Balmer and Sulzberger, 1999):

$$2HO_2/\cdot O_2^- + H^+ \rightarrow H_2O_2 + O_2 \quad (3\text{-}51)$$

$$Fe^{2+} + \cdot HO_2/\cdot O_2^- + H^+ \rightarrow Fe^{3+} + H_2O_2 \quad (3\text{-}52)$$

Whilst the radical produced by Reaction 3-49 can react as described by Reaction 3-53 (Balmer and Sulzberger, 1999):

$$\cdot CO_2- + Fe^{3+}(C_2O_4)_3^{3-} \rightarrow Fe^{2+} + CO_2 + 3C_2O_4^{2-} \quad (3\text{-}53)$$

For iron, Pliego *et al.*, 2014, notes that the speciation of dissolved iron in aqueous solution in the presence of oxalic acid depends on the competition between the formation of iron–hydroxyl and iron–oxalate complexes. Zuo and Hoigné 1992, reported that under mildly acidic conditions, pH range of 3 to 5, Fe^{2+} mainly occurs in the form of the hydrated cation $[Fe(OH)x]^{2-}$. Fe^{3+} is present but mainly in the form of the dissolved Fe^{3+}–oxalate. In the absence of oxalate, Fe(III) would form ferric hydroxides and oxyhydroxides in this pH range, it was concluded that the amount of oxalic acid oxidised to CO_2 was similar in concentration to the amount of Fe^{2+} in solution, produced under UV and inert conditions according to the following overall reaction, Reaction 3-54 (Zuo and Hoigné, 1992):

$$2\ Fe(C_2O_4)_n^{(3-2n)} \xrightarrow{h\nu} 2\ Fe^{2+} + (2n-1)C_2O_4^{2-} + 2CO_2 \quad (3\text{-}54)$$

This reaction, though thermodynamically favourable, requires high activation energy (Pleigo *et al.*, 2014), thus, the reaction must be promoted by photons or by thermal energy.

Per Pliego *et al.*, 2014, the degradation of ferric oxalates at high-temperature proceeds through a thermal/chemical cycle involving Fe^{3+}, oxalic acid, and O_2. Increasing the temperature promotes an electron-transfer from a complexing oxalate ligand to the central Fe^{3+} ion. The homolytic breaking (i.e. breaking in which the bonding electron pair is split evenly between the products) of a Fe^{3+}–O coordination bond of the oxalate ligand gives rise to Fe^{2+} ion, and

oxalate anion, and oxalate radical anion. Then, the oxalate radical can reduce another Fe^{3+}–oxalate complex with the overall mechanism for oxalate mineralisation. This is summarised by Reaction 3-55 and 3-56 (Pliego *et al.*, 2014):

$$Fe(C_2O_4)_n^{(3-2n)+} \rightarrow Fe^{2+} + (n-1)C_2O_4^{2-} + \cdot C_2O_4^- \quad (3\text{-}55)$$

$$Fe(C_2O_4)_n^{(3-2n)+} + \cdot C_2O_4^- \rightarrow Fe^{2+} + nC_2O_4^{2-} + 2CO_2 \quad (3\text{-}56)$$

According to Pliego *et al.*, 2014, the oxalate radical released yields CO_2 and the radical anion $\cdot CO_2^-$ by Reaction 3-57. In the presence of oxygen, the oxalate radical also reacts with dissolved O_2 to produce the superoxide ion, $\cdot O_2^-$, from Reaction 3-58:

$$\cdot C_2O_4^- \rightarrow CO_2 + \cdot CO_2^- \quad (3\text{-}57)$$

$$\cdot C_2O_4^- + O_2 \rightarrow 2CO_2 + \cdot O_2^- \quad (3\text{-}58)$$

It is interesting to note that the thermally promoted reaction sequence of Reactions 3-55 to 3-58 is directly analogous to the previously discussed photonically promoted sequence of Reactions 3-47 to 3-50.

According to Pliego *et al.*, 2014, when Fe^{2+} is added to an oxygen-saturated aqueous solution of oxalic acid, two pathways for the mineralisation can be proposed. On the one hand, Fe^{2+} is oxidised to Fe^{3+} as discussed with the Fe^{3+} ions forming Fe^{3+}-oxalate complexes with the oxalate anions present. This shown by Reaction 3-59.

$$Fe^{2+} + O_2 \rightarrow Fe^{3+} + \cdot O_2\text{-} \quad (3\text{-}59)$$

The ferric ions tend to form ferric oxalate complexes with the oxalate anions present in the reaction media. Also to a lesser extent, metal complexation remains unchanged during one-electron transfer between metal complexes and O_2, as shown in Reaction 3-60. In both cases, mineralisation occurs through the decomposition of the Fe^{3+}-oxalate complexes formed.

$$Fe^{2+}(C_2O_4)_n^{(2-2n)} + O_2 \leftrightarrow Fe^{3+}(C_2O_4)_n^{(3-2n)} + \cdot O_2^- \quad (3\text{-}60)$$

This less favoured pathway (i.e. Reaction 3-60) was confirmed by experiments with pure Fe(II) oxalate complexes in the presence of O_2. Under these conditions, the reaction rate observed for the TOC decomposition was lower than one obtained when iron (II) and oxalic acid were added separately.

3.6 Factors Decreasing Decomposition Effectiveness

Various factors may decrease decomposition effectiveness of AOP and non-radical pathway decomposition processes.

3.6.1 Oxidant Scavengers

Oxidant scavengers discussed in this section include scavengers of hydroxyl radicals, ozone, and hydrogen peroxide. They are called scavengers because the will consume oxidants, resulting in lower decompositional effectiveness.

3.6.1.1 Carbonate and Bicarbonate

The detrimental impact of alkalinity (defined as the ability of water bodies to neutralise acids) on the effectiveness of AOPs has been comprehensively studied (Kommineni *et al.,* 2001). Both alkaline carbonate and bicarbonate will scavenge hydroxyl radicals to create carbonate radicals which, in turn, react with other organic or inorganic compounds present, albeit at a much slower rate (Hoigné and Bader, 1983a and b; (Kommineni *et al.,* 2001). The reaction for the scavenging of hydroxyl radicals by bicarbonate ions is shown below in Reaction 3-61 (Morel and Hering, 1993; Kommineni *et al.,* 2001):

$$OH\cdot + HCO_3^- \xrightarrow{k_{OH\cdot}} \cdot CO_3 + H_2O \quad (3\text{-}61)$$

The rate constants for the reactions of hydroxyl radicals with carbonate and bicarbonate at neutral conditions are 3.8×10^{8} and 8.5×10^{6} $M^{-1}sec^{-1}$, respectively (Buxton *et al.,* 1988). Of relevance to the oxalate-based systems under study in this thesis is the observation that the rate constants in near neutral conditions (i.e. pH of around 7) are slower than the reaction rate constant of hydroxyl radicals with oxalate, 10^{9} $M^{-1}sec^{-1}$ (Munter, 2001) at the same pH. At near neutral conditions, the hydroxyl radical reactions with carbonate and bicarbonate are second-order reactions. That is the reaction rate, r, is a function of the relevant rate parameter, $k_{OH\cdot}$, the hydroxyl radical concentration, [OH·], and the concentration of carbonate or bicarbonate, [CO_3 or HCO_3]. Equation 3-1 shows the reaction of hydroxyl radicals with carbonate or bicarbonate.

$$r = k_{OH\cdot}[OH\cdot][CO_3 \text{ or } HCO_3] \quad \text{(eq. 3-1)}$$

Water can contain carbonate and bicarbonate ions at concentrations several orders of magnitude higher than oxalate and, thus, the reaction of hydroxyl radicals with carbonate and bicarbonate can proceed as fast as their reaction with oxalate (Munter, 2001; Kommineni *et al.,* 2001). For oxalate decomposition, the scavenging effect of hydroxyl radicals by carbonate and bicarbonate can be significant. The potential significance is because carbon dioxide and water are the primary products associated with the oxidative mineralisation of oxalate (Davis *et al.,* 2009; Zuo and Deng, 1997; Lagunova *et al.,* 2012; Minakata *et at.,* 2011). Per Munter, 2001, CO_2 readily dissolves in water, a process that becomes more favourable as pH increases with bicarbonate formation dominating at pH > 6.4 and carbonate formation predominating at pH > 10.3. Therefore, the significance of bicarbonate and carbonate as scavengers becomes even more substantial as the oxalate destruction proceeds and both the amount of CO_2 generated and the pH of the slurry increases.

With the solubility of carbonate and bicarbonate exceeding that of ozone (Minakata *et al.,* 2011; Battino *et al.,* 1983; Glaze and Kang, 1989), its effect could quickly dominate over other scavengers. In fact, when investigated by Battino *et al.*, 1983; Glaze and Kang, 1989; Olson and Barbier, 1994; Chiang *et al.,* 2006, it was concluded that carbonate actively lowers the TOC removal rates, while bicarbonate could completely inhibit TOC removal. To mitigate against this impedance, waters high in carbonate and bicarbonate ions can be:

1) Treated with carbon dioxide stripping (e.g. by sparging with oxygen) before AOP treatment (Peyton *et al.,* 1998),

2) Administered higher concentrations of ozone (Kommineni *et al.,* 2001; Munter, 2000), or

3) Exposed for longer ozonation times (Kommineni *et al.,* 2001; Munter, 2000).

3.6.1.2 Nitrates, Nitrites, Phosphates, and Sulfates

Nitrite is another commonly identified scavenger for both hydroxyl radicals and ozone. Published rate constants for the reaction of nitrite with ozone and hydroxyl radicals under neutral conditions are 4×10^{8} $M^{-1}sec^{-1}$ and 1×10^{10} $M^{-1}sec^{-1}$ respectively (Neta *et al.,* 1988; Farhataziz and Ross, 1977) – highly competitive with the rate constant for the reaction of hydroxyl radicals with oxalate.

Phosphates, PO_4^{3-}, and sulfates, SO_4^{2-}, also have the potential to scavenge ozone and hydroxyl radicals. However, they are extremely slow in reacting with OH· (Gottschalk *et al.,* 2000; Kommineni *et al.,* 2001), and their scavenging effect can usually be neglected for ozone/peroxide/UV systems (Hoigné, 1998).

Since nitrate, nitrite, phosphates and sulfates all are present in HLW sludge, their concentration and potential scavenger impact to the ECC process will require evaluation.

3.6.2 Impacts to UV Light Effectiveness

Since the conceptual design process for ECC discussed in Section 2.3 includes UV, impacts to UV light in both AOP and non-AOP water-treatment processes were investigated as part of the literature review.

Although different terms and quantifications are used by the various authors, the impacts could be group into two general categories.

The first impact category, entitled solution properties, includes factors directly associated with the characteristics of the solution being oxidised. The factors can be summarised as transmissivity, turbidity, and suspended solids, and metals concentrations (Karim and Gehr, 2001).

It is important to note that any UV light absorbing constituent present in solution undergoing ozonation will decrease the rate of formation of radicals, this includes the effects of common anions such as nitrite/nitrate.

The second category includes UV lamp sheath fouling, breakage, and ageing.

3.6.2.1 Solution Properties

Anion Concentrations

Nitrates and nitrites adsorb UV light in the range of 230 to 240 nm and 300 to 310 nm; consequently, high nitrate and nitrite concentrations (either >1 mg/litre) have been shown to limit the effectiveness of UV transmissivity (Calgon, 1996; Kommineni *et al.,* 2001).

Water Quality Measured Properties

UV transmissivity (UVT), refers to the percentage of light that passes through a solution sample at a specific wavelength, normally 254 nm. It is usually reported for a path length of 1 cm. Related properties include turbidity, hardness, and pH.

Turbidity is a measure of the degree to which the water loses its transparency due to the presence of suspended particulates (Gottschalk *et al.,* 2000). Similar to the effect from suspended solids, systems relying on UV irradiation for the dissociation of H_2O_2 or O_3 exhibit a decrease in efficiency as turbidity increases. Turbidity lowers the transmittance of the light into solution and, thus, increased turbidity drops the penetration of the UV radiation into the water (Kommineni *et al.,* 2001; Gottschalk *et al.,* 2000; Avramescu *et al.,* 2008).

pH, which affects the solubility of metals and thus compromises water clarity. The ideal value for suspended solids is < 10 ppm, for UVT is > 85% at a 254 nm wavelength (Kommineni *et al.,* 2001).

3.6.2.2 Fouling, Breakage, and Ageing

Concerns associated UV system degradation include lamp fouling, subsequent lamp sleeve cleaning. Lamp breakage and ageing are other potential problems since UV intensity output decreases with time. Water quality parameters used as possible predictors of fouling were COD, suspended solids, temperature, pH, UV transmission, and metal concentrations, mainly Fe and Ca (Karim and Gehr, 2001).

According to Peng *et al.,* 2005, a significant problem with UV disinfection of wastewater is the accumulation of fouling materials at sleeve-water interfaces. Even though techniques cleaning has been perfected in the last 20 years, some permanent fouling will occur. Although often automated, chemical and mechanical cleaning can remove most fouling materials

satisfactorily, permanent foulants, which cannot be wholly eradicated using conventional cleaning operations, remain on the quartz sleeves and reduce effectiveness (Peng *et al.,* 2005).

3.7 Summary of Literature Review

The main findings of the above review that are relevant to the enhanced chemical cleaning (ECC) oxalate decomposition tests are discussed in the next two chapters, are as follows:

1) Oxalate is a highly refractory compound that is resistant to oxidative decomposition.

2) Oxalate is particularly resistant to mineralisation via direct ozonation at low pH values but can be oxidised by indirect ozonation at basic pH values due to the higher availability of OH^- as a precursor to $OH\cdot$.

3) Metals and metal oxides have been shown to catalyse oxalate mineralisation by three mechanisms:

    - ONE – a heterogeneous non-AOP mechanism where the target organic adsorbs onto the surface of solid metal oxide at a so-called active site, followed by ozone attack on the sorbed organic. In the case of oxalic acid, the extent of adsorption, as a function of pH is dependent upon the pK_a of the acid, (i.e. negative log to the base 10 of the acid dissociation constant, K_a) and the pH at the point of zero charge (PZC) of the metal oxide surface.

    - TWO – a homogeneous non-AOP mechanism that operates under low pH acidic conditions and which involves complexation of the catalysing metal ion with oxalate, followed by ozone attack on the complex.

- THREE – a homogeneous AOP mechanism that operates at a basic pH and which involves metal ions catalysing the formation of hydroxyl radicals from ozone, with the said hydroxyl radicals then driving the oxalate decomposition.

4) In terms of water quality impacts, ozone, hydrogen peroxide, and hydroxyl radical scavengers can limit decomposition effectiveness and must be considered. Additionally, solution properties, such as nitrite concentrations, and water quality measured properties will affect UV effectiveness. Even though UV has become commonplace in both AOPs and non-AOPs, and cleaning techniques have been perfected over the last 20 years, the various potential impacts on the effectiveness of UV remain.

4. DECOMPOSITION TESTING USING SIMULANT BASED SLURRIES

4.1 Overview

In this chapter, the competing and synergistic catalytic effects of highly loaded metal ion mixtures on the rates of decomposition of oxalic acid by ozonation in acidic oxalate-rich slurries are studied for the first time.

Although research on general organic and, specifically, oxalate decomposition has been widely performed using single transition metal catalysts, the decomposition of oxalate using a mixture of transition metals and metal oxalates, with each potentially competing or aiding the decomposition, has not been well studied.

However, this study is not merely driven by scientific curiosity. As described in Chapter 1, the SRS near Aiken, South Carolina, USA remains home to forty-three very large, underground, carbon steel tanks, storing a total of approximately 1.2×10^8 litres of liquid radioactive HLW. To inhibit corrosion of tank fabric, the liquid waste is first rendered heavily alkaline, with a hydroxide concentration typically > 1 M. However, these conditions result in metal ion precipitation from the HLW liquid, forming a sludge that is predominately comprised of the oxides and hydroxides of iron, aluminium, and manganese and mainly compacted into a solid mass. Each of these forty-three tanks must eventually be emptied, cleaned, and closed.

Although the bulk of the sludge in each tank can be removed using a hydraulic slurrying technique, use of chemically aided techniques to partially digest remaining sludge, thus rendering it more amenable to suspension with subsequent removal via slurrying, have been deployed. Given the high metal hydro(oxide) concentration of the sludge, digestion using

technologies adapted from other uses in the nuclear industry, particularly decontamination methods, have been explored.

As discussed in Chapter 2.3, the new process identified to clean the HLW tanks was termed Enhanced Chemical Cleaning (ECC), wherein the process, dry oxalic acid and make-up water are combined to make a dilute oxalic acid solution. The oxalic acid solution is added to the tank being cleaned, lowering the pH and digesting the sludge. After the sludge solids are digested, they are suspended through use of slurring or mixer pumps. The suspended solids are then transferred out of the HLW tank being cleaned, as part of a spent acid slurry. The spent acid slurry is then treated with ozone and UV, where the oxalate decomposes into CO_2 and then is off-gassed. The oxalate decomposition process increases the pH causing sludge oxide solids to reform as a result of hydroxide-promoted precipitation. The thick slurry containing sludge oxide solids are transferred out of the oxalate decomposition process. Using an existing Evaporator, a significant fraction of the liquid will be separated/removed from the thick slurry. The resultant (mostly) dewatered solids are transferred to the deposition tank (where the solids are combined with other HLW sludge to become eventual feed to vitrification), while the evaporator condensate is transferred back towards the tank being cleaned, as fluid to be recycled/refreshed/restored. As part of regenerating the acid, anhydrous oxalic acid is added to the recycled-fluid immediately before the fluid is returned to the HLW tank being cleaned. The regenerated/refreshed cleaning fluid is then added back into the HLW Tank Being Cleaned for further digestion of the sludge.

The slurries created from oxalate-assisted digestion of HLW sludges would have the potential to be highly radioactive. Therefore, use of an immersed UV lamp (i.e. a quartz encased UV lamp as detailed in Section 4.5.1) is considered problematic in both providing the regulatory required pedigree of primary containment, as well as from a maintenance/cleaning perspective.

Thus, an alternative to the conceptual design ECC process for post-decontamination oxalate degradation was sought.

Given both the high oxalate and dissolved transition metal loadings in the recovered slurries, the focus of the search changed to determine whether the metal catalysts already present within the slurries can catalyse the oxalate decomposition to an endpoint of < 100 ppm (1.1×10^{-3} M) within an acceptable period of time.

In addition to addressing SRS's objective to close its radioactive liquid HLW tanks in a timely manner, such a study allows for a number of generic knowledge gaps to be confronted. With concepts for ozonation chiefly originating from well-characterised minimal-constituent dilute water-type systems (e.g., water treatment), there is a fundamental lack in understanding of the crucial factors affecting the decomposition rate of spent organic acids in highly loaded metal slurries (e.g. spent decontamination solutions, metal etch sludge waste, etc.). Additionally, although research on general organic and oxalate decomposition has been primarily performed using single transition metals, the decomposition of oxalate making use of a mixture of transition metals, with each potentially competing or aiding the decomposition also is a system not studied to date.

Because of the unique concerns associated with radioactive liquid waste, caustic additions, i.e. NaOH, known to optimise the hydroxyl radical yield (Zepp *et al.*, 1992), before any treatment with ozone, would only add additional waste and further complicate downstream processing. Thus, the preference is to work under the as received low pH slurry conditions (i.e. a starting pH ~2), so affording an opportunity to investigate ozone-initiated oxalate decomposition under less studied acidic conditions.

Since testing using real HLW (detailed in Chapter 5) necessitated its performance in a laboratory shielded hot cell – and hence, had significant safety controls and size limitations

imposed on it – the process tests performed to understand the oxalate decomposition mechanisms were performed with simulant and are discussed in Chapter 4[25,26], while the results of Chapter 5 are provided to show confirmation of applicability.

Section 4.2 provides an overview of the purpose/goals associated with each of the simulant based oxalate decomposition tests. Section 4.3 provides a synopsis on making the sludge simulants used in making the *simulant decomposition test slurries*, as well as the associated nomenclature used for identifying the slurries. Section 4.4 provides an overview of the *Simulant Decomposition Test Apparatus* design, including the *UV Lamp Apparatus* design, as well as general procedures associated with performing the simulant based oxalate decomposition (with Appendix 3, containing a detailed equipment list (including model numbers) and additional design performance details. Section 4.5 determines if UV light is vital to decompose the oxalate in an industrially relevant time frame (i.e. less than 24 hours required to decompose the oxalate concentration to 1.1×10^{-3} M in each approximate 60 litre batch of simulant based slurry). Section 4.6 determines the impact of the three competing transition metals, Fe, Ni, and Mn on the decomposition process. Section 4.7 demonstrates that pH can be used as a field measure to confirm when oxalate decomposition is complete (as stated above, taken to be corresponding to < 100 ppm / 1.1×10^{-3} M oxalate in solution). Section 4.8 summarizes the results of a study, which strongly suggests that the observed oxalate

[25] Similar to Chapters 1, 2, and 3 where components, functions, and streams associated with the process being presented by the respective chapter are italicised, the components, functions, and streams associated with the Simplified *Simulant Decomposition Test Apparatus*, shown by Figure 9, are italized within this chapter.

[26] For or completeness, the full set of simulant based decomposition test data are included in Table 41 through Table 43, which are found in Appendix 5, while the full set of real HLW based decomposition test data are contained in Table 44 through 47, also contained in Appendix 5.

decomposition, especially under the initial acid conditions, is not the result of a hydroxyl radical-driven process.

4.2 Purpose/Goals of Simulant Based Tests

To ensure that decomposition of oxalic acid would occur to less than 1.1×10^{-3} M total oxalate within an industrial acceptable timeframe, the effects of highly loaded transition metal ion mixtures on the amount of ozonation required to successfully decompose acidic oxalate-rich slurries are studied.

4.2.1 Questions Being Addressed with Simulant Based Testing

Using the *Simulant Decomposition Test Apparatus* based on the conceptual process flowsheet for ECC previously shown in Figure 7, deployed on *simulant decomposition test slurries* (as further detailed in Section 4.3.2), answers to the following questions are investigated:

1) Is UV needed to photo-catalytically aid oxalate decomposition? Can an oxalate concentration of less than 1.1×10^{-3} M be reached without UV stimulated photo-catalysis, on an industrially relevant time scale (i.e. decomposition complete in less than 24 hours)?

2) How do the different Fe, Mn, and Ni concentrations impact the oxalate decomposition rate?

3) Can pH be used confirm when oxlate decomposition is complete?

4) Are hydroxyl radicals driving the oxalate decomposition, especially under acidic conditions? That is, is the ECC process an AOP? If not, what are the reactions?

4.2.2 Answering the Simulant Questions

1) *Is UV light needed?*

With significant issues associated with using UV light, a simple test contrasting the required ozonation time to result in an oxalate concentration of less than 1.1×10^{-3} M is used to quantify the benefits of using UV light. The testing was performed: 1) with clean UV light; 2) without UV; and 3) with a so-called fouled UV, where a film was allowed to build up on the quartz sheath that is in contact with the *simulant decomposition test slurries.* Depending on the results of the testing, the goal was to remove the UV light from the design, greatly simplifying the ECC Process. From an industry perspective, the test will demonstrate if similar processes, such as the CORD UV process using ozone, require UV light to decompose the oxalate on an industrially relevant time scale (i.e. oxalate decomposed 1.1×10^{-3} M to less than 24 hours). This effort is detailed in Section 4.5.

2) *What effect do the concentrations of Fe, Mn, and Ni have on the oxalate decomposition rate?*

Based on variations of Fe, Mn, and Ni concentrations of the *simulant decomposition test slurries*, the decomposition rates are compared and the significance of each transition metal evaluated. From an industry perspective, an understanding of the significance that each transition metal play during at the beginning and near the end of the decomposition process.

3) Can pH be used to confirm when oxalate decomposition is complete?

While the *Simulant Decomposition Test Apparatus* used in these studies uses an inline Total Organic Carbon (TOC) analyser, equipped with a 680°C combustion catalytic oxidation system to measure remaining oxalate concentration, this is a more complicated technique than using a simple pH probe. Thus, the use of pH probe is evaluated as a potential field instrument

which can be used to confirm when the oxalate concentration has reached its defined endpoint of 1.1×10^{-3} M. The implications to industry would be a potentially significantly more robust, reliable, and inexpensive field instrument that can be used for determining when the oxalate decomposition is complete.

4) Are hydroxyl radicals driving the oxalate decomposition?

Since bicarbonate/carbonate produced during the oxalate decomposition are hydroxyl radical scavengers that have been credited as potentially stopping AOP reactions (Battino *et al.,* 1983; Glaze and Kang, 1989; Olson and Barbier, 1994; Chiang *et al.,* 2006), and nitrite scavengers, which scavenges hydroxyls with a rate constant, $k_{OH\cdot}$ of the order of $\sim10^8$ (Neta *et al.,* 1988; Farhataziz and Ross, 1977), are also present in the as-prepared slurries, the impact of these scavengers on the decomposition rate is evaluated. If the impacts from these scavengers are shown to be negligible then, based on their respective rate constants, it can be deduced that the oxalate decomposition may, in fact, not be hydroxyl radical driven.

From an industry perspective, the ECC process is an adaptation of the CORD UV process. Testing may confirm that the CORD UV process with ozone, commonly explained as a hydroxyl radical based AOP (Davis et al., 2009; Bradbury, 2000) may, in fact, be a non-radical based decomposition process.

4.3 Making of the Simulant Based Slurries

4.3.1 Sludge Simulants

As discussed in Chapter 2, the SRS HLW sludges digested to produce the simulant based *simulant decomposition test slurries* are of two general types. According to Eibling, 2010, the first type of sludge is an Fe-rich sludge containing varying concentrations of magnetite (Fe_3O_4), goethite (α-FeOOH), hematite (α-Fe_2O_3), and maghemite (γ-Fe_2O_3), with the exact

ratios mostly dependent on the HLW and radiochemical separations processing specifics. The second type of sludge is an Al/Mn-rich sludge containing varying concentrations of gibbsite ($Al(OH)_3$) and boehmite (AlOOH), also principally dependent on the HLW and radiochemical separations processing specifics.

The two non-radioactive, non-hazardous (except for containing some of the applicable U.S. Resource Conservation and Recovery Act (RCRA) metals and radionuclides) simulants were developed by the SRNL based on being chemically similar to representative to real SRS F-Area HLW sludge (i.e. F-Area sludge is the Fe-rich sludge) and real SRS H-Area HLW sludge (i.e. the H-Area sludge is the Al/Mn-rich sludge) (Eibling, 2010). As part of developing the simulants, each digestion behaviour was evaluated, with heat treatment applied and content also adjusted to ensure digestion behaviour was similar to that of real HLW sludge. The details of the significant effort to develop the sludge simulants are contained in Eibling, 2010. Table 6 summarises the wet characterisation the two final HLW sludge simulants used to make the *simulant decomposition test slurries (*Eibling, 2010).

Table 6. Simplified wet characterisation of the two sludge simulants used to make the *decomposition test slurries.*

Constituent	"Wet" Fe-rich simulant (mg/kg)	"Wet" Al/Mn-rich simulant (mg/kg)
Silver (Ag)	$4.6\times10^{+1}$	$1.5\times10^{+2}$
Aluminium (Al)	$9.0\times10^{+3}$	$6.3\times10^{+4}$
Barium (Ba)	$3.0\times10^{+2}$	$4.4\times10^{+2}$
Calcium (Ca)	$3.0\times10^{+3}$	$1.1\times10^{+3}$
Cadmium (Cd)	LTD[1]	LTD[1]
Cerium (Ce)	$3.0\times10^{+2}$	$1.2\times10^{+2}$
Cobalt (Co)	NA[2]	NA[2]
Chromium (Cr)	$3.1\times10^{+2}$	$1.2\times10^{+2}$
Copper (Cu)	$1.5\times10^{+2}$	$8.9\times10^{+1}$
Chloride (Cl)	$1.5\times10^{+3}$	0.0
Fluoride (F)	LTD[1]	LTD[1]
Iron (Fe)	$3.2\times10^{+4}$	$5.4\times10^{+3}$
Gadolinium (Gd)	NA[2]	NA[2]
Mercury (Hg)	$1.6\times10^{+3}$	$2.8\times10^{+3}$
Potassium (K)	$1.7\times10^{+2}$	$2.5\times10^{+2}$
Lanthanum (La)	$1.8\times10^{+2}$	$5.8\times10^{+1}$
Lithium (Li)	$1.6\times10^{+2}$	$1.3\times10^{+2}$
Magnesium	$1.4\times10^{+2}$	$1.0\times10^{+3}$
Manganese (Mn)	$4.1\times10^{+3}$	$5.6\times10^{+3}$
Molybdenum	NA[2]	NA[2]
Sodium (Na)	$1.2\times10^{+4}$	$7.4\times10^{+3}$
Sulfur (S)	$4.2\times10^{+2}$	$6.9\times10^{+1}$
Strontium (Sr)	$1.1\times10^{+2}$	$3.0\times10^{+1}$
Nickel (Ni)	$3.6\times10^{+3}$	$5.5\times10^{+2}$
Phosphorus (P)	$5.6\times10^{+1}$	$2.2\times10^{+1}$
Nitrite (NO_2^-)	$9.1\times10^{+3}$	$6.1\times10^{+2}$
Nitrate (NO_3^-)	$2.6\times10^{+3}$	$3.2\times10^{+3}$
Hydroxide (OH^-)	$1.3\times10^{+3}$	$9.6\times10^{+1}$
Lead (Pb)	$1.3\times10^{+2}$	$1.5\times10^{+2}$
Silicon (Si)	$1.3\times10^{+3}$	$2.6\times10^{+2}$
Titanium (Ti)	NA[2]	NA[2]
Uranium	NA[2]	NA[2]
Zinc (Zn)	$3.7\times10^{+2}$	$6.9\times10^{+1}$
Zirconium (Zr)	$5.5\times10^{+2}$	$2.2\times10^{+2}$
pH	12.34	12.54
wt% solids	13.55%	17.20%
density (kg/litre)	1.12	1.15

Notes: [1] LTD refers to less than detectable.
[2] NA refers to a component not added.

4.3.2 Digesting to Make Simulant Based Slurries

The *simulant decomposition test slurries* were prepared from the two sludge simulants characterized in Table 6.

First, each sludge was thrice sequentially digested using either 1 or 2.5 wt% oxalic acid solution, with the wt% oxalic acid solution(s) determined based on which of the simulant tests were being performed. The analyses are considered to support the following determinations:

Section 4.5. Is UV Light Required?

Section 4.6. Differing Role of Metal Catalysts During Ozonation.

Section 4.7. Using pH to Confirm Completion of Oxalate Decomposition.

Section 4.8. Is Decomposition Hydroxyl Radical Driven?

Specifics of the digestion process used to make the slurries, are as follows.

Sludge Digestion Procedure: Approximately 61 litres of oxalic acid solution were added to a standard 114-litre capacity 304 stainless steel drum that had previously been loaded with sludge simulant.

Based on the expected digestion capacity of the oxalic acid solution of 3 gram/litre cation digestion, conservatively assuming iron, aluminium and nickel contribution only, and the cation content of each simulant, the equivalent of approximately 2.0 kg dry weight of Fe-rich simulant and 3.3 kg dry weight of H-Area simulant were the minimum required amounts of simulant to ensure sufficient loading was available for digestion. The moisture was determined using a moisture analyser (Mettler Toledo, Hal Moisture Analyser HE53). The equivalent dry simulant sludge loadings used for the sequential digestions are shown in Table 7.

Table 7. Dry sludge simulant loadings used to support three sequential digestions.

Simulant decomposition test slurries[1]	Initial wet simulant (kg)	Measured average wt% moisture	Eq. dry simulant (kg)
1-Fe-x.no	5.20	61.06	2.03
1-Fe-x. clean	5.05	59.91	2.03
1-Fe-x. fouled	4.80	57.67	2.03
1-Al/Mn-no	10.40	66.51	3.47
1-Al/Mn-clean	11.09	68.79	3.46
1-Al/Mn-fouled	10.95	68.31	3.47
2.5-Fe-x-no	12.68	60.01	5.07
2.5-Fe-x-clean	12.09	57.89	5.09
2.5-Fe-x-fouled	12.36	58.32	5.15
2.5-Al/Mn-x.no	20.86	58.41	8.68
2.5-Al/Mn-clean	20.29	57.61	8.60
2.5-Al/Mn-fouled	20.60	58.01	8.65

Note: [1]the nomenclature used to identify the simulants is provided in Table 8.

Maintaining the drum temperature at 70±5ºC, the acid digests the sludge for approximately 24 hours, with mild agitation applied for roughly the first three and last three hours (i.e. using an approximate 19 litres/minute Titan electric drum pump for recirculation). Better agitation was not supplied, in attempt to roughly emulate the limitations associated with slurrying the HLW tank (i.e. the goal of this mixing was not to ensure a well-mixed tank that would maximise digestion, but instead mimic the limited mixing in a HLW tank). The pH was monitored throughout digestion, with the digestion assumed to have gone to completion once the pH value stabilised in the pH range 1.5 to 2.5. Using the electric transfer pump, approximately 61 litres of the *simulant decomposition test slurry* were transferred out of the drum, of which ~1 litre was placed in a sample vial for metals characterisation by Atomic Absorption Spectroscopy (AA). The bulk of the slurry was transferred to the *Simulant Decomposition Test Apparatus* to initiate oxalate decomposition testing (*vide infra*).

After transferring the *simulant decomposition test slurry* out of the "digestion" drum, the drum was replenished with approximately 61 litres of fresh oxalic acid of the same original concentration (i.e. 1 or 2.5 wt% depending on the specific testing). The above procedure was then performed again, digesting the sludge simulant sequentially two additional times, resulting in 3 slurries, ~61 litres each, of *simulant decomposition test slurry*. All of the steps were then repeated for the other sludge simulant, thus creating a total of six *simulant decomposition test slurries* for the specific acid strength. Depending on the test(s) to be performed (i.e. with the four tests and analyses detailed in Chapter 4.5, Chapter 4.6, Chapter 4.7, or Chapter 4.8), the procedure was repeated using the appropriate UV light testing protocols, as well as the appropriate oxalic acid concentration.

Derived from the acid concentration and HLW sludge simulant digestion matrix used for making the *simulant decomposition test slurries*, the nomenclature applied for naming (i.e. identifying) the slurries are shown by Table 8.

Table 8. Acid/sludge simulant digestion matrix and resultant *simulant decomposition test slurry* nomenclature.

Acid concentration used for sludge digestion	**Type of sludge digested**	
	Fe-rich simulant	**Al/Mn-rich simulant**
	NAME OF *SIMULANT DECOMPOSITION TEST SLURRY*	
1 wt% oxalic acid	1 wt% oxalic acid applied to Fe-rich simulant, named 1-Fe-x.y	1 wt% oxalic acid applied to Al/Mn-rich simulant, named 1-Al/Mn-x.y
2.5 wt% oxalic acid	2.5 wt% oxalic acid applied to Fe-rich simulant, named 2.5-Fe-x.y	2.5 wt% oxalic acid applied to Al/Mn-rich simulant, named 2.5-Al/Mn-x.y

Where:

- "x" refers to the digestion sequence of the sludge simulant by the addition of oxalic acid, either "1," 2, or "3." (i.e. the number of times the subject sludge simulant was treated with acid to create the specific *simulant decomposition test slurry*).

- "y" refers to one of the three UV light protocols used during testing. That is, "no" refers to no UV light (i.e. without UV) added during ozonation. "Clean" refers to the UV lamp energised with the *UV lamp sheath* maintained clean (i.e. cleaned with 5 wt% oxalic acids after the oxalate decomposition of each *simulant decomposition test slurry*) as the result of ozonation. "Fouled" refers to the UV lamp being energised, with the UV lamp sheath only cleaned before the beginning the decomposition of the 1st sequentially created *simulant decomposition test slurry*.

In addition to "no," "clean," and "fouled" UV light protocols, the "clean" and "fouled" are largely limited to the tests performed as part of Section 4.5 - Is UV Light Required? With the other three simulant tests (Section 4.6 through 4.8) done only under the "no" UV light protocol.

Since solids are formed throughout the decomposition of the oxalate, application in actual HLW use would prohibit the use of a filter because of operational/personnel exposure concerns. Therefore, no filter was used in *simulant decomposition test apparatus.*

4.4 Test Apparatus for Simulant Based Testing

Figure 9 shows a simplified schematic of the *Simulant Decomposition Test Apparatus*, with an operational overview supplied immediately following the figure. A detailed equipment list,

including vendor model numbers, and additional design details are also provided as part of Appendix 3.

As previously discussed in Chapter 2, an early decision was made to use ozone instead of hydrogen peroxide for tank cleaning because of the potential safety concerns with using peroxide. Therefore, the simulant testing was based on adding ozone.

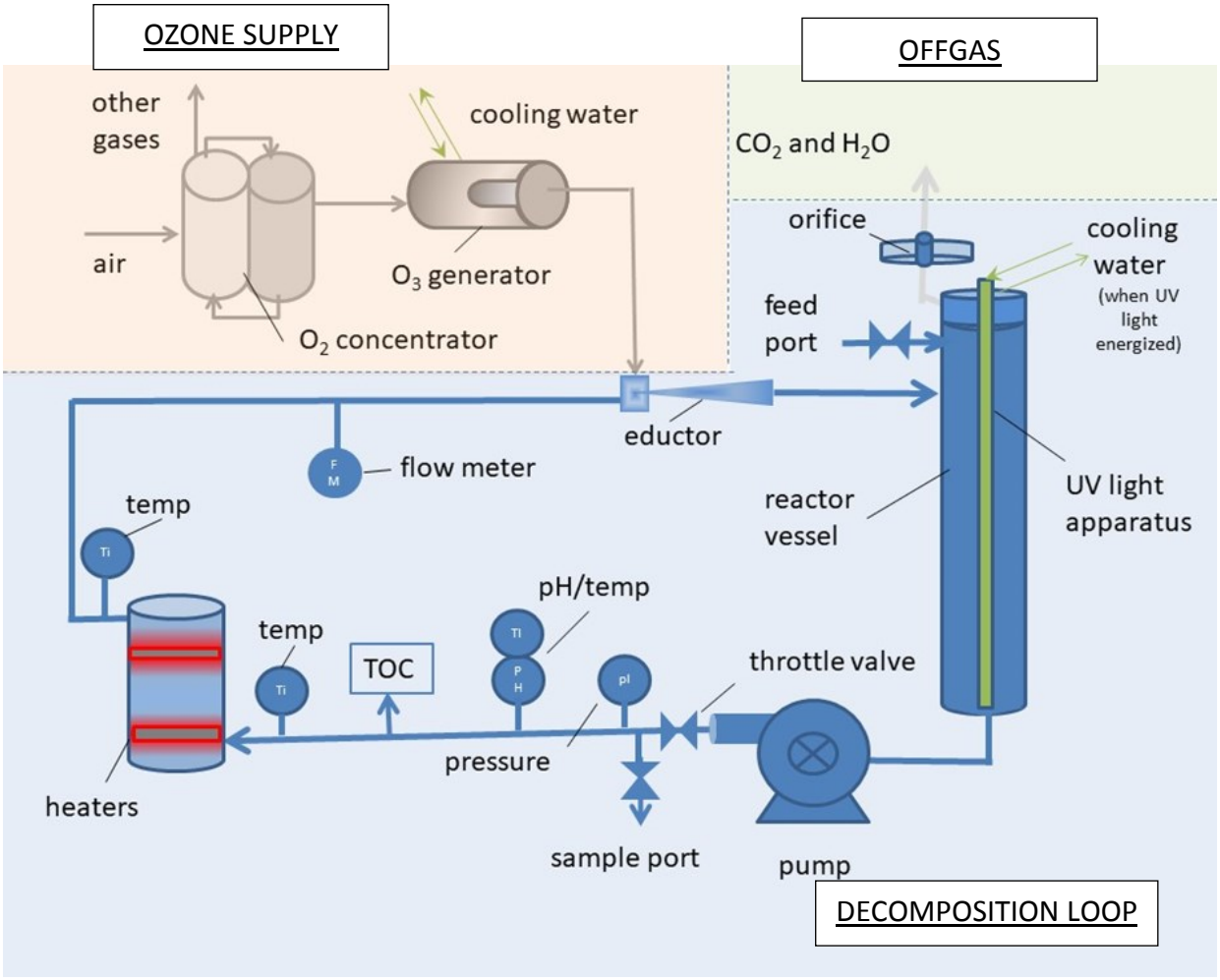

Note: Equipment details, including model numbers, are found in Appendix 3.

Figure 9. *Simulant Decomposition Test Apparatus*.

Based on purpose, the apparatus can be considered to consist of three sections as shown in Figure 9. Each is discussed, as follows:

Ozone Supply

- Air is supplied to the *Oxygen Concentrator*. The *Oxygen Concentrator* removes other gases and concentrates the oxygen to 93 wt% oxygen (7 wt% air), providing the concentrated oxygen at 9.4 litres/minute to the *Ozone Generator.*

- *Ozone Generator* converts the concentrated oxygen mix to 15% ozone, supplying ozone at 1.7×10^{-2} kg/sec. The ozone is injected into the *Decomposition Loop* via the *Eductor.*

Decomposition Loop

- The *simulant decomposition test slurry* is transferred to the *Test Apparatus* via the *Feed Port*.

- After the approximate 60 litres of the *simulant decomposition test slurry* (with its making discussed in Section 4.3.2) is added to the D*ecomposition Loop*, the *Recirculation Pump* is energised, and the *Throttle Valve* adjusted to maintain a recirculation flow rate of 6.7 litres/second, with a 1.7×10^{5} Pa backpressure maintained by the *Orifice, Pump* and *Throttle Valve*

- The *Eductor* injects the ozone into the *simulant decomposition test* slurry. Based on the 1.7×10^{5} Pa backpressure maintained by the *Orifice, Pump* and *Throttle Valve*, the ozone solubility is calculated as 6.3×10^{-4} M based on Henry's Law.

- The *Pressure Gage, pH meter*, and *thermocouples* are used to measure the pressure, pH and temperature periodically during the oxalate decomposition. The locations of each are shown in Figure 9.

- The *TOC Analyser* provides an inline measurement of the oxalate concentration.

- *The Heater Vessel* with two *Band Heaters* maintains the *decomposition slurry* temperatures at 70±5ºC throughout the oxalate decomposition.

- The *Flow Meter* provides confirmation that the flowrate in the *Decomposition Loop* is maintained at approximately 6.7 litres/second.

- The *Reactor Vessel* provides residence time, as well as contains the *UV Lamp Apparatus.* Depending on the appropriate UV protocol applied during the testing, the *UV Lamp* may be energised and operated as clean, or fouled, or not energised.

    - The *US Lamp apparatus* consists of a *UV Lamp Sheath* to protect the actual *UV Lamp* and allow for cleaning and cooling the *UV lamp*. The *UV Lamp* is a synthetic quartz medium pressure 1.5 kW UV lamp.

- As the *simulant decomposition test slurry* is recirculated through the *Decomposition Loop*, and the ozone is injected into the slurry, the ozone initiates the decomposition of oxalate into CO_2, water vapour, and potential *other gasses*. (The indirect ozone mechanism(s) driving the oxalate decomposition are investigated as part of Section 4.8.).

- The CO_2, water vapour, and potential *other gasses* exit the ECC process through an *Orifice* connected to the *Reactor Vessel.*

OFFGAS

The CO_2, water vapour, and potential *other gasses* are off-gassed (i.e. released into the environment).

OTHER

Cooling water is fed to the decomposition test apparatus not shown in Figure 9. Well water (WW) at approximately 15ºC was filtered (using 10-micron mesh) and supplied as cooling water to the *UV Lamp Apparatus* (when energised) at a measured flow rate of 1 litre/minute, while it was also provided to the Ozone Generator at a confirmed flow rate of 1.5 litres/minute. Upon removing the excess heat associated with the UV lamp and the ozone generator, the cooling water was collected, periodically monitored, and released to the SRS sanitary-drains.

The *simulant decomposition test slurry* flow rate has already been defined at approx. 40 litres/minute based on maintaining the solubility of ozone in solution.

The slurry is ozonated until the TOC analyser determines that the oxalate concentration is less than the defined endpoint of 1.1×10^{-3} M oxalate. The decomposition data for each of the *simulant decomposition test slurry*, as recorded during the testing is provided in Table 41 through Table 43 of Appendix 5.

4.4.1 General Procedures and Operation

Each *simulant decomposition test slurry* was fed into the *Decomposition Test Apparatus.* Throughout ozonation, the oxalate concentration was measured using the inline *TOC analyser*, while samples were periodically withdrawn using the S*ample Port* of the *Decomposition Test Apparatus* and analysed by AA analysis.

The TOC concentrations corresponding to the point-in-time when the AA samples were taken, were also recorded for analysis. Also, because of metal complexation, standard titration of the oxalate by permanganate with sulfuric acid (Jeffery *et al.*, 1989) was used to confirm the initial and final oxalate concentrations of each *simulant decomposition test slurry*. Throughout the

ozonation/decomposition, the pH of the *simulant decomposition test slurries was* also measured but not adjusted, while the temperature was maintained at 70 ± 5°C.

TOC Analyser. Throughout ozonation, the concentration of oxalate remaining in the *simulant decomposition test slurries* was determined by catalyst combustion oxidation with nondispersive infrared detection using an inline *Total Organic Carbon (TOC) Analyser* equipped with a 680°C combustion catalytic oxidation system. The TOC model was chosen since it is recommended for use on slurries containing significant amounts of mineral salts (Shimazdu, 2013). Additional details on the *TOC Analyser* are provided in Appendix 3.

AA Spectrometry**.** The concentrations of soluble Fe, Mn, and Ni were periodically measured in grab samples, which were periodically withdrawn from the *Decomposition Test Apparatus,* using the *Sample Port*. The soluble concentrations of the metals were recorded as a function of ozonation time. Additional details on the *AA Spectrometer* are also provided in Appendix 3.

4.5 Is UV Light Required?

4.5.1 UV Light Design

There are two UV lamp-types which are most commonly used in UV systems. The two types are a medium pressure (MP) and low pressure (LP) lamp. As discussed in Section 3.4.2 UV lamps should have a maximum radiation output at 254 nm to maximise conversion efficiency. However, MP lamps have a significantly higher electrical power input compared to LP lamps. MP-UV lamps with a UV-flux per unit arc length of up to 35 W/cm compared to LP lamps with an average of approximately 1 W/cm (Schalk *et al.,* 2005).

UV-dose also called fluence refers to UV intensity (fluence rate) and residence time, where residence time is given as the volume/flow rate. This relationship between UV dose and intensity shown by Equation 4-1.

$$UV\ dose = UV\ intensity \times residence\ time \quad \text{(eq. 4-1)}$$

When designing UV systems, a commonplace to start, such as for AOPs associated with water treatment is with the Beer-Lambert Law. The Beer-Lambert Law can be stated as shown in Equation 4-2:

$$A = \varepsilon\, bc \quad \text{(eq. 4-2)}$$

Where A is the absorbance of a substance at a specified wavelength λ, in units of nm for light in the ultraviolet and visible regions of the electromagnetic spectrum. b is the length of the light path through the sample, usually in cm. ε is the molar absorptivity (also called the extinction coefficient) of the absorbing species at λ, in $M^{-1}cm^{-1}$. c is the concentration in M. The absorbance is defined by 1-T, where T is the transmission as shown by Equation 4-3.

$$T = I/I_o \quad \text{(eq. 4-3)}$$

Where I/I_o refers to the ratio of the intensity of the transmitted light (I) to the intensity of the incident light (I_o).

In common dilute applications, such as drinking water AOPs, % UV transmittance is used when designing UV systems. UVT is a measure of the 100% of the light entering and exiting water, usually reported for a path length of 1 cm. As UV absorbance increases, UV transmittance decreases, with the relationship shown by Equation 4-4.

$$\% UVT = 100 \times 10^{-UVA} \quad \text{(eq. 4-4)}$$

Where UV absorption, UVA is equal to -log (T).

4.5.2 Problems with Using UV Light

The conceptual design of the ECC process, as discussed in Section 2.3 makes use of a UV light. The slurries created from oxalate-assisted digestion of HLW sludges would have the potential to be highly radioactive. Therefore, use of an immersed UV lamp (i.e. a quartz encased UV lamp) is considered problematic in providing the required regulatory pedigree of primary containment.

Complicating this issue is the fact UV lamps have a limited lifetime. For example, most MP UV lamps have a guaranteed life range from only 4,000 to about 8,000 hours (Schalk *et al.,* 2005), meaning that the guaranteed life is slightly less than 1-year continuous operation. Assuming a 6-month duration to clean a tank with the proposed process, suggests that the UV lamps could likely require replacement even before the completion of cleaning a second tank.

Since parts of the UV light assembly, such as the UV light sheath, will be in contact with HLW, maintenance would represent a significant effort and likely include radiological contamination/personnel exposure risk. As a related issue, with increasing ferric iron concentration the UVT decreases, as shown in Figure 10 (Mackey *et al.,* 2004).

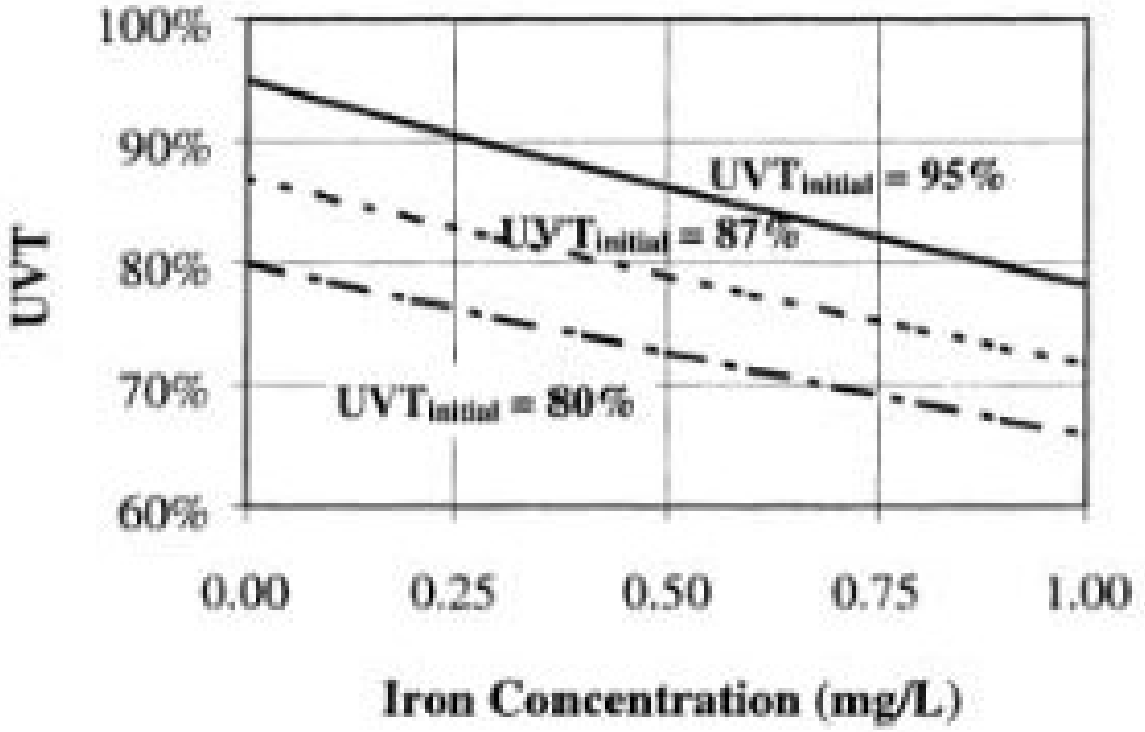

Figure 10. Impact of ferric iron concentration on UVT (Used with permission; Mackey *et al.,* 2004).

With the initial iron concentrations being on the order of 10^{-3} M for 1 wt% oxalic acid based decomposition slurries and 10^{-2} M for 2.5 wt% oxalic acid based solutions, it can be inferred from Figure 10 that the UVT would be near zero for the initial operation of the ECC process.

Since UVT approaches zero, because of the ferric ion concentration in the ECC process, the UV light was sized merely by installing a 1.5-kW MP-UV lamp sized to allow a 20:1 scale-up for field installation. That is, a similar 30 kW UV lamp is available from the same UV lamp manufacturer and represents the maximum available SRS HLW tank-top power which could be used for the UV lamp.

Although fouling is customarily considered to take an extended period, the rate of fouling in a UV reactor is highly variable between water sources with the time required for significant fouling to occur in a UV reactor is reported to range from a few hours to several months (Black

and Veatch, 2010). Figure 11 compares a fouled UV lamp sheath from preliminary testing after operating the decomposition process for only about 10 hours to a clean UV lamp sheath.

Figure 11. Fouled UV lamp sheath after operating the decomposition process for 10 hours vs a clean UV lamp sheath.

A major factor also considered was the changing opacity of the *simulant decomposition test slurries* from ozonation. As the metal oxalate in solution is decomposed and metal oxide particles form, the solution turns a dark brown colour. Figure 12 and Figure 13 show samples collected throughout an UV assisted ozonation of both an Fe-rich and an Al/Mn-rich *simulant decomposition test slurry*. The Fe-rich *simulant decomposition test slurry* started becoming

dark after about 3 hours, while the Al/Mn-rich *simulant decomposition test slurry* exhibited the same behaviour in less than 1 hour.

With the solution becoming less opaque with ozonation, the penetrability of the UV light into the solution would decrease, which would likely reduce the effectiveness of the UV light in creating hydroxyl radicals, meaning the lights would be less effective. However, based on Figure 10, the UVT is already zero.

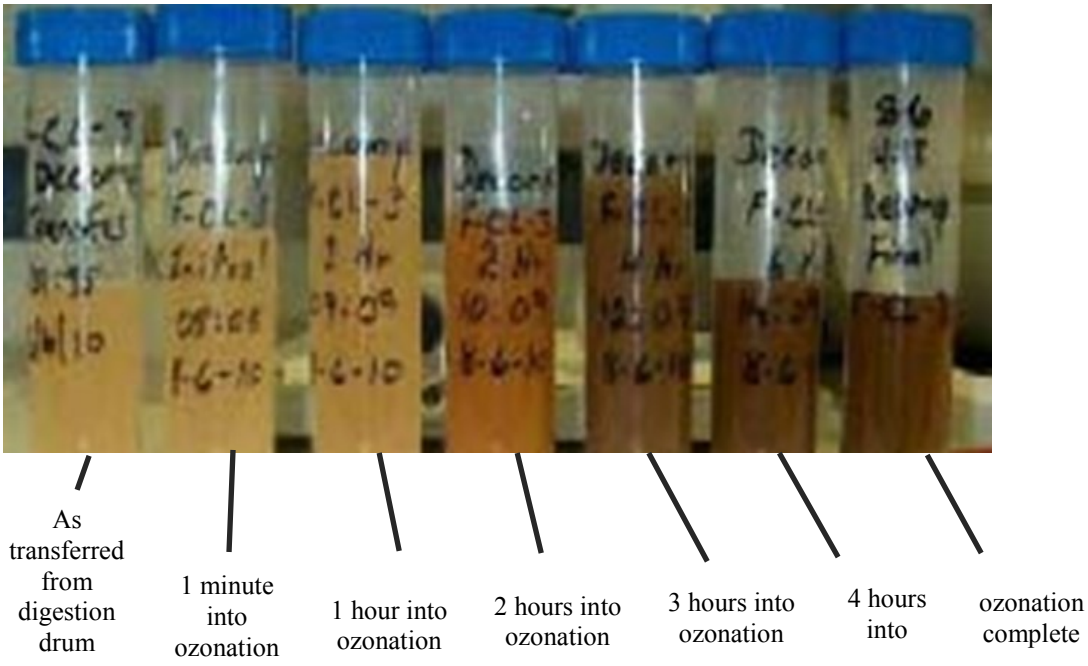

Figure 12. Opacity of the 1-Fe-1.clean *simulant decomposition test slurry* throughout ozonation/oxalate decomposition.

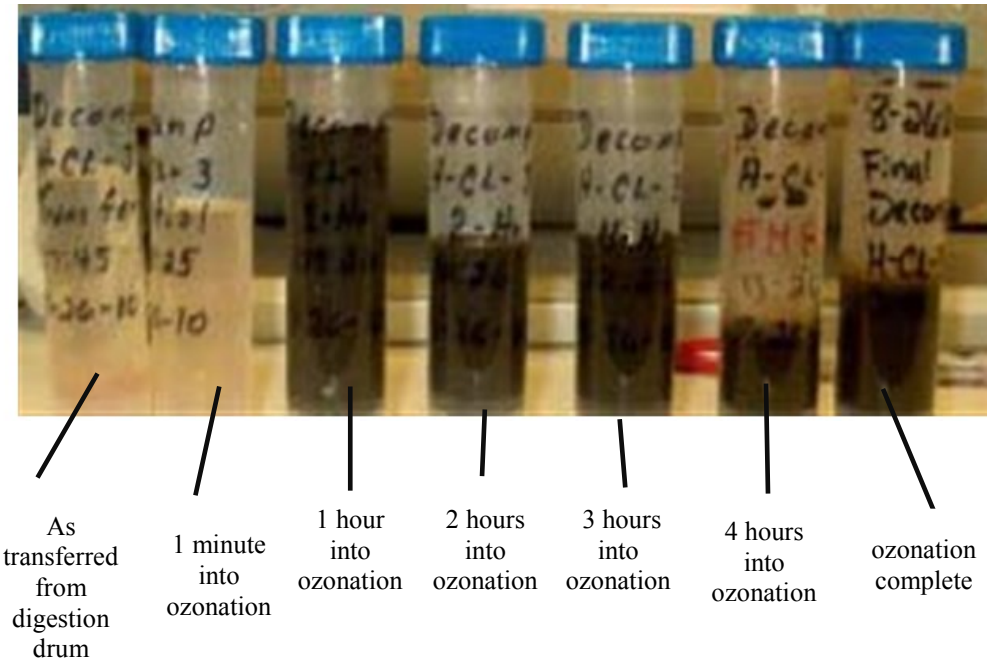

Figure 13. Opacity of the 1-Al/Mn-1.clean *simulant decomposition test slurry* throughout ozonation/oxalate decomposition.

Thus, with all the problems associated with the use of UV, an alternative to the conceptual design ECC process for post-decontamination oxalate decomposition was sought. The purpose of this analyses was to determine if UV light was needed to photo-catalytically aid the decomposition process, such that with ozonation an oxalate concentration of less than 1.1×10^{-3} M could be achieved in an industrial relevant time frame (i.e. < 24 hours).

4.5.3 Spent Acid Slurries for UV Testing

Only *simulant decomposition test slurries* made with 1 wt% oxalic acid were used for determining the benefit of the UV light testing. Since the UV light failed during before the start of 2.5 wt% oxalic acid testing, use of UV light during the testing was limited to slurries created from 1 wt% oxalic acid.

In addition, the justification for continuing without the UV light using 2.5 wt% acid was based on the assumption that the oxalate decomposition rate was related to the transition metal concentrations contained in the *simulant decomposition test slurries,* with the UV catalytic benefit the result of its interaction with ozone (per Reaction 3-16). Since the 1 wt% *simulant decomposition test slurries* would contain a lower concentration of iron compared to 2.5 wt%, the transmissivity of the 1 wt% slurry would be highest. Therefore, the benefit of the UV light to the 1 wt% *simulant decomposition test slurry* was deemed to likely have the greatest effect (i.e. result in the greatest oxalate decomposition rate). As such, the testing to confirm that UV light was not required, was limited to using only the 1 wt% *simulant decomposition test slurries*.

4.5.3.1 Simulant Slurries for No UV Light Decomposition Testing

Figure 14 shows the oxalate and soluble Fe, Mn, and Ni concentrations as a function of time for the 1-Fe-x and the 1-Al/Mn-x slurries throughout decomposition, run without UV light.

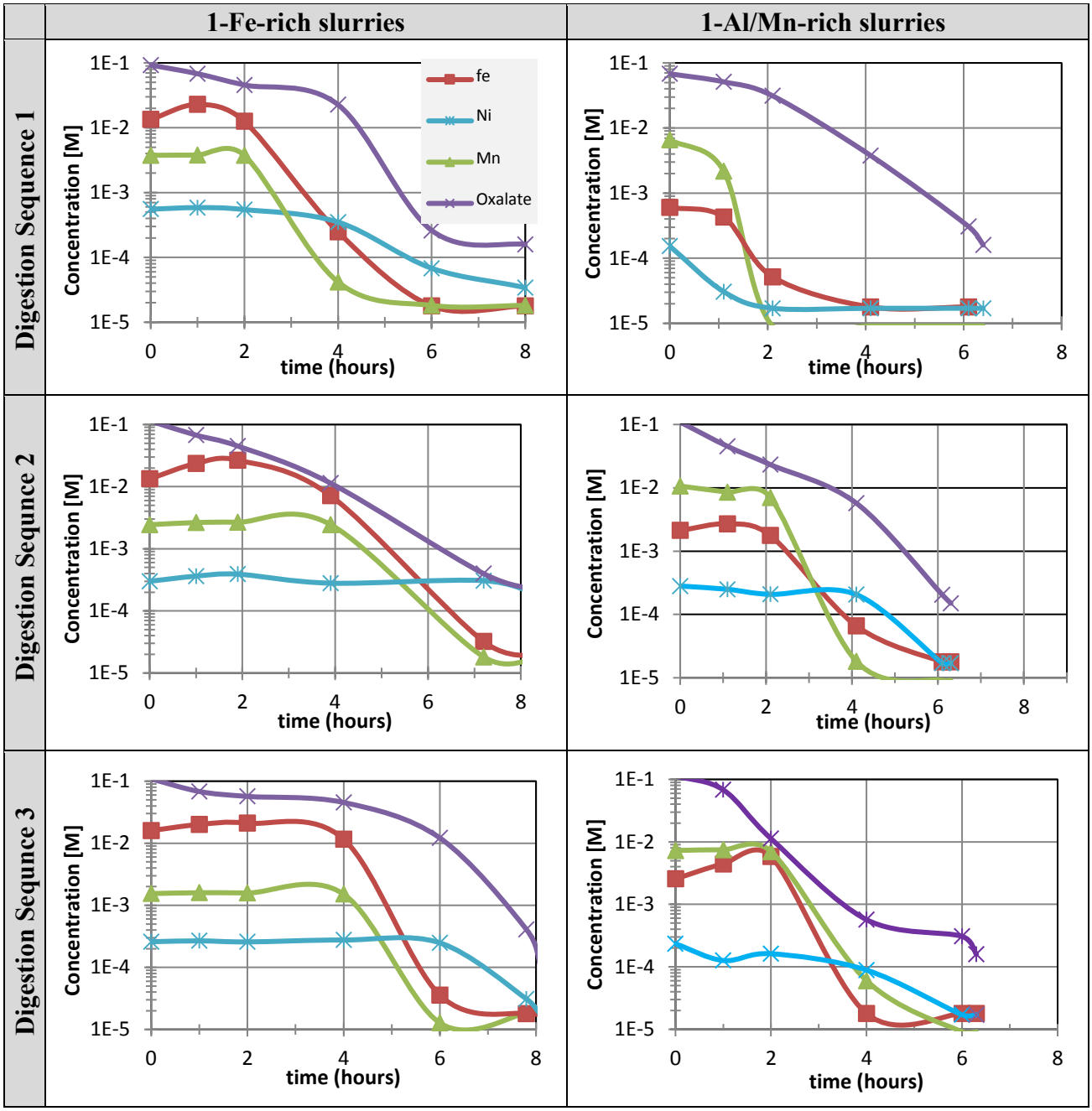

Figure 14. Oxalate and soluble Fe, Mn, and Ni concentrations for the 1-Fe-x and the 1-Al/Mn-x slurries throughout decomposition, run without UV light.

4.5.3.2 Simulant Slurries for Clean UV Light Decomposition Testing

Figure 15 shows the decomposition of the 1 wt% slurries using a maintained clean UV lamp.

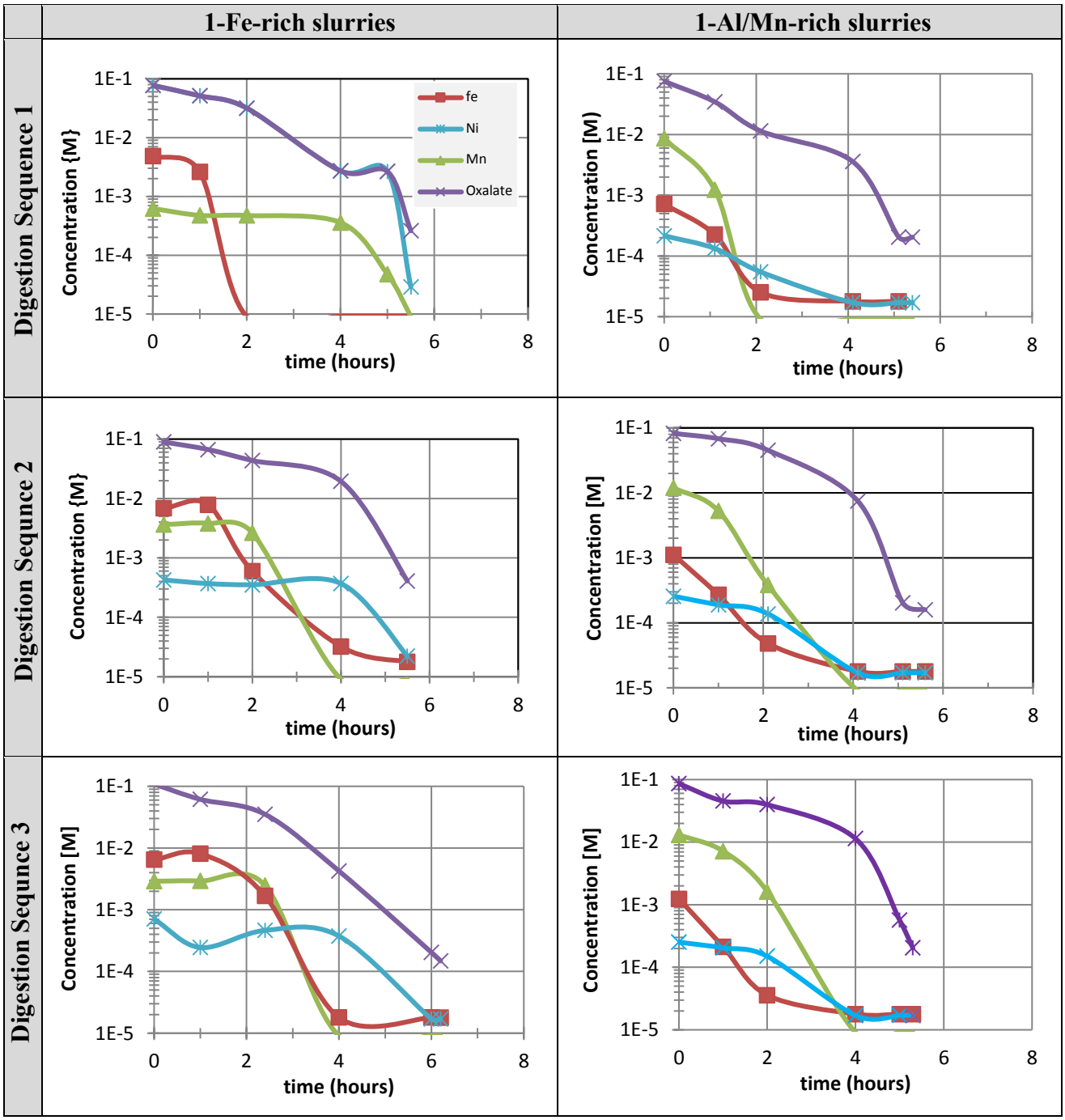

Figure 15. Oxalate and soluble Fe, Mn, and Ni concentrations for the 1-Fe-x and the 1-Al/Mn-x slurries throughout decomposition, run with a "maintained" clean UV lamp.

4.5.3.3 Simulant Slurries for Fouled UV Light Decomposition Testing

Figure 16 shows the same with a non-maintained UV light.

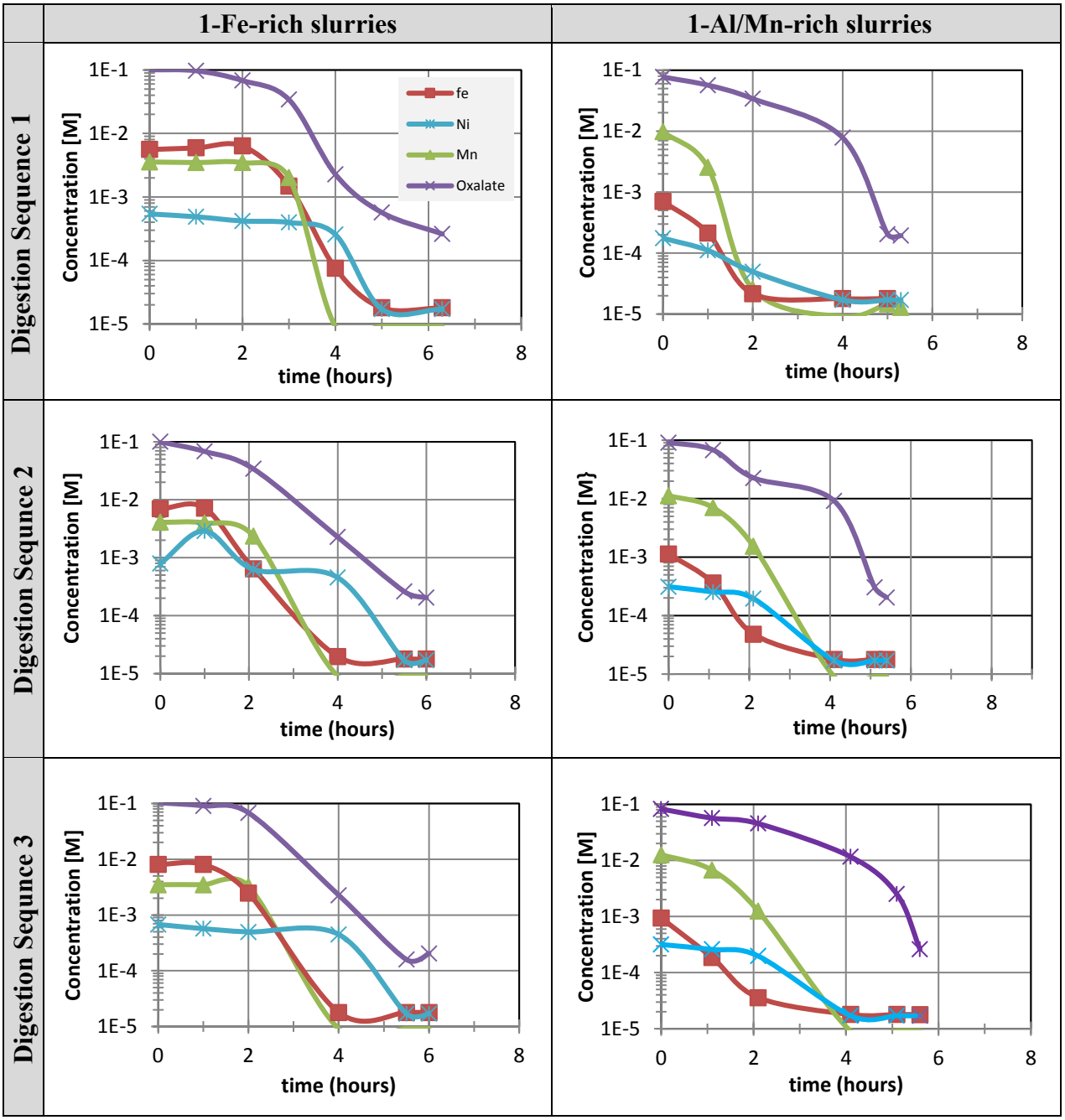

Note: The term "fouled" is used for slurry UV light protocol identification, with the 1-Fe-1.fouled and the 1-Al/Mn-1.fouled actually "clean" as defined at the start of slurry decomposition.

Figure 16. Oxalate and soluble Fe, Mn, and Ni concentrations for the 1-Fe-x and 1-Al/Mn-x slurries throughout decomposition, run with a "fouled" UV light during decomposition.

4.5.4 Results and Discussion of UV Light Significance

Table 9 summarises the ozonation/decomposition times required to reach an oxalate concentration of 1.1×10^{-3} M for the *simulant decomposition test slurry* created using 1 wt% oxalic acid under different UV light protocols.

Table 9. Comparison of required ozonation times for the 1 wt% *simulant decomposition test slurries* with different UV light protocols to reach an oxalate concentration of 1.1×10^{-3} M.

Simulant decomposition test slurry	**With no UV (hours)**	**With maintained/clean UV (hours)**	**With fouled UV (hours)**
1-Fe-1.y	5.9	5.3	4.7*
1-Fe-2.y	7.0	5.4	5.4
1-Fe-3.y	7.7	5.6	5.2
1-Al/Mn-1.y	5.6	4.8	4.7*
1-Al/Mn-2.y	5.8	5.0	5.0
1-Al/Mn-3.y	5.7	5.0	5.4

Note: *The term "fouled" is used for slurry identification purposes only, with the 1-Fe-1.fouled and the 1-Al/Mn-1.fouled being clean at the start of testing.

As can be seen in Table 9, UV slightly increases the decomposition rate. However, all the slurries reached an oxalate concentration of less than 1.1×10^{-3} M in an industrial relevant time frame (e.g., << 24 hours). Therefore, the UV light was deemed not to be required and removed from additional testing as part of *decomposition testing of spent acid slurries*.

As discussed in Section 3.2, the TRIZ homogeneous hydroxyl radical based AOP, and where according to Reaction 3-17, the UV catalytically interacts directly with the ozone. However, with the transmissivity of the solution so low, the UV would be hindered from penetrating into the solution. The enhancement to the rate of oxalate destruction in the presence of UV over and above the non-UV based ozonation baseline was observed, but not regarded as being of sufficient economic benefit to justify investment in the necessary equipment and equipment

modifications required to support a UV driven process. Thus, the UV light was again deemed not to be required and removed from additional testing as part of the decomposition testing of spent acid slurries.

4.5.5 Conclusion of UV Significance

Based on Figure 10, the % UVT associated with using a UV-lamp in the process is estimated as zero. Based on *simulant decomposition test slurries* created from 1 wt% oxalic acid, it was demonstrated that UV light was not needed as a catalyst to aid in the decomposition of oxalate, such that an oxalate concentration of less than 1.1×10^{-3} M would be achieved in an industrial relevant time frame (i.e. < 24 hours). As shown in Column 2 of Table 9, the maximum required ozonation time without UV for all the 1 wt% slurries was 7.7 hours, significantly less than 24 hours.

The original overall goal was to be able to clean an HLW tank within six months in each area, with a maximum number of tanks to be cleaned per area being two per year (for a total of four). This desired throughput was based on operations resource loading constraints, available operating volume with each tank farm, the amount of time required to prepare/wash a vitrification feed batch. In addition to the issues with using the UV light, studies were performed which showed that decreasing the time required for oxalate decomposition to less than 24 hours per slurry, would not increase the annualized throughput.

4.6 Differing Role of Metal Catalysts During Ozonation

As previously discussed in Section 3, the presence of increased concentrations of soluble Fe-Mn-Ni in the slurries will increase the decomposition rate, with the onset of reaction completion being first observed after only about 6 hours of ozonation. With Fe, Mn and Ni being first-row transition metals that exhibit broadly similar chemistries, (Beltrán *et al.*, 2005;

Logager *et al.*, 1992; Gottschalk *et al.*, 2002; Olson and Barbier, 1994; Von Gunten, 2003; Tomiyasu *et al.*, 1985; Portjanskaja, 2007; Jacobsen *et al.*, 1998; Kasprzyk-Hordern *et al.*, 2003), they were the metals analysed as part of simulant based decomposition testing to understand their effect on the oxalate decomposition rate. In contrast, and based on their very limited initial concentrations, titanium, vanadium, chromium, cobalt, copper and zinc were considered to be minor contributors to any catalytic effect compared to Fe, Ni and Mn and so were not made subject to any further analysis.

Thus, in view of metal catalyst derived enhancement to oxalate decomposition during ozonation and the lack of industrially meaningful enhancement to the decomposition afforded by in-process UV, this section analyses the oxalate concentration, soluble Fe-Mn-Ni metals concentrations, and required ozonation time to reach an oxalate concentration of $\leq 1.1\times10^{-3}$ M for each of twelve *simulant decomposition test slurries* in order to better quantify and understand the individual effect of these metals. The initial metals and oxalate concentration of the twelve slurries used are summarised in Table 10.

Table 10. Summary of twelve (initial) *simulant decomposition test slurries* used for determining the catalytic significance of Fe, Mn, and Ni.

Twelve *simulant decomposition test slurries*	**pH**	**C_2O_4 (M)**	**Fe (M)**	**Mn (M)**	**Ni (M)**
1-Fe-1.no	1.74	9.27E-2	1.34E-2	3.76E-3	5.55E-4
1-Fe-2.no	1.83	1.15E-1	1.34E-2	2.44E-3	3.00E-4
1-Fe-3.no	1.90	1.09E-1	1.60E-2	1.55E-3	2.59E-4
1-Al/Mn-1.no	2.53	6.81E-2	6.07E-4	6.62E-3	1.53E-4
1-Al/Mn-2.no	1.68	1.09E-1	2.13E-3	1.07E-2	2.81E-4
1-Al/Mn-3.no	1.53	1.14E-1	2.57E-3	7.28E-3	2.33E-4
2.5-Fe-1.no	1.32	2.40E-1	1.14E-2	4.79E-3	7.26E-4
2.5-Fe-2.no	1.25	2.51E-1	1.49E-2	4.64E-3	8.13E-4
2.5-Fe-3.no	1.03	2.56E-1	1.92E-2	3.90E-3	7.12E-4
2.5-Al/Mn-1.no	1.32	2.58E-1	1.12E-2	4.10E-3	4.55E-4
2.5-Al/Mn-2.no	1.49	2.76E-1	1.10E-2	2.05E-3	2.68E-4
2.5-Al/Mn-3.no	1.30	2.86E-1	6.87E-3	1.22E-3	1.82E-4

Histograms showing the initial Fe, Mn, and Ni concentrations (i.e. starting levels) for each of the twelve test slurries are shown in Figure 17 and Figure 18, respectively.

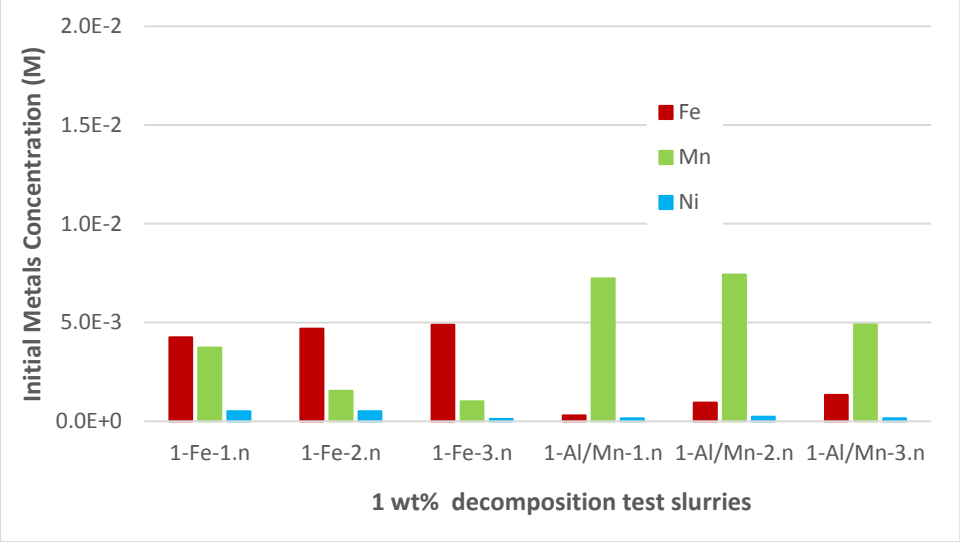

Figure 17. Initial Fe, Mn, and Ni concentrations for the 1-Fe-x.no and 1-Al/Mn-x.no slurries.

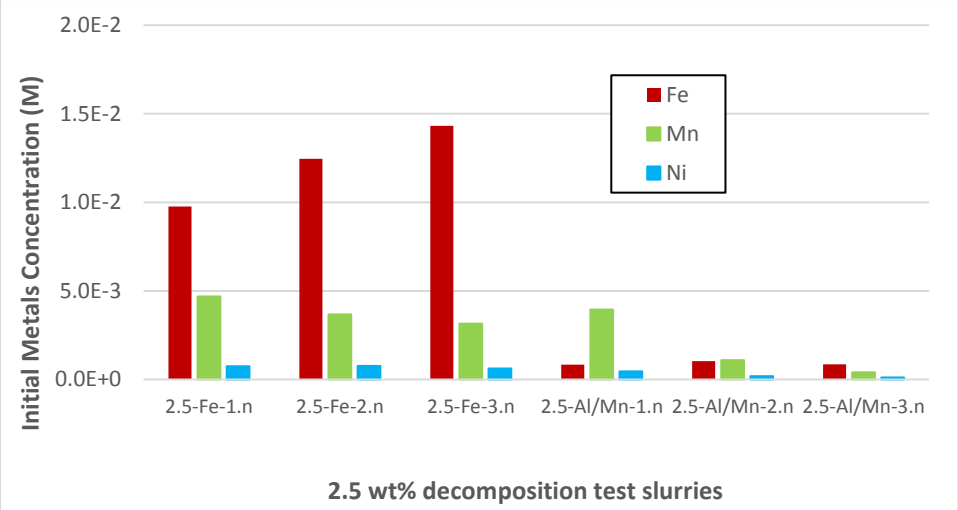

Figure 18. Initial Fe, Mn, and Ni concentration for 2.5-Fe-x.no and 2.5-Al/Mn-x.no slurries.

4.6.1 Results and Discussion

Figure 19 through Figure 22 show the concentrations of oxalate and the Fe, Mn, and Ni remaining in the twelve no-UV slurries as a function of ozonation time.

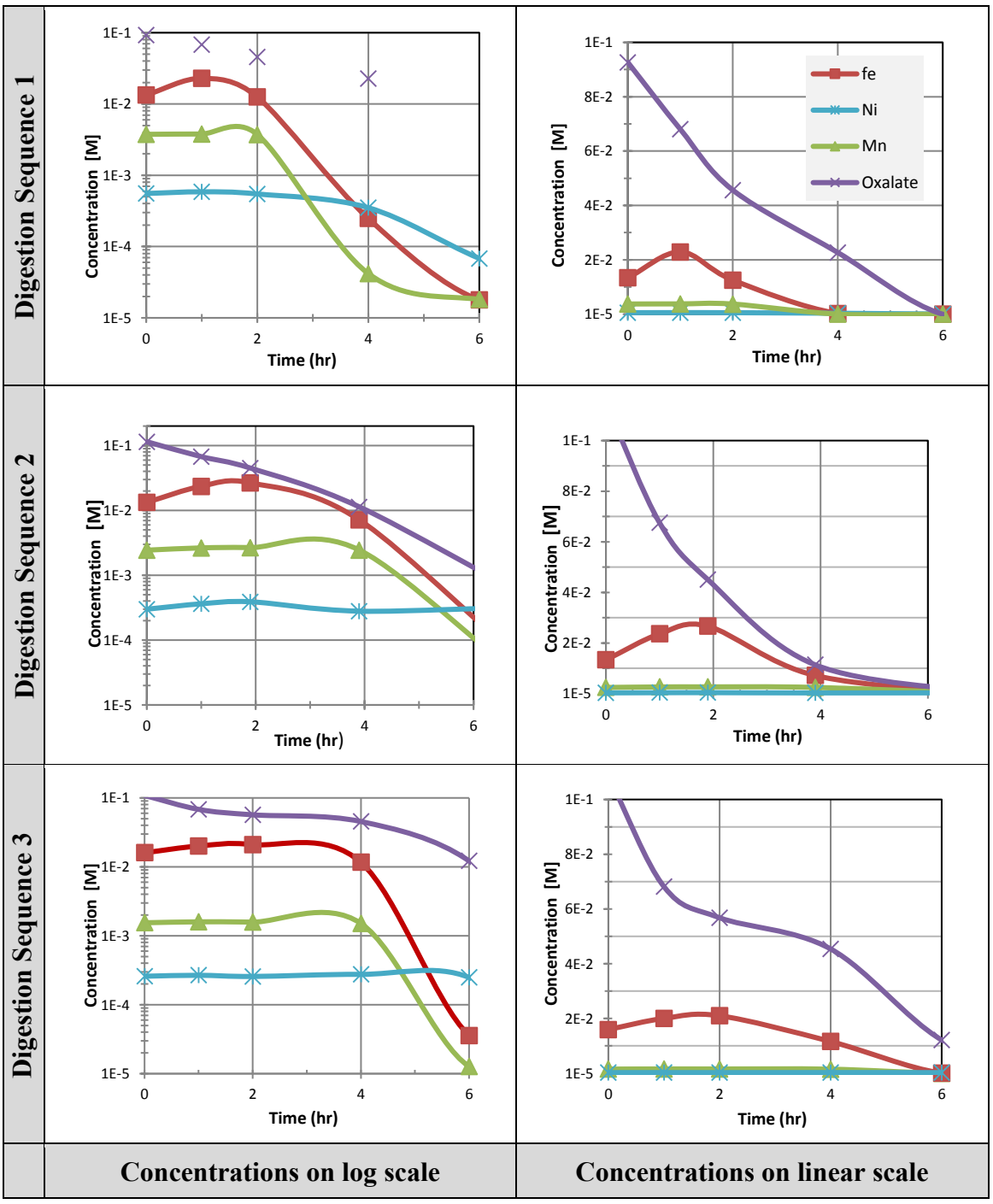

Figure 19. Oxalate and metal concentration vs ozonation time for the 1-Fe-x.no slurries.

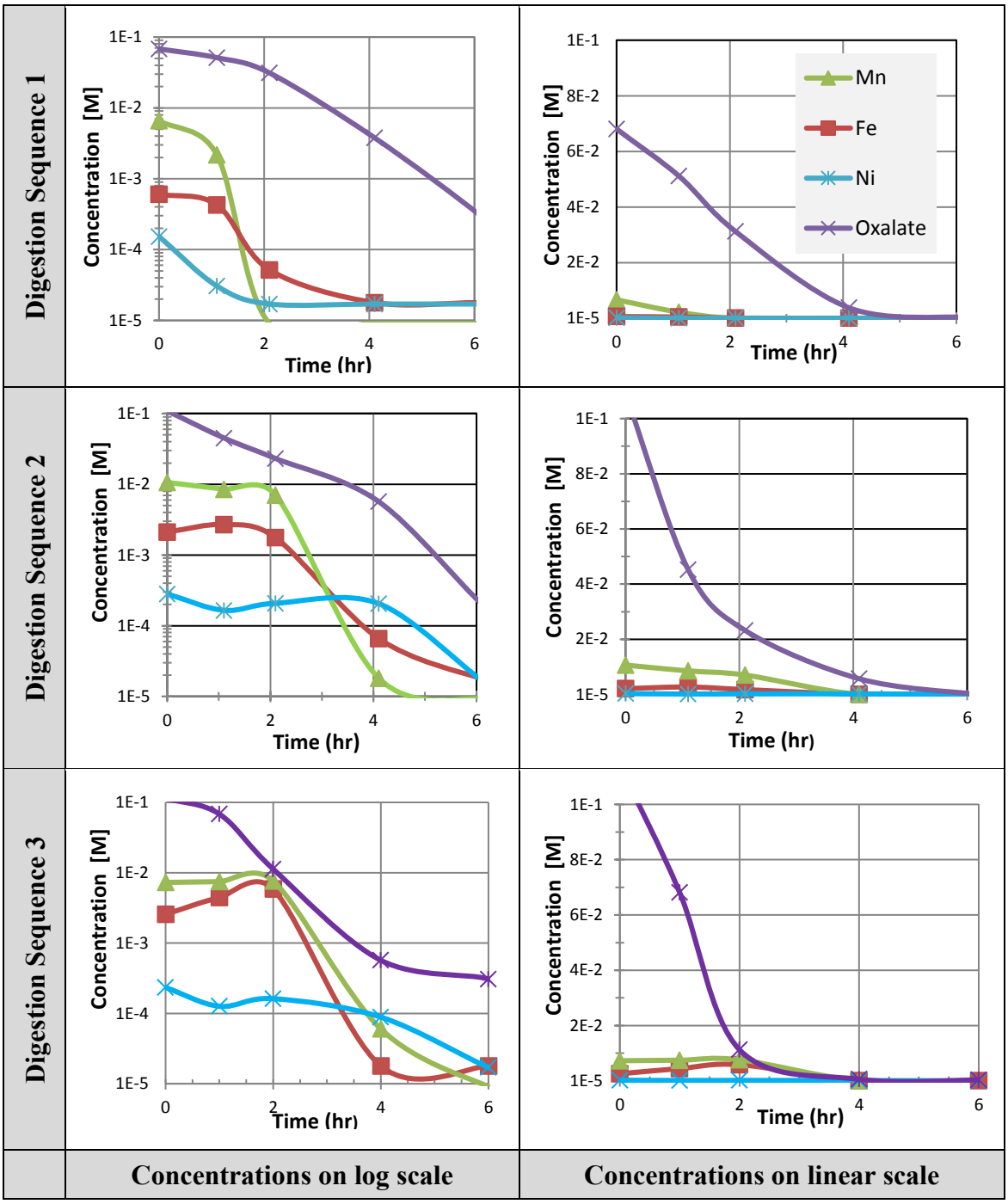

Figure 20. Oxalate and metal concentration vs ozonation time for the 1-Al/Mn-x.no slurries.

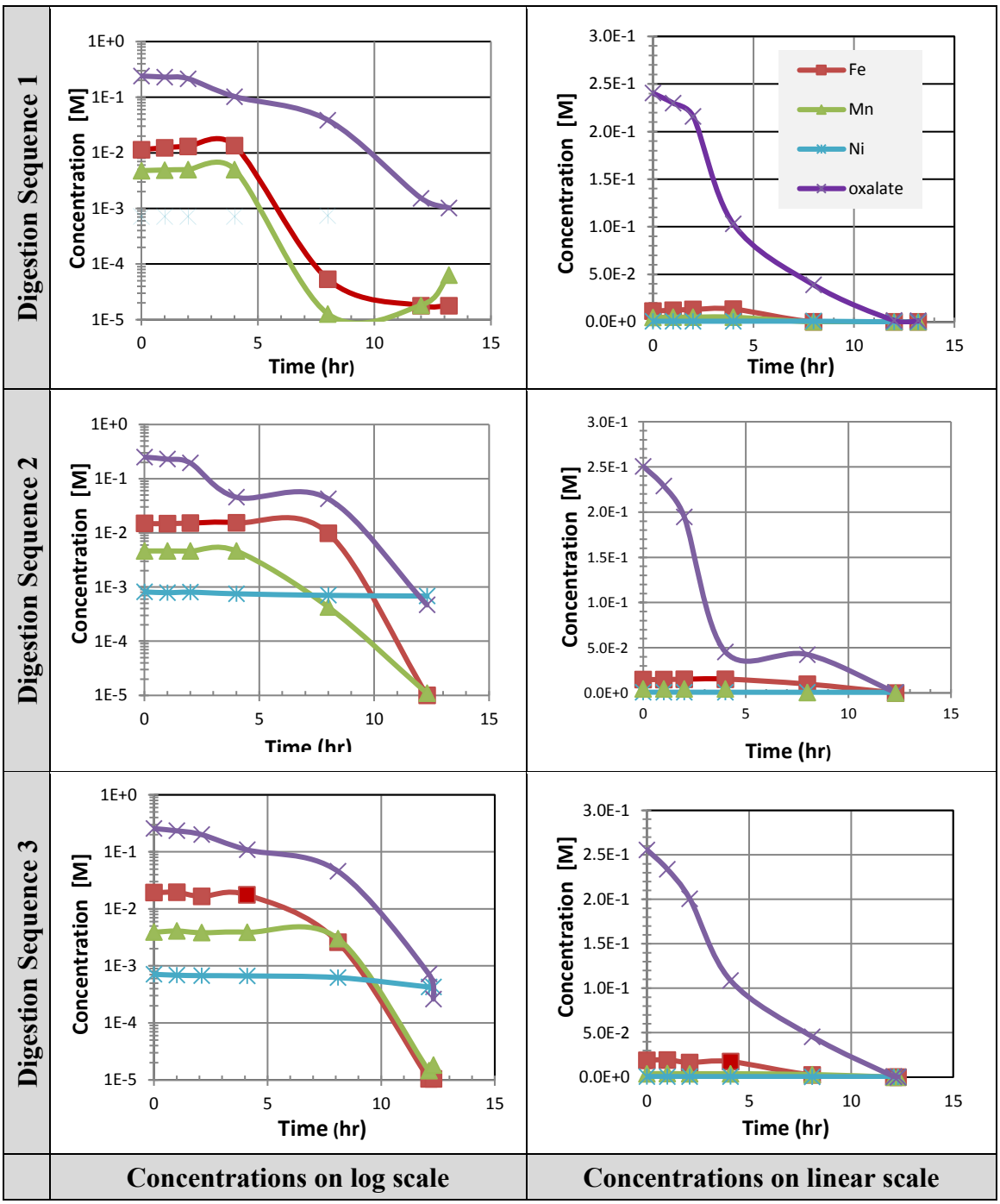

Figure 21. Oxalate and metal concentration vs ozonation time for the 2.5-Fe-x.no slurries.

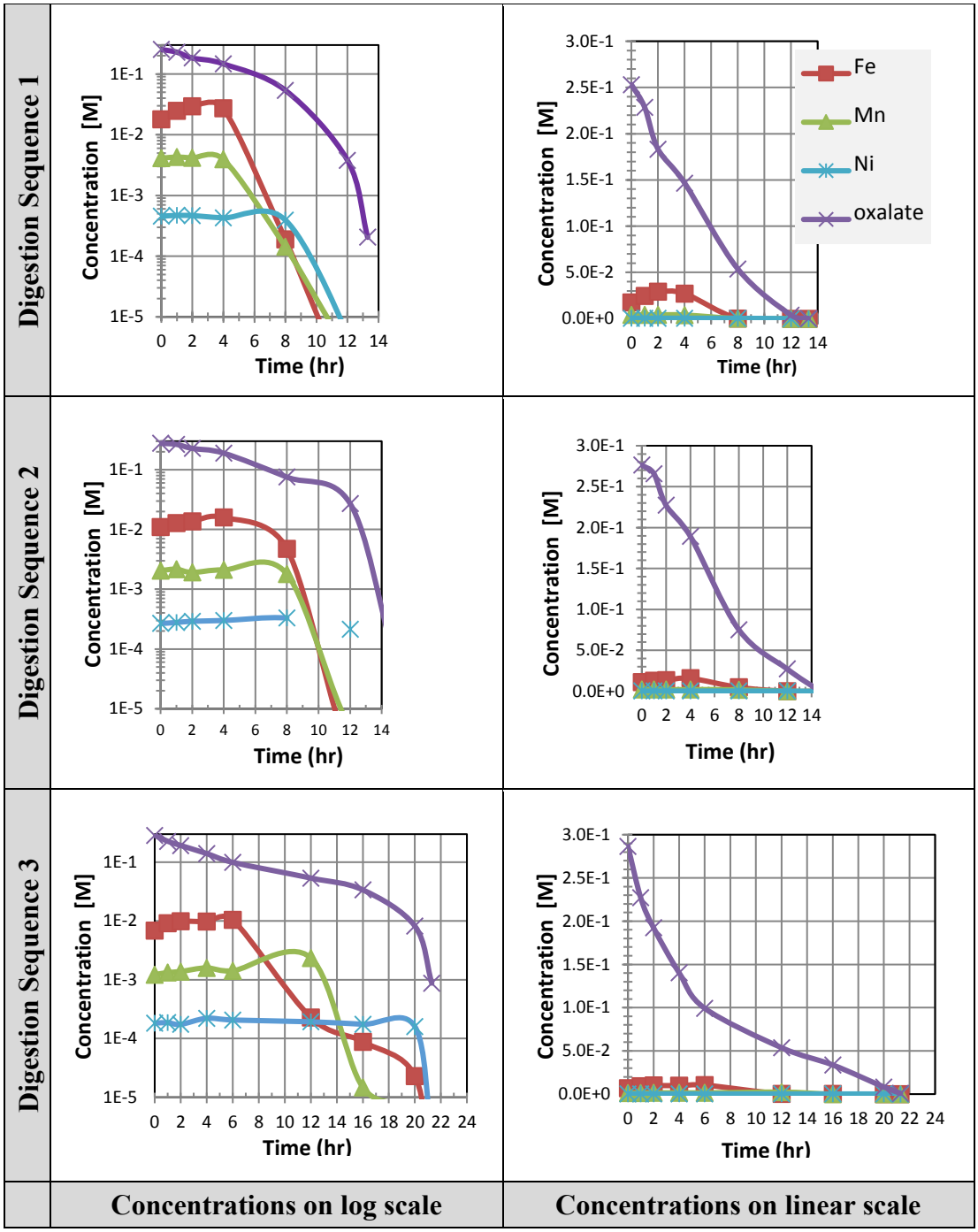

Figure 22. Oxalate and metal concentration vs ozonation time for the 1-Al/Mn-x.no slurries.

As ozonation continues throughout the decomposition process, the slurry's oxidative stress will increase. Inspection of E_h-pH (also called Pourbaix) diagrams (Takeno, 2005), indicates that Fe oxides can be expected to precipitate at pH of around 4.5 to 5.0 as either the sesquioxide, hydroxide or hydro(oxide) when under a solution oxidative stress of as little as from +0.5 to +1.0 V vs Normal Hydrogen Electrode (NHE). Such oxidative stress is not inconsistent with the prevailing experimental conditions here, given the continuous sparging by ozone and the presence of highly oxidising ozone derived hydroxyl radicals (as evidenced by the observed destruction of oxalate).

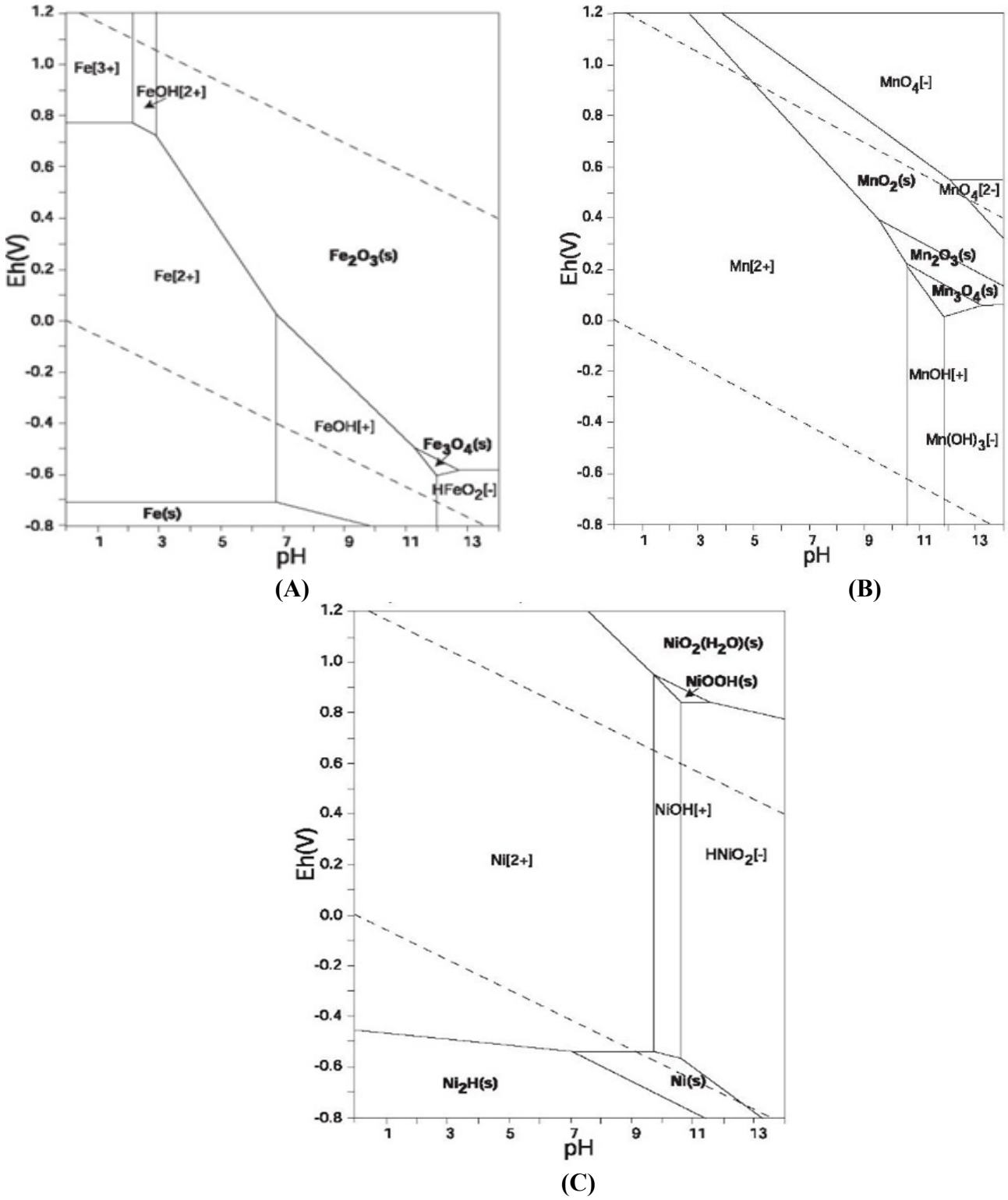

Figure 23. Pourbaix diagram for A) Fe; B) Mn; and C) Ni.

At the other extreme, the E_h-pH diagram for the Ni-H_2O system (Takeno, 2005), Figure 23 C) indicates that precipitation as $Ni(OH)_2$ should not occur until pH values greater than ~10. Before this oxide precipitation-derived decrease of soluble metal ion concentration

at long ozonation times, Ni concentrations are constant, while Fe and to some degree Mn exhibits an initial increase in soluble metal concentration at a short ozonation time.

For Fe(II) with ozone, the oxidation of Fe(II) requires only a one electron transfer and, therefore, is kinetically facile (Beltrán *et al.*, 2005; Logager *et al.*, 1992; Ngadi *et al.*, 2006; Gottschalk and Saupe, 2002; Von Gunten, 2003; Chetty *et al.*, 2012; Jacobsen *et al.*, 1998; Buxton *et al.*, 1995; Legube and Leitner, 1999; Kasprzyk-Hordern *et al.*, 2003). In Fe(II)- rich systems such as at the start of the ozonation process, this oxidation can be considered to proceed by Reactions 4-13 and 4-14.

$$Fe^{2+} + O_3 \rightarrow FeO^{2+} + O_2 \quad (4\text{-}13)$$

$$FeO^{2+} + Fe^{2+} + 2H^+ \rightarrow 2Fe^{3+} + 2H_2O \quad (4\text{-}14)$$

This results in the formation of Fe^{3+} ions, increasing the total concentration of soluble iron in solution as observed at short ozonation times in Figure 19 to Figure 22. At longer ozonation times, as can also be seen from Figure 19 to Figure 22, the increased soluble Fe^{3+} ions complex with the oxalate, resulting in the total soluble Fe concentration eventually decreasing once oxalate decomposition has resulted in both the oxalate concentration having fallen below a critical value and the solution pH starting to increase.

Since Mn and Ni are also first-row transition elements, they will also exhibit similar types of reactions to Reaction 4-13 (Kasprzyk-Hordern *et al.*, 2003; Gracia *et al.,* 1995; Gracia *et al.*, 1996). However, as can be seen from the Pourbaix diagrams of Figure 23 C), aqueous Ni(III) is unstable with respect to hydroxide precipitation, as is Mn(III) with respect to insoluble MnO_2 formation. The reactions for Ni seem to preclude any net increase in solubility of the sort demonstrated by the Fe data of Figure 19 and 22. While the E_h-pH diagram of Ni, Figure 23 C) leads us to expect the observed behaviour of the Ni concentration as a function

of time (i.e. expect no net increase as a function of time), the E_h-pH diagram for Mn, Figure 23 B), could be taken to indicate the feasibility of a net increase in the Mn concentration with ozonation time. Such an increase could be facilitated by Mn(II) oxidation to permanganate (i.e. Mn(VII)) which is soluble across the pH range used in the decomposition testing. Indeed, over-oxidation of Mn(II) to Mn(VII) is a well-documented undesirable consequence of excessive ozonation during treatment of drinking water for manganese removal (Gottschalk and Saupe, 2002; Von Gunten, 2003; Portjanskaja, 2007; Jacobsen *et al.*, 1998). However, the absence of any substantial increase in Mn concentration upon the commencement of ozonation seems to indicate that the ozone doses used here were not high enough to generate the oxidative stresses necessary to drive Mn(VII) formation.

The ECC process would perform ozonation in the decomposition loop, above-grade, outside of the HLW Tank Being Cleaned. Since the ECC process is an out-of-tank process, and the half-life for ozone is very short (Lenntech, 2017), the decomposed slurry would be recirculated in the stainless steel Decomposition Loop after adequate time has elapsed to ensure the ozonation reactions are complete, before transferring the decomposed slurry to a real HLW (deposition) tank. The HLW Deposition Tank would have been previously pre-staged with excess caustic rich supernatant to return the deposited slurry mix to within SRS normal tank farm corrosion control parameters. Thus, any impact to the HLW tank fabric could likely be minimised. To further ensure/confirm the impact to the HLW tank fabric would be minimal, independent corrosion studies including those associated with the oxalate decomposed slurries, and its effect on the deposition tank are planned to be performed (Wiersma, 2011).

Thus, in summary, the dependences shown in Figure 19 through 22 can be considered to exhibit two distinct phases dependent upon metal ion nature.

1) **The initial phase: For Fe**: an increase in metal ion concentration due to the action of ozone on the sludge constituents; For **Mn**: no initial increase upon ozonation due to instability of Mn(III) ions to precipitation; with precipitation of ions in the +2 oxidation state inhibited by complexation with oxalate. For **Ni:** the pH is too low to show any effect.

2) **The second phase** at longer ozonation times: a decrease in metal ion concentration as a result of decreasing the oxalate concentration and increasing the *spent acid slurry* pH. The former effect results in decomplexation of metal ions, rendering them vulnerable to precipitation as insoluble metal hydro/oxides at the elevated pH values that arise due to the latter effect.

Having considered the metal ion concentration data of Figure 19 through 22, the associated oxalate data is considered in terms of what it reveals about the kinetics of the three metal catalysts in promoting oxalate decomposition. Using the data of Figure 19 through Figure 22, Figure 24 shows plots of the oxalate decomposition after one-hour vs initial concentrations of Fe, Mn, and Ni for the twelve *simulant decomposition test slurries*, thereby enabling the significance of each of the metals to be compared to the first-hour oxalate decomposition. Using the same dataset, Figure 25 shows analogous plots for the time required to decompose the oxalate to a concentration $\leq 1.1\times10^{-3}$ M vs the initial metal concentrations, enabling the significance of each of the metals to be compared to the required decomposition time (in hours) to reach the defined oxalate decomposition endpoint of 1.1×10^{-3} M.

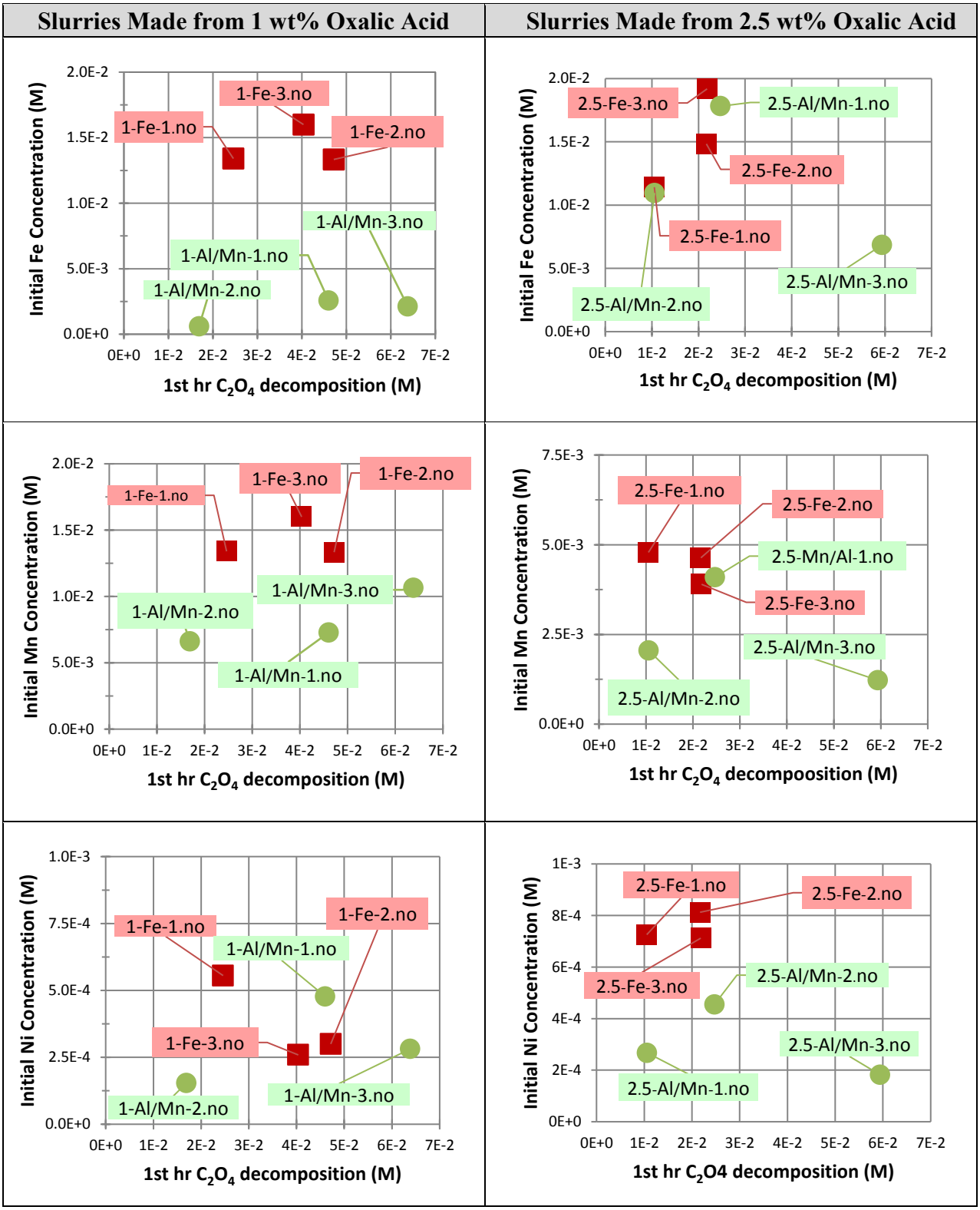

Figure 24. Initial rate of oxalate decomposition vs concentrations of Fe, Mn, and Ni ions for the *simulant decomposition test slurries*.

From 24, the initial oxalate decomposition rate data obtained from Al/Mn-rich slurries created using 1 wt% oxalic acid – i.e. at low soluble Fe concentrations such as $< 1\times10^{-2}$ M, reveals that initial decomposition rate increases with all three metal ion concentrations individually. Initial rate data obtained from the Fe-rich slurries created using 1 wt% oxalic acid with a higher level of soluble Fe (i.e. $> 1\times10^{-2}$ M), exhibit no discernable dependence on soluble Mn or Ni concentration. This lack of discernable dependence on Mn and Ni is presumably due to any effect in the rate from these ions being swamped by the effect of the now substantially more abundant Fe.

Also Figure 24, as evidenced by the bunching at higher Fe concentrations $> 1\times10^{-2}$ M (i.e. bunching and a shift to the right) from slurries prepared using 2.5 wt% oxalate (vs the same data for slurries created from 1 wt% oxalic acid), it appears that high initial oxalate concentrations support Fe solubilizing - as it does during rust removal.

Unfortunately, this means that the effect of iron on the initial decomposition rate masks that of the Mn or Ni for these 2.5 wt% oxalic acid created slurries, an effect that will be expected to maintain until the Fe has precipitated, i.e. long ozonation times, with the effect clearly shown after long ozonation times. Figure 25 shows plots for the ozonation time required for the oxalate concentration to be decomposed to < 100 ppm oxalate (i.e. $\leq 1.1\times10^{-3}$ M) as a function of the initial concentrations of the individual metal ions Fe, Mn and Ni. Such a low concentration of oxalate is typically obtained only after long ozonation times of 6 hours or greater, corresponding to conditions where much of the Fe has usually precipitated (Figure 19 through Figure 22). This means that the Mn and Ni derived effects may be more readily observed after long ozonation times vs the initial rate data of Figure 24.

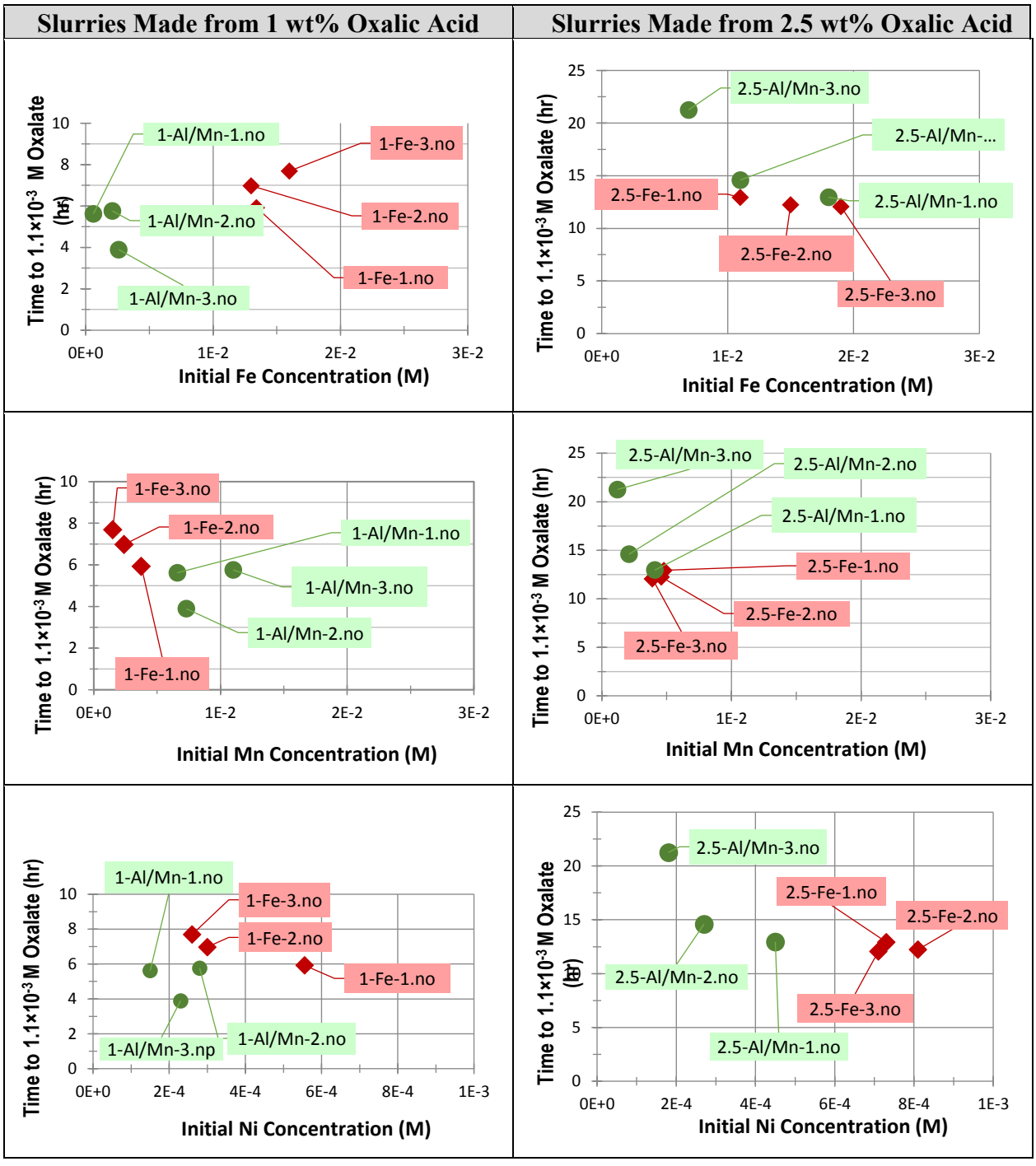

Figure 25. Time in hours to reach 1.1×10^{-3} M oxalate vs initial concentrations of Fe, Mn, and Ni ions for the *simulant decomposition test slurries*.

As shown by the left side of Figure 25, the 1 wt% oxalic acid data for both slurries exhibits no real dependence on initial Fe concentration, as most of the iron has precipitated by the time an

oxalate concentration of 1.1×10^{-3} M is approached. This behaviour is in agreement with the Pourbaix diagrams of Figure 23 which indicate that, as pH rises during oxalate decomposition, Fe will precipitate before Mn, which will precipitate before Ni. Thus, Ni will persist in solution even when an oxalate concentration of < 100 ppm / < 1.1×10^{-3} M is achieved. However, the 1 wt% oxalic acid data of Figure 25 (i.e. the left side) also exhibits no real dependence on initial Ni concentration, indicating that Ni plays only a small role, if any, in promoting the overall oxalate decomposition. In contrast, increases in the initial concentration of Mn, which remains in solution well into the time domain / pH range where the oxalate concentration approaches 100 ppm / 1.1×10^{-3} M, would result in a decrease in the amount ozonation/time required to reach the defined oxalate decomposition endpoint.

This solubility based behaviour, taken in the context of the dominating effect of Fe concentration on the initial rate data of Figure 19 through 22 strongly suggests that the Fe initially dominates the catalysis of ozonation-driven oxalate decomposition of the slurries at short ozonation times, partially due to solubility and its associated high rate parameter for reaction with ozone. However, as a result of oxalate decomposition and the associated pH increase, the Fe precipitates at longer ozonation times, with Mn starting to dominate oxalate decomposition by Mn oxalate complex formation followed by ozone attack as before.

The 2.5 wt% oxalic acid data for both slurries (i.e. 2.5-Fe-x.no and 2.5-Al/Mn-x.no), shown by the right side of Figure 25, was again recorded at high initial Fe concentrations with the required amount of ozonation time to result in an oxalate concentration of 1.1×10^{-3} M decreasing with increasing initial concentrations of Fe, Mn, and Ni. This indicates either that the Fe, Mn, and Ni ions all play a role in determining the time to reach the defined

decomposition endpoint, or that non-catalytic Fe, Mn, and Ni are released at the same time as catalytic Fe, Mn, and Ni during the three sequential oxalic acid digestions used in this dataset.

4.6.2 Conclusions on Role of Metal Catalysts

Metal ions such as Fe(II), Mn(II) and Ni(II), already present within the slurries as a result of sludge mobilisation, catalyse oxalate decomposition. Results show that mineralisation of the oxalate with metal catalysts occurs at a rate higher than observed during simple ozonation conducted in their absence.

Single metal ion systems have been widely researched in the metal oxalate systems. Less well studied are systems employing a mixture of metal catalysts, and that may provide insights into inter-metal ion competition or synergistic effects. The *simulant decomposition test slurry* experiments presented here fall into the latter category and indicate that the three main metal catalysts present both compete with and complement each other in the overall catalytic process. However, this is complemented in the slurries studied here by a reverse order solubility exhibited as the oxalate destruction process proceeds. As this destruction proceeds, pH increases from ~1 to as high as ~9 (*vide supra*) leading to the precipitation of the metal catalysts as metal hydro/oxides. E_h-pH diagram data indicates that Fe precipitates at pH values lower than Mn, which in turn precipitates at pH values lower than Ni – meaning that as oxalate decomposition proceeds and pH increases concomitantly (as seen in, Fe precipitates before Mn before Ni). Thus, Fe(II) oxalate catalysis dominates the overall oxalate decomposition rate at short ozonation times. At intermediate ozonation times, once the Fe has started to precipitate due to the increasing pH, Mn oxalate catalysed decomposition dominates the process. Finally, typically close to the process endpoint of 1.1×10^{-3} M oxalate in solution, Ni oxalate catalysis dominates.

Of these three metal ions, the solubility behaviour of Fe is the most involved. Initially, upon the onset of ozonation, there is an increase in solution Fe concentration due to the oxidative action of ozone on the metal oxide components of the sludge; precipitation is inhibited by complexation with oxalate. This complexation, also makes the oxalate susceptible to decomposition by direct attack of ozone in the context of the metal complexation catalyse mechanism for oxalate destruction discussed here. At longer ozonation time, there is a decrease in Fe ion concentration as a result of oxalate decomposition, so decreasing the oxalate concentration, as well as increasing the *slurry* pH. The decrease in oxalate concentration results in decomplexation of Fe (as well as Mn and Ni) ions, rendering them vulnerable to precipitation as insoluble metal (hydro)oxides at the elevated pH values that arise due to the increasing the *slurry* pH. Thus, overall, oxalate decomposition in the slurries studied can be regarded as exhibiting four distinct stages:

Stage One (short ozonation times): ozone decomposes Fe oxalates and solubilise Fe from ozone action on the metal oxide constituents of the sludge;

Stage Two (intermediate ozonation times): As a result of the loss of the solution capacity to complex (and so solubilise) Fe, Mn, and Ni ions due to O_3 driven oxalate decomposition, as well as the pH increase that accompanies that decomposition, Fe begins to precipitate. Hydroxyl radical generation from ozone is still primarily catalysed by Fe ions during this stage.

Stage Three (intermediate ozonation times): Fe precipitation is near complete, and oxalate decomposition is now driven by ozone attack on Mn complex oxalate – Mn playing a major role in determining the final to process endpoint of 100 ppm / 1.1 x 10^{-3} M oxalate in solution

Stage Four (long ozonation times): Process endpoint with Mn precipitation now near completion and Ni being the dominant metal ion in solution.

4.7 pH as Measure of Remaining Oxalate

Lagunova *et al.*, 2012 purports that simple oxalic acid solutions at an initial pH of 2 can be decomposed with ozone at 70°C. Figure 26 shows pH vs time plots derived from previously conducted much smaller scale ozone-driven oxalate decomposition experiments using real HLW, than those based on simulant. Full details as to the performance of the tests whose results are shown in Figure 26 are given in Chapter 5. They are presented here, juxtaposed with Lagunova's data, to demonstrate the effect that the presence of Fe, Mn and Ni metal ions has on the rate of oxalate decomposition by ozonation.

All three slurry decompositions shown in Figure 26 were conducted at the same temperature (i.e. 70°C) and similar initial pH (i.e. pH≈2), using simple (metal free) 2 wt% oxalic acid solutions and slurries made from two real HLW sludges (the composition of which the currently used simulants are primarily based (Eibling, 2010 and detailed in Section 5)). The decomposition data (pH vs time) associated with the two HLW based waste slurries, identified as 2-Fe-3.no and 2-Al/Mn-3.no, and the comparable data for the pure 2 wt% oxalic acid solution is contained in Appendix 5, as Tables 44 through 47.

As can be seen from Figure 26, the presence of metal ions such as Fe and Mn substantially accelerates the rate at which the pH of the samples under study increases, with Fe ions having the most significant accelerating effect. However, this also raises the question as to what the increase in pH is due to, and whether it can be used, as an indicator of residual oxalate concentration.

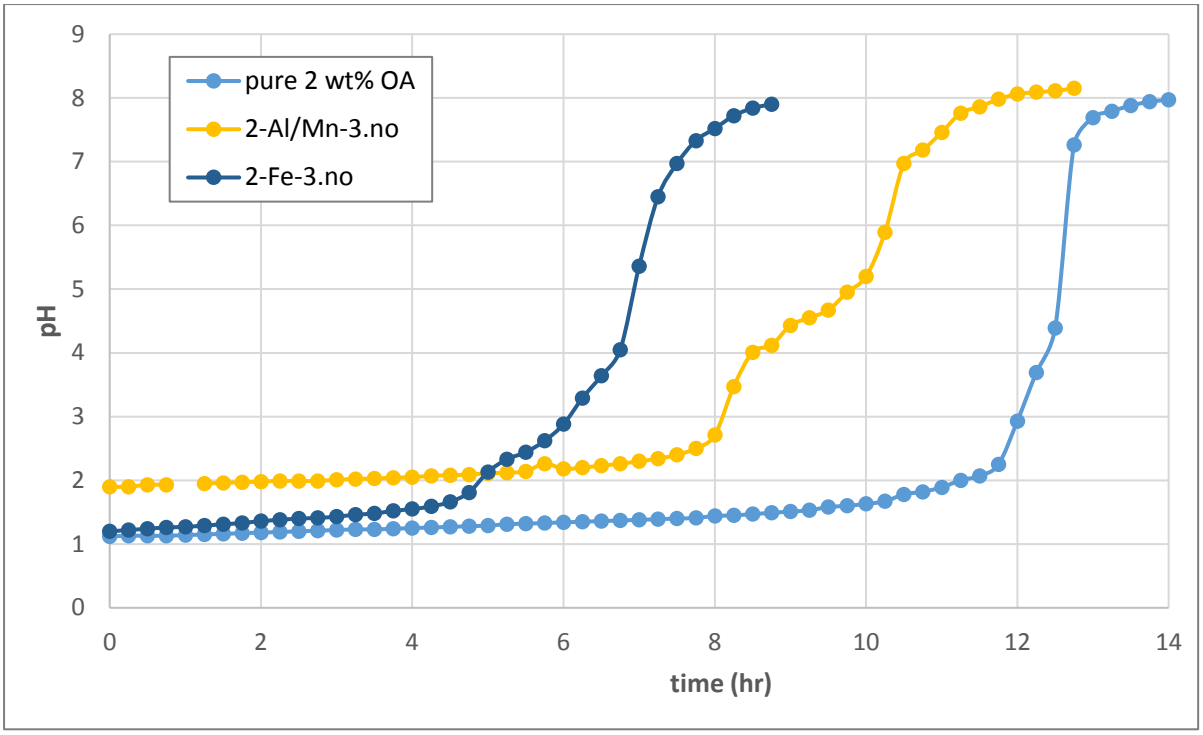

Figure 26. pH vs ozonation time for slurries created with real HLW sludge and pure 2 wt% oxalic acid.

As the oxalic acid concentration plays a major role in determining solution proton concentration, it is reasonable to conclude that the pH values recorded for Figure 26 are causally related to oxalate concentration and can be taken to indicate the degree of oxalate decomposition. Specifically, low pH will indicate high oxalate concentration and high pH, the reverse. This correlation is seen by the oxalate concentration vs time and pH vs time data recorded from simulant test slurries shown in Figure 27 through Figure 30.

In agreement with Lagunova *et al.*, 2012, the data of Figure 26 show that simple oxalate solutions are indeed decomposed by ozonation, with the onset of reaction completion in the simple oxalate solution indicated by the sudden increase in pH observed after 12 to 13 hours of O_3 sparing. However, Figure 26 also shows that the presence of soluble Fe-Mn-Ni in the *simulant decomposition test slurries* increases the rate of oxalate decomposition, with the onset of reaction completion being observed after only about 6 hours of ozonation.

Thus, in light of the *Real HLW decomposition testing,* transition metal derived enhancement to oxalate decomposition during ozonation demonstrated in Figure 26, the results from simulant based decomposition experiments were used to better quantify and understand the individual effect of each of the metals/metal complexes.

4.7.1 pH vs Oxalate Concentration Testing with Simulant

Figure 27 through 30 show the effect of ozonation on remaining oxalate concentration and pH as a function of time for twelve *simulant decomposition test slurries*. Specifically, Figure 27 shows the remaining oxalate and the corresponding pH vs ozonation time for test slurries created using the Fe-rich simulant and 1 wt% oxalic acid, with the plots on the left side showing the remaining oxalate using a log scale, while the plots on the right side showing the remaining oxalate using a linear scale. Since the remaining oxalate concentration varies greatly, the log scale is included showing the general relationships of remaining oxalate to pH vs time (the plots in the left column), while the linear scale for remaining oxalate is shown (plots on the right) to provide visual magnitude. Figure 28 shows the same for the test slurries created using the Al/Mn-rich sludge simulant and 1 wt% oxalic acid. Figure 29 shows the same for the test slurries created using the Fe-rich sludge simulant and 2.5 wt% oxalic acid, while Figure 30 shows the same for the test slurries created using the Al/Mn-rich sludge simulant and 2.5 wt% oxalic acid.

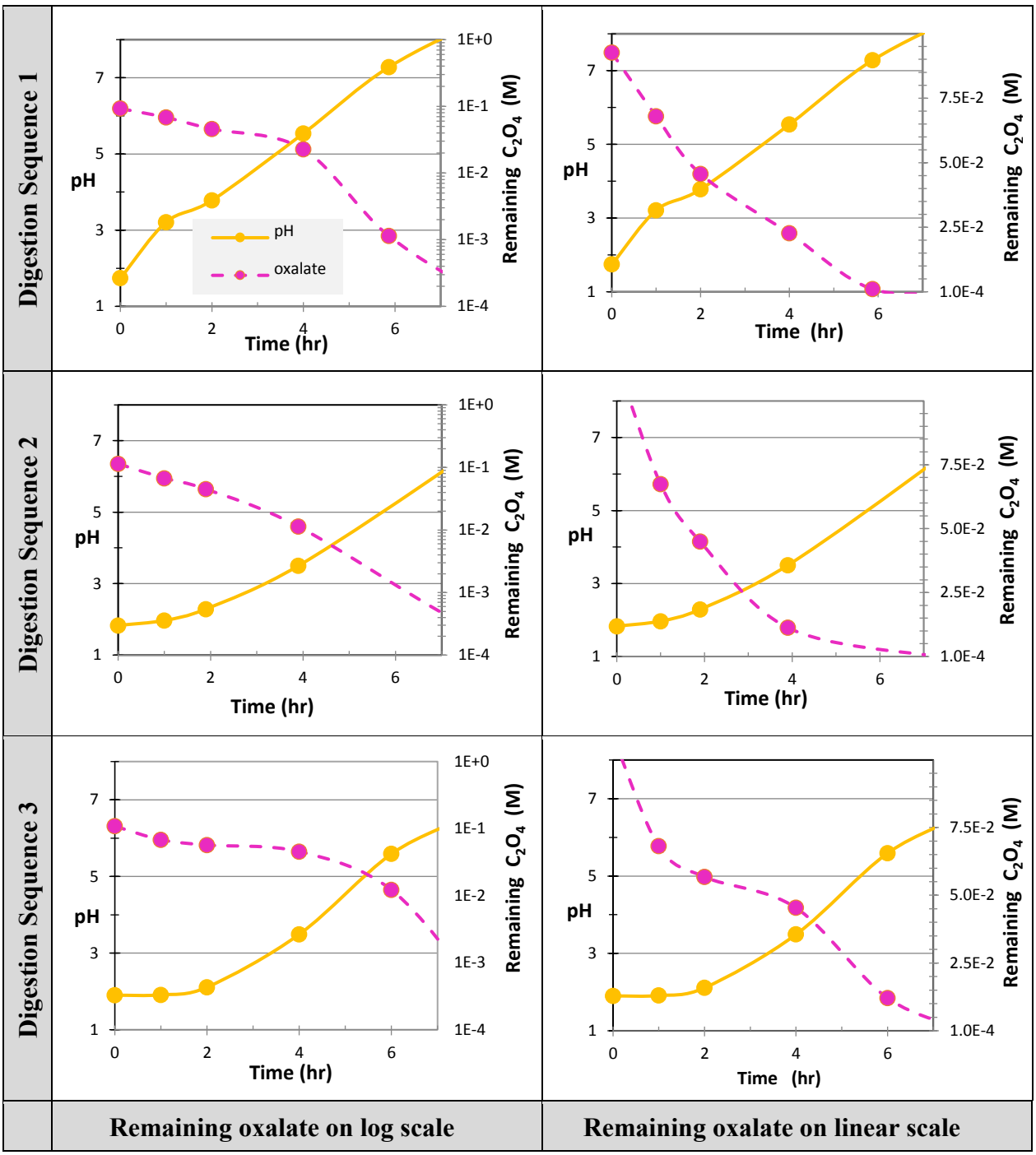

Figure 27. Oxalate remaining and pH ozonation time for 1-Fe-x.no slurries.

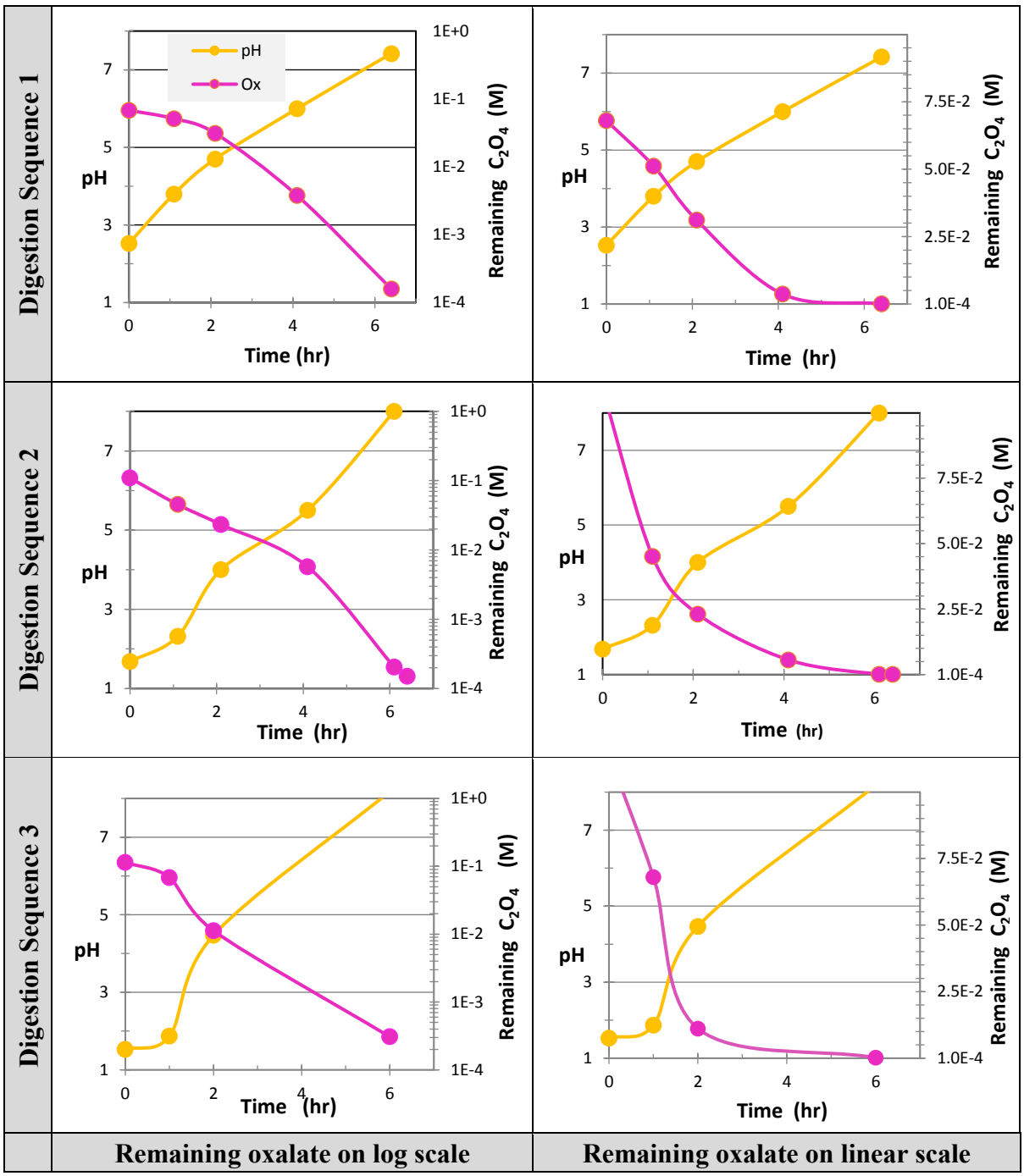

Figure 28. Oxalate remaining and pH vs ozonation time for 1-Al/Mn-x.no slurries.

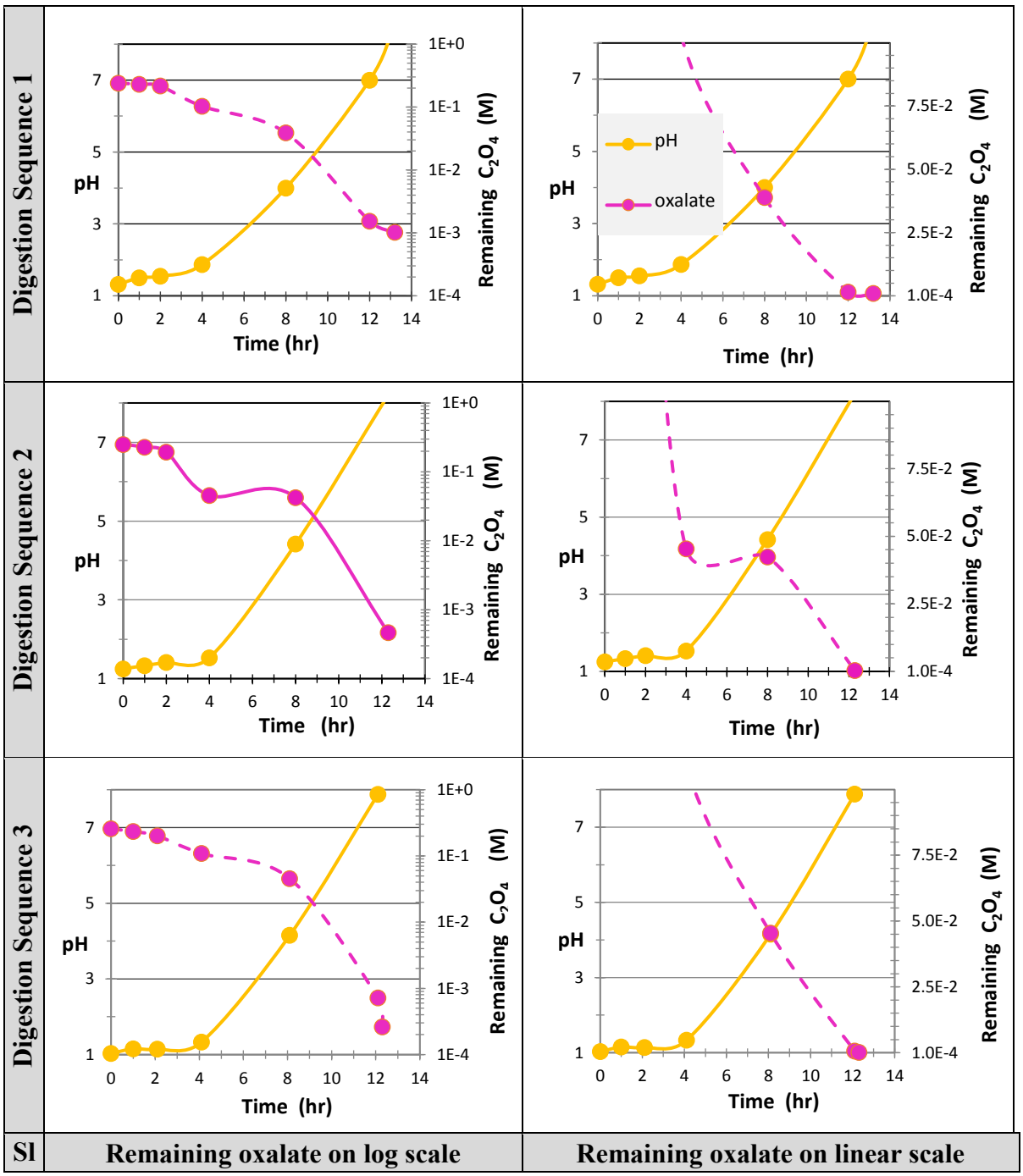

Figure 29. Oxalate remaining and pH vs ozonation time for 2.5-Fe-x.no slurries.

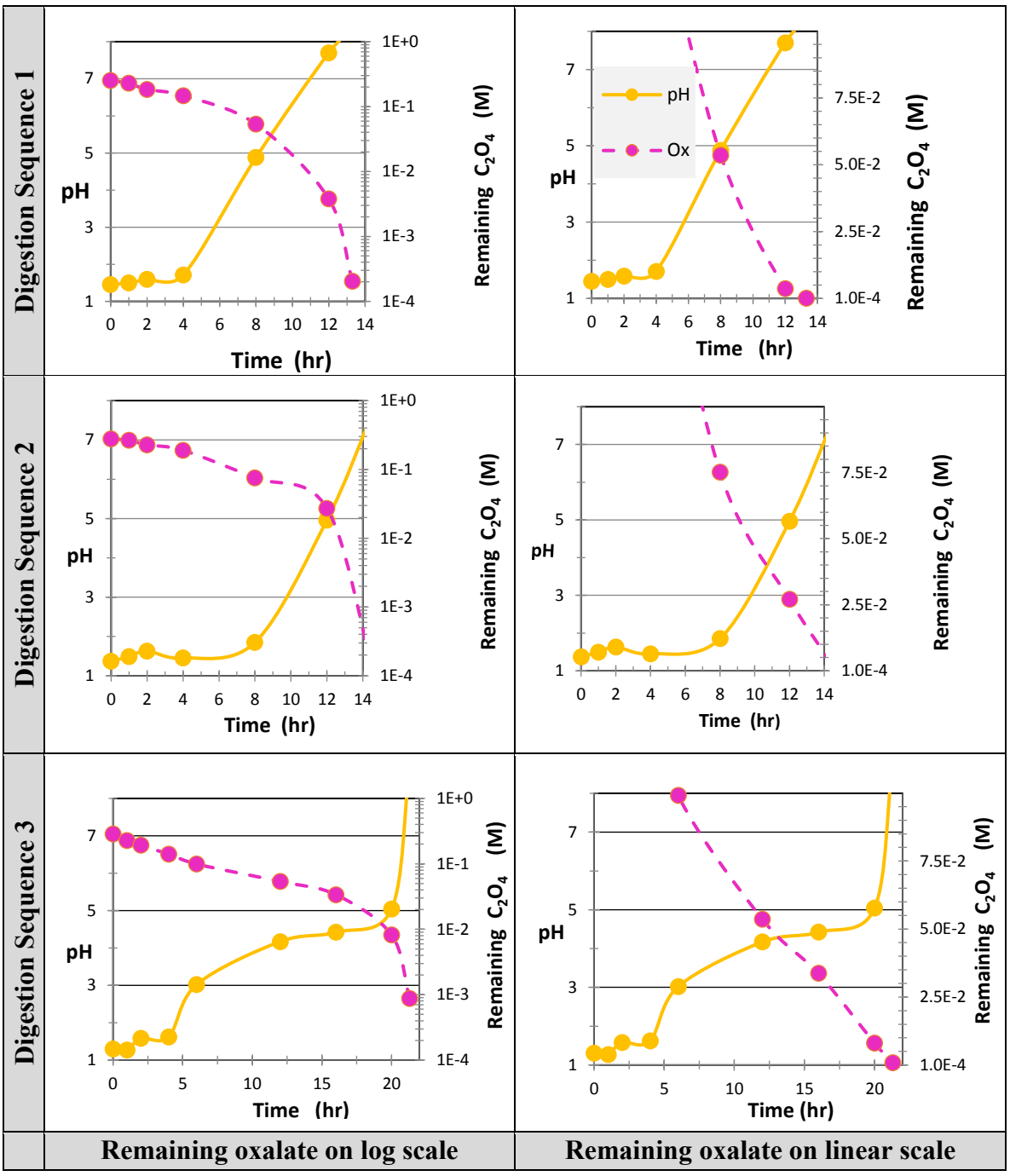

Figure 30. Oxalate remaining and pH vs ozonation time for 2.5-Al/Mn-x.no slurries.

Similar behaviour is observed in the variation of pH with ozonation time, pH typically increasing from a pH of around 2 up to the region of pH ≈ 7 to 8 when decomposition is judged to be complete (i.e. oxalate concentration has reached less than 1.1×10^{-3} M).

4.7.2 pH as Measurement of Remaining Oxalate

Oxalic acid is a diprotic acid, which means it has two acid dissociation constants, K_a values. For convenience, pK_a values are used. The relationship between K_a and pK_a values is shown by Equation 4-5.

$$pK_a = -log\ (K_a) \qquad \text{(eq. 4-5)}$$

pK_a values for oxalic acid, $H_2C_2O_4$ at 25ºC are quoted as 1.27 and 4.29 (Purich, 2017). pK_a is a measure of acid strength, while pH is a measure of $[H^+]$ in a solution. For acids, the smaller the pK_a, the more acidic the substance (i.e. the more easily a proton is lost, thus the lower the pH). For a weak acid, the relationship between pKa and pH can be shown by the Henderson-Hasselbalch equation, Equation 4-6.

$$pH = pK_a + log\ ([A^-]/[HA]) \qquad \text{(eq. 4-6)}$$

Where $[A^-]$ refers to the concentration of the conjugate base of the acid, and [HA] is the concentration of the acid. Since pK_a values are constants, the Henderson-Hasselbalch equation can be modified as shown by Equation 4-7.

$$\Delta pH \propto \Delta\ log\ ([A^-]/[HA]) \qquad \text{(eq. 4-7)}$$

Assuming much of the acid, [HA], has already reacted and could be approximated as a constant would mean that the log of any change in oxalate concentration would result in a proportional change in pH.

In order to access the ability of pH to be used to confirm that oxalate decomposition is complete, for each *simulant decomposition test slurry* the -log of oxalate concentration vs pH is graphed (i.e. 1-Fe-x.no, 1-Al.Mn-x.no, 2.5-Fe-x.no, 2.5-Al/Mn-x.no, and an all-combined). Using regression analysis, the Coefficient of Determination (R^2) values are determined. The results are shown in Figure 31 through 35.

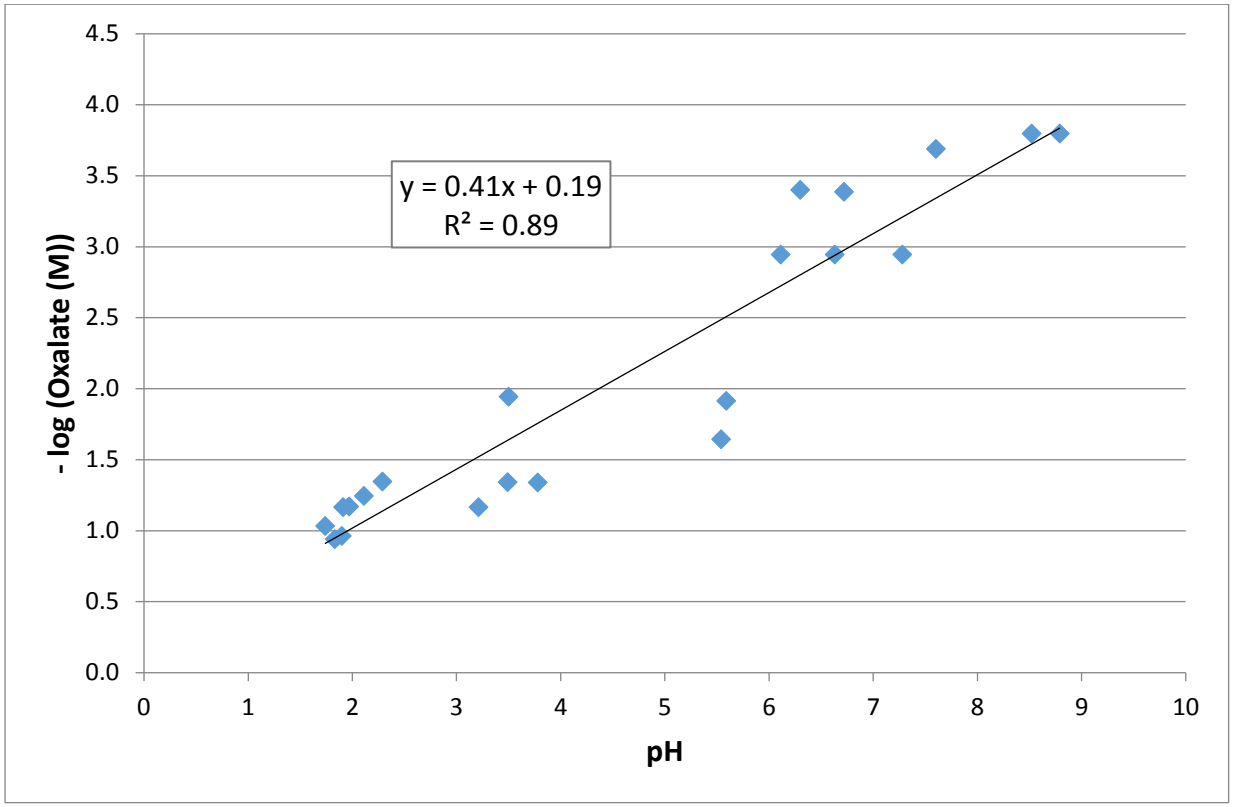

Figure 31. Linear regression analysis of negative log of oxalate concentration vs pH of the 1-Fe-x.no slurries.

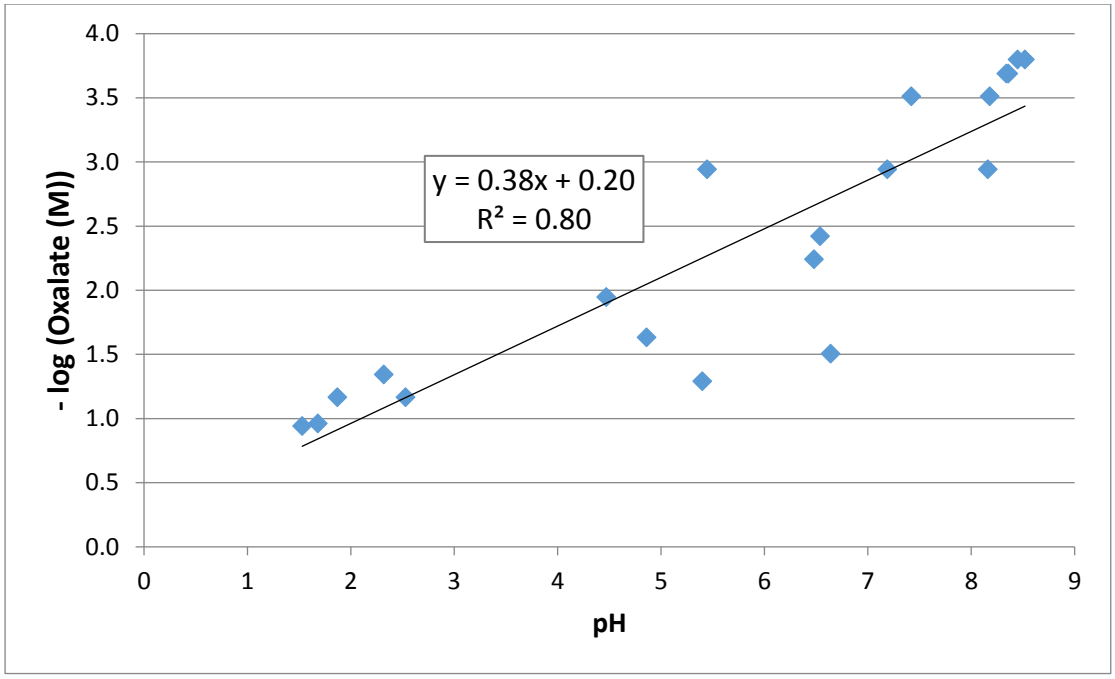

Figure 32. Linear regression analysis of negative log of oxalate concentration vs pH of the 1-Al/Mn-x.no slurries.

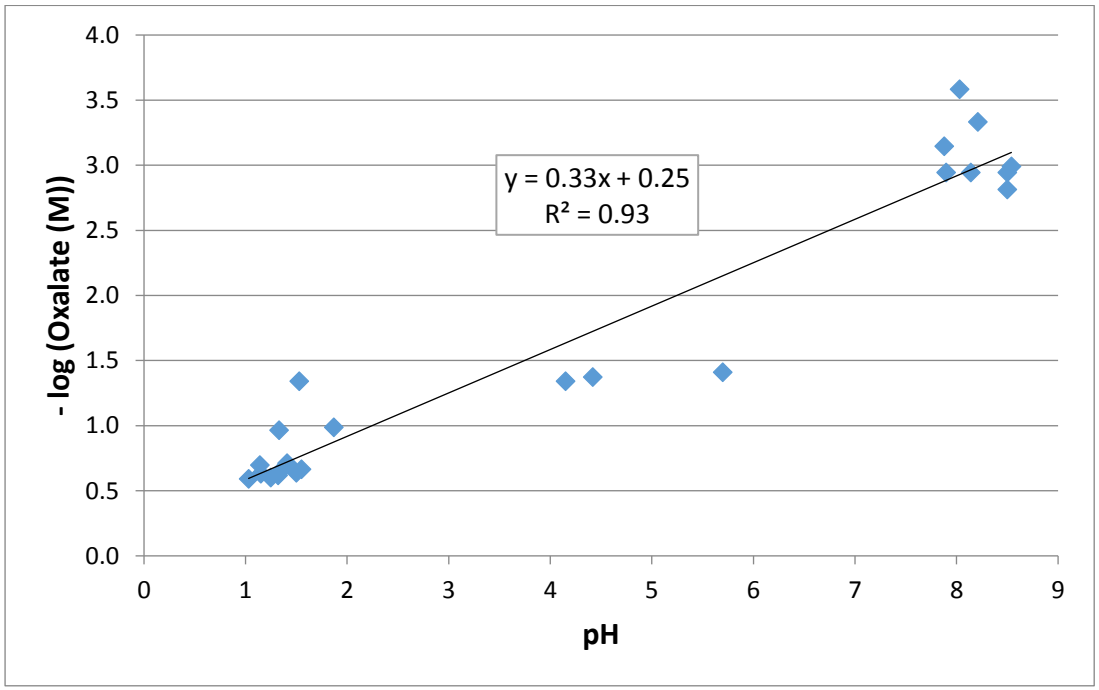

Figure 33. Linear regression analysis of negative log of oxalate concentration vs pH of the 2.5-Fe-x.no slurries.

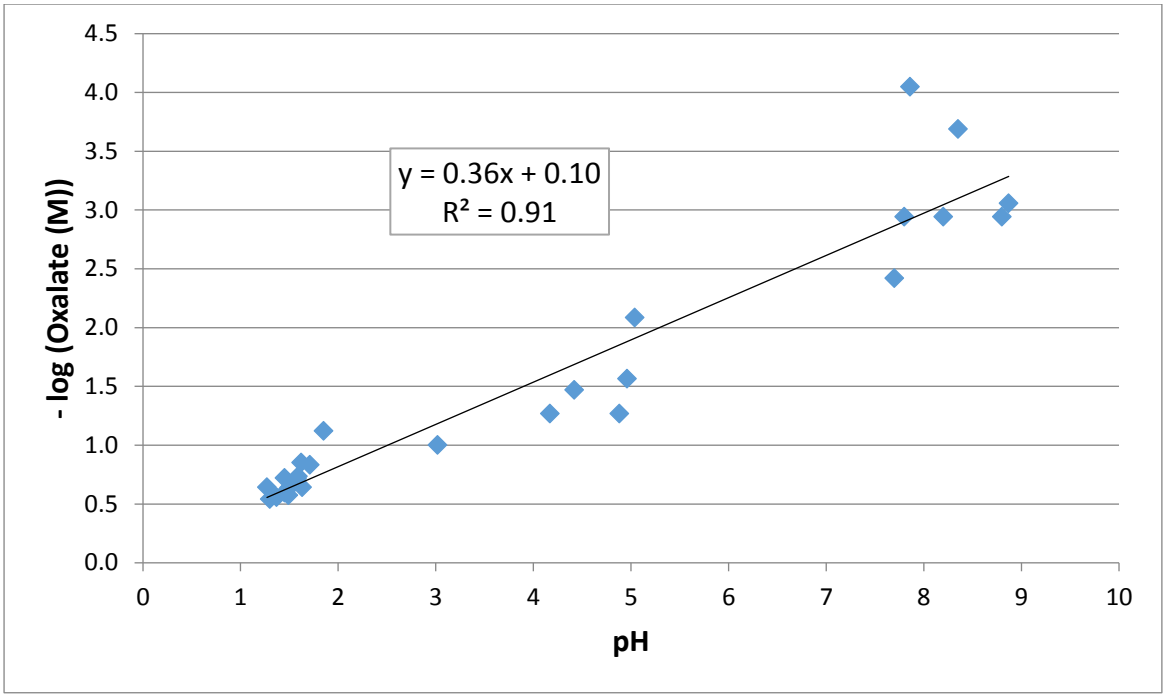

Figure 34. Linear regression analysis of negative log of oxalate concentration vs pH of the 2.5-Al/Mn-x.no slurries.

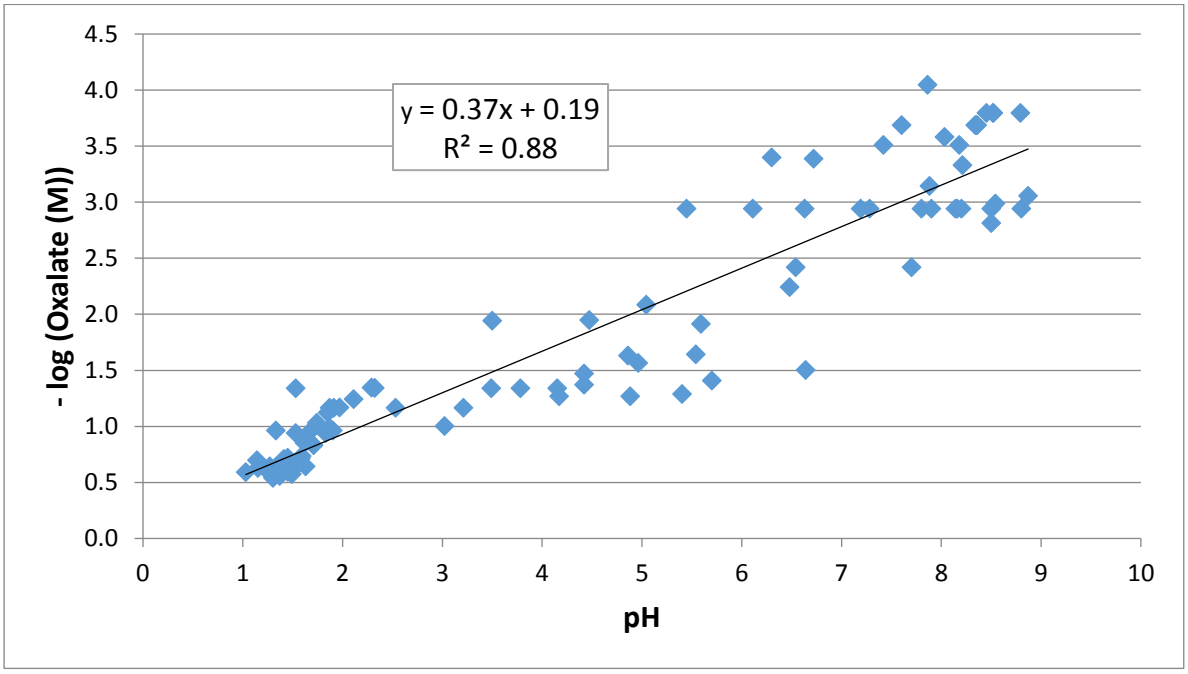

Figure 35. Linear regression analysis of negative log of oxalate concentration vs pH for the combined 1-Fe-x.no, 1-Al/Mn-x.no, 2.5-Fe-x.no, and 2.5-Al/Mn-x.no slurries

Based on regression analyses, the R^2 values of Figure 31 through Figure 35 are all greater than 0.80, demonstrating correlation, hence, confirming that as a field measurement, pH can be used to confirm when oxalate decomposition is complete.

4.8 Is Decomposition Hydroxyl Radical Driven?

The presence of hydroxyl radicals in AOP type processes is confirmed using fluorometric detection methods in solution, or spectroscopic analysis of a hydroxyl radical probe compound, such as p-chlorobenzoic acid, known as pCBA, $C_7H_5ClO_2$, (Pines and Reckhow, 2002) 2,4-dichlorophenoxyacetic acid, known as 2,4-D, $C_8H_6CL_2O_3$, or even atrazine, $C_8H_{14}CIN_5$ (Zhang *et al.*, 2012). However, such compounds are most commonly deployed in a single component, well-characterised systems where probe compound response can be unambiguously attributed to the presence of hydroxyl radicals. In contrast, because of the complicated slurry chemistry associated with the *ECC process*, such testing would be fraught with interferences, thus reporting false positives. Use of an added probe was therefore unsuitable for studying the remediation of spent oxalic acid nuclear decontamination solutions using ozone associated with HLW tank cleaning, so an alternate approach to the interrogation of the role of hydroxyl radical was sought. However, before initiating the alternate approach, the reaction pathways for the decomposition of oxalate by ozone were first reviewed.

4.8.1 Graphs of Reaction Rate vs Concentration

As stated above in Section 4.8.1, indirect decomposition of oxalate is commonly accepted as being second-order. Plots of the inverse of "$[C_2O_4^{2-}]$" as a function of time, therefore would result in a straight line. Since the reaction rate (i.e. oxalate decomposition rate), "r_{ox}," is equivalent to the negative inverse of time, the graph represents reaction rate vs concentration

(i.e. $1/r_{ox}$ vs $1/[C_2O_4^{2-}]$). Plots of "$1/r_{ox}$ vs $1/[C_2O_4^{2-}]$" were constructed as shown in Figure 36 and 37.

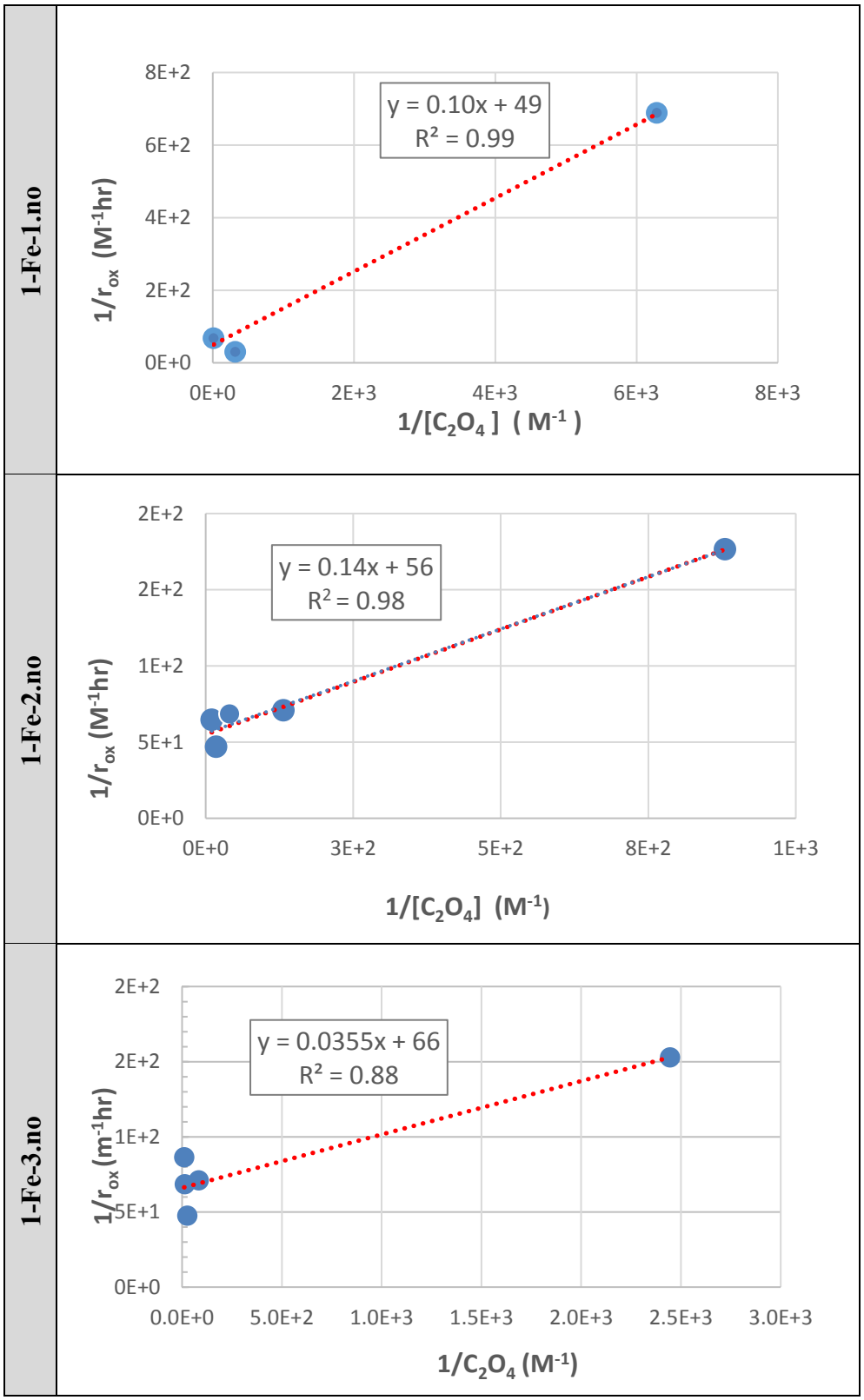

Figure 36. Plots of $1/r_{ox}$ vs $1/[C_2O_4^{2-}]$ for 1-Fe-x.no slurries.

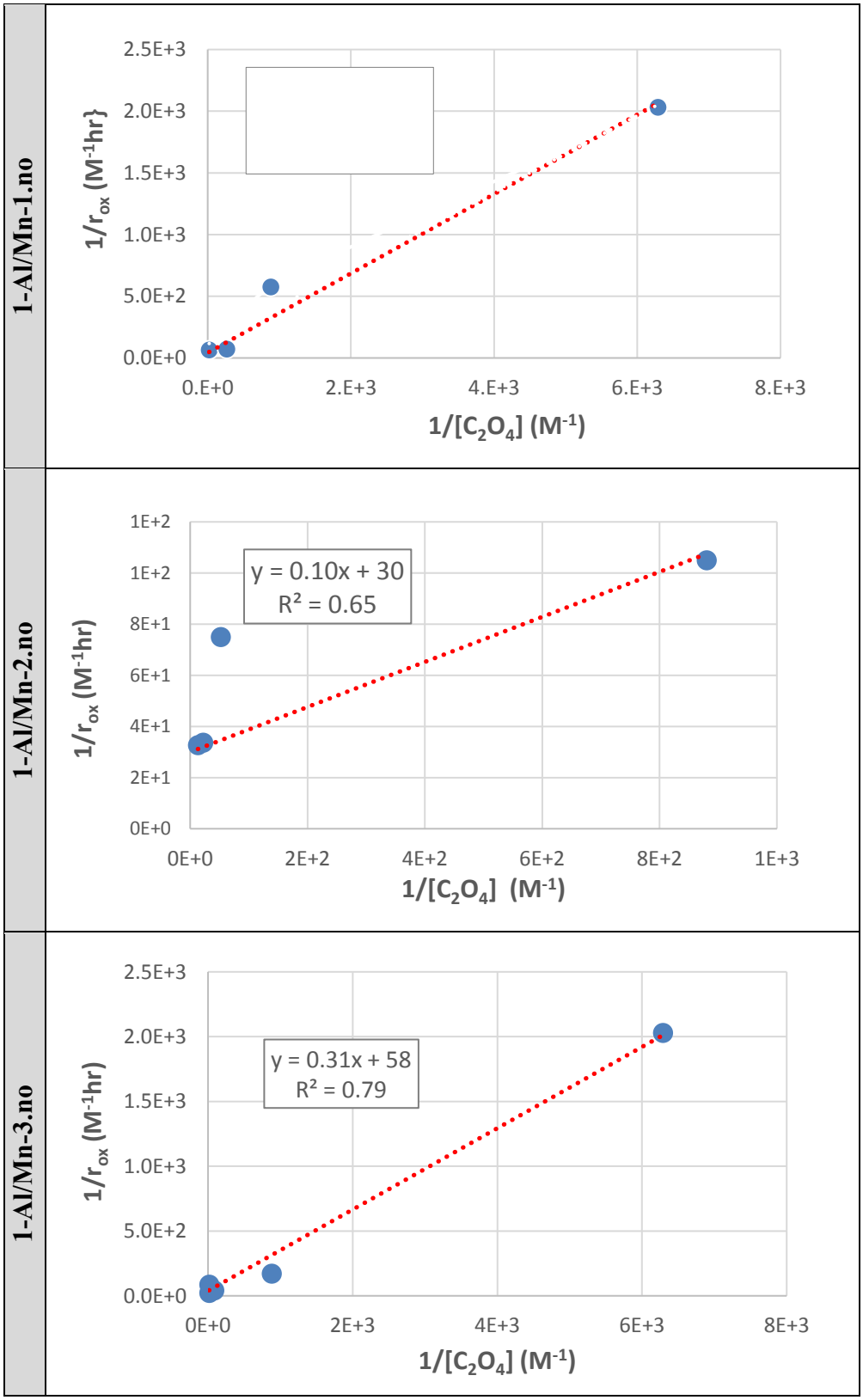

Figure 37. Plots of $1/r_{ox}$ vs $1/[C_2O_4^{2-}]$ for 1-Al/Mn-x.no slurries.

4.8.1.1 Determination of g-values

From the plots, the slope-intercept, which is also the 1/g-value can be determined. Using data provided in Appendix 3 (i.e. Table 41 through 43 for the 1 wt% slurries and the 2.5 wt% slurry decomposition data), the g-values for the decomposition of the simulant decomposition test slurries were determined. The results are shown in Table 11.

Table 11. Estimated *g-values* derived from decomposition test data**.**

Simulant decomposition test slurry	***g*-value ($M \cdot hour^{-1}$)**	
1-Fe-1.no	3.0×10^{-2}	Stable
1-Fe-2.no	1.8×10^{-2}	
1-Fe-3.no	2.1×10^{-2}	
1-Al/Mn-1.no	9.1×10^{-3}	No trend
1-Al/Mn-2.no	3.3×10^{-2}	
1-Al/Mn-3.no	1.7×10^{-2}	
2.5-Fe-1.no	1.3×10^{-2}	No trend
2.5-Fe-2.no	1.5×10^{-2}	
2.5-Fe-3.no	2.0×10^{-3}	
2.5-Al/Mn-1.no	1.6×10^{-2}	No trend
2.5-Al/Mn-2.no	2.0×10^{-2}	
2.5-Al/Mn-3.no	1.2×10^{-3}	

The g-values, including those prepared by dilution with oxalate during sequential oxalic acid strikes (e.g. 1-Fe-1.no, 1-Fe-2.no, 1-Fe-3.no, etc.) are similar, with some decreasing and others increasing but with an average value of around 1.6×10^{-2} M hr^{-1}. Further, the *g-values* for sequentially created slurries shows no general pattern consistent with scavenger dilution that results from each sequential digestion. As discussed above, the decrease in concentration of those scavengers present as part of the initial slurry composition (e.g. nitrite) with each digestion would be expected to lead to a net increase in *g-values*, the hydroxyl radical generation rates.

The fact that no such "scavenger dilution" trend is observed *in g-values* (i.e. Table 11 does not show an increase in g-values with sequential digestions) is good evidence that the effect of initial Table 11 scavengers (i.e. nitrite) on the oxalate decomposition rate is negligible – casting doubt upon whether metal-catalysed oxalate destruction at low pH is hydroxyl radical driven. The fact that no such "scavenger dilution" trend is observed in g-values in Table 11 is good evidence that the effect of initial scavengers (i.e. nitrite) on the oxalate decomposition rate is negligible – casting doubt upon whether metal-catalysed oxalate destruction at low pH is hydroxyl radical driven.

4.8.1.2 Ratio of Scavenger Reactions to Oxalate Decomposition

Based on Equation 4-20, the slope shown in Figure 36 and Figure 37 is mathematically equivalent to "$k_{OH\cdot}[scav_{OH\cdot}]/(g\text{-value}\times k_{OH\cdot})$." Multiplying this term by the applicable g-values in Table 11, then dividing by the applicable oxalate concentration results in $k_{OH\cdot}[scav_{OH\cdot}]/k_{OH\cdot}[C_2O_4^{2-}]$," which for simplicity is referred to as the "Hydroxyl radical scavenged fraction."

"Hydroxyl radical scavenged fraction" provides a comparison of the hydroxyl radicals lost to scavengers vs hydroxyl radicals consumed in the decomposition of oxalate. Values for the "Hydroxyl radical scavenged fraction" are provided by the second column in Table 12.

Table 12. Hydroxyl radical scavenged fraction.

Simulant decomposition test slurry	Hydroxyl radical scavenged fraction
1-Fe-1.no	4.0×10^{-2}
1-Fe-2.no	2.6×10^{-2}
1-Fe-3.no	1.9×10^{-2}
1-Al/Mn-1.no	5.7×10^{-2}
1-Al/Mn-2.no	4.4×10^{-2}
1-Al/Mn-3.no	7.6×10^{-2}
2.5-Fe-1.no	1.9×10^{-2}
2.5-Fe-2.no	4.6×10^{-3}
2.5-Fe-3.no	8.8×10^{-3}
2.5-Al/Mn-1.no	6.8×10^{-3}
2.5-Al/Mn-2.no	7.4×10^{-2}
2.5-Al/Mn-3.no	6.8×10^{-2}

Table 12 shows the calculated values for *Hydroxyl radical scavenged fraction. The value* provides a ratio of the rate of hydroxyl radical reactions with scavengers to the rate of hydroxyl radical reactions with oxalate. The values show that the hydroxyl scavenger losses early on in the process are very low, providing evidence that the decomposition of oxalate is not driven by hydroxyl radicals. If the process under acid conditions is genuinely an AOP, the rate of oxalate decomposition would be inhibited. Since however, the impacted is minimal, the evidence strongly suggests that the decomposition is not hydroxyl radical driven.

4.8.2 Possible Reaction Pathways

As previously discussed, decomposition of oxalate under acidic conditions may be initiated by simple oxidants, such as ozone, hydroxyl radicals (Beltrán *et al.*, 2005; Logager *et al.*, 1992; El-Raady and Nakajima, 2006; Zepp *et al.*, 1992; Grosse *et al.*, 1998; Ngadi *et al.*, 2006), or other radicals.

When studying ozonation, the decomposition of dissolved organics in aqueous media in the absence of catalysing metal ions is considered in terms of two reaction pathways:

1) A direct reaction with ozone vs reaction with a free radical intermediate (Beltrán *et al.*, 2005; Logager, 1992; El-Raady and Nakajima, 2006; Zepp *et al.*, 1992; Grosse *et al*., 1998; Ngadi *et al.*, 2006; Rodriquez, 2003; Hislop and Bolton, 1999; Zuo and Deng, 1997); or,
2) The indirect pathway which first includes the generation of the intermediate.

These two pathways were previously discussed as part of Figure 8. A second-order (Pines and Reckhow, 2002) mechanism are commonly accepted for both pathways with an overall reaction rate, r_{ox}, for the decomposition of organics (shown as oxalate) given by Equation 4-8 (Gottschalk *et al.*, 2000; Ketusky, 2015).

$$r = (k_{O3}[O_3] + k_{OH\cdot}[OH\cdot]) \times [C_2O_4^{2-}] \quad \text{(eq. 4-8)}$$

where $[C_2O_4^{2-}]$, $[O_3]$ and $[OH\cdot]$ represent the concentrations of oxalate, ozone, and hydroxyl radicals. In context, k_{O3} represents the rate parameter associated with the direct reaction of ozone with oxalate, and $k_{OH\cdot}$ represents the rate parameter associated with the reaction of hydroxyl radicals with oxalate.

4.8.3 Using Scavengers as an OH· Probe

Table 13 lists key constituents present in the *simulant decomposition test slurries* that could theoretically act as scavengers for ozone, the hydroxyl radicals, or both.

Table 13. Average rate constants[27] for ozone and hydroxyl radical scavengers at pH~7.

Scavenger	Rate constant with O_3 ($M^{-1}sec^{-1}$) (Neta *et al.*, 1988)	Rate constant with $OH\cdot$ ($M^{-1}sec^{-1}$) (Neta *et al.*, 1988)
Carbonate (CO_3^{2-})	1×10^{-1}	4×10^{8}
Bicarbonate (HCO_3^{-})	2×10^{3}	4×10^{7}
Chloride (Cl^{-})	1×10^{-3}	1×10^{6}
Nitrite (NO_2^{-})	4×10^{8}	1×10^{10}
Nitrate (NO_3^{-})	1×10^{-4}	5×10^{5}
Phosphate (PO_4^{3-})	1×10^{-4}	1×10^{7}
Sulfite (SO_3^{2-})	4×10^{5}	6×10^{9}

Instead of using the previously discussed hydroxyl radical detection/probe chemicals, it is reasoned that the already present hydroxyl scavenger(s) could be used as probe(s), where the absence of any anticipated decrease in the oxalate decomposition rate arising from the presence of known hydroxyl scavengers would strongly suggest that oxalate decomposition is not hydroxyl radical driven.

The two types of scavengers most applicable to this effort are carbonate/bicarbonate and nitrite, the former created as the result of oxalate decomposition – specifically from the CO_2 generated

[27] The rate constants, shown in Table 13, are supplied to support qualitative comparisons. Although the rate constants are known to be pH dependent (Zepp et al., 1992; Munter, 2001), reference values for the full set of the listed scavengers were found at a pH of 7 (Neta et al., 1988; Farhataziz and Ross; 1977). Since the oxalate decomposition in the ECC process is initiated at the initial pH value of around 2, it is important to understand that the rate constants for both ozone and hydroxyl radicals will be orders of magnitude lower when the initial pH is ~2 (i.e. the rate constants for both ozone and hydroxyl radical decrease with a decreasing pH).

as the result of oxalate decomposition, while nitrite is a constituent in the sludge. As such, both are present in the *simulant decomposition test slurries.*

Nitrite is considered the most significant anion type scavenger and considered for evaluation because:

1) Concentrations of chlorides, phosphates, and sulfites are strictly minimised within the SRS HLW process as part of the corrosion control program (HLW, 2009), while nitrite is not restricted, but is in fact deliberately added as part of the corrosion control process; and,
2) The rate constant for nitrite is significantly larger than the other anion scavengers with ozone and hydroxyl radicals, as was previously shown in Table 13.

Nitrite

Nitrite is a commonly identified scavenger for both hydroxyl radicals and ozone with published rate constants of 4×10^{8} $M^{-1}sec^{-1}$ and 1×10^{10} $M^{-1}sec^{-1}$ for reacting with ozone and hydroxyl radicals, respectively (Neta *et al.*, 1988; Farhataziz and Ross; 1977). Given that it is plentiful within both the SRS HLW Fe-rich and the Al/Mn-rich sludge, nitrite would be one of the most prominent initial scavengers, even potentially overwhelming the effects of other scavengers.

Because up to three sequential digestions occur during the creation of the simulant *decomposition test slurries*, the nitrite concentration associated with each sequentially created simulant decomposition test slurry decreases as the digestion sequence (value) increases (i.e. first from 1 to 2, and then from 2 to 3). With decreasing ozone scavengers, more hydroxyl radicals would be created. For example, the concentration of available hydroxyl radicals would increase when decomposing 2.5-Fe-2.no vs the previously decomposed 2.5-Fe-1.no, and again the concentration of hydroxyl radicals would increase when decomposing 2.5-Fe-3.no vs a

previously decomposed 2.5-Fe-2.no. This increase in available hydroxyl radicals would decrease in required ozonation times, meaning that 2.5-Fe-3.no would decompose faster than 2.5-Fe-2.no, which would decompose faster than 2.5-Fe-1.no.

The fact that such a decrease in required ozonation time is not observed from the increased dilution (in the previously shown Figure 19, Figures 19 and 20, and Figures 29 and 30), as summarized in Figure 38, provides substantial qualitative evidence that the hydroxyl radical pathway is not the major reaction pathway for the decomposition of oxalate during ozonation.

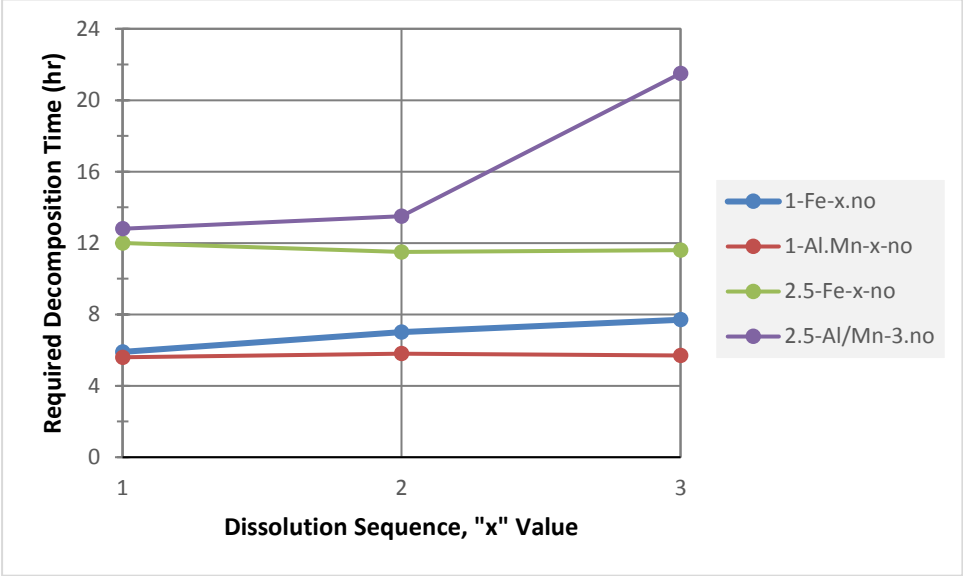

Figure 38. Required decomposition time to reach an oxalate concentration of 1.1×10^{-3} M for both the 1 wt% and 2.5 wt% simulant decomposition slurry series without UV.

Since nitrite is present (i.e., its concentration is 9.1×10^{3} mg/kg in the Fe-rich sludge simulant and 6.1×10^{2} mg/kg in the Al/Mn-rich simulant), relatively soluble, and has a large reaction rate constant for reacting with hydroxyl radicals, as previously shown in Table 13, the required slurry decomposition times should decrease when moving from the left to the right of Figure 36, should decrease. This is not observed. The fact that such a decrease in required ozonation time is not observed from the increased dilution (as previously shown in Figures 19 and 20,

and Figures 29 and 30), as summarised in Figure 38, provides substantial qualitative evidence that the hydroxyl radical pathway is not the major reaction pathway for the decomposition of oxalate during ozonation

Carbonate/Bicarbonate

Carbon dioxide is the primary product of the oxidative mineralisation of oxalate (Davis *et al.*, 2009; Zuo and Deng, 1997; Lagunova *et al.*, 2012; Minakata *et al*., 2011). Carbon dioxide readily dissolves in water, a process that becomes more favourable as pH increases with bicarbonate formation predominating at pH > 6.4 and carbonate formation predominating at pH > 10.3. Based on Table 13, both CO_3^{2-} and bicarbonate would act as major scavengers for hydroxyl radicals during the ozonation – their roles as scavengers becoming ever more important as oxalate destruction proceeds and both the amount of CO_2 generated and the pH of the *simulant decomposition test slurry* (and thus (bi)carbonate solubility) increases.

With the solubility of carbonate/bicarbonate exceeding that of ozone (Minakata *et al.*, 2011; Battino *et al.*, 1983; Glaze and Kang,1989), its effect could quickly dominate over the effects from all other scavengers, and in fact become proportional to the oxalate decomposition. In fact, when investigated by Olson and Barbier, 1994, it was concluded that carbonate would strongly inhibit TOC removal rates, while bicarbonate could wholly inhibit TOC removal (Battino *et al.*, 1983; Glaze and Kang, 1989). The fact that such an effect was not observed with all decomposition tests reaching an oxalate concentration of less than 1.1×10^{-3} M provides additional qualitative evidence that the hydroxyl radical pathway is not the major reaction pathway for the decomposition of oxalate in the slurries as the result of ozonation.

4.8.4 Scavenging Modelling

If the known to be present hydroxyl scavengers are shown to have negligible impact on the oxalate decomposition rate, the scavengers are acting similar to a hydroxyl radical probe, with the probe(s) showing that the oxalate decompositions are not radical driven, but instead likely a direct type of reaction of the ozone with the oxalate.

To better understand the effect of nitrites and carbonates/bicarbonates previously qualitatively discussed, and to attempt to quantify these effects, a mathematical model is constructed. In constructing the model, the primary chemical reactions associated with ozone and hydroxyl radical generation and the subsequent reactions leading to the decomposition of oxalate are identified, with associated mathematical equations developed. The overall goal is summarized in the following:

1) Develop a mathematical equation for the oxalate decomposition rate,

2) Enable the effects of the scavengers between the different *simulant decomposition test slurries* to be quantitatively compared.

Assuming an AOP (i.e. the decomposition of oxalate under acid conditions is driven by the concentration of hydroxyl radicals, with the direct reaction of oxalate with ozone assumed to be slow in comparison) allows for the direct reactions of oxalate with ozone to be discounted. This discounting of the direct reaction of oxalate with ozone can be assumed based on an estimated derived rate constant for ozone reacting with oxalate as low as 10^2 $M^{-1}s^{-1}$ at a near neutral pH (Hoigne and Bader, 1983b) vs that of the hydroxyl radical. The hydroxyl radical reacts with most organics at near neutral pH conditions ranging from 10^6 and 10^9 $M^{-1}sec^{-1}$ (Kasprzyk-Hordern et al., 2003). Therefore, from the decomposition test data, the associated oxalate

decomposition rate, "r" is estimated based on the calculated hydroxyl radical concentrations and measured oxalate concentrations.

4.8.5 Discussion and Results

4.8.5.1 Reactions

Ozone

The primary reaction schemes for O_3 as part of ozonation were previously shown in Figure 8. They include both direct and indirect ozonation. In addition, the reduced effectiveness from O_3 scavengers must be considered. Therefore, possible reactions for O_3 during the ozonation of oxalate under acid conditions can be summarised as including:

1) Direct reaction of O_3 with oxalate, as discussed in Section 3.5;

2) Direct reaction of O_3 with ozone scavengers, reducing overall decomposition effectiveness of the O_3, as discussed in Section 3.6; and,

3) The creation of hydroxyl radicals from the ozone, as discussed in Section 3.4.

Based on simplifications of Reactions 3-13 to 3-14, the creation of hydroxyl radicals can be shown as Reaction 4-1, with k_{O3} representing the effective rate constant for the catalytic creation of hydroxyl radicals from ozone reacting with a catalyst (in water).

$$O_3 + M^n \quad (+ H_2O) \xrightarrow{k_{O3}} M^{n+1} + OH\cdot + OH^- + O_2 \qquad (4\text{-}1)$$

Where the following definitions and common notation apply:

- O_3 refers to the ozone maintained in the *simulant decomposition test slurry*, whose

concentration will be a function of, *inter alia*, ozone sparged rate and solubility under prevailing conditions.

- k_{O3} is the rate constant for the direct reaction of O_3 with the applicable reactant, with metal catalysts. The subscript is used to aid/provide clarification when developing mathematical equations.

- M^n refers to the oxidation state dependent iron, manganese and nickel that act as catalysts.

In addition to the direct catalytic reaction of ozone with a metal to create hydroxyl radicals, Reaction 4-2 expresses the direct reaction of ozone with scavengers.

$$O_3 + scav_{O3} \xrightarrow{k_{O3}} scav_{O3}\text{-product} \qquad (4\text{-}2)$$

Where, $scav_{O3}$, refers to (direct) ozone scavengers and $scav_{O3}$-product refers to the product(s) created from reacting O_3 directly with the scavengers.

Although the direct reactions of ozone with metals catalysts likely vary based on the metal catalyst specifics, as evidenced by the many different non-AOP ozone to metal catalyst reactions discussed in Section 3.5, using a simplification of Reactions 3-35 through 3-37 as an example, allows for a direct ozone decomposition of oxalate reaction to be shown. See Reaction 4-3.

$$2O_3 + \ldots M^{2+}C_2O_4^{2-} \xrightarrow{k_{O3}} 2CO_2 + M^{2+} + 2O_3^{-} \qquad (4\text{-}3)$$

Where $C_2O_4^{2-}$ refers to the oxalate in the slurry, and CO_2 refers to the carbon dioxide generated by the decomposition of oxalate.

Hydroxyl Radicals

As part of assuming the decomposition process is an AOP, the reaction of hydroxyl radicals with oxalate ion is provided as an example and expressed as Reaction 4-4 (Yoon and Jeong, 2005).

$$OH\cdot + C_2O_4^{2-} \xrightarrow{k_{OH\cdot}} CO_2 + \cdot CO_2^- + OH^- \quad (4\text{-}4)$$

Where $k_{OH\cdot}$ refers to the rate constant for the reaction of OH· with the applicable reactant, in this case, oxalate. The reaction of the hydroxyl radicals with a scavenger (i.e. a hydroxyl radical lost to a scavenger) decreasing the hydroxyl radical effectiveness, as well as the overall ozone effectiveness is shown as Reaction 4-5.

$$OH\cdot + scav_{OH\cdot} \xrightarrow{k_{OH\cdot}} scav_{OH\cdot}\text{-product} \quad (4\text{-}5)$$

Where "$scav_{OH\cdot}$" refers to the hydroxyl radical scavengers and "$scav_{OH\cdot}$-product" refers to the product created from reactions of OH· with the scavengers.

4.8.6 Derivation of Equations

4.8.6.1 G-Value Basic Equation

Based on Reaction 4-1, the metal-catalysed hydroxyl radical generation rate, *g-value,* can be given as shown in Equation 4-10.

$$g\text{-}value = k_{O3}\,[O_3][M^n] \quad (\text{eq. } 4\text{-}10)$$

As previously discussed in Chapter 3, the mechanism of Equation 4-10, the process that this rate equation relates to, has been described by Pera *et al.*, 2000, and Sauleda and Brillas, 2001,

and, in the case of Fe^{2+} is commonly expressed using previously presented Reactions 3-13 and 3-14.

$$Fe^{2+} + O_3 \rightarrow FeO^{2+} + O_2 \quad (3\text{-}13)$$

$$FeO^{2+} + H_2O \rightarrow Fe^{3+} + OH\cdot + OH^- \quad (3\text{-}14)$$

A similar mechanism has been researched by Beltrán *et al.* for cobalt (Beltrán *et al.*, 2003a) and by Jacobsen *et al.* for manganese (Jacobsen *et al.*, 1998), indicative of its general applicability to the first-row transition metals – an observation of relevance to the results being considered here as the main constituents of the simulant decomposition test slurries being studied include Fe, Mn and Ni (e.g. see Figure 2). Also of relevance is the fact that both Reactions 3-13 and 3-14 are independent of pH; as test solution pH is principally controlled by the oxalic acid concentration as confirmed in Section 4.7, suggesting that the *g-value* is independent of the extent of oxalate destruction, allowing for the development of simplified kinetic analysis.

4.8.6.2 Simplified Oxalate Decomposition Rate for an AOP

As previously discussed, a second-order mechanism is commonly accepted for both the direct and indirect reaction pathways for the reaction of oxalate with ozone and hydroxyl radicals, respectively (Gottschalk *et al.,* 2000; Ketusky, 2015). In basic terms the, oxalate decomposition rate, r_{ox}, can either be the result of direct and indirect reactions with the O_3. This is shown in Equation 4-11:

$$r_{ox} = k_{O3}[O_3][C_2O_4^{2-}] + k_{OH\cdot}[C_2O_4^{2-}][OH\cdot] \quad \text{(eq. 4-11)}$$

The required oxalate decomposition time will be reciprocally related to the experimentally

observed rate parameter for oxalate decomposition (i/r_{ox} α required oxalate decomposition time).

As discussed in Section 4.8.2, instead of adding the previously discussed hydroxyl radical detection/probe chemicals, it was reasoned that the already present hydroxyl scavenger(s) could be used as probe(s), where the absence of any anticipated decrease in the oxalate decomposition rate arising from the presence of known hydroxyl scavengers would strongly suggest that oxalate decomposition is not hydroxyl radical driven. Therefore, for the sake of argument, an AOP driven reaction is assumed (i.e. as previously discussed in Section 4.8.3, the oxalate decomposition can be considered to be hydroxyl radical driven, with the goal of Section 4.8 to disprove this AOP reaction assumption). Therefore, as an assumed AOPs, where hydroxyl radicals are largely responsible for the decomposition, Equation 4-11 is simplified to Equation 4-12:

$$r_{ox} = k_{OH\cdot}[C_2O_4^{2-}]\,[OH\cdot] \qquad \text{(eq. 4-12)}$$

4.8.6.3 G-Value, Application of Steady State Analysis

Under steady state conditions, the rate of hydroxyl radical generation (i.e. g-value as defined by Equation 4-10) would also be equal to the combined hydroxyl radical reaction rate. That is, the hydroxyl radical reaction rate with oxalate plus the hydroxyl radical reaction rate with indirect scavengers "$scav_{OH\cdot}$" are also equal to the "g-value," resulting in the g-value expressed in indirect terms. This is shown in Equation 4-13:

$$g\text{-}value = k_{OH\cdot}[C_2O_4^{2-}][OH\cdot] + k_{OH\cdot}[scav_{OH\cdot}][OH\cdot] \qquad \text{(eq. 4-13)}$$

Where $k_{OH\cdot}[scav_{OH\cdot}]$ represents the equivalent of a kinetic rate parameter for the reaction of hydroxyl radicals with scavengers present in the slurry. Rearranging Equation 4-13 in terms of hydroxyl radical results in Equation 4-14:

$$[OH\cdot] = g\text{-}value / [k_{OH\cdot}[C_2O_4^{2-}] + k_{OH\cdot}[scav_{OH\cdot}]] \quad \text{(eq. 4-14)}$$

4.8.6.4 Ozone Cross-over Rate, Steady State Analysis

As stated in stated by Equation 4-10, the g-value is defined as the hydroxyl radical generation rate based on the catalytic reaction of O_3 with the metal catalysts. This O_3, however, is referring only to the O_3 in solution, not the O_3 created a gas. Therefore, a new term is introduced, that is the rate at which ozone crosses the gas/liquid interface during ozonation, R_{O3}. In addition, the pH is independent (and so oxalate concentration independent) of both of the following:

i. The rate of the metal-catalysed reaction of ozone with water to generate radicals; and,
ii. The rate of direct scavenging of O_3 by $scav_{O3}$.

Using these three facts, a steady state balance for the rate of ozone cross-over from gas to liquid equal to the rate ozone is used in creating hydroxyl radicals plus the loss of ozone due to direct scavengers is shown by Equation 4-15:

$$r_{ox} = k_{O3}[M^n][O_3] + k_{O3}[scav_{O3}][O_3] \quad \text{(eq. 4-15)}$$

Rearranging Equation 4-15 in terms of system ozone concentration results in Equation 4-16.

$$[O_3] = R_{O3} / [k_{O3}[M^n] + k_{O3}[scav_{O3}]] \quad \text{(eq. 4-16)}$$

4.8.6.5 G-Value including Cross-over

Upon substitution of the right side of 4-16 for $[O_3]$ back into Equation 4-10 (i.e. g-value = $k_{O3}[O_3][M^n]$), allows the rate hydroxyl radical generation, g-value, to be equated by Equation 4-17 (Ketusky, 2015).

$$g\text{-}value = R_{O3}\left[k_{O3}[M^n] \;/\; (k_{O3}[M^n] + k_{O3}[scav_{O3}])\right] \quad \text{(eq. 4-17)}$$

4.8.6.6 Oxalate Decomposition Rate, Accounting for G-value and Scavengers

Starting with Equation 4-12 (i.e. $r = k_{OH\cdot}[C_2O_4^{2-}][OH\cdot]$), and substituting in the right side of Equation 4-14 for [OH·] (i.e. $[OH\cdot] = \text{g-value}/[k_{OH\cdot}[C_2O_4^{2-}] + k_{OH\cdot}[scav_{OH\cdot}]$) enables the oxalate decomposition rate to be mathematically determined using indirect terms and the g-values, as shown in Equation 4-18.

$$r_{ox} = k_{OH\cdot}[C_2O_4^{2-}] \times \left[g\text{-}value \,/\, (k_{OH\cdot}[C_2O_4^{2-}] + k_{OH\cdot}[scav_{OH\cdot}])\right] \quad \text{(eq 4-18)}$$

Equation 4-18 is then re-arranged as Equation 4-19.

$$r_{ox} = \left(k_{OH\cdot}[C_2O_4^{2-}] / (k_{OH\cdot}[C_2O_4^{2-}] + k_{OH\cdot}[scav_{OH\cdot}])\right) \times g\text{-}value \quad \text{(eq 4-19)}$$

4.8.6.7 Oxalate Decomposition Rate, Direct, Indirect and Cross-Over Rate

Substituting the right side of Equation 4-18 (i.e. right side of "$\text{g-value} = R_{O3}[k_{O3}[M^n]]/[k_{O3}[M^n] + k_{O3}[scav_{O3}]]$") into Equation 4-19, allows the rate at which ozone crosses the gas/liquid interface to be mathematically included. It is noteworthy, that the resulting equation, Equation 4-20, represents the overall oxalate decomposition reaction rate equation. Equation 4-20 includes terms accounting for indirect oxalate decomposition, the direct generation of hydroxyl radical, both direct and indirect scavenger effects, as well as a term to account for the rate at which ozone crosses the gas/liquid interface.

$$r_{ox} = \left[k_{OH\cdot}[C_2O_4^{2-}] / (k_{OH\cdot}[C_2O_4^{2-}] + k_{OH\cdot}[scav_{OH\cdot}])\right] \times \left[R_{O3} \times k_{O3}[M^n] / [k_{O3}[M^n] + k_{O3}[scav_{O3}]]\right] \quad \text{(eq 4-20)}$$

Equation 4-20 shows that the presence of hydroxyl radical scavengers (i.e. $[scav_{OH\cdot}]$) will

decrease the oxalate decomposition rate, while the presence of ozone scavengers (i.e. [$scav_{O3}$]) will divert O_3 away from the catalytic reaction with metals that initiate the creation of radicals in the first place. In contrast, Equation 4-20 also shows that an increase in metal concentration [M^n] will lead to an increase in the overall oxalate decomposition rate.

It is highly likely there are two common possibilities associated with the hydroxyl radical scavenger. The first consideration is that the term "$k_{OH\cdot}[scav_{OH\cdot}]$" is dominated by one, possibly two scavenger species – specifically a single component associated with the sludge, e.g. nitrite (see Section 4.8.2.1) and carbonate (see Section 4.8.2.2). However, these effects are difficult to deconvolute and so "$k_{OH\cdot}[scav_{OH\cdot}]$" is treated as a lumped parameter. Equation 4-18 can then be rewritten in the slope-intercept form of a linear equation (i.e. y = mx + b), as shown in Equation 4-21:

$$1/r_{ox} = [(k_{OH\cdot}[scav_{OH\cdot}] \times g\text{-}value \times k_{OH\cdot}) \times [1/C_2O_4^{2-}]) + 1/g\text{-}value] \quad \text{(eq. 4-21)}$$

That is y is represented by "$1/r_{ox}$." The m, slope, is represented by the "($k_{OH\cdot}[scav_{OH\cdot}]$ × g-value × $k_{OH\cdot}$)." The x, as part of the slope-intercept form of a linear equation, is represented by the "[$1/C_2O_4^{2-}$])" and the b is represented by the "1/g-value."

4.8.7 Conclusion on Role of Hydroxyl Radicals

The results of the work in this section show that the effect of known scavengers such as nitrite and bicarbonate/carbonate on the oxalate decomposition rate can be used as a mechanistic probe for hydroxyl radicals at low pH.

It is found that the oxalate decomposition kinetics are largely unaffected by the concentration of these potential radical scavengers. In particular, the scavenging effects of oxalate mineralisation-derived carbonate are extremely small, demonstrating that, under acid conditions, the primary decomposition reaction of oxalate is not an AOP involving generated

hydroxyl radicals. Instead, it is most likely direct reaction, involving the reaction of ozone with metal-complexed oxalate – as described in Section 3.5 above and for the 2+ metal state shown by Reaction 4-9 though Reaction 4-12.

$$M^{2+} + C_2O_4^{2-} \leftrightarrow MC_2O_4 \quad (4\text{-}9)$$

$$MC_2O_4 + O_3 \rightarrow MC_2O_4^{+} + O_3^{-} \quad (4\text{-}10)$$

$$MC_2O_4^{+} \rightarrow M^{2+} + \cdot C_2O_4^{-} \quad (4\text{-}11)$$

$$\cdot C_2O_4^{-} + O_2, O_3, OH\cdot \rightarrow 2CO_2 + O_2^{-}, O_3^{-}, OH^{-} \quad (4\text{-}12)$$

Where:

M^{2+} = 2+ metals state of iron, manganese, or nickel.

Note: Metal can be in another oxidation state but is shown as 2+ to maintain reaction simplicity.

In summary, the most likely mechanism for the metal-catalysed, ozone-driven decomposition of oxalate in the slurries studied here can be considered a direct, non-AOP involving ozone attack on metal-complexed oxalate. Each metal ion within the slurry (e.g. Fe, Mn, Ni) will influence this catalysis to a different extent due both to their kinetics and prevailing solution conditions.

5. TESTING USING REAL HLW BASED SLURRIES

Based on the initial findings of Chapter 4, decomposition testing was conducted using slurries made from real HLW. An SRS Tank 5F sludge sample and a 12H sludge sample were digested to create the slurries.

Differing somewhat from the matrix used for creating the Chapter 4 simulant decomposition test slurries, the making of the slurries involved trice sequentially digesting the sludge samples using 2 wt% oxalic acids at 70ºC. Six test slurries were created, then sub-dividing to support the two UV light protocols performed as part of the decomposition testing.

Because of limitations associated with working in SRNL's shielded cells, ozonation was performed using only 5 wt% percent ozone. Because of power and cooling water limitations associated with the shielded cells, An LP UV light used for the real HLW test apparatus. Similar to simulant based testing, the temperature of the real HLW based slurries were maintained at 70ºC during decomposition testing. The system backpressure maintained on the real HLW slurries during decomposition testing was maintained at a slightly lower process backpressure of 1.5×10^5 Pa.

A comparison of the Simulant based decomposition test apparatus vs the HLW based decomposition test apparatus is provided in Table 14.

Table 14. Comparison of key aspects of the *Simulant Based Test Apparatus* vs the *HLW Based Test Apparatus.*

Attribute	Simulant Based	Real HLW Based
Nominal decomposition test apparatus volume	60 L	3.2 L
Back Pressure	1.7×10^5 Pa	$1.5\text{x}10^5$ Pa
Ozone concentration	10 wt%	5 wt%
Acid concentrartion	1 wt% and 2.5 wt%	2 wt%
UV light (when used)	MP 1.5 KW	LP 400 W
Recirculation rate	40.3 litres/minute	5.7 litres/minute

As further discussed in Section 5.3, under the clean UV light protocol, decomposition testing of the third sequentially created slurry from Tank 5F and Tank 12H sludge was not tested.

5.1 Purpose/Goals

Because of the safety and size limitations associated with performing experiments using real HLW, the goals of the testing were limited to confirming that the *real HLW based slurries* would have similar behaviour to the *simulant decomposition test slurries*. Specifically, the primary goal of the HLW based decomposition testing is to confirm that the oxalate could be decomposed to a concentration of $< 1.1\times10^{-3}$ M using ozone, in an industrial relevant timeframe (i.e. less than 24 hours). In addition, the use of pH as a measure remaining oxalate was also investigated.

5.2 Making of the Real HLW Based Slurries

5.2.1 Real HLW Sludge Samples

With Tank 5 being in F-Area, the Tank 5 sludge being Fe-rich. The waste was generated from the PUREX process. Tank 12 is in H-Area, with the Tank 12 sludge being Al/Mn-rich. The waste was generated from the SRS HM process.

Both the Tank 12 and Tank 5 sludge characterisations were previously performed (Martino and King, 2011) and were not re-analysed as part of this effort, but simply restated. The characterisation of sludge constituents measured in terms of mg/kg, with their associated method of determination, are summarised in Table 15, while those measured in terms of dpm/gram, with their corresponding method of determination, are summarised in Table 16 (Martino *et al.*, 2011).

Table 15. Characterisation of real HLW sludge constituents measured in terms of mg/kg used for making real HLW based slurries.

Element/ analyte	Method	Tank 5F Fe-rich sludge (mg/kg)	Tank 12H Al/Mn-rich sludge (mg/kg)
Ag	ICP-ES	< LOD	8.91×10^{1}
Al	ICP-ES	1.64×10^{4}	2.62×10^{5}
Ba	ICP-ES	1.63×10^{3}	5.09×10^{2}
Ca	ICP-ES	4.57×10^{3}	3.29×10^{3}
Cd	ICP-ES	8.00×10^{1}	< LOD
Ce	ICP-ES	2.29×10^{3}	8.39×10^{2}
Co	ICP-ES	2.29×10^{2}	< LOD
Cr	ICP-ES	4.77×10^{2}	2.31×10^{2}
Cu	ICP-ES	4.62×10^{2}	5.51×10^{2}
Fe	ICP-ES	3.62×10^{5}	4.52×10^{4}
Gd	ICP-ES	< LOD	1.645×10^{2}
K	ICP-ES	6.62×10^{2}	3.27×10^{3}
La	ICP-ES	9.98×10^{2}	4.00×10^{2}
Li	ICP-ES	$4.38\times10^{28.06}$	1.12×10^{2}
Mg	ICP-ES	5.88×10^{2}	1.14×10^{3}
Mn	ICP-ES	6.68×10^{4}	2.81×10^{4}
Mo	ICP-ES	1.66×10^{2}	< LOD
Na	ICP-ES	3.37×10^{4}	4.23×10^{4}
Ni	ICP-ES	3.60×10^{4}	4.62×10^{3}
P	ICP-ES	< LOD	7.58×10^{2}
Pb	ICP-ES	3.89×10^{2}	< LOD
Si	ICP-ES	8.07×10^{3}	2.66×10^{3}
Sr	ICP-ES	7.80×10^{2}	2.16×10^{2}
Th	ICP-ES	< LOD	1.55×10^{2}
Ti	ICP-ES	1.99×10^{2}	1.08×10^{2}
U	ICP-ES	7.88×10^{4}	6.00×10^{3}
Zn	ICP-ES	2.45×10^{2}	3.43×10^{2}
Co	ICP-MS	2.21×10^{2}	2.73×10^{1}
Hg	CVAA	6.95×10^{2}	1.85×10^{4}
Pb	ICP-MS	374	30.7
Th-232	ICP-MS	10.4	15,200
U-233	ICP-MS	NR	11.1
U-234	ICP-MS	6.06	10.3
U-235	ICP-MS	490	96.3
U-236	ICP-MS	25.4	13.3
Np-237	ICP-MS	51.1	13.5
U-238	ICP-MS	7.90×10^{4}	5.20×10^{3}
Pu-239	ICP-MS	103	202
Pu-240	ICP-MS	8.69	21.6

Note: LOD refers to the level of detectability, while NR refers to not recorded.

Table 16. Characterisation of real HLW sludge constituents measured in terms of dpm/gram used for making real HLW based slurries.

Key radionuclide concentrations	Detection method	Tank 5F HLW sludge (dpm/gram)	Tank 12H HLW sludge (dpm/gram)
Pu-238	PuTTA	4.04×10^{6}	7.18×10^{8}
Pu-239/240		2.04×10^{7}	3.06×10^{7}
Co-60	gamma scan	1.74×10^{7}	4.42×10^{5}
Cs-137		2.39×10^{9}	2.48×10^{8}
Eu-154		2.52×10^{7}	3.15×10^{8}
Am-241		9.69×10^{7}	3.90×10^{7}
Sr-90	Sr-90 LS	7.81×10^{10}	2.04×10^{10}
Am-243	Am/Cm*	5.79×10^{5}	3.53×10^{4}
Am-242m		1.89×10^{5}	2.83×10^{4}
Cm-242		1.57×10^{5}	2.34×10^{4}
Cm-244		5.297×10^{6}	1.03×10^{6}

Note: *Am/Cm – is a separation and measurement method developed by SRNL.

5.2.2 Digesting Sludge to Make Real HLW Based Slurries

Using 48.1 grams of Tank 12H and 65.1 grams of Tank 5F real HLW sludge, three sequential digestions of the sludge were performed using 3.2 litres of 2 wt% oxalic acid solution at 60ºC (i.e. using 3.2 litres of 2 wt% oxalic acid for each of the three sequential digestions).

The total percent of the sludge that was removed after completion of the 3rd sequential digestion is shown in Table 17, with "removal" including both digestion of soluble components and partial transfer of insoluble solids. Each of the first real HLW sludge sample sequential digestions efforts lasted approximately 12.1 hours, with sequential digestion 2 and 3 both constrained to eight hours. Thus, the real HLW based slurry decomposition process no longer emulates the planned ECC process. In the planned field use of the ECC process, the in-tank digestion process would effectively be a minimum of one day as the waste tank inventory will be fed in small batches to the ECC process (Martino and King, 2011).

The final percent mass removed as the result of the three sequential digestions of real HLW Sludge using 2 wt% oxalic acids, resulting in the real HLW based decomposition slurries are summarised in Table 17.

Table 17. Percent mass removed resulting from three sequential digestions of real HLW sludge using 2 wt% oxalic acid.

Metal	Starting Mass of Tank 12H sludge (mg)	% Mass removed after 3rd digestion of Tank 12H sludge	Starting Mass of Tank 5F sludge (mg)	%Mass removed after 3rd digestion of Tank 5F sludge
Iron	2.36×10^{4}	78%	2.17×10^{3}	75%
Aluminium	1.07×10^{3}	46%	1.26×10^{4}	95%
Manganese	4.35×10^{3}	95%	1.35×10^{3}	90%
Nickel	2.34×10^{3}	68%	2.22×10^{2}	69%
Thorium	2.34×10^{3}	37%	7.46	16%
Strontium	5.08×10^{1}	79%	10.40	92%
Uranium	2.34×10^{3}	99%	2.89×10^{2}	99.9%
Plutonium	7.23	62%	9.72	87%
Total Mass	3.89×10^{4}	73%	1.67×10^{4}	80%

As shown above in Table 17, the result of three sequential digestions showed an approximate 73% mass removed of Tank 12H solids, while the result of three sequential digestions showed an approximately 80% mass removed for Tank 5F.

Residuals remaining at the conclusion of digestion testing using the Tank 12H sludge were primarily aluminium (90% of the mass as boehmite) with small amounts of iron and manganese. Residuals remaining at the conclusion of digestion testing using the Tank 5F sludge were primarily iron (66% of the mass as hematite) with small amounts of manganese and nickel.

Table 18 shows the characterisation of the each of the initial *real HLW based test slurries* in terms of its concentrations of key first-row transition elements and pH.

Table 18. Characterisation of initial *real HLW decomposition slurries* before decomposition/ozonation.

Slurry Name	pH	C_2O_4 (M)	Fe (M)	Mn (M)	Ni (M)
2-Al/Mn-1.no	2.34	9.15E-2	7.93E-3	5.84E-3	1.53E-4
2-Al/Mn-2.no	2.01	1.70E-1	3.53E-5	1.82E-3	2.81E-4
2-Al/Mn-3.no	1.90	3.29E-1	1.34E-3	3.33E-7	2.33E-4
2-Fe-1.no	2.2	4.26E-2	4.87E-2	1.60E-2	7.45E-4
2-Fe-2.no	1.27	1.18E-1	2.54E-2	3.19E-3	2.68E-4
2-Fe-3.no	1.20	1.83E-1	1.46E-2	1.48E-3	1.74E-4
2-Al/Mn-1.clean	1.65	3.22E-2	6.543E-3	4.57E-3	2.78E-4
2-Al/Mn-2.clean	1.13	9.70E-2	2.45E-3	7.97E-4	3.50E-5
2-Fe-1.clean	1.35	1.59E-1	1.83E-2	5.13E-3	3.87E-5
2-Fe-2.clean	1.11	1.14E-1	1.20E-2	3.59E-4	3.61E-4

5.3 Test Apparatus for Real HLW Based Slurries

Figure 39 shows the *Real HLW Oxalate Decomposition Test Apparatus*. A distribution on how the test apparatus operates is supplied immediately following Figure 39. The associated equipment list, including vendor model numbers, and additional design details provide in Appendix 4.

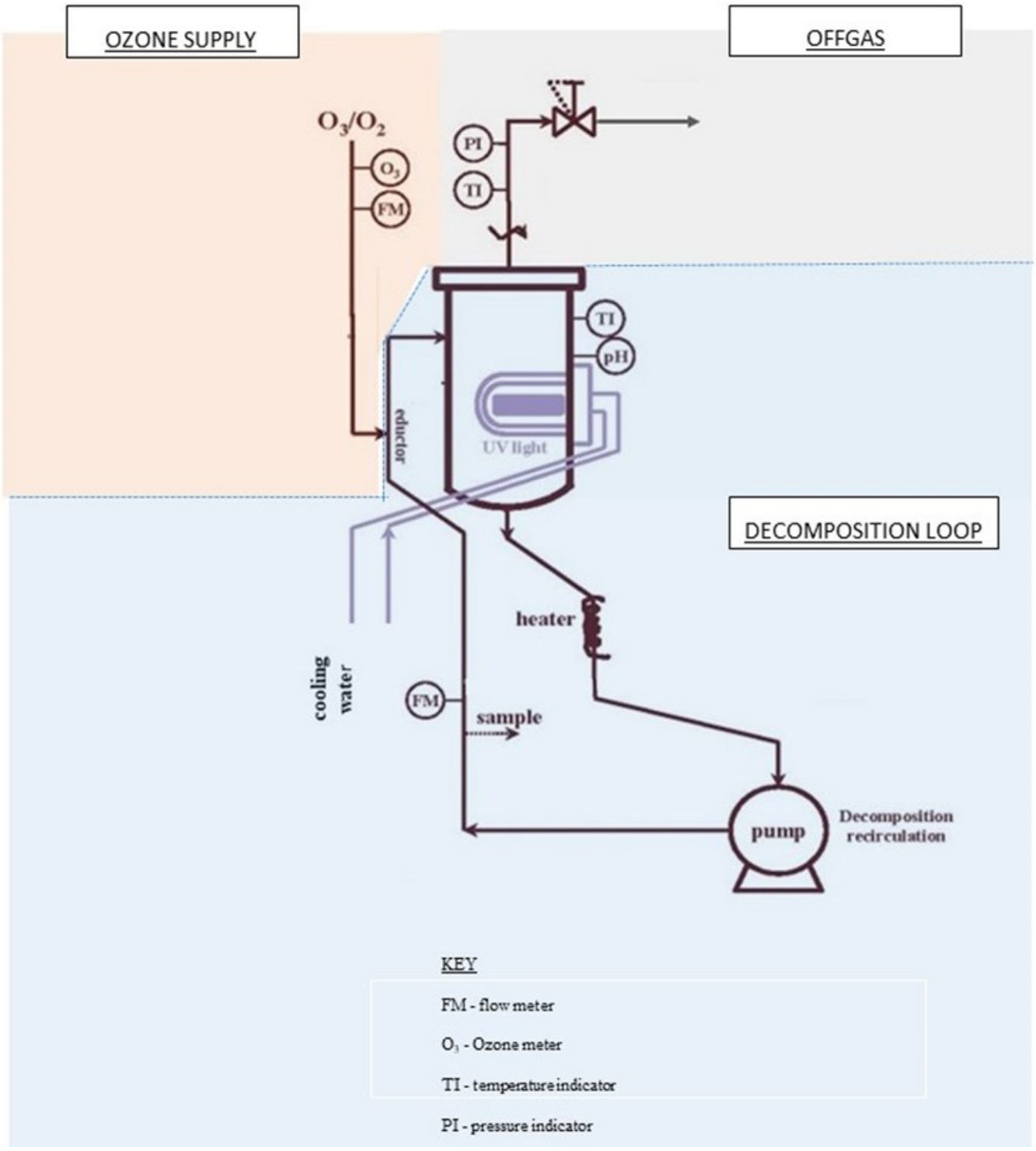

Figure 39. Simplified Schematic of the *Real HLW based Slurry Decomposition Test Apparatus.*

EQUIPMENT AND PIPING

Ozone Supply

- *Ozone Generator* supplying approximately 13 gram/hour ozone, air cooled, containing an *Integrated Oxygen Concentrator*.
- *Flow meter* – for measuring gas flowrate from the ozone generator.
- *Ozone Monitor* confirms the concentration of ozone from the ozone generator before entering decomposition loop.

Decomposition Unit

- *Sample Port* used for withdrawing samples from decomposition loop.
- *Eductor* used for injecting ozone gas into the recirculated slurries
- *Decomposition Vessel is self*-made from schedule 80 ss pipe. Vessel Contains:
  - *pH Probe* to monitor pH of the slurry in decomposition loop.
  - *Thermocouple* used to monitor the temperature in decomposition loop.
  - *UV Lamp Sheaths* protects UV lamp and allows for cooling.
  - *Cooling Water* supplied to UV quartz sheath.
  - *UV Light* - LP UV light.
- *Ceramic Rectangle Heaters used* to maintain the temperature of decomposition loop at approximately 70±5ºC.
  - *Recirculation Pump* - pump used to maintain decomposition loop slurry flowrate at approximately 5.7 litres/minute.

- *Flow meter* – used for measuring flowrate in slurry decomposition loop.

Offgas

- *Back Pressure Regulator* used for maintaining system backpressure.

5.4 Decomposition Testing

Sludge (48 to 63 grams) was trice digested using 3.2 litres of recirculated 2 wt% oxalic acid, heated to 70°C. The first sequential digestion lasted for approximately 12 hours, with each the 2nd and 3rd lasting approximately eight hours each. The *real HLW test slurries* made from the two HLW sludge samples were fed to the *Decomposition Module*. With the *Decomposition Module* containing the *real HLW test slurries*, it was recirculated and heated to 70°C with ozone was injected into the slurry through the eductor. Operation of the test apparatus continue until the fluid pH, and the sample analysis indicates that the oxalate concentration is less than 1.1×10^{-3} M.

An ozone generator located outside of the shielded cells (i.e. behind the cells) provided 2 litres/minute of 5 wt% O_3 in O_2 with a backpressure maintained at 1.5×10^5 Pa. The oxalic acid decomposition was performed under mostly a no UV light protocol, but also included limited clean UV light testing.

The use of *real HLW waste based slurries* limited the scale-down of the test, with the *Decomposition Module* being between 1:2400 and 1:3000 of the scale when compared to the volume of the planned field implementation (Ketusky, 2009; Ketusky and Subramanian, 2012).

During ozonation/decomposition testing, samples were periodically withdrawn from the test apparatus using the sample port. Soluble fractions of each sample were quantified by the filtrate that passed through 0.45-micron nylon filters. Sample preparation for soluble fraction analysis was by dilution in 3 M nitric acid, and preparation for bulk or insoluble fraction analysis

involved digestion by aqua regia. Analysis of metals concentrations were performed using ICP-ES.

The two real HLW sludges used in this testing represent the two main types of waste sludge in the SRS Tank Farm. The Tank 5F sludge sample is from the heel of sludge remaining after bulk waste removal from an F-Area PUREX waste tank, thus being the Fe-rich sludge. The Tank 12H material is sludge contained in slurries sampled during bulk waste removal in an H-Area HM waste tank, thus being an Al/Mn-rich sludge. The primary component of Tank 5F material is iron (as hematite), and the primary component of Tank 12H material is aluminium (as boehmite) (Hay *et al.*, 2008).

For real HLW, both oxalic acid decomposition of the subsequent slurries was performed. Similar to Chapter 4 simulant based testing, decomposition of the real HLW slurries was performed using both the clean UV protocol and no UV protocol. Differing from Chapter 4, no decomposition testing was performed using the fouled UV lamp protocol. For simplification, the applicable UV light protocol terminology used for real HLW will follow similar notation as that used for the simulant based slurries in Chapter 4. That is, the applicable UV light protocols for real HLW based slurries are termed “clean,” “no,” and “fouled,” without a “fouled” UV protocol test performed on real HLW based slurries.

However, the slurries made for clean UV light decomposition testing were stored/aged an additional six months before decomposition. In addition, in the clean UV light protocol, the slurries associated with the 3rd digestion sequence could not be tested because of issues tied to extended long-term outages in the shielded cell facility.

5.4.1 Results and Discussion

Oxalate decomposition testing was performed on the *real HLW test slurries* created from the digestion of sludge from Tanks 12H and 5F by application of 5 wt% ozone at a pressure of 1.5×10^5 Pa at 70°C with clean UV and no UV. The decomposition data for each of the *real HLW based slurries*, as recorded during the testing is contained in Table 44 through 46 of Appendix 5.

Table 19 records the measured soluble components of Tank 12H slurries during decomposition without UV, while Table 20 shows the same for Tank 5F slurries. Table 21 records the measured soluble components of Tank 12H slurries during decomposition with maintained clean UV light, while Table 22 shows the same for Tank 5 F.

Table 19. Measurement of soluble components of Tank 12H slurries during decomposition without UV light.

Simulant decomposition test slurry	Time (hour)	pH	Oxalate (M)	Fe (M)	Mn (M)	U-238 (M)
2-Al/Mn-1.no	0	2.34	9.15E-2	7.93E-3	5.84E-3	3.39E-4
	1.1	3.5	1.69E-2	6.48E-5	7.10E-6	2.68E-4
	4.6	7.3	4.54E-3	6.07E-6	1.81E-5	1.07E-4
	7.6	8.4	5.44E-4	8.90E-6	5.82E-5	1.42E-4
2-Al/Mn-2.no	0	2.0	1.70E-1	3.51E-3	1.82E-3	9.79E-5
	3.5	2.2	3.27E-2	4.73E-3	2.69E-3	1.20E-4
	6.8	6.0	8.09E-3	2.01E-4	5.95E-5	8.78E-5
	10.8	8.7	5.66E-4	9.87E-6	3.80E-5	1.11E-5
2-Al/Mn-3.no	0	1.9	3.29E-1	1.34E-3	3.33E-7	1.72E-5
	4.2	2.1	1.02E-1	3.00E-3	1.00E-6	5.34E-5
	8.5	4.0	1.18E-2	1.70E-3	8.78E-7	4.79E-5
	10.3	6.2	3.31E-3	1.29E-5	5.63E-7	2.87E-5
	12.5	8.1	7.09E-4	1.27E-5	2.87E-5	1.06E-7

Table 20. Measurement of soluble components of Tank 5F slurries during decomposition without UV light.

Simulant decomposition test slurry	Time (hour)	pH	Oxalate (M)	Fe (M)	Mn (M)	U-238 (M)
2-Fe-1.no	0	2.2	4.26E-2	4.87E-2	1.60E-2	1.74E-1
	2.5	NR	3.56E-3	1.52E-2	1.32E-2	1.50E-1
	5.1	NR	7.40E-3	9.78E-4	3.28E-4	8.15E-2
	9.7	NR	1.01E-3	9.81E-5	8.39E-5	3.11E-2
	10.9	NR	8.88E-4	9.10E-5	3.11E-2	3.10E-2
2-Fe-2.no	0	1.3	1.18E-1	2.54E-2	3.19E-3	1.72E-1
	3.5	3.2	1.02E-2	1.48E-2	5.24E-3	3.01E-1
	5	6.4	4.59E-3	6.45E-5	8.76E-6	1.32E-1
	7.6	8.5	9.32E-4	8.22E-5	3.17E-5	1.86E-2
2-Fe-3.no	0	1.2	1.83E-1	1.46E-2	1.48E-3	1.31E-1
	3.3	1.5	1.09E-3	2.60E-2	2.84E-3	3.62E-1
	5.8	2.7	1.06E-3	1.33E-2	2.86E-3	2.62E-1
	7.3	6.5	1.08E-3	8.04E-5	4.24E-6	8.45E-2
	8.6	7.8	9.07E-4	3.08E-5	8.45E-2	2.70E-3

Table 21. Measurement of soluble components of Tank 12H slurries during decomposition with maintained clean UV.

Simulant decomposition test slurry	Time (hour)	pH	Oxalate (M)	Fe (M)	Mn (M)	U-238 (M)
2-Al/Mn-1.clean	0	1.7	3.22E-1	6.54E-3	4.57E-3	2.78E-4
	1.2	3.1	8.68E-2	5.51E-3	4.33E-2	2.59E-4
	2.5	4.0	6.86E-2	1.70E-4	3.91E-5	2.02E-4
	5.0	6.0	1.61E-2	8.67E-5	1.30E-5	1.58E-4
	7.9	8.0	1.51E-3	8.83E-6	3.69E-5	1.31E-5
2-Al/Mn-2.clean	0	1.1	9.70E-2	2.45E-3	7.97E-4	3.50E-5
	1.3	1.3	3.07E-2	2.35E-3	7.70E-4	3.10E-5
	3.4	2.7	4.07E-3	8.95E-5	3.11E-5	1.82E-5
	4.4	4.2	1.02E-3	7.70E-6	4.40E-6	1.88E-7
	6.4	6.3	1.14E-3	1.16E-5	4.93E-6	2.11E-7

Table 22. Measurement of soluble components of tank 5F slurries during decomposition with maintained clean UV.

Simulant decomposition test slurry	Time (hour)	pH	Oxalate (M)	Fe (M)	Mn (M)	U-238 (M)
2-Fe-1.clean	0	1.4	1.59E-1	1.83E-3	5.13E-3	5.63E-1
	0.7	2.5	5.15E-2	1.37E-3	4.44E-3	1.77E-1
	1.4	4.1	3.18E-2	1.92E-4	6.90E-4	3.50E-2
	2.1	6.1	2.26E-2	2.60E-4	6.70E-4	3.73E-2
	5.5	8.5	1.07E-3	6.09E-5	3.44E-5	2.20E-2
2-Fe-2.clean	0	1.1	1.14E-1	1.20E-3	3.59E-4	1.51E-1
	1.2	3.1	5.34E-3	1.10E-3	2.49E-4	1.45E-1
	1.6	4.9	2.23E-3	9.78E-5	3.48E-5	1.45E-1
	2.0	6.7	1.07E-3	2.90E-5	4.64E-6	3.17E-2
	4.5	8.4	1.09E-3	4.87E-5	9.03E-6	3.17E-2

Oxalate decomposition to a concentration of 1.1×10^{-3} M with clean UV light was accomplished in less than 8.5 hours with the aid of UV, with clean UV light appearing to speed up the oxalate decomposition. However, in all cases, oxalate decomposition was completed, well before approaching 24 hours. As such, it is obvious that clean UV light is not required to result in oxalate decomposition being complete on an industrial significant time scale (i.e. less than 24 hours).

Figures 39 through 42 show both the oxalate concentration and pH vs ozonation time for the different slurries under maintained clean UV light and no UV light.

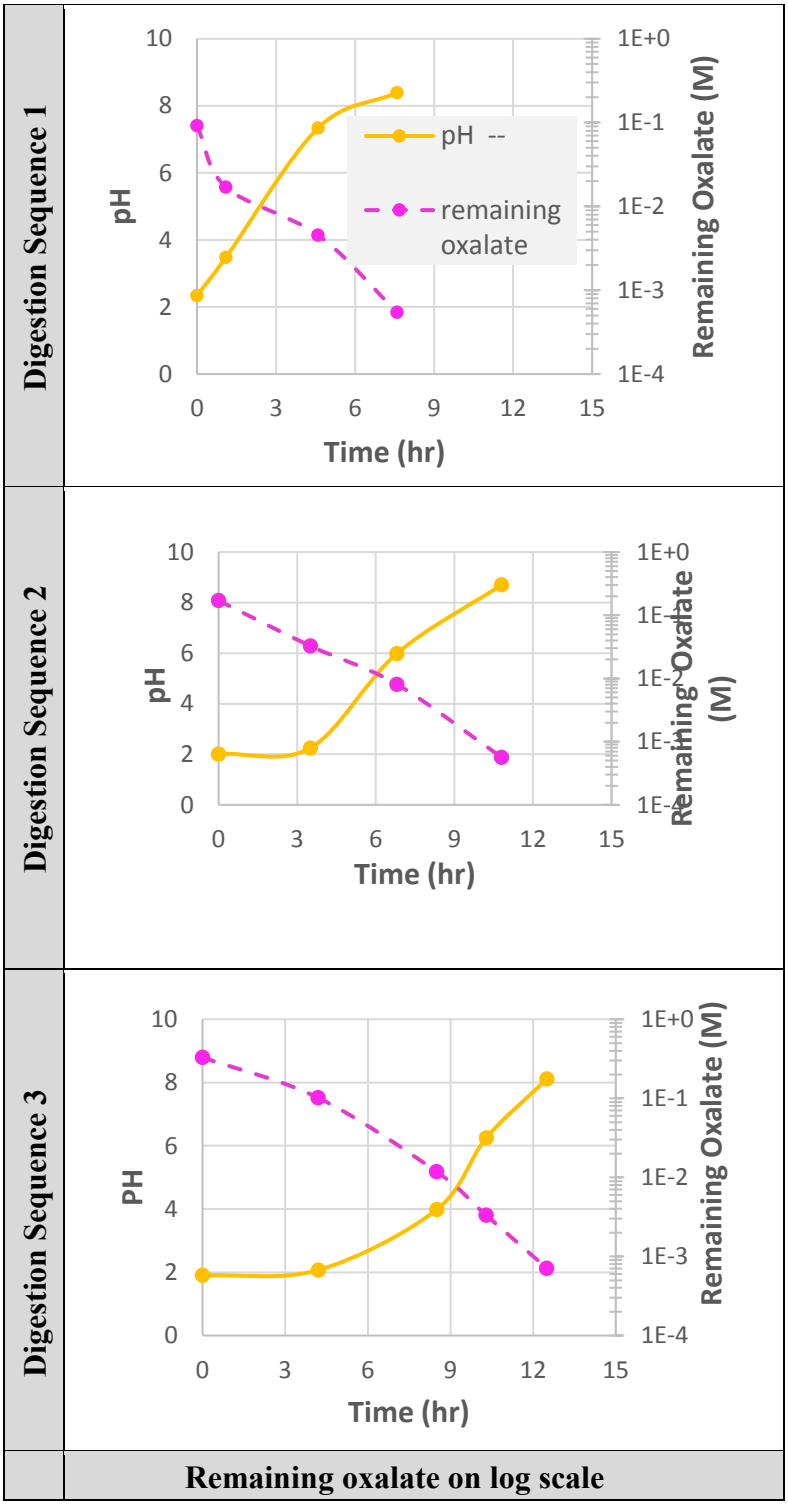

Figure 40. Oxalate remaining and pH vs ozonation time for 2-Al/Mn-x.no slurries

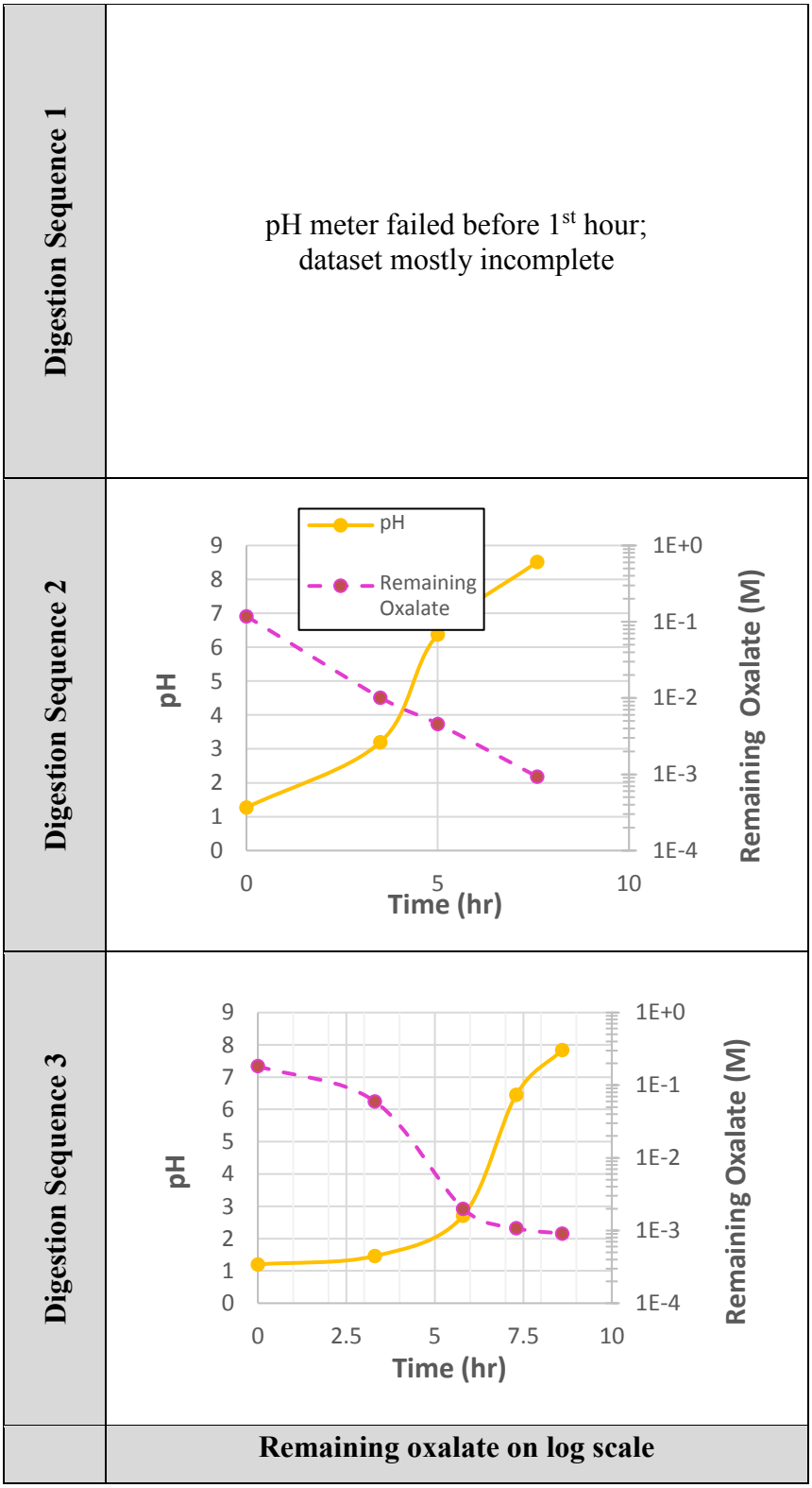

Figure 41. Oxalate remaining and pH vs ozonation time for 2-Fe-x.no slurries.

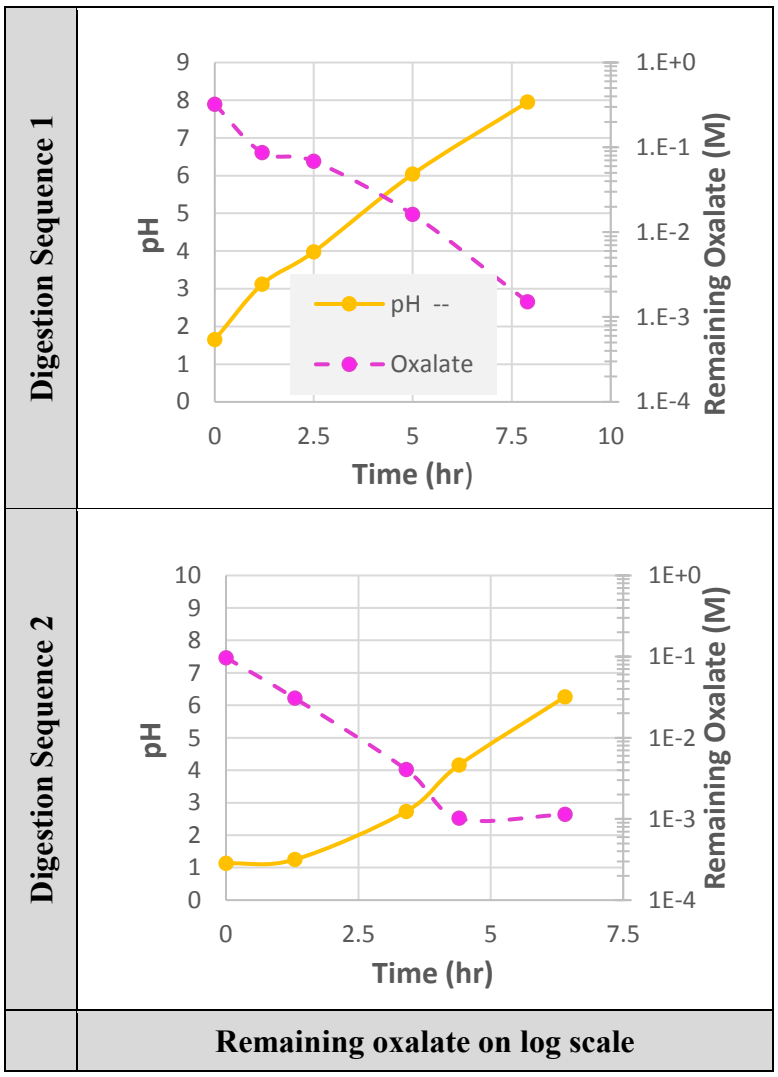

Figure 42. Oxalate remaining and pH vs ozonation time for 2-Al/Mn.clean slurries.

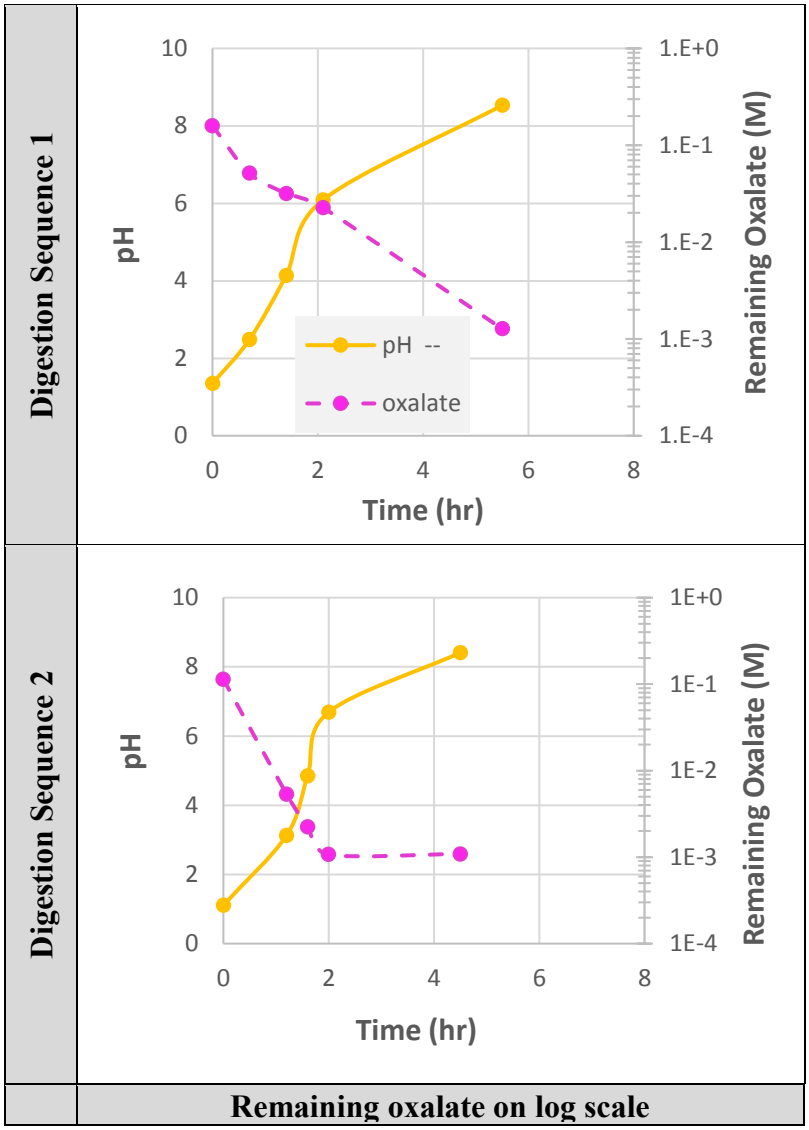

Figure 43. Oxalate remaining and pH vs ozonation time for 2-Fe-x.clean slurries.

As seen in Figures 39 through 42, the real HLW decomposition testing resulted in the same types of similarities between pH vs oxalate concentration, both as a function of ozonation time.

Figure 43 shows the pH curves vs time curves for the three sequential digestions conducted for 2-Al/Mn-x.no; however, the other tests obtained similar results.

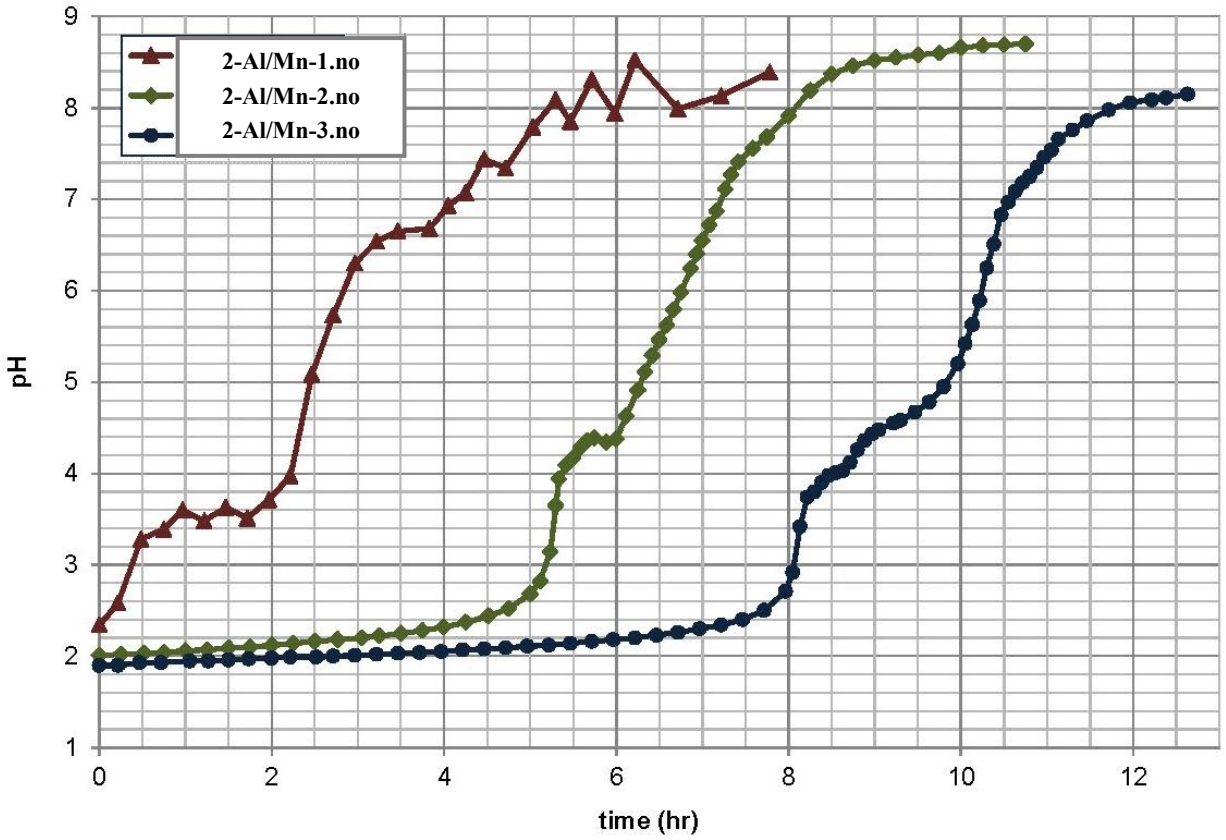

Figure 44. Measured pH change during oxalate decomposition process for Tank 12H slurries without UV (i.e. 2-Al/Mn-x.no).

As seen from Figure 44, the subsequent batch required longer oxalate decomposition times. The longer required decomposition times are likely due to the higher starting pH, and the possibly lower soluble oxalate content in the earlier dissolved sludge batches.

As described in Chapters 3 and 4, several metals present in SRS sludge have been shown to catalyse ozone and photochemical reactions for the decomposition of organics (Al-Raady and Nakajima, 2006; Zepp et al., 1992; Beltrán et al., 2005; Pines and Reckhow, 2002; Logager 1992). Also, the pure 2 wt% oxalate decomposition where the "slurry" was pure oxalic acid solution (i.e. did not contain metals) required the longest decomposition time (i.e. 14 hours).

All decomposition datasets from the simulant and real slurries, as well as only pure oxalic acid (with no sludge), are contained in Appendix 5.

The sampling frequency of each test was based on the observed changes the pH. Samples taken at short times exhibit the highest solubility of many metal components – presumably due to the low pH values/high acidities in such samples. Samples taken at long decomposition times, i.e. from near to the end of the decomposition process, typically had the lowest soluble level of sludge components, indicating that sludge precipitates as the oxalate decomposes and the pH increases.

During Real HLW slurry decomposition testing without UV, every 4 moles of ozone fed to the *Decomposition Module* decomposed 1 mole of oxalate. This molar ratio was higher than the 3:1 ozone to oxalate ratios attained during the simulant based testing detailed in Chapter 4 (Ketusky and Subramanian, 2012). All of the ozone can be assumed to have reacted since the half-life of ozone in water at a pH of approximately 7, at 35ºC, is 8 minutes (Lenntech, 2017). The less efficient utilisation of ozone in the HLW testing may be due to several factors. The ozone generator was located an extended distance from the apparatus in the shielded cells, potentially allowing a portion of the ozone to decompose before introduction to the decomposition module (e.g., ozone is known to decompose into oxygen). This distance resulted in some ozone feed conditions being lower than the process baseline conditions developed using simulants, including the in-stream concentration of ozone (5 wt% vs the baseline 10 wt%) and feed pressure 1.5×10^5 Pa vs the Chapter 4 simulant based test pressure of 1.7×10^5 Pa. This lower backpressure means that the concentration of ozone maintained in solution was less than that used for the simulant testing.

5.5 Conclusions from Real HLW Testing

During real HLW based slurry testing, the introduction of ozone was successful in decomposing oxalate to below the target levels. The results from these tests confirm observations made during the larger scale testing with waste simulants described in Chapter 4 (Ketusky and Subramanian, 2012). This real HLW based slurry decomposition testing, however, had a decreased utilisation of ozone, requiring approximately 4 moles of ozone per mole of oxalate decomposed.

Decomposition of oxalates in sludge dissolved in 2 wt% oxalic acids to levels near 100 ppm / 1.1×10^{-3} M oxalate using required 8 to 12.5 hours with no UV, and 4.5 to 8 hours with maintained clean UV, both showing that oxalate decomposition could be achieved, even without UV, in an industrial relevant timeframe.

The pH was tracked during decomposition testing, showing a correlation between remaining oxalate concentration (i.e. in terms of -log[M]) and pH. Soluble Fe, Mn, and Ni were tracked during oxalate decomposition, showing the highest soluble levels in the initially dissolved sludge and early decompositions, and exhibit lower soluble levels as oxalate decomposition progressed.

6. CONCLUSIONS AND RECOMMENDATIONS

The impact from the application of the Historical Baseline Chemical Cleaning Process was quantified. With the only two removal paths for waste out of the tank farm being vitrification and salt processing, and the typical sodium and hydroxide concentrations well-known throughout the process, and the very limited solubility of sodium oxalate, a model was constructed to determine the fate of the oxalate.

The model was built primarily using OLI Stream Analyser® to estimate the chemical speciation associated with reactions within the tank farm and the additional feed to vitrification. The vitrification feed batch additional washing required to meet waste acceptance criteria and the associated volumetric impacts on salt processing were then determined using a simple sodium dilution/washing models.

Results of the model show that regardless of the chosen oxalate handling strategies (i.e. add the formed sodium oxalate solids to a pre-washed sludge batch to minimise the additional required washing, or combine the sodium oxalate solids with an unwashed batch then wash, the following are required:

1) Significant additional washing to decrease sodium concentration and solid sodium oxalate loading of the vitrification feed, required to support glass quality; and,

2) Copious volumes of Future Additional Feed for salt Processing would be created from dissolving the oxalates precipitates that would form in the evaporator system salt heels.

The modelling output of Table 38 in Appendix I, shows that pre-washing (before adding the sodium oxalate solids created as part of tank cleaning from two or three tanks) results in five or seven wash cycles being required as part of preparing the vitrification feed (vs eight/nine or 12 wash batches required if washing is performed only after adding the oxalate to the vitrification feed batch). The future impacts to salt processing range from 1.2 to 1.6×10^6 litres of additional feed to salt processing, when solidified requiring 0.7 to 0.8 of the volume of a current-design-vault as the result of cleaning just one HLW tank. However, based on the number of planned sludge batches and HLW tanks to be cleaned, it is anticipated that the sodium oxalate solids from cleaning two or three HLW tanks would need to be added to each future feed batch. Table 38 of Appendix I shows that a resulting minimum of 1.2 vaults would be needed for the cleaning of two HLW tanks and a minimum of 2.16 vaults as the result of cleaning three tanks with the resultant sodium oxalate solids added per each vitrification feed batch.

Using TRIZ, a modified form of the backend of the CORD UV was initially identified as an analogous but already solved problem, that could be adapted for remediation of spent oxalic acid generated as the result of HLW tanks cleaning. Based on the CORD UV process, a preliminary process called Enhanced Chemical Cleaning (ECC) was envisioned.

Switching from the Historical Baseline Chemical Cleaning Process, which uses a concentrated 8 wt% oxalic acid with inhibited washes, to decomposition based regenerative technology using a dilute oxalic acid, which closely monitors and controls pH. Although the Historical Baseline Chemical Cleaning Process used an 8 wt%, the pH value obtained during the Historic Baseline Chemical Cleaning Process using 8 wt% oxalic acid never reached a pH value of less than 3.5, despite multiple references clearly pointed out that iron-rich sludge digestion would be most effective at a pH of ~2. This high pH value was the result of highly inhibited water

and even supernatant being used a to make the acid cleaning solution. Preliminary testing showed that with adequate pre-washing of the sludge to decrease the pH to around 10, a pH of 2 could be readily obtained by adding a simple 1 wt% oxalic acid solution to both the simulant and the real HLW.

With most of the technology adapted from the water treatment industry, there was a significant reason to believe that the proposed ECC process was an AOP. Therefore, the early stages of the literature review focused on understanding decomposition methods associated with both AOPs and UV enhanced AOPs. However, since hydroxide would not be readily available at acid conditions to form hydroxyl radicals, ferrioxalate like and type mechanisms (e.g., metal oxalate chelates/ligands) were also investigated. Although it is well known that ozone readily absorbs UV at 254 nm wavelength producing H_2O_2 as an intermediate, which then decomposes to $OH^{\cdot}$, there were multiple issues with using UV. Most importantly, testing shows that it is not needed to result in the slurry decomposition being complete in less than 24 hours.

Based on the literature review, there are three possible non-UV enhanced decomposition mechanisms. They are: 1) a heterogeneous non-AOP mechanism where the target organic adsorbs onto the surface of solid metal oxide at a so-called active site, followed by ozone attack on the sorbed organic. In the case of carboxylic acids such as oxalic, the extent of adsorption could be a function of pH, dependent upon the pKa of the acid and the pH of the PZC of the metal oxide surface; 2) a homogeneous non-AOP mechanism that operates under low pH acidic conditions and which involves complexation of the catalysing metal ion with the oxalate followed by ozone attack on the complex; or, 3) a homogeneous AOP mechanism that operates at a high basic pH and which involves metal ions catalysing the formation of hydroxyl radicals from ozone, said hydroxyl radicals then driving oxalate decomposition.

Early testing and design efforts revealed that there were assorted concerns associated with using the UV light. First, the UV Lamp Sheath required to keep the real UV light from being in contact with the HLW slurry would not provide the appropriate safety pedigree mandated for containment. That is, the required quartz sheath would represent a facility safety analysis issue. Other complications included the quick formation of a film forming on the UV Lamp Sheath, minimising the penetration ability/effectiveness of the UV light to act on the slurry. In addition, the simulant decomposition test slurries become opaque after only 1 to 3 hours of ozonation, depending on if the slurry was created from an Al/Mn-rich sludge, or Fe sludge, respectively.

Process sized testing was performed using slurries created from three subsequent digestions of an Fe-rich simulant and an Al/Mn-rich simulant with both 1 and 2.5 wt% oxalic acid. Analysis was performed to substantiate if UV was needed to photo-catalytically aid oxalate decomposition. All slurries tested under the different UV light protocols (i.e. UV, no UV, and fouled UV), were decomposed to an oxalate a concentration of less than 1.1×10^{-3} M (i.e. 1.1×10^{-3} M was deemed the point at which oxalate decomposition is complete) on an industrially relevant time scale (i.e. in less than 24 hours). As such, it is substantiated that UV is not required, and no further testing with UV was performed.

Each of the three sequentially created slurries created using an Fe-rich sludge simulant and an Al/Mn-rich sludge simulant with 1 wt% and 2.5 wt% oxalic acid were decomposed with ozone without application of UV. R^2 analysis show correlation of pH to remaining oxalate concentration, confirming that as a field measurement, pH can be used to confirm when the remaining oxalate concentration is $< 1.1\times10^{-3}$ M.

The presence of known nitrite and bicarbonate/carbonate scavengers are used as probe chemical for hydroxyl radicals. With nitrite being a known constituent of sludge, nitrite

concentrations would be diluted as sequential digestions occur in the making of the slurries. Therefore, the effect of nitrite would decrease as sequential slurries were tested, meaning that the oxalate decomposition rate would increase. This nitrite concentration decreasing, as seen by increasing hydroxyl radical g-values/increase in oxalate decomposition rates was not observed. In addition, the scavenger effect from carbonate/bicarbonate was shown to very small, discounting the scavenging significance that carbonate/bicarbonate played. Therefore, the minimal impact from both scavengers highly suggests that the oxalate decomposition is likely not hydroxyl radical driven. Instead, the decomposition is either:

1) A heterogeneous non-AOP mechanism where the target organic adsorbs onto the surface of a solid metal oxide at a so-called active site, followed by ozone attack on the sorbed organic; or
2) A homogeneous non-AOP mechanism that operates under low pH acidic conditions and which involves complexation of the catalysing metal ion with the oxalate followed by ozone attack on the complex.

Metal ions such as Fe(II), Mn(II) and Ni(II), already present within the slurries as a result of sludge mobilisation, have been shown to catalyse oxalate decomposition. Associated results show that mineralisation of the oxalate with metal catalysts occurs at a rate higher than observed during simple ozonation conducted in their absence. Further, the kinetics of the oxalate removal were found to be highly correlated with the rate of process initiation via the concentrations of the three-principle hydroxyl radical promoting metal ions in the slurries, specifically Fe(II), Mn(II) and Ni(II). Single metal ions systems have been widely researched in the metal oxalate systems. Less well studied are systems employing a mixture of metal catalysts, and that may provide insights into inter-metal ion competition or synergistic effects. The decomposition slurry experiments here consist of three main metal catalysts that have the

potential to compete as catalysts. However, this is complemented in the slurries studied here by a reverse order solubility exhibited as the oxalate destruction process proceeds. As this destruction proceeds, pH increases from ~1 to as high as ~9 (vide supra) leading to the precipitation of the metal catalysts as metal hydro(oxides). Eh-pH diagram data indicates that Fe precipitates at pH values lower than Mn which in turn precipitates at pH values lower than Ni – meaning that as oxalate decomposition proceeds and pH increases concomitantly. As seen in Figure 24, Fe precipitates before Mn before Ni. Thus, Fe(II) oxalate catalysis is found to dominate overall oxalate decomposition rate at short ozonation time; at intermediate ozonation times, once the Fe has started to precipitate due to the increasing pH, Mn oxalate catalysed decomposition dominates the overall process; finally, and typically close to the process endpoint of 1.1×10^{-3} M oxalate in solution, Ni oxalate catalysis dominates.

An initial nominal concentration of the metals before ozonation has begun would be as follows:

1) For the Fe-rich slurries, the Fe concentration is the latest (a maximum of ~ 1.2×10^{-2} M for both, with Mn concentration being half that of iron for both, and the Ni concentration for both being approximately 7 or 8×10^{-4} M.

2) For the Al/Mn-rich slurries, the Mn concentration is about six times larger than the Fe concentration (the Fe concentration for the 1 wt% slurry has a maximum value of 1.1×10^{-3}). While for the 2.5 wt%, the Fe rages from 1.8×10^{-2} to 6.9×10^{-3}). The Mn concentration for both the 1 wt% about five times larger than the same concentration for the Fe, while for the concentration for the 2.5 wt% Mn it is about five times lower than the concentration for the 2.5wt% Fe. Both the 1 wt% and 2.5 wt%, the Ni concentration range from 2 or 3×10^{-4} M. Of these three metal ions, the solubility behaviour of Fe is the most complex. As shown by Figure 19 through Figure 22, initially, upon the onset of ozonation, there is an increase in solution Fe concentration

due to the oxidative action of ozone on the metal oxide components of the sludge; precipitation is inhibited by complexation with oxalate. At longer ozonation time, there is a decrease in Fe ion concentration as a result of oxalate decomposition, so decreasing the oxalate concentration, as well as increasing the simulant decomposition test slurry pH. The decrease in oxalate concentration results in decomplexation of Fe (as well as Mn and Ni) ions, rendering them vulnerable to precipitation as insoluble metal hydro(oxides) at the elevated pH. Thus, overall, oxalate decomposition in the slurries studied can be regarded as exhibiting four distinct stages:

Stage One (short ozonation times): ozone decomposes Fe oxalates and solubilise Fe from ozone action on the metal oxide constituents of the sludge;

Stage Two (intermediate ozonation times): As a result of the loss of the solution capacity to complex (and so solubilise) Fe, Mn, and Ni ions due to O_3 driven oxalate decomposition, as well as the pH increase that accompanies that decomposition, Fe begins to precipitate. Hydroxyl radical generation from ozone is still primarily catalysed by Fe ions during this stage.

Stage Three (intermediate ozonation times): Fe precipitation is near complete, and oxalate decomposition is now driven by ozone and radicals generated by Mn catalysis – Mn playing a major role in determining the final to process endpoint of 1.1×10^{-3} M oxalate in solution.

Stage Four (long ozonation times): Process endpoint with Mn precipitation now near completion and Ni being the dominant metal ion in solution.

Using known to be present nitrite and bicarbonate/carbonate as probe chemicals, it was found that the oxalate decomposition kinetics were largely unaffected by the concentration of these

potential radical scavengers; in particular, the scavenging effects of oxalate mineralisation-derived carbonate were extremely small, demonstrating that, under acid conditions, the primary decomposition reaction of oxalate is not an indirect AOP involving generated hydroxyl radicals, but is most likely a so-called direct reaction, involving the reaction of ozone with metal-complexed oxalate.

Real HLW based testing was performed, but because of limitations with testing using real HLW, its function was limited to confirmatory testing. For real HLW testing, the introduction of ozone was successful in decomposing oxalate to below the target levels. The results from these tests confirm that UV is not required and that decomposition can be completed in an industrial relevant timeframe, and pH can likely be used as an indication of remaining oxalate. The real HLW testing, however, had a decreased utilisation of ozone, requiring approximately four moles of ozone per mole of oxalate decomposed vs simulant testing which required three moles of ozone per mole of oxalate decomposed. For the real HLW testing, this was explained as the result of ozone losses associated with the distance from the ozone generator to the shielded cell which house the Decomposition Module. In addition, the slightly lower backpressure maintained of on decomposition test apparatus (i.e. 1.5×10^5 Pa for the real HLW based testing vs 1.7×10^5 Pa for the simulant based testing) would have also contributed to the difference.

Decomposition of oxalates in sludge dissolved in 2 wt% oxalic acids to levels near of 1.1×10^{-3} M oxalate required 8 to 12.5 hours without the aid of UV, while requiring only 4.5 to 8 hours with the aid of UV. The pH was tracked during decomposition testing. Sludge components were tracked during oxalate decomposition, showing that most components have the highest soluble levels in the initially dissolved sludge and early decomposition samples and exhibit lower soluble levels as oxalate decomposition progresses.

The main postulate of this thesis is that, in the context of the ECC process, ozonation alone can be effectively used to decompose spent oxalic acid in HLW tank nuclear decontaminations solutions in an industrially relevant time frame. This ability to decompose oxalates on an industrial relevant time period was proven using both simulant decomposition test slurries and real HLW based slurries.

That observed minimal impacts on oxalate decomposition rates observed during simulant based testing as a result of the hydroxyl radical scavengers during oxalate decomposition testing clearly demonstrates that, at least under acid conditions, the decomposition of oxalate is not hydroxyl radical driven.

Recommendations for the future would likely include a revised test setup for real HLW based testing, focusing on ensuring the setup is designed to support material balance determinations (e.g. designed the minimise hold-up). In addition, the concentrations of more of the soluble multi-valent transition metals should be measured throughout testing (i.e. more than just Fe, Mn and Ni). Creating and decomposing slurries created with each of the single metal catalysts, to understand each metal's individual catalytic effect would be invaluable. Additionally, effort should be invested to determine why real HLW based slurries had a decreased utilisation of ozone, requiring approximately five moles of ozone per mole of oxalate decomposed vs simulant testing which required four.

Finally, the decomposition data fails to take into account the potential of oxalate decomposition from radioactive fields. Very limited testing has been performed, with the latest focused on varied strength gamma exposure (Gurbnov et al. 2015). Although the decomposition would be expected to be low, testing should be considered to quantify the potential decompositions rates in both acids exposed to different radioactive sources and strengths.

7. REFERENCES

Adu-Wusu, K., Barnes, M., Bibler, N., Cantrell, J., Fondeur, F., Hamm, B., Hobbs, D., Ketusky, E., Singleton, M., Stallings, M., Stevens, W. and Wiersma, B. (2003). *Waste Tank Heel Chemical Cleaning Summary, WSRC-TR-2003-00401*. Aiken, South Carolina: Washington Savannah River Company.

Andreozzi, R., Insola, A., Caprio, V., and Amore, M. (1992). The kinetics of Mn(II)-catalysed ozonation of oxalic. *Water Research*, Vol. 26, Issue 7, pp. 917-921.

Andreozzi, R., Insola, A., Caprio, V., Marotta, R. and Tufano, V. (1996). Kinetics of Oxalic Acid Ozonation Promoted by Heterogeneous MnO_2 Catalysis. *Applied Catalysts B*, Vol. 138, Issue 1, pp. 75-81.

Andreozzi, R., Caprio, V., Insola, A., Marotta, R. and Tufano, V. (1997). Kinetics of Oxalic Acid Ozonation Promoted by Heterogeneous MnO_2 Catalysis. *Industrial and Engineering Chemistry Research*, Vol. 36, No. 11, pp. 4774-4778.

Arslan, I., Balcioglu, A. and Tuhkanen, T. (1999). Oxidative treatment of simulated dyehouse effluent by UV and near-UV light assisted Fenton's reagent. *Chemosphere*, Vol. 39: pp. 2767-2783.

Asano, M., Hinokio, R., Jiku, F. and Saito, K. (2008). The Treatment of the Humic Substance from A Domestic Wastewater Treatment Device Effluent. In: *Proceedings of Taal2007: The 12th World Lake Conference.* Jaipur, India*,* 29 October - 2 November 2008: pp. 941-943.

Avramescu, S., Bradu, C., Udrea, I., Mihalache, N. and Ruta, F. (2008). Degradation of oxalic acid from aqueous solutions by ozonation in presence of Ni/Al_2O_3 catalysts. *Catalysis Communications*, Vol. 9, pp. 2386–2391.

Bahnemann, D., Bockelmann, D. and Goslich, R. (1991) Mechanistic studies of water detoxification in illuminated TiO_2 suspensions. *Solar Energy Materials and Solar Cells*, Vol. 24, pp. 564–583.

Baig, S. and Liechti, P. (2001). Ozone treatment for biorefractory COD removal. *Water Science and Technology*, Vol. 43, pp. 197–204.

Balmer, M. and Sulzberger, B (1999). Atrazine Degradation in Irradiated Iron/Oxalate Systems: Effects of pH and Oxalate. Environmental Science and Technology, Vol. 33, No. 14, pp. 2418–2424.

Battino, R., Rettich, T. and Tominaga, T. (1983). The Solubility of Oxygen and Ozone in Liquids. *Journal of Physical and Chemical Reference Data,* Vol. 12, No. 2, pp. 163-178.

Barbusiński, K. (2009). Fenton Reaction - Controversy Concerning the Chemistry. *Ecological Chemistry and Engineering*, Vol. 16, No. 3, pp. 347-358.

Bauman, L. and Stenstrom, M. (1990). Removal of Organohalogens and Organohalogen Precursors in Reclaimed Wastewater. I. *Water Research*, 24(8), pp. 957-964.

Benito, Y., Arrojo, S., Hauke, G. and Vidal, P. (2005). Hydrodynamic Cavitation as a Low-Cost AOP for Wastewater Treatment: Preliminary Results and a New Design Cost Approach. *WIT Transactions on Ecology and the Environment: Water Resources Management* III, Vol. 80.

Beltrán, F., Rivas, F. and Montero-de-Espinosa, R. (2003a). Ozone-Enhanced Oxidation of Oxalic Acid in Water with Cobalt Catalysts. 1. Homogeneous Catalytic Ozonation. *Industrial and Engineering Chemistry Research*, Vol. 42, pp. 3210-3217.

Beltrán, F., Rivas, F. and Montero-de-Espinosa, R. (2003b). Ozone-Enhanced Oxidation of Oxalic Acid in Water with Cobalt Catalysts. 2. Heterogeneous Catalytic Ozonation. *Industrial and Engineering Chemistry Research*, Vol. 42, pp. 3218-3224.

Beltrán, F., Rivas, F. and Montero-de-Espinosa, R. (2005). Iron Type Catalysts for the Ozonation of Oxalic Acid in Water. *Water Research,* Vol. 39, Issue 15, pp. 3553-3564.

Benitez, F., Beltrán-Heredia, J., Acero, J. and Rubio, F. (1999). Chemical Decomposition of 2,4,6-Trichlorophenol by Ozone. Industrial Engineering Chemistry Research, Vol. 38, pp. 1341-1349.

Bischof, H., Höfl, C., Schönweitz, C., Sigl, G., Wimmer, B. & Wabner, D. (1996). UV-activated hydrogen peroxide for ground and drinking water treatment – development of technical process. In: *Proc. Reg. Conf. Ozone, UV-light, AOPs Water Treatment,* 24-26 September 1996. Amsterdam, Netherlands, pp.117–131.

Black and Veatch Corporation (2010). *White's Handbook of Chlorination and Alternative Disinfectants*, 5th edition, Hoboken, New Jersey, USA: John Wiley and Sons.

Bokare, A. and Choi, W. (2014). Review of iron-free Fenton-like systems for activating H_2O_2 in advanced oxidation processes. *Journal of Hazardous Materials*, Vol. 275, pp. 121-35.

Bowers, A., Gaddipati, P., Eckenfelder, W. and Monsen, R. (1989). Treatment of toxic or refractory wastewater with hydrogen peroxide. *Water Resources*, Vol. 21(6), pp. 477–486.

Bradbury, D. (2001). Review of Decontamination Technology Development 1977-2000. In: British Nuclear Energy Conference (Ed.) Water Chemistry of Nuclear Reactor Systems 8, Vol. 1, pp. 173-178, Thomas Telford, London.

Bushart, S., Wood, C., Bradbury, D. and Elder, G. (2003). The EPRI DFDx Chemical Decontamination Process, In: *Waste Management Symposium 2003* Conference, *23 – 27 February 2003*, Tucson, Arizona.

Buxton, G., Mulazzani, Q. and Ross, A. (1995). Critical Review of Rate Constants for Reactions of Transients from Metal Ions and Metal Complexes in Aqueous Solutions. *Journal of Physical and Chemical Reference Data*, Vol. 24, No. 3, pp. 1056-1349.

Cacuci, D. (2010). Handbook of Nuclear Engineering, Vol. 1, Nuclear Engineering Fundamentals, Springer Reference.

Calderón, G., Rodríguez, J., Ortiz-Méndez, U. and Torres-Martínez, L. (2000). Iron Leaching of a Mexican Clay of Industrial Interest by Oxalic Acid. *AZojomo*, Vol. 1.

Calgon (1996). *AOT Handbook*. Markham, Ontario, Canada: Calgon Carbon Oxidation Technologies.

Canton, C., Esplugas, S. and Casado, J. (2003). Mineralisation of phenol in aqueous solution by ozonation using iron or copper salts and light. *Applied Catalysis B: Environmental*, Vol. 43, pp. 139–149.

Carey, J. (1992). An introduction to AOP for destruction of organics in wastewater. *Water Pollution Research Journal of Canada*, Vol. 27, pp. 1–21.

Chemical Speciation and Reactivity in Water Chemistry and Water Technology a Symposium in Honor of James J. Morgan (2000). Pages 608-611 in reprints of Extended Abstracts, Vol. 40, No. 2, 20-24 August 2000, Washington D.C., USA: American Chemical Society.,

Chamarro, E., Marco, A., Prado, J. and Esplugas, S. (1996). Tratamiento de aguas y aguas residuales mediante utilizacion de procesos de oxidacion avanzada. *Quımica & Industria, Sociedad Chilena de Quımica*, Vol. 1/2, pp. 28–32.

Chetty, E., Maddila, S., Southway, C. and Jonnalagadd, S. (2012). Ozone Initiated Ni/Metal Oxide Catalysed Conversion of 1,2 Dichlorobenzene to Mucochloric Acid in Aqueous Solutions. *Industrial and Engineering Chemistry Research*, Vol. 51 (7), pp. 2864–2873.

Chew, D. and Hamm, B. (2010). *Liquid Waste System Plan,* SRR-LWP-2009-00001, Rev 15. Aiken, South Carolina, USA: Savannah River Remediation.

Chiang, Y., Liang, Y., Chang, C. and Chao, A. (2006). Differentiating ozone direct and indirect reactions on decomposition of humic substances. *Chemosphere*, Vol. 65, pp. 2395–2400.

Chung, D., Kim, E., Shim, Y., Yoo, J., Choi, C. and Kim, J. (2001). Decomposition of Oxalate by Hydrogen Peroxide in Aqueous Solution. *Journal of Radioanalytical and Nuclear Chemistry Letters*, Vol. 96, pp. 495-507.

Cornell, R. and Schindler, P. (1987). Photochemical dissolution of goethite in acid/oxalate solution. *Clays and Clay Minerals,* Vol. 35, No. 5, pp. 347-352.

Cortés, S., Sarasa, J., Ormad, P., Gracia R., and Ovelleiro, J. (2000). Comparative efficiency of the systems $_{O3}$/high pH and O_3/catalyst for the oxidation of chlorobenzenes in water. *Ozone: Science and Engineering*, Vol. 22, No. 4, pp. 415–426.

Cortés, S., Sarasa, J., Ormad, P., Gracia, R. & Ovelleiro, J. (1998). Comparative efficiency of the systems O_3/high pH and O_3/CAT for the oxidation of chlorobenzenes in water. In: *Proc. Int. Reg. Conference. Ozonation and AOPs in Water Treatment*, 23-25 September 1998, Poitiers, France, 14-1–15-1.

Crittenden J., Zhang Y., Hand D., Perram, D. and Marchand, E. (1996). Solar Detoxification of Fuel Contaminated Groundwater using Fixed-Bed Photocatalysts. *Water Environment Research*, Vol. 68, Number 3, pp. 270-278.

Davis, N and Dickert, G. (2011). *Completion of Tank 11H Bulk Waste Removal Efforts*, SRR-WRC-2011-0003, Aiken, South Carolina, USA: Savannah River Remediation.

Davis, N., Ketusky, E., Spires, R., Beatty, R., Jones, S., Remark, J. and Wojtaszek, P. (2009). Enhanced Chemical Cleaning: A New Process for Chemically Cleaning Savannah River Waste Tanks-9100, In: *Waste Management Symposium 2009 Conference*, *1 – 5* March 2009, Phoenix, Arizona, USA.

Dorfman, L. and Adams, G. (1973). *Reactivity of the hydroxyl radical in aqueous solutions*, NSRDS-NBS-46. Washington D.C., USA: U.S. National Bureau of Standards.

Duguet, J., Brodard, E., Dussert, B. and Mallevialle, J. (1985). Improvement in the effectiveness of ozonation of drinking water through the use of hydrogen peroxide. *Ozone Science and Engineering*, Vol. 7, pp. 241–258.

DOW Chemical. (1977). *Technical Study for The Chemical Cleaning of Dresden-1*, DNS-01-016, Volume I, NSRDS-NBS-46. Midland, Michigan, USA: DOW Chemical.

Eibling, R. (2008). *Development of an Insoluble Salt Simulant to Support Enhanced Chemical Cleaning Tests,* WSRC-STI-2008-00079. Aiken, South Carolina, USA: Washington Savannah River Company.

Eibling, E. (2010). *Development of Hazardous Sludge Simulants for Enhanced Chemical Cleaning Tests,* SRNL-STI-2010-00170. Aiken, South Carolina, USA: Savannah River National Laboratory.

El-Raady, A. and Nakajima, T. (2006). Effect of UV Radiation on the Removal of Carboxylic Acids from Water by H_2O_2 and O_3 in the Presence of Metallic Ions. *Ozone Science and Engineering,* Vol. 28, pp. *53-58.*

EPRI. (1988). *A Review of Plant Decontamination Methods 1988 Update*. EPRI NP-6169, Palo Alto, California, USA: Electric Power Research Institute.

EPRI. (1996). *TECHCOMMENTARY: Advanced Oxidation Processes for Treatment of Industrial Wastewater.* An EPRI Community Environmental Centre Publication No. 1, Palo Alto, California, USA: Electric Power Research Institute.

Ershov, B. and Morozov, P. (2009). The kinetics of ozone decomposition in water, the influence of pH and temperature. *Chemical Kinetics and Catalysis, Russian Journal of Physical Chemistry A*, Vol. 83, Issue 8, pp. 1295-1299.

Esplugas, S., Gimenez, J., Contreras, S., Pascual, E. and Rodrıguez, E. (2002). Comparison of different advanced oxidation processes for phenol degradation. *Water Research,* Vol. 36, pp. 1034–1042.

Farhataziz, P. and Ross, A. (1977). *Selected Specific Rates of Reactions of Transients from Water in Aqueous Solutions,* NSRSDS-NBS-59. National Standards Reference Data Series, National Bureau of Standards.

Faust, B. and Zepp, R. (1993). Photochemistry of aqueous iron (III)-polycarboxylate complexes: roles in the chemistry of atmospheric and surface waters. *Environmental Science and Technology*, Vol. 27, Issue 12, pp 2517-2522.

Fenton, H. (1884). Oxidative properties of the H_2O_2/Fe_2^+ system and its application. *Journal of the Chemical Society*, Vol. 65, pp. 889–899.

Fowler, J. (1980). *Effect of Temperature on Sodium Oxalate Solubility*, DPST-80-265. Aiken, South Carolina, USA: DuPont De Nemours.

Garoma, T. and Gurol, M. (2005). Modelling Aqueous Ozone /UV Using Oxalic Acid as a Probe Chemical. *Environmental Science and Technology*, Vol. 39, pp. 7964-7969.

Garoma, T., Gurol, M., Osibodu, O. and Thotakura, L. (2008). Treatment of groundwater contaminated with gasoline components by an ozone/UV process, *Chemosphere*, Vol. 73, pp. 825–831.

Gehringer, P. and Eschweiler, H. (1996). Ozone/Electron Beam Process for Water Treatment: Design, Limitations and Economic Considerations, *OF*-4767, In: *2nd International Symposium on Environmental Applications of Advanced Oxidation Technologies*, 28 February – 1 March 1996, San Francisco, California, USA.

Glaze, W. and Kang, J. (1989). Description of a Kinetic Model for the Oxidation of Hazardous Materials in Aqueous Media with Ozone and Hydrogen Peroxide in a Semibatch Reactor. *Industrial and Engineering Chemistry Research*, Vol. 28, No. 11, pp. 1573-1580.

Gogate, P. and Pandit, A. (2003). A review of imperative technologies for wastewater treatment I: oxidation technologies at ambient conditions. *Advances in Environmental Research,* Vol. 8, pp. 501–551.

Gottschalk, C., Libra, J. and Saupe, A. (2000). *Ozonation of Water and Wastewater: A Practical Guide to Understanding Ozone and its Application,* 2nd Edition. Weinheim, Germany: Wiley VCH.

Grosse, D., Lewis, N., Cooper, W., Chapman, T., Kawahara, F., Sahle-Demessie, E. and Gallardo, V. (1998). *Handbook on Advanced Photochemical Oxidation Processes*, EPS/625/R-98/004. Cincinnati, Ohio, USA: United States Environmental Protection Agency.

Gracia, R., Aragües, J., Cortés, S. and Ovelleiro, J. (1995). Study of the catalytic ozonation of humic substances in water and their ozonation byproducts. In: *Proceedings of the 12th World Congress of the International Ozone Association*, Lille, France, 15–18 May: 75.

Gracia, R., Aragües, J. and Ovelleiro J. (1996). Study of the catalytic ozonation of humic substances in water and their ozonation byproducts. *Ozone Science and Engineering*, Vol. 18, pp. 195-208.

Guo, Y., Yang, L., Cheng, X., Wang, X. (2012) The Application and Reaction Mechanism of Catalytic Ozonation in Water Treatment. Journal of Environmental and Analytical Toxicology, Vol. 2, Issue 7, pp. 1-6.

Gurol, M. and Singer, P. (1982). Kinetics of Ozone Decomposition, a dynamic approach. *Environmental Science and Technology*, Vol. 16, No. 7, pp. 377-383.

Gurol, M. and Vatistas, R. (1987). Oxidation of phenolic compounds by ozone and ozone/UV Radiation: A comparative study. *Water Research*, Vol. 21, pp. 895–903.

Harneed, B. and Lee, T. (2008). Degradation of malachite green in aqueous solution by Fenton Process. *Journal of Hazardous Materials*, Vol. 164, pp. 468-472.

Hernandez-Alonso, M., Coronado, J., Maira, A., Soria, J., Loddo, V. and Augugliaro, V. (2002). Ozone enhanced activity of aqueous titanium dioxide suspensions for photocatalytic oxidation of free cyanide ions. *Applied Catalysis B: Environmental*, Vol. 39, Issue 3, pp 257-267.

Hislop, K. and Bolton, J. (1999). The photochemical generation of hydroxyl radicals in the UV-vis/ferrioxalate/H_2O_2 system. *Environmental Science and Technology*, Vol. 33, pp. 3119–3126.

Hirvonen, A., Tuhkanen, T. and Kalliokoski, P. (1996). Treatment of TCE- and TCE-contaminated groundwater using UV/H_2O_2 and O_3/H_2O_2 oxidation processes. *Water Science and Technology*, Vol. 33, pp. 67–73.

HLW Engineering (2009). *Waste Characterisation System WCS 1.5 (process database)*. Aiken, South Carolina, USA: Savannah River Remediation.

HLW Engineering (2008). *Ntank Database (NTank51, NTank47, NTank 38, and NTank 30).* Aiken, South Carolina, USA: Savannah River Remediation.

Hoigné, J. (1982). Mechanisms, rates and Selectivities of oxidations of organic compounds initiated by ozonation of water, In: *Handbook of Ozone Technology and Applications*. Ann Arbor Science Publishing, Ann Arbor, Michigan.

Hoigné, J. and Bader, H. (1983a). Rate constants of reaction of ozone with organic and inorganic compounds in water. Part I. Non-dissociating organic compounds. *Water Research,* Vol. 17, pp.173–183.

Hoigné, J. and Bader, H. (1983b). Rate constants of reaction of ozone with organic and inorganic compounds in water. Part II. Dissociating organic compounds. *Water Research*, Vol. 17, pp. 185–194.

Huang, Y, Liu, C. and Chen, H. (2007). Study of oxalate mineralisation using electrochemical oxidation technology, *Journal of Environmental Engineering Management,* Vol. 17, Issue 5, pp. 345-349.

Ince, N. (1998). Light-Enhanced Chemical Oxidation for Tertiary Treatment of Municipal Landfill Leachate, *Water Environment Research*, Vol. 70, No. 6, pp. 1161-1169.

Ince, N. and Apikyan, I. (2000). Combination of Activated Carbon Adsorption with Light-Enhanced Chemical Oxidation via Hydrogen Peroxide, *Water Research*, Vol. 34, pp. 4169-4176.

Ince, N., Stephen, M. and Bolton, J. (1997). UV/ H_2O_2 degradation and toxicity reduction of textile azo dyes. *Journal of Advanced Oxidation Technology*, Vol. 2, pp. 442-448.

Ince, N. (1998). Light enhanced chemical oxidation for tertiary treatment of municipal landfall leachate. *Water Environmental Research,* Vol. 70, pp. 1161-1168.

Ince, N. and Tezcanli, G. (1999). Treatability of textile dyebath effluents by advanced oxidation: preparation for reuse. *Water Science Technology*, Vol. 40, pp. 183-190.

Jacobsen, F., Holcman, J. and Sehested, K. (1998). Oxidation of Manganese(II) by ozone and reduction of Manganese(III) by hydrogen peroxide in acidic solution. *International Journal of Chemical Kinetics*, Vol. 30, Issue 3, pp. 207-214.

Jeffery, G., Bassett, J., Mendham, J. and Denney, R. (1989). *Vogel's Textbook of Quantitative Chemical Analysis*, 5th edition. New York, USA: John Wiley & Sons, 370 10.95.

Jones, D. (2008). *Savannah River Site Salt Simulant AREVA,* 51-9077712-000, Lynchburg, Virginia, USA: AREVA N.P.

Kasprzyk-Hordern, B., Ziółek, M. and Nawrockia, J. (2003). Catalytic ozonation and methods of enhancing molecular ozone reactions in water treatment. *Applied Catalysis B: Environmental*, Vol. 46, pp. 639–669.

Karim, S. and Gehr, R., (2001). *Fouling of UV Lamp Sleeves: Exploring Inconsistencies in The Role of Iron*. Montreal, Canada: McGill University.

Kavitha, V. and Palanivelu, K. (2004). The role of ferrous ion in Fenton and Photo-Fenton processes for the degradation of phenol, Chemosphere, Vol. 55, pp.1235–1243.

Kavitha, V. and Palanivelu, K. (2005). Destruction of cresols by Fenton oxidation process, *Water Research*, Vol. 39, pp. 3062–3072.

Ketusky, E. (2008). *Percent Oxalic Acid for Enhanced Chemical Cleaning Sludge Dissolution*, LWO-CES-2008-00014. Aiken, South Carolina, USA: Washington Savannah River Company.

Ketusky, E. (2015). Mathematically Determined Scavenger Impacts during Ozonalysis of Oxalic Acid Waste Slurries-15600. In: *Waste Management Symposium 2015 Conference*, 5-9 March 2015, Phoenix, Arizona, USA.

Ketusky, E., Huff, T., Sudduth, C., Jones, S., Remark, J. and Sillanpaa, M. (2011). Enhanced Chemical Cleaning: Effectiveness of the UV Lamp to Decompose Oxalates -10502. In: *Waste Management Symposium 2011 Conference*, 1-5 March 2011, Phoenix, Arizona, USA.

Ketusky, E. and Subramanian, K. (2012). *SRS SRR AOP Decomposition Testing with* Ozone, SRR-LWE-2012-00006. Aiken, South Carolina, USA: Savannah River Remediation.

Ketusky, E., Subramanian, K. and Wiersma, B. (2011). Savannah River Tank Cleaning: Corrosion Rate for One Versus Eight Percent Oxalic Acid 12534, In: *Waste Management Symposium 2011* Conference*,* 27 February – 3 March 2011, Phoenix, Arizona, USA.

Kim, E., Chung, D., Park, J. and Yoo, J. (2012). Dissolution of oxalate precipitate and destruction of oxalate ion by hydrogen peroxide in nitric acid solution. *Journal of Nuclear Science and Technology*, Vol. 37, Issue 7, pp. 601-607.

Kommineni, S., Zoeckler, J., Stocking, A., Liang, S., Flores, A., and Kavanaugh, M. (2001). Chapter 3: Air Stripping, Advanced Oxidation Process, Granular Activated Carbon, Synthetic Resin Sorbents. *Treatment Technologies for Removal of Methyl Tertiary*

Butyl Ether (MTBE) from Drinking Water, 2nd ed. Fountain Valley, California: National Water Research Institute, pp. 111–208.

Krichevskaya, M., Malygina, T., Preis, S. and Kallas, J. (2000). Photocatalytical oxidation of de-icing agents in aqueous solutions and aqueous extract of jet fuel. In: *Proc. 2nd Int. Conf. Oxidation Technologies for Water and Wastewater Treatment*, 28–31 May 2000, Clausthal-Zellerfeld, Germany, pp. 6–12.

Kusakabe, K., Aso, S., Wada; T., Hayashi, J., Moroka, S. and Isomuta, K. (1991). Destruction rate of volatile organochlorine compounds in water by ozonation with ultraviolet radiation. *Water Researc*h, Vol. 25, Issue 10, pp. 1199–1203.

Lagunova, Y., Seliverstov, A, Ershov, B. and Basiev, A. (2012). Oxidative decomposition of oxalate ions in water solutions of concentrated ozone. *Atomic Energy*, Vol. 113, No. 2. pp. 112–116.

Langlais, B., Reckhow, D. and Brink, D. (1991). *Ozone in Water Treatment: Application and Engineering*; Lewis Publishers Inc., New York, USA.

Ledakowicz, S., Miller, J. and Olejnik, D. (2001). Oxidation of PAHs in water solution by ozone combined with ultraviolet radiation, *International Journal of Photoenergy*, Vol. 3, pp. 95-101.

Legube, B., Delouane, B., Karpel Vel Leitner, N. and Luck, F. (1996). Catalytic ozonation of salicylic acid in aqueous solution: Efficiency and mechanisms. In: *Proc. Reg. Conf. Ozone, UV-light, AOPs Water Treatment*, 24–26 September 1996, Amsterdam, Netherlands, 509–514.

Legube, B. and Karpel Vel Leitner, N. (1999). Catalytic ozonation: a promising advanced oxidation technology for water treatment. *Catalysts Today,* Vol. 53, pp. 61-72.

Leitner, N., Delanoe, F., Acedo, B., Papillault, F. and Legube, B. (1998). Catalytic ozonation of succinic acid in aqueous solution: A kinetic approach. In: *Proc. Int. Reg. Conf. Ozonation and AOPs in Water Treatment*, Poitiers, France, 23-25 September 1998, 15-1–16-1.

Lenntech. (2017), *Ozone Decomposition*, Delft, Netherlands; Lenntech B.V.

Li, F., Chen, J., Liu, C., Dong, J. and Liu, T. (2006). Effect of iron oxides and carboxylic acids on Photochemical Degradation of Bisphenol, *Biology Fertility Soils*, Vol. 42, pp. 409-417.

Li, X., Cubbage, J., Tetzlaff, T. and Jenks, W. (1999). Photocatalytic Degradation of 4-Chlorophenol. 1. The Hydroquinone Pathway, *Journal of Organic Chemistry*, Vol. 64, pp. 8509-8524.

Li, Q., Zhou, O., and Tao Hua, T. (2010). Removal of Organic Matter from Landfill Leachate by Advanced Oxidation Processes: A Review. *International Journal of Chemical Engineering*, Vol. 2010, Article ID 270532, 10 pages. [online] Available at:<. http://WWw.hindawi.com/journals/ijce/2010/270532/ [Accessed 2 January 2015].

Liao, C., Kang, S., and Wu, F. (2001). Hydroxyl radical scavenging role of chloride and bicarbonate ions in the H_2O_2/UV process. *Chemosphere*, Vol. 44, pp. 1193-1200.

Logager, T., Holcman, J., Sehested, K. and Pedersenf, T. (1992). Oxidation of Ferrous Ions by Ozone in Acidic Solutions. *Inorganic Chemistry,* Vol. 31, pp. 3523-3529.

Ma, J. and Graham, N. (1999). Degradation of atrazine by manganese-catalysed ozonation: Influence of humic substances. *Water Research,* Vol. 33, No. 3, pp. 785-793.

Mackey, E., Cushing, R., Janex-Habibi, M., Picard, N., and Laine, J. (2004). Bridging Pilot-Scale Testing to Full Scale Design of UV Disinfection Systems, 1st Edition. Denver, Colorado, USA: American Water Works Research Association.

Marin, M., Arques, S., Antonio, L., Amat, A. and Miranda, M. (2012). Organic Photocatalysts for the Oxidation of Pollutants and Model Compounds. *Chemical Reviews*, Vol. 112, pp. 1710–1750.

Martell, A. (1968). Catalytic Effects of Metal Chelate Compounds. *Pure and Applied Chemistry*, Vol. 17, No. 1, pp. 129-178.

Martin, C., Martin, I. and Rives, V. (1995). Effect of sulfate removal on the surface texture and acid-base properties of TiO2 (anatase). *Journal of Mathematical Sciences*, Vol. 30, 3847–385

Martino, C. and King, W. (2011). *Testing of Enhanced Chemical Cleaning of SRS Actual Waste Tank SF and Tank 12H Sludge, SRNL-STI-2011-00360*, Aiken, South Carolina, USA: Savannah River Laboratory.

Martino, C., King, W. and Ketusky, E. (2012). Actual-Waste Tests of Enhanced Chemical Cleaning for Retrieval of SRS HLW Sludge Tank Heels and Decomposition of Oxalic Acid-12256, In: *Waste Management Symposium 2012* Conference, 26 February – 1 March 1 2012, Phoenix, Arizona, USA.

Masschelein, W. (1992). *Unit Processes in Drinking Water Treatment*, CRC Press, New York< USA.

Matavos-Aramyan, S. and Moussavi, M. (2017). Advances in Fenton and Fenton Based Oxidation Processes for Industrial Effluent Contaminants Control – A Review. *International Journal of Environmental Science and Natural Resources*, Vol. 2, pp. 1-17.

Matthews, R. (1986). Photo-oxidation of organic material in aqueous suspensions of titanium dioxide. *Water Research*, Vol. 20, pp. 569–578.

Mazellier, P. and Sulzberger, B (2001). Diuron Degradation in Irradiated, Heterogeneous Iron/Oxalate Systems: The Rate-Determining Step. Environmental Science Technology, Vol. 35, pp. 3314-3320.

Miller, C. and Valentine, R. (1999) Mechanistic studies of surface catalysed H_2O_2 decomposition and contaminant degradation in the presence of sand. *Water Research*, Vol. 33(12), pp. 2805–2816.

Mills, A., O'Rourke, C. and Moore, K. (2015) Powder semiconductor photocatalysis in aqueous solution: An overview of kinetics-based reaction mechanisms. *Journal of Photochemistry and Photobiology A: Chemistry,* Vol. 310, pp. 66-101.

Minakata, D., Song, W. and Crittenden, J. (2011). Reactivity of Aqueous Phase Hydroxyl Radical with Halogenated Carboxylate Anions: Experimental and Theoretical Studies, *Environmental Science and Technology*, Vol. 45, pp. 6057–6065.

Miyittah, M., Tsyawo, F., Kumah, K., Stanley, C. and Rechcigl, J. (2016), Suitability of Two Methods for Determination of Point of Zero Charge (PZC) of Adsorbents in Soils. *Communications in Soil Science and Plant Analysis*, Vol. 47, Issue 1, pp. 101-111.

Mokrini, D. and Esplugas, S. (1997). Oxidation of Aromatic Compounds with UV Radiation/Ozone/Hydrogen Peroxide. *Water Science and Technology*, Vol. 35 Issue 4, pp. 95-102.

Morel, F. and Hering, J. (1993). *Principles and Applications of Aquatic Chemistry*. New York, USA: John Wiley & Sons.

Munter, R. (2001). Advanced Oxidation Processes – Current Status and Prospects, *Proc. Estonian Academy of Science Chemistry*, Vol. 50, Issue 2, pp. 59–80.

Munter, R., Kallas, J., Preis, S., Kamenev, S., Trapido, M. and Veressinina, Y. (1995). Comparative studies of AOP for aromatic and PAH destruction. In: *Proceedings of 12th World Ozone Congress*, 15–18 May 1995, Lille, France, pp. 395–406.

Nagargoje, R., Atalay, S., Eroz, G. and Palas, B. (2014). Photo-Fenton Oxidation of Azo Dyes in Textile Wastewaters in the Presence of Fe/AC and Fe-TiO2/AC Catalysts, *Bombat Technologist*, Vol. 64, Issue1, pp. 59–80.

National Academy of Science (2006). *Tank Waste Retrieval, Processing, and On-Site Disposal at Three Department of Energy Sites*, Washington D.C., USA: National Academies Press.

Neta, P., Huie, R. and Ross, A. (1988). Rate Constants for Reactions of Inorganic Radicals in Aqueous Solution, *Journal of Physical Chemistry Reference Data*, Vol. 17, No. 3, pp. 1027-1083.

Ngadi, N., Amin, N., Tak, K., Lian, L. and Keong, L. (2006). Catalytic Ozonation of 2-Hydroxy-1,2,3-Propanetricarboxylic Aid. *Jurnal Teknologi,* Vol. 44(C), pp. 13–22.

Nicole, I., Laat, J. and Dore, M. (1991). Evaluation of reaction rate constants of OH· radicals with organic compounds in diluted aqueous solutions using H_2O_2/UV process. In: *Proc. 10th Ozone World Congress*, March 1991, Monaco, 1, 279–290.

Nichols, T., Barnes, C., Lauerhass, L., and Taylor, D. (2001), *Selection of Steady-State Process Simulation Software to Optimize Treatment of Radioactive and Hazardous Waste,* INEEL/EXT-01-00485, Idaho Falls, Idaho, USA: Idaho National Engineering and Environmental Laboratory.

Nuclear Energy Agency (2008). *Decontamination Techniques Used in Decommissioning Activities: A Report by the NEA Task Group on Decontamination*, Issy-les-Moulineaux, France: Nuclear Energy Agency.

Ollis, D. (1993). Comparative Aspects of Advanced Oxidation Processes. In: *Emerging Technologies in Waste Management II, ACS Symposium Series 518*. Washington, D.C., USA, 1993, p. 18–34.

Olson, T. and Barbier, F. (1994). Oxidation kinetics of natural organic matter by sonolysis and ozone. *Water Research*, Vol. 28, No. 6, pp. 1383-1391.

Oppenlander, T. (2003). *Photochemical Purification of Water and Air (Advanced Oxidation Processes (AOPs): Principles, Reaction Mechanisms, Reactor Concepts,* Weinheim, Germany: Wiley VCH.

Paillard, H., Brunet, R. and Dore, M. (1988). Optimal conditions for applying an ozone/hydrogen peroxide oxidising system. *Water Research,* Vol. 22, pp. 91–103.

Paillard, H., Dore, M. and Bourbigot, M. (1991). Prospect concerning applications of catalytic ozonation in drinking water treatment. In: *Proc. 10th Ozone World Congress*, Monaco, 1, 313–331.

Panias, D., Taxiarchou, M., Paspaliaris, I., and Kontopoulos, A. (1996). Mechanisms of dissolution of iron oxides in aqueous oxalic acid solutions. *Hydrometallurgy,* Vol. 42. Pp. 257-265.

Palanivelu, K. and Kavitha, V. (2004). Role of ferrous ion in Fenton and Photo-Fenton processes for the degradation of phenol. *Chemosphere*, Vol. 55, pp. 1235–1243.

Pareizs, J. (2002). *Washing Demonstration Using Nonradioactive Simulated Tank 7 Sludge Slurry, WSRC-TR-2003-00401*. Aiken, South Carolina, USA: Westinghouse Savannah River Company.

Penkett, S., Jones, B., Brich, K. and Eggleton, A. (1978). The importance of atmospheric ozone and hydrogen peroxide in oxidising sulfur dioxide in cloud and rainwater. *Atmospheric Environment*, Vol. 13, Issue 1, pp.123-137.

Perez, M., Torradesa, F., Domenech, X. and Peral, J. (2002). Fenton and Photo-Fenton oxidation of textile effluents. *Water Research*, Vol. 36, pp. 2703–2710.

Peyton G., Bell O., Girin E., LaFaivre, M. and Sanders, J. (1998). *Effect of Bicarbonate Alkalinity on Performance of Advanced Oxidation Processes*. Denver, Colorado, USA: American Water Works Association Research Foundation (AWWRF).

Pham, N., Xing, G., Miller, C. and Waite, T. (2013). Fenton-like copper redox chemistry revisited: Hydrogen peroxide and superoxide mediation of copper-catalysed oxidant production, *Journal of Catalysis*, Vol. 301, pp. 54–64.

Piera, E., Calpe, J., Brillas, E., Domènech, X. and Peral, J. (2000). 2,4-Dichlorophenoxyacetic acid degradation by catalysed ozonation: TiO_2/UVA/O_3 and Fe(II)/UVA/O_3 systems, *Applied Catalysts B: Environmental*, Vol. 27, pp. 169-177.

Pike, J., Badheka, N. and Ketusky, E. (2004). *Flowsheet for SRS Waste Tank Heel Removal Using Oxalic Acid*, WSRC-TR-2004-00317, Rev. 0. Aiken, South Carolina, USA: Savannah River Remediation.

Pines, D. and Reckhow, D. (2002). Effect of dissolved cobalt (II) on the ozonation of oxalic acid. *Environmental Science and Technology*, Vol. 36, Issue 19, pp. 4046-4051.

Pinker, B. and Henderson, W. (1996). The effect of ozonation on the performance of GAC. In: *Proc. Reg. Conf. Ozone, UV-light, AOPs Water Treatment*, 24-26 September, 1996, Amsterdam, Netherlands, 307–318.

Pliego, G., Zazo, J., Casas, J. and Rodriquez, J. (2014). Fate of iron oxalates in aqueous solution: The role of temperature, iron species and dissolved oxygen. *Journal of Environmental Chemical Engineering*, Vol. 2, pp. 2236-2241.

Portjanskaja, E. (2008). Ozone reactions with inorganic and organic compounds in water, in Ozone Science and Technology. In: *Rein Munter (Ed.). Encyclopedia of Life Support Systems (EOLSS) (6.192)*. EOLSS Publishers.

Pouran, S., Raman, A. and Daud, W. (2014). Review on the application of modified iron oxides as heterogeneous catalysts in Fenton reaction. *Journal of Cleaner Production,* Vol. 64, pp 24-35.

Preis, S., Retentive, Y. and Rozkov, A. (1997). Photocatalytic oxidation of phenolic compounds in wastewater from oil shale treatment. *Water Science Technology*, Vol. 35, pp. 165–174.

Preis, S., Krichevskaya, M. and Kharchenko, A. (1997). Photocatalytic oxidation of aromatic amino compounds in aqueous solutions and groundwater from abandoned military bases. *Water Science and Technology*, Vol. 35, pp. 265–272.

Preis, S., Krichevskaya, M., Terentyeva, Y., Moiseev, A. and Kallas, J. (2000). Treatment of phenolic and aromatic amino compounds in polluted waters by photocatalytical oxidation. *Journal of Advanced Oxidation Technology*, Vol. 5, pp. 1–8.

Prousek, J. (1995). Fenton Reaction After a Century, *Chem. Listy*, Vol. 89, pp. 11-21.

Purich, D. (2017). *The Inhibitor Index: A Desk Reference on Enzyme Inhibitors, Receptor Antagonists, Drugs, Toxins, Poisons, Biologics, and Therapeutic Leads*. Boca Ranton, Florida, USA: CRC Press.

Raut-Jadhav, S., Pinjari, D., Saini, D. and Pandit, A. (2013). Synergetic effect of combination of AOP's (hydrodynamic cavitation and H_2O_2) on the degradation of Neonicotinoid class insecticide. *Journal of Hazardous Materials*, Vol. 261, pp.139-147.

Ravikumar, J. and Gurol, M. (1994). Chemical oxidation of chlorinated organics by hydrogen peroxide in the presence of sand. *Environmental Science and Technology*, Vol. 28(3), pp. 394–400.

Remark, J. (1989). A review of plant decontamination methods, NP-6169, Marietta, GA: Applied Radiological Control, Inc.

Riess, R., Odar, S. and Kysela, J. (2007). Decontamination and Steam Generator Chemical Cleaning, Skultuna, Sweden: Advanced Nuclear Technology International.

Rodriguez, M. (2003). *Fenton and UV-vis Based Advanced Oxidation*, PhD Thesis, University of Barcelona, Spain.

Ruppert, G., Bauer, R., Heisler, G. and Novalic, S. (1993). Mineralisation of cyclic organic water contaminants by the Photo-Fenton reaction. Influence of structure and substituents. *Chemosphere*, Vol. 27, pp. 1339–1347.

Safarzadeh-Amiri, A., Bolton, J. and Cater, S. (1997). Ferrioxalate-mediated photo degradation of organic pollutants in contaminated water. *Water Research,* Vol. 31, pp. 787–798.

Saldivar, E. (2002). Savannah River Site Waste Removal Program Past, Present, and Future in: *Waste Management Symposium 2002 Conference*, 24-28 February 2002, Phoenix, Arizona, USA.

Sauleda, R. and Brillas, E. (2001). Mineralisation of aniline and 4-chlorophenol in acidic solution by ozonation catalysed with Fe^{2+} and UVA light, *Applied Catalysis B: Environmental*, Vol. 29, pp. 135-145.

Schalk, S., Volker, A., Arnold, E., Briedent, K., Voronov, A. and Witzke, H., (2005). UV-lamps for Disinfection and Advanced Oxidation-Lamp Types, Technologies and Applications: *Novel Lamps, Sleeves and Reactors*, UV Congress, May 2005, Whistler, British Columbia, Canada.

Schmelling, D., Gray, K. and Kamat, P. (1997). The influence of solution matrix on the photocatalytic degradation of TNT in TiO_2 slurries. *Water Research*, Vol. 31, pp.1439–1447.

Shafer, A. (2010). *Waste Acceptance Criterial for Sludge, ARP, and MCU Process Transfers to 512-S and DWPF*, X-SD-G-00008. Aiken, SC, USA: Savannah River Remediation.

Shimazdu Corporation (2013). *Measurement of TOC in Electroplating Solutions by TOC-LCSH, Application News No. 45,* LAAN-A-TCE021. Kyoto, Japan: Shimazdu Corporation.

Silva, L. and Jardim, W. (2006). Trends and strategies of ozone application in environmental problems. *Quımica Nova*, Vol. 29, No. 2.

Son, Y. (2016). Advanced Oxidation Processes Using Ultrasound Technology for Water and Wastewater Treatment, *Handbook of Ultrasonic and Sonochemistry*. Singapore: Springer, pp. 1-22.

Stallings, M., Hobbs, D. and Wiersma, B. (2004). *Dissolution of Simulated and Radioactive Savannah River Site High-Level Waste Sludges with Oxalic Acid and Citric Acid Solutions, WSRC-TR-2004-0042*. Aiken, South Carolina, USA: Washington Savannah River Company.

Stumm. W. and Morgan J. (1996). *Aquatic Chemistry: Chemical Equilibria and Rates in Natural Waters, 3rd Edition*. New York, New York, USA: A Wiley Interscience Publication, John Wiley and Sons.

Subosits, S. (1994). *Actinide Removal Process Material Balance with Low Curies Salt Feed*, X-CLC-S-00113. Aiken, South Carolina, USA: Savannah River Remediation.

Sun, Y. and Pignatello, J. (1993). Photochemical reactions involved in the total mineralisation of 2,4-D by $Fe^{3+}/H_2O_2/UV$. *Environmental Science and Technology,* Vol. 27, pp. 304–310.

Sundström, D., Weir, B., Barber, T. and Klei, H. (1990). Purification and disinfection of water by UV light and hydrogen peroxide. In: *Proc. Symp. AOP*s, June 4–5, 1990, Toronto, Canada, Session 2, pp. 55–65.

Takahashi, N. (1990). Ozonation of several organic compounds having low molecular weight under UV irradiation. *Ozone: Science and Engineering*, Vol. 12, pp. 1–18.

Takeno, N. (2005). *Atlas of Eh-pH diagrams inter-comparison of thermodynamic databases Geological Survey of Japan Open File Report No.419*. Japan: National Institute of Advanced Industrial Science and Technology Research Centre for Deep Geological Environments.

Taxiarchou, M., Panias, D., Douni, I., Paspaliaris, I. and Kontopoulos, A. (1997). Dissolution of hematite in acidic oxalate solution, *Hydrometallur*gy, Vol. 44, pp. 287-299.

Teel, A., Warberg, C., Atkinson, D. and Watts, R. (2001). Comparison of mineral and soluble iron Fenton's catalysts for the treatment of trichloroethylene. *Water Research*, Vol. 35, No. 4, pp. 977–984.

Thomas, D., Coggon, M., Lignell, H., Schilling, K., Zhang, X., Schwantes, R., Flagon, R., Seinnfeld, J. and Beauchamp, Real time studies of iron oxalate-mediated Oxidation of Glycolaldehyde as a Model for Photochemical Ageing of Aqueous Aerosols, *Environmental Science and Technology,* (Accepted for publication).

Thomas, J. (2004). *Documentation of Tanks 30, 36, 41, and 47 Sludge Volumes*, CBU-LTS-2004-00177. Aiken, South Carolina, USA: Savannah River Remediation.

Tomiyasu, H., Fukutomi, H. and Gordon, G. (1985). Kinetics and Mechanism of Ozone Decomposition in Basic Aqueous Solution, *Inorganic Chemistry*, Vol. 24, pp. 2962-2966.

Tong, S., Li, W., Zhao, S. and Ma, C. (2010) Titanium (IV)-improved H_2O_2/O_3 Process for Acetic Acid Degradation under Acid Conditions, *Ozone: Science and Engineering*, Vol. 33, Issue 6, pp. 441-448.

Tong, S., Zhao, S., Lan, X. and Ma, C., (2011). A kinetic model of Titanium (IV)-improved H_2O_2/O_3 Process in aqueous solution. *Journal of Environmental Sciences*, Vol. 23, Issue 12, pp. 2087-2092.

Trapido, M. (2007). Ozone-based advanced oxidation processes. In: *Rein Munter (Ed.). Encyclopedia of Life Support Systems (EOLSS) (6.192)*. EOLSS Publishers.

Trapido, M., Hirvonen, A., Veressinina, Y., Hentunen, J. and Munter, R. (1997). Ozonation, ozone/UV and UV/H_2O_2 degradation of chlorophenols. *Ozone: Science and Engineering*, Vol. 19, pp. 75–96.

Trapido, M. and Kallas, J. (2000). Advanced oxidation processes for the degradation and detoxification of 4-nitrophenol. *Environmental Technology*, Vol. 21, pp. 799–808.

United States Department of Energy-Savannah River Operations Office (2000). *High-Level Waste Tank Closure Environmental Impact Statement*, DOE/EIS-0303D, Aiken, South Carolina, USA: United States Department of Energy-Savannah River Operations Office.

United States Department of Energy-Savannah River Operations Office (2014). *Basis for Section 3116 Determination for Closure of the H-Tank Farm at the Savannah River Site*, DOE/SRS-2014-001, Aiken, South Carolina, USA: United States Department of Energy-Savannah River Operations Office.

United States Government Accountability Office (2017*).*

Report to Congressional Addressees: Nuclear Waste

Opportunities Exist to Reduce Risks and Costs by Evaluating Different Waste

Treatment Approaches at Hanford, GAO-17-306, Washington, D.C., USA: United States Government Accountability Office.

Vogelpohl, A, and Kim, S. (2004). *A*dvanced Oxidation Processes (AOPs) in Wastewater Treatment, *Journal of Industrial Engineering Chemistry*, Vol. 10, No. 1, pp. 33-40.

Von Gunten, U. (2003). Ozonation of drinking water: Part I. Oxidation kinetics and product formation. *Water Research*, Vol. 37, No. 7, pp. 1443–1467.

Waite, T., Feitz A., and Aplin, R. (2000). Broadening the Scope of Modified Photo-Fenton Processes in Water and Wastewater Treatment through Ferric Complex Design. In: Chemical Water and Wastewater Treatment VI, Proceedings of the 9th Gothenburg Symposium 2000, 2-4 October, 2000. Istanbul, Turkey.

Wang, F. and Lum, B. Photolytic Destruction of Oxalate in Aqueous Mixed Waste, UCRL-JC-119739, In: *Third Mixed Waste Symposium*, 1995, Baltimore, Maryland, USA, 7-11 August 1995.

Watts, R., Sarasa, J., Loge, Frank J. and Teel, A. (2005). Oxidative and Reductive Pathways in Manganese-Catalysed Fenton's Reactions. *Environmental Engineering*, Vol. 131, pp. 158-164.

Way, T. and Wan, C. (1991). Heterogeneous photocatalytic oxidation of phenol with titanium dioxide powders. *Industrial and Engineering Chemistry Research*, Vol. 30, pp. 1293–1300.

Weber, C. (2001). *Thermodynamic Modelling of Savannah River Evaporators, ORNL/TM-2001/1023*. Oak Ridge, Tennessee, USA: Oak Ridge National Laboratory.

Wiersma B. (2011). *Treatment Tank Corrosion Studies for the Enhanced Chemical Cleaning Process,* SRNL-STI-2010-00535, Rev. 1 Aiken, South Carolina, USA: Savannah River National Laboratory.

Wiersma, B., Mickalonis, J., Subramanian, K. and Ketusky, E. (2012). Corrosion Testing of Carbon Steel in Oxalic Acid Chemical Cleaning Solutions, In: *ACE Corrosion Conference and Expo 2012*, Salt Lake City, Utah, USA, 11-15 March 2012: Vol. 6, pp. 4353-4370.

Wilde, E., Berger, L., and Berger, J. (1984). *Cleaning Agents for Reactor Heat Exchangers, DP-12670*. Aiken, South Carolina, USA: Savannah River Laboratory.

Wiley, J. (1978). *Sodium Oxalate Solubility in Simulated SRP Waste Solutions, DPST-78-480*. Aiken, South Carolina, USA: DuPont de Nemours.

Wille, H. and Berthaldt, H. (2000). Lessons Learned in Full System Decontamination by Application of the CORD Family Concept British Nuclear Energy Society, In: *British*

Nuclear Energy Society, Water chemistry of nuclear reactor systems 8, 22-26 October 2000, Bournemouth, UK. 179-185.

Wille, H., Berthaldt, H. and Roumiguiere, F. (1997). Chemical Decontamination with the CORD UV Process: Principle and Field Experience*, 4th Regional Meeting Nuclear Energy in Central Europe*, 19 September 1997, Bled, Slovenia.

Yoo, J. and Kim, E. (2002). *Decomposition of Oxalate Precipitates by Photochemical Reaction*. Korea: Korea Atomic Energy Research Institute.

Yoon, J. and Jeong, J. (2005). pH effect on OH radical production in photo/ferrioxalate system. *Water Research*, Vol. 39, pp 2893–2900.

Zepp, R., Faust, B. and Holgne, J. (1992). Hydroxyl Radical Formation in Aqueous Reaction (pH 3-8) of Iron (II) with Hydrogen Peroxide: The Photo-Fenton Reaction, *Environmental Science and Technology*, Vol. 26, pp. 313-319.

Zhang, Y., Kailay, N. and Matijevic, E. (1985). *Interactions of Metal Hydrous Oxides with Chelating Agents 7. Hematite-Oxalic Acid and Citric Acid systems*. *Langmuir*, Vol. 1, Issue 2, pp. 201–206.

Zhang, Y., Crittenden, J., Hand, D. and Perram, D. (1994). Fixed-bed photocatalysts for solar decontamination of water. *Environmental Science and Technology*, Vol. 28, pp. 435–442.

Zhang, T., Li, W. and Croué, J. (2011). Catalytic ozonation of oxalate with a cerium supported palladium oxide: an efficient degradation not relying on hydroxyl radical oxidation. *Environmental Science and Technology*, Vol. 45, pp. 9339-9346.

Zhang, T. and Croué, J. (2014). Catalytic ozonation not relying on hydroxyl radical oxidation: a selective and competitive reaction process related to metal–carboxylate complexes, *Applied Catalysis B: Environmental*, Vol. 144, Pages 831–839.

Zuo, Y. and Hoigné, J. (1992). Formation of hydrogen peroxide and depletion of oxalic acid in atmospheric water by photolysis of iron(III)-oxalate complexes. *Environmental Science and Technology*, Vol. 26, Issue 5, pp. 1014-1022.

Zuo, Y. and Deng, Y. (1997). Iron(II) Catalysed Photolysis of Organic Compounds in Atmospheric Water. *Chemosphere*, Vol. 35, pp. 2051-2058.

APPENDICES

APPENDIX 1.

MODEL TO DETERMINE IMPACT OF TANK CLEANING

One disadvantage of using oxalic acidic to clean SRS HLW tanks is that oxalic acid must be carefully managed during decontamination applications because of the sparing solubility of its sodium salt in representative HLW process supernatant equaling about 0.028 M (Weber, 2001; Wiley, 1978). Because of the low solubility, sodium oxalate precipitates form from the oxalic acid solutions in the sodium-rich environment.

During the Historical Baseline Chemical Cleaning Process, a total of about 491,000 litres of 8 wt% oxalic acid solution is added to the HLW *tank being chemically cleaned*.

The impacts are the product of the very high sodium concentrations throughout the HLW process, combined with the limited solubility of sodium oxalate. The solubility of sodium oxalate as a function of sodium concentration is shown in Figure 45.

Where Pike *et al.,* 2004, analysed various SRS applicable sodium oxalate solubility studies including that for the following:

1) A Tank 8 sludge-slurry simulant (with 33 wt% total solids) using 0.24-gram of NaC_2O_4 added per gram of solids, 33 wt% total solids, simulated supernatant includes sodium salts of chloride, hydroxide, carbonate, and sulfate, with a Na concentration of 4.21 M, nitrite concentration of 1.75 M, and a nitrate at concentration of 0.19 M (Pareizs, 2002).
2) Tests where varying amounts of sodium nitrate were added to a 1 M NaOH solution. An excess of NaC_2O_4 was then added to each solution and allowed to equilibrate. The test was then run at three temperatures so the change in solubility with temperature could be estimated (Fowler, 1980).
3) Similar to 2), with the addition of tests where the simulated solution consisted of only sodium nitrate (Wiley, 1978).
4) Tests using a complex simulated waste solution, with the additional components of sodium aluminate, sodium carbonate, and sodium sulfate (Wiley, 1978).

As a result of the comparison, Pike *et al.,* 2004, concluded that "all the data shows the sodium oxalate solubility is relatively insensitive to the anions in solution and the oxalate solubility could be closely estimated as simply a function of the total sodium concentration."

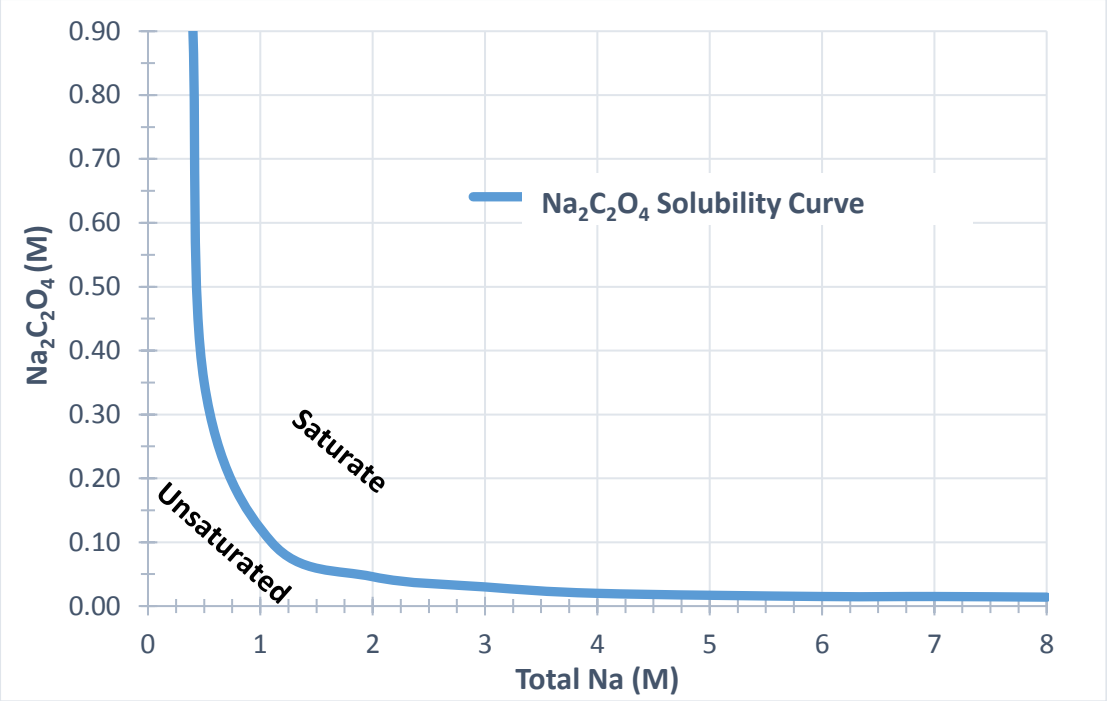

Figure 45. Solubility of sodium oxalate vs sodium concentration.

As a result of the extremely high sodium concentration in the process, use of oxalic acid to chemically clean the SRS HLW tanks results in significant downstream quantities of sodium oxalate precipitate, resulting in significant waste volumes issues. These resultant quantities are calculated within this Appendix.

To summarise: The alkali-treated *hydroxide restored slurry* (which itself will be rich in precipitated sodium oxalate) is subsequently routed to the *Vitrification Feed Preparation (Washing) Tank* (also for convenience referred to as simply the Prep Tank). The combined mix is washed to a sodium concentration of $\leq$ 1 M and to a current maximum sodium oxalate solids loading of 14 wt%. Meantime, the *excess liquid* and *spent wash water* from the *vitrification feed prep tank*, and *free liquid* from the *hydroxide restoration tank* (all saturated with dissolved sodium oxalate) are routed to the *evaporator concentrate receipt tank*, where sodium oxalate will precipitate and become part of the sparingly-soluble *salt heel.* The future dissolving of the *salt heel to* remove the sodium oxalate precipitate will require significant

amounts of additional *salt heel removal water* creating a copious additional *feed for salt processing*. As part of *salt processing*, the supernatant output from the evaporator, containing a large fraction of the oxalate, is mixed with grout and immobilised (i.e. turned into "saltstone)." With salt processing having a typical feed-to-grout ratio of 10 vol%, significant volumes of saltstone will be created. Disposal of the significant volumes of saltstone will consume significant saltstone vault space.

Since the sodium oxalate from the Historical Baseline Chemical Cleaning Process predominantly forms sodium oxalate precipitate in the *hydroxide restoration t*ank, most are transferred as a *hydroxide restored slurry* to the *vitrification feed preparation (washing) tank*. The combined *hydroxide restored slurry* and *vitrification sludge feed batch* will be washed to reduce the sodium concentration, and weight percent loading of sodium oxalate solids, a large fraction of the sodium oxalate solids that are added to the *Vitrification Feed Preparation Tank* will be solubilised (Pike *et al.*, 2004). The solubilised sodium oxalate exits the *Vitrification Feed Preparation Tank* with the *excess liquid* and *spent wash water*. Because of limited free operating volume within the HLW process, both the *excess liquid* and *spent wash water are* sent to the *evaporator concentrate receipt tank.* Because of the high sodium concentration, the vast majority of solubilised oxalate will re-precipitate, becoming part of a sparingly-soluble *salt heel.*

Preparing the combined *hydroxide restored slurry* and *existing vitrification sludge feed* as vitrification feed requires the application of multiple wash-cycles (add water, wash, then drain) to decrease the sodium concentration to Na $\leq$ 1 M (Pike *et al.*, 2004; Shafer, 2010). Also, the sodium oxalate solids loading in the *feed to vitrification* must be maintained at $\leq$ 14 wt% (Pike *et al.*, 2004).

As part of this research, a detailed model was developed to better understand and quantify the effects from performing the Historical Baseline Chemical Cleaning Process on the SRS HLW tanks. Based on operational experience, a representative historical baseline for chemically cleaning of a tank could be defined as the starting with approximately 18,900 litres of sludge using three digestions of 8 wt% oxalic acids in 20:1, 13:1 and 13:1 volume ratios of fresh oxalic acid solution to sludge (Adu-Wusu *et al.*, 2003).

Based on 43 HLW tanks needing to be cleaned with oxalic acid before closure, and the planned total number of *vitrification feed batches* for the life of the vitrification process (about 20 remaining) (Chew and Hamm, 2010), the *hydroxide restored slurry* transferred out of the *hydroxide restoration tank* from the oxalic acid cleaning of two or three HLW tanks would need to be: 1) combined with an *existing vitrification sludge feed batch*, then washed; or, 2) combined with a pre-washed *existing vitrification sludge feed batch,* with the possibility for the need of additional washing.

Based on the solubility of sodium oxalate as a function of sodium concentration, a model was constructed using OLI Stream Analyser® chemical thermodynamic equilibrium modelling software. OLI Stream Analyser® was chosen because of its extensive solubility database specifically properties database and thermodynamic models (Nichols *et al.,* 2001). The model's purpose is to determine the fate of sodium oxalate in the *hydroxide restored slurry* when combined with either a pre-washed or unwashed *existing vitrification sludge feed batch*, with a maximum allowed sodium concentration of 1 M (Pike *et al.*, 2004), and the maximum sodium oxalate solids loading weight fraction. As part of the model, the following variables are evaluated:

- Washing strategy – Combine the *hydroxide restored slurry* to either a pre-washed or unwashed *existing vitrification sludge feed batch*.

- Increasing the weight percent of sodium oxalate solids loading sent in the *feed to vitrification* from the current 14 wt% to 20 wt% based on assuming such an increase will occur because of hypothetical frit improvements.

- The impact of combining the *hydroxide restored slurry* from cleaning either two or three tanks with an *existing vitrification sludge feed batch*.

The impacts were evaluated in terms of:

- Additional washing (i.e. wash-cycles) needed to reduce the sodium concentration in the feed *to vitrification* to both: 1) an acceptable sodium concentration; as well as, 2) an acceptable sodium oxalate solids weight fraction, both required as part of the feed requirements for maintaining vitrification product quality.

- Due to the additional *salt heel* formed in the evaporator, significant quantities of *salt heel removal water* will be required *to* dissolve the *salt heel. When dissolved, this will create a copious additional amount of feed for salt processing*, upon grouting, this will require even more additional *grout* disposal volume.

This study differs from previous reports and material balances in two main ways:

1) The focus is on quantifying the impacts, recognising that the historical processing flowsheet and associated chemistry is very well defined, with significant changes unlikely. The impacts quantified include:

    a. The increase in the amount of washing (i.e. wash cycles) required to prepare the combined *hydroxide restored slurry* and *existing vitrification sludge feed batch* as *feed to vitrification.*

b. The future *feed for salt processing* is expressed in "disposal terms" of current-design-vault space required for disposing of the future copious additional *feed for salt processing* by making of saltstone by solidifying the *feed for salt processing* with grout.

2) Since OLI Stream Analyser® chemical equilibrium models[28] have been shown to require less acid to digest the sludge compared to the SRNL recommended volume ratios for digesting sludge based on laboratory testing (Pike *et al.*, 2004)[29], the model carries the difference (i.e. unspent oxalic acid from the tank chemical cleaning step) and adds it, as unreacted acid, to the *hydroxide restoration tank.*

In the *hydroxide restoration tank,* the free hydroxide concentration is restored to > 1 M using *caustic rich excess process supernatant* (see above). Accounting for inter-model differences in acid requirements in this way ensures that unreacted acid and solids formation can be conservatively factored into determining impacts on vitrification and salt processing.

As previously stated, up to 43 HLW tanks needing to be cleaned with oxalic acid before closure, and the planned total number of vitrification feed batches before closure of the vitrification process (Chew and Hamm, 2010), each planned *vitrification sludge feed batch* will need to accommodate the *hydroxide restored slurry* formed from the cleaning of multiple tanks.

---

[28] OLI Stream Analyser® is a preferred software for thermodynamic modelling digestion of SRS HLW sludge because of the software's extensive databank.

[29] One explanation for the difference between OLI Stream Analyser® based HLW sludge digestion models and reality is that the model does not account for the physical form of the material, such as porosity, including Oswald ripening/ageing.

Because up to 43 tanks will need to be chemically cleaned, the impact assessment is based on the Historical Baseline Chemical Cleaning Process being applied to two or three tanks, with the free hydroxide of the *spent acid slurry* restored by combining the *slurry* with the caustic rich excess process in the *hydroxide restoration tank*. The resultant *hydroxide restored slurry* containing formed sodium oxalate precipitates, is transferred from the *hydroxide restoration tank* to the *vitrification feed preparation (washing) tank* where it is combined with the *existing vitrification sludge feed batch*. As previously shown in Figure 6, there are only two current possible paths for the waste to be removed from the SRS HLW process. That is as 1) f*eed to vitrification*; or, 2) *feed for salt processing*. For oxalate, this can be mathematically shown by Equation 1-1, restated here for completeness.

Sodium oxalate eventually processed to salt processing	=	*total sodium oxalate*	-	*sodium oxalate removed through vitrification*	(eq. 1-1)

- Where, because of the sparing solubility of sodium oxalate, and a significant amount of washing required, the quantities of sodium oxalate sent to *vitrification* can be approximated as the non-solubilised oxalate in the *feed to vitrification*.

- Total sodium oxalate equals include that initially present even before the Historical Baseline Chemical Cleaning Process was applied. The initially present sodium oxalates sources include radiochemical separations, as well as various other activities, including spent decontamination solutions associated with various historical SRS activities. Per Pike *et al.*, 2004, average *salt heels* can be expected to contain 0.45 wt% sodium oxalate, or on a HLW tank basis, about 3.8×10^6 litres of saltcake should contain about 23,500 kg of sodium oxalate, while each *existing vitrification sludge feed batch* before

adding the *hydroxide restored slurry* from the *Hydroxide Restoration Tank* can be assumed to initially contain about 10,000 kg of sodium oxalate solids.

During vitrification feed preparation (washing), the sodium concentration is diluted by each wash cycle. As the sodium concentration decreases and approaches 1 M, the sodium oxalate solubility begins to increase exponentially. As mentioned previously, because of limited free operating volume in the HLW process, the spent wash water containing copious amounts of solubilised sodium oxalate is sent to the *evaporator concentrate receipt tank*.

The oxalate solubility curve as a function of sodium concentration was previously shown in

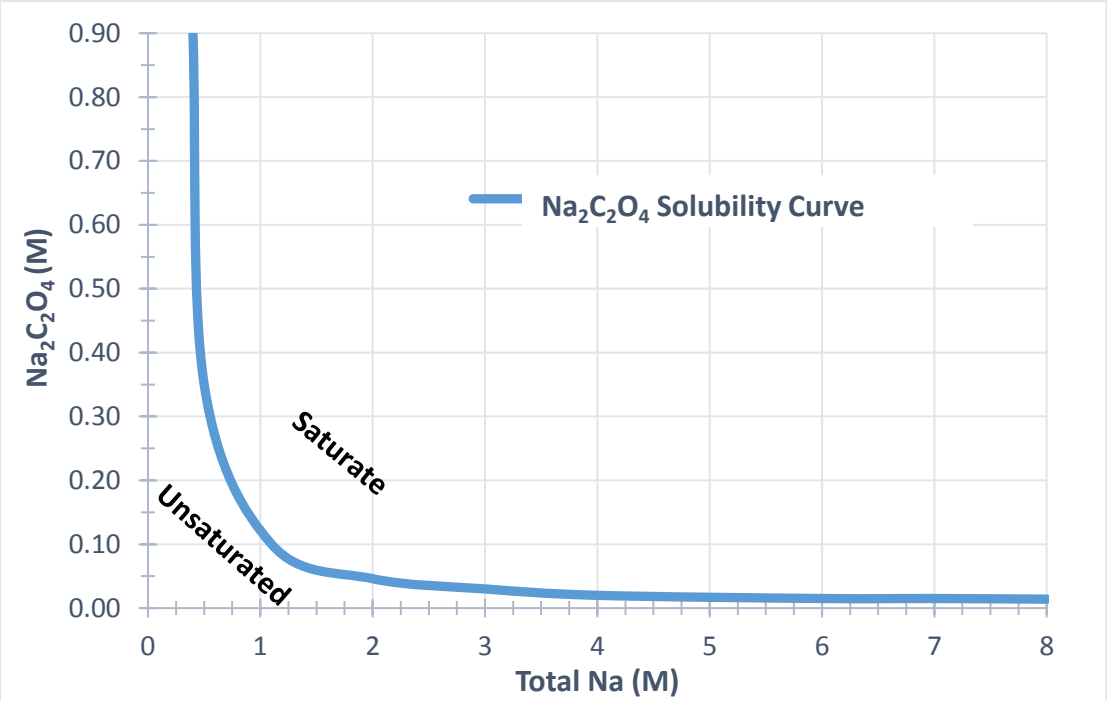

Figure 45 (Pike *et al.*, 2004). Figure 46 shows the same oxalate solubility curve with the current acceptable sodium concentration for *feed to vitrification* on the left, the lowest expected sodium concentration of the *evaporator concentrates receipt tank* on the far right.

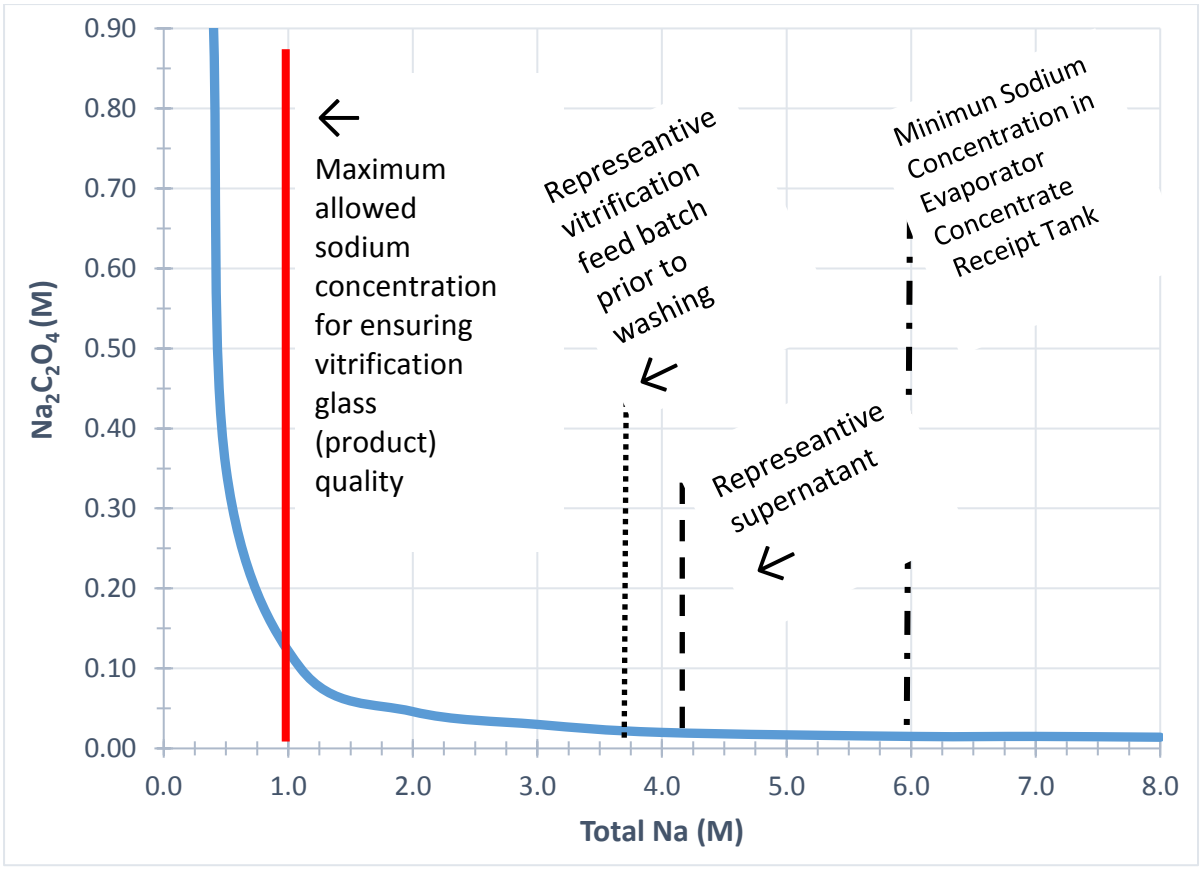

Figure 46. Annotated sodium oxalate solubility vs key sodium concentration for SRS HLW Process.

If the sodium oxalate as part of a *hydroxide restored slurry* is not sent to the *Vitrification Feed Prep Tank*, almost all of would precipitate-out and become part of a sparingly-soluble *salt heel* in the *Evaporator Concentrate Receipt Tank* (Pike *et al.*, 2004). Based on Pike *et al.*, 2004, this addition to the *salt heel* would eventually require using about additional 1,890,000 litres of water to be dissolved. Therefore, when this salt heel is dissolved, the approximate additional 1,890,000 litres of resultant salt solution would become additional *future feed for salt processing*. This additional feed for salt processing from salt heel digestion is shown as Equation A-1.

$$\textit{additional feed for salt processing from cleaning of one tank} = \textit{water required to dissolve sodium oxalate precipitate in salt heel} \times (1 - \textit{fraction of oxalate vitrified}) \quad \text{(eq. A-1)}$$

Where:

- Fraction of the oxalate vitrified is simply that, i.e. the fraction of sodium oxalate from tank cleaning that is eventually vitrified.

- The estimated additional *feed for salt processing* created from digestion of the sodium oxalate contained within an existing sparingly-soluble *salt heel* is 1,890,000 litres (Pike *et al.*, 2004).

A1.1 Modelling Approach

The modelling approach used to estimate the impacts of *Historical Baseline Chemical Cleaning Process* can be best understood as consisting of two different phases:

Phase I – Determining the amount sodium oxalate created from applying the *Historical Baseline Chemical Cleaning Process* on two or three HLW tanks, each with an assumed 18,900 litres of sludge to be digested (Adu-Wusu *et al.*, 2003). Much of this effort is based on SRNL sludge digestion test data, as well using OLI Stream Analyser® for speciation.

Phase II – Based on the known solubility of sodium oxalate, and normal washing parameters/strategies associated with the *vitrification feed preparation (washing) tank*, determine the amount of washing (i.e. wash cycles) required to prepare the *feed to vitrification*. More specifically, this includes:

a. Constructing a simple dilution/wash cycle model replicating the effect of washing on the soluble sodium concentration.

b. Combining the dilution/wash cycle model with the sodium oxalate solubility curve in Figure 46 estimating both the sodium concentration and sodium oxalate solids loading after each wash cycle.

c. Determining the number of wash cycles that are required to decrease the soluble sodium concentration and solid sodium oxalate loading in the *feed to vitrification* using one of the two possible washing strategies:

    i. Combining the *hydroxide restored slurry* from the *hydroxide restoration tank* to an unwashed *existing vitrification sludge feed batch*, and then washing.

    ii. Combining the *hydroxide restored slurry* from the *hydroxide restoration tank* to a pre-washed *existing vitrification sludge feed batch*, with the goal of minimising both the total number of wash cycles, as well as the number of wash cycles required after combing the *hydroxide restored slurry* with the *existing vitrification sludge feed batch.*

d. Calculating the fraction of sodium oxalate that ultimately remains part of the *feed to vitrification*.

e. Determine the impacts to salt processing by:

    i. Using Equation A-1 to calculate the additional future volume of *feed for salt processing*.

ii. Knowing the feed-to-grout ratio used to make saltstone, as well as the volume of the current *saltstone vault design*, determine the additional vault space needed to accommodate the copious additional feed for salt *processing* from cleaning two or three tanks.

The initial pH of the sludge in the *tank being cleaned* before adding the oxalic acid solution, based on previous waste removal efforts will have a pH of approximately 10.5 (Adu-Wusu *et al.*, 2003). The solid's mass in *sludge being digested* at the time of initiating the *Historical Baseline Chemical Cleaning Process* has been shown to be about one kg of dry solids per 3.78 litres of "wet" sludge (Thomas, 2004). As previously stated, the volume of the sludge in the tank to be cleaned before initiation of historical baseline chemical cleaning has been shown to typically be 18,900 litres (Adu-Wusu *et al.*, 2003).

A1.2 Inputs, Models, and Results

A1.2.1 Phase I of Model – Sodium Oxalate Produced

As previously discussed, the historical baseline oxalic acid cleaning process for the HLW tanks shows that the *tank to be cleaned* has undergone bulk sludge removal (i.e. significant rinsing) and therefore has pH is approximately 10.5 (Adu-Wusu *et al.*, 2003). The solid's mass in the sludge is approximately 1 kg per 3.78 litres (Thomas, 2004). The volume of the sludge at the start of *Historical Baseline Chemical Cleaning Process* is based on previous cleaning campaigns and typically about 18,900 litres. The unwashed solids contributing greater than 1 wt% of the solid's mass in a representative F-Area tank and a representative H-Area tank are representative of the sludge before tank mechanical cleaning.

The *Historical Baseline Chemical Cleaning Process* uses 8 wt% oxalic acid. The SRNL recommended volume ratio for the first digestion is 20 to 1 oxalic acid solution to sludge, while

both subsequent ratios are 13 volume parts of oxalic acid solution to 1 volume part sludge. The ratios are based on years or SRNL testing (Adu-Wusu *et al.*, 2003). Table 23 shows the SRNL recommend quantities of acid if using the *Historical Baseline Chemical Cleaning Process* (Adu-Wusu *et al.*, 2003).

Table 23. SRNL recommended quantities of 8 wt% oxalic acid for the *Historical Baseline Chemical Cleaning Process*.

Constituent	1st digestion (kg)	2nd digestion (kg)	3rd digestion (kg)
Water	378,000	73,700	36,900
Dry Oxalic Acid	30,200	5,900	2,950
Acid Solution to Sludge (vol/vol)	20:1	13:1	13:1

Using OLI Stream Analyzer®, a flow sheet was constructed for of the process described in Figure 6-Area using both F-Area and H-Area waste tanks. The detailed flowsheet is graphically shown as Figure 47 with the additional feed to vitrification modelled using OLI Stream Analayzer® with values shown by Table 24 and Table 25.

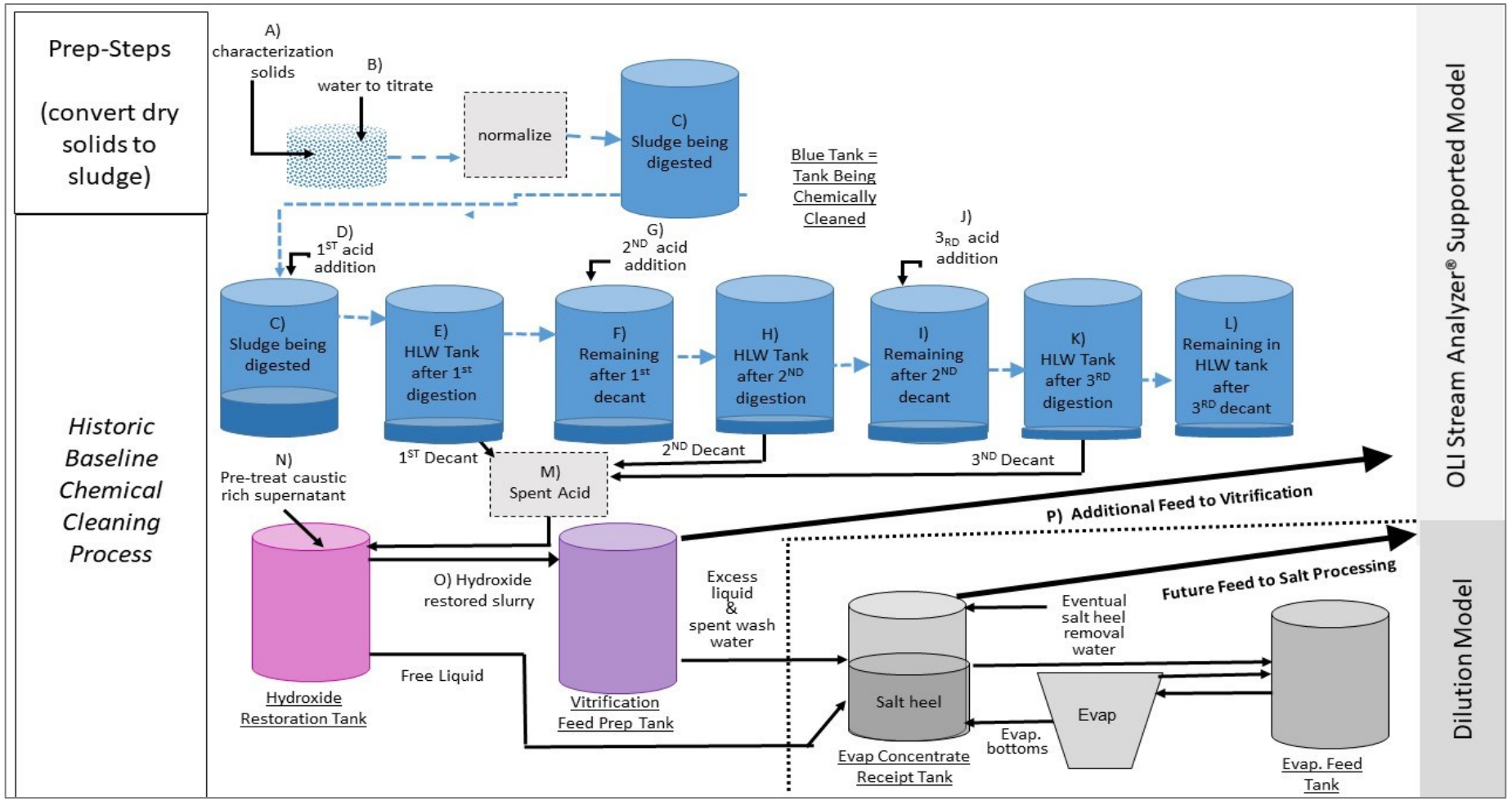

Note: Multiple Evaporator Feed Tanks, Evaporators, and Evaporator Concentrate Receipt Tanks exist at SRS, with only one overall D) Evaporator System shown to maintain clarity.

Figure 47. Flowsheet of *Historical Baseline Chemical Cleaning Process* for cleaning SRS HLW tanks.

Prep-Steps (Prior to Chemical Cleaning) - Converting Dry Solids Data to Sludge

As a prerequisite, prior to beginning chemical cleaning to represent the sludge being digested, the dry solids characterisation is converted to a representative sludge characterisation (Column A of Table 24 and 25). The dry solids represent the solid constituents accounting for at least 95 wt% of the solid sludge mass. Using the chemical thermodynamic equilibrium software (i.e. the OLI Stream Analyser®), the contents are modelled as "titrated" to a pH of 10.5, then normalised to ~18,900 kg aqueous and ~5,000 kg solids, being representative of the quantity of *sludge being digested* in a *HLW tank being cleaned.* The titration to a pH of 10.5 is shown by Column B of Tables 24 and 25. The resultant values for the sludge to be digested are shown by Column C of Tables 24 and 25.

Historical Baseline Chemical Cleaning Process

Column C represents the sludge in the HLW tank immediately before initiation of the *Historical Baseline Chemical Cleaning Process*.

Only the necessary fraction of acid to achieve the SRNL observed approximate 70 wt% digestion of the original solids (i.e. about 30% of the original sludge solid's mass remains), followed by approximate 50 wt% digestion of what remains (i.e. about 15% of the original sludge solid's mass remains), followed by an approximate 25 wt% digestion (i.e. about 11% of the original sludge solid's mass remains) is used in the digestion segment of the model. To ensure representative modelling of oxalate formed and solids remaining, the remainder of the acid is carried forward as unreacted acid and added to the *Hydroxide Restoration Tank,* (i.e. cumulative approx. unreacted acid in Column M for F and H-Area equals 33,300 kg).

The 1st 2nd and 3rd sequential acid additions are shown by Column D, G, and J, with Columns E, H and K showing the result from the acid addition immediately after digestion. Columns F, I, L show the contents remaining in the HLW tank being chemically cleaned after all decants.

The combined *spent acid* transferred out of both the F-Area and H-Area tanks are approximately equal, with the Approx. Total of each for both F and H being 520,000 kg each. Column M is then added to the *Caustic Rich (Excess) Supernatant,* Column N.

Specifically, using OLI Stream Analyser® chemical thermal dynamic equilibrium software, the *Spent Acid Sent to the Hydroxide Restoration Tank*, Column M and just enough Ca*ustic Rich Supernatant,* are combined to achieve a free hydroxide concentration just > 1 M. Column O shows the speciation of the *hydroxide restored slurry.*

Using an 8:3 mass ratio of the *hydroxide restored* slurry aqueous (i.e. aq. in Column O) to solids, a slurry is created and transferred to the *Vitrification Feed Prep Tank* and either: 1) combined with a pre-washed *existing vitrification sludge batch*; or, 2) combined with an *existing vitrification sludge batch*, then washed.

The *free liquid* in the *hydroxide restoration tank* not required to support making the 8:3 slurries for transfer to the *Vitrification Feed Preparation Tank* are sent directly to the *Evaporator Concentrate Receipt Tank.* (However, the aq. used to make the transfer slurry will also be returned and sent to the *Evaporator Concentrate Receipt Tank*, as part of the spent wash water created from sludge washing). After draining the *excess liquid* and *spent wash water* to *Evaporator Concentrate Receipt Tank*, the transferred solids added to *Vitrification Feed Prep Tank* are shown in Column P of Tables 24 and 25. As shown in Column O of Tables 24 and 25, for both the F and H-Area HLW tanks, about 51,000 kg of sodium oxalate, $Na_2C_2O_4$, solids from the *Historical Baseline Chemical Cleaning Process* can be assumed to be transferred to the *Vitrification Feed Prep Tank* and combined with the *existing vitrification sludge feed batch.*

Table 24. F-Area tank cleaning flowsheet, from initial tank sludge solids through solids being transferred to vitrification feed batch (i.e. OLI® Based Model).

Constituent	A	B	C		D	E		F		G	H		I		J	K		L		M	N	O		P
	F-Area sludge solids		Sludge in HLW Tank before Chemical Cleaning		1st acid addition to HLW tank	HLW Tank after 1st digestion		Remaining in HLW tank after 1st decant		2nd acid addition to HLW tank	HLW Tank after 2nd digestion		Remaining in HLW tank after 2nd decant		3rd acid addition to HLW tank	HLW Tank after 3rd digestion		Remaining in HLW tank after 3rd decant		Spent acid sent to OH Restore	Pre-treat caustic rich	OH restored slurry		Additional Feed to Vitrified-
	(mass faction)		aq. (kg)	solid (kg)	aq. (kg)	aq. (kg)	solid (kg)	aq. (kg)	solid (kg)	aq. (kg)	aq. (kg)	solid (kg)	aq. (kg)	solid (kg)	aq. (kg)	aq. (kg)	solid (kg)	aq. (kg)	solid (kg)	(kg)	(wt%)	aq. (kg)	solid (kg)	solid (kg)
$Al(OH)_3$	0.21		0	1200	0	0	800	0	800	0	0	160	0	160	0	0	0	0	0	0	0	0	9700	9700
AlOOH	0		0	0	0	350	0	5	0	0	490	0	20	0	0	150	0	70	0	950	0	410	0	0
$Ca(OH)_3$	0.04		0	0	0	0	0	0	0	0	0	0	0	0	0	0	0	0	0	0	0	0	0	0
CaO	0		0.1	0	0	0.1	0	0	0	0	0	0	0	0	0	0	0	0	0	0.1	0	0.1	0	0
$CaCO_3$	0		0	0	0	0	0	0	0	0	0	0	0	0	0	0	0	0	0	0	0	0.1	0	0
CO_2	0		0.04	0	0	62	0	1	0	0	1	0	0	0	0	0	0	0	0	62	0	3900	0	0
$Fe(OH)_3$	0.4		0	2400	0	0	0	0	0	0	0	0	0	0	0	0	0	0	0	0	0	0	2400	2400
$Fe_2(C_2O_4)_3$	0		0	0	0	4200	0	60	0	0	60	0	2	0	0	2	0	1	0	4200	0	18.1	0	0
H_2O	0		18900	0	380000	399300	0	5700	0	74000	79000	0	2800	0	37000	40000	0	18900	0	50000	67.4	803000	0	0
$H_2C_2O_4$	0		0	0	30000	800	0	10	0	5900	1500	0	60	0	3,000	900	0	447	0	3200	0	4100	0	0
HCl	0		0.04	0	0	0	0	0	0	0	0	0	0	0	0	0	0	0	0	0	0	0	0	0
HNO_2	0		0	0	0	0	0	0	0	0	0	0	0	0	0	0	0	0	0	0	0	9,200	0	0
HNO_3	0		0.05	0	0	0	0	0	0	0	0	0	0	0	0	0	0	0	0	0	0	51400	0	0
HgO	0		0	0	0	4	0	0.1	0	0	0.1	0	0	0	0	0	0	0	0	4	0	4	0	0
MnO_2	0.04		0	0	0	0	0	0	0	0	0	0	0	0	0	0	0	0	0	0	0	0	0	0
$Mn(OH)_2$	0		0	90	0	0	0	0	0	0	2	0	0.1	0	0	0	0	0	0	2	0	0	140	140
$MnCO_3$	0		0	160	0	0	0	0	0	0	0	0	0	0	0	0	0	0	0	0	0	0	0	0
$MnC_2O_4 2H_2$	0		0	0	0	0	200	0	200	220	0	170	0	170	0	0	160	0	160	0	0	0	0	0
MnC_2O_4	0		0	0	0	0	0	0	0	0	45	0	2	0	0	12	0	6	0	55	0	0	0	0
NaCl	0.01		0	0	0	0	0	0	0	0	0	0	0	0	0	0	0	0	0	0	0	0	0	0
$NaNO_3$	0.01		0	0	0	0	0	0	0	0	0	0	0	0	0	0	0	0	0	0	15.8	0	0	0
$NaNO_2$	0		0	0	0	0	0	0	0	0	0	0	0	0	0	0	0	0	0	0	3.1	0	0	0
NaOH	0.04		0	0	0	0	0	0	0	0	0	0	0	0	0	0	0	0	0	0	7.6	0	0	0
Na_2O	0		0.02	0	0	0.2	0	0	0	0	0	0	0	0	0	0	0	0	0	0.2	0	45600	0	0
$NaAlO_3$	0		0	0	0	0	0	0	0	0	0	0	0	0	0	0	0	0	0	0	2.2	0	0	0
Na_2CO_3	0		0	0	0	0	0	0	0	0	0	0	0	0	0	0	0	0	0	0	2.1	0	0	0
$Na_2C_2O_4$	0		0	0	0	0	0	0	0	0	0	0	0	0	0	0	0	0	0	0	0	0	51000	51000
KOH	0		0	0	0	0	0	0	0	0	0	0	0	0	0	0	0	0	0	0	0.1	0	0	0
K_2O	0		0	0	0	0	0	0	0	0	0	0	0	0	0	0	0	0	0	0	0	270	0	0
$Ni(OH)_2$	0.04		0	230	0	0	0	0	0	0	0	0	0	0	0	0	0	0	0	0	0	0	7	7
NiC_2O_4	0		0	0	0	11	0	0.2	0	0	0.2	0	0.1	0	0	0	0	0	0	14	0	0.1	0	0
$NiC_2O4.2H_2$	0		0	0	0	0	430	0	430	0	0	430	0	0	0	0	0	0	0	0	0	0	0	0
SiO_2	0.01		0	0	0	0.1	0	0	0	0	0	0	0	0	0	0	0	0	0	0.1	0	14	0	0
$UO_2(OH)_2$	0.15		0	880	0	1000	0	15	0	0	15	0	0.5	0	0	0.5	0	0.3	0	1000	0	0	0	0
$UO_2C_2O_4$	0		0	0	0	0	0	0	0	0	0	0	0	0	0	0	0	0	0	0	0	1000	0	0
Sum	0.95		18900	5000	410000	410000	1500	5800	1500	80000	81000	765	2900	770	40000	41000	590	2200	590	520000	NA	900000	60000	60000
Unreacted acid			NA	NA	NA	29500	NA	NA	NA	NA	4300	NA	NA	NA	NA	2000	NA	1040	NA	33300	NA	0	0	0
Cumulative of unreacted acid			NA	NA	NA	29500	NA	NA	NA	NA	33800	NA	NA	NA	NA	35800	NA	2,500	NA	33300	NA	0	0	0

Titate to pH=10.5

Note: All minor mass constituents are not shown.

Table 25. H-Area tank cleaning flowsheet, from initial tank sludge solids through solids being transferred to vitrification feed batch (i.e. OLI® Based Model).

Constituent	A	B	C		D	E		F		G	H		I		J	K		L		M	N	O		P
	H-Area sludge solids		Sludge in HLW Tank before Chemical cleaning		1st acid addition to HLW tank	HLW Tank after 1st digestion		Remaining in HLW tank after 1st decant		2nd acid addition to HLW tank	HLW Tank after 2nd digestion		Remaining in HLW tank after 2nd decant		3rd acid addition to HLW tank	HLW Tank after 3rd digestion		Remaining in HLW tank after 3rd decant		spent acid slurry sent to OH Restoratn Tank	Pre-treat caustic rich	OH restored slurry		Additional Feed to Vitrified-cation
	(mass fractio		aq.	solid	aq.	aq.	solid	aq.	solid	aq.	aq.	solid	aq.	solid	aq.	aq.	solid	aq.	solid			aq.	solid	solid
			(kg)		(kg)	(kg)		(kg)		(kg)	(kg)		(kg)		(kg)	(kg)		(kg)		(kg)	(wt%)	(kg)		(kg)
$Al(OH)_3$	0.46		0	2800	0	0	1000	0	1000	0	0	320	0	320	0	0	130	0	1127	0	0	0	9700	9700
AlOOH	0		0.03	0	0	1400	0	20	0	0	540	0	20	0	0	170	0	80	0	2000	0	410	0	0
$C_2H_2O_4$	0		0.1	0	0	0	0	0	0	0	0	0	0	0	0	0	0	0	0	0	0	0	0	0
$Ca(OH)_3$	0.01		0	0	0	1	0	0	0	0	0	0	0	0	0	0	0	0	0	0	0	0	0	0
CaO	0		1	0	0	0.2	0	0	0	0	0	0	0	0	0	0	0	0	0	0.3	0	0.1	0	0
$CaCO_3$	0		0	80	0	0	0	0	0	0	0	0	0	0	0	0	0	0	0	0	0	0.1	0	0
CaC_2O_4	0.003	Titrate to pH = 10.5	0	0	0	0	0	0	0	0	0	130	0	130	0	0	130	0	133	0	0	0	0	0
$CaC_2O_4.H_2O$	0		0	20	0	0	130	0	130	0	0	0	0	0	0	0	0	0	0	0	0	0	0	0
CO_2	0		0.1	0	0	40	0	0.5	0	0	1	0	0	0	0	0	0	0	0	40	0	3900	0	0
$Fe(OH)_3$	0.26		0	1600	0	0	0	0	0	0	0	0	0	0	0	0	0	0	0	0	0	0	2400	2400
$Fe_2(C_2O_4)_3$	0		0	0	0	2800	0	40	0	0	60	0	1	0	0	1	0	1	0	2800	0	18.1	0	0
H_2O	0		18700	0	380000	400000	0	5700	0	74000	80000	0	2800	0	37000	40000	0	18900	0	507000	67.4	803000	0	0
$H_2C_2O_4$	0		0	0	30000	3800	0	50	0	5900	1700	0	60	0	3000	560	0	267	0	5900	0	4100	0	0
HCl	0		5	0	0	5	0	0.1	0	0	0.1	0	0	0	0	0	0	0	0	5	0	0	0	0
HNO_2	0		0	0	0	0	0	0	0	0	0	0	0	0	0	0	0	0	0	0	0	9200	0	0
HNO_3	0		60	0	0	60	0	1	0	0	0	0	0	0	0	0	0	1	0	260	0	51400	0	0
HgO	0.04		1	260	0	260	0	4	0	0	4	0	0.1	0	0	0.1	0	0	28	4	0	4	0	0
MnO_2	0.03		0	0	0	0	0	0	0	0	0	0	0	0	0	0	0	0	0	0	0	0	0	0
$Mn(OH)_2$	0		0	180	0	0	0	0	0	0	2	0	0.1	0	0	0	0	0	0	2	0	0	140	140
$MnCO_3$	0		0	3	0	0	0	0	0	0	0	0	0	0	0	0	0	19256	544	0	0	0	0	0
$MnC_2O_4\,2H_2O$	0		0	0	0	0	220	0	220	0	0	150	0	150	0	0	130	80	0	0	0	0	0	0
MnC_2O_4	0		0.1	0	0	120	0	2	0	0	60	0	2	0	0	15	0	0	127	190	0	0	0	0
$NaNO_3$	0.04		0	0	0	0	0	0	0	0	0	0	0	0	0	0	0	0	0	0	15.8	0	0	0
$NaNO_2$	0		0	0	0	0	0	0	0	0	0	0	0	0	0	0	0	0	0	0	3.1	0	0	0
NaOH	0.03		0	0	0	0	0	0	0	0	0	0	0	0	0	0	0	0	0	0	7.6	0	0	0
Na_2O	0		70	0	0	70	0	1	0	0	1	0	0	0	0	0	0	0	0	70	0	46000	0	0
$NaAlO_3$	0		0	0	0	0	0	0	0	0	0	0	0	0	0	0	0	0	0	0	2.2	0	0	0
Na_2CO_3	0		0	0	0	0	0	0	0	0	0	0	0	0	0	0	0	0	0	0	2.1	0	0	0
$Na_2C_2O_4$	0		0	0	0	0	0	0	0	0	0	0	0	0	0	0	0	0	0	0	0	0	51000	51000
K_2O	0		0	0	0	0	0	0	0	0	0	0	0	0	0	0	0	0	0	0	0	270	0	0
$Ni(OH)_2$	0.004		0	25	0	0	0	0	0	0	0	0	0	0	0	0	0	0	0	0	0	0	7	7
NiC_2O_4	0		0	0	0	10	0	0.2	0	0	3	0	0.1	0	0	0	0	0	0	14	0	0	0	0
$NiC_2O4.2H_2O$	0		0	0	0	0	32	0	32	0	0	29	0	29	0	0	0	0	0	0	0	0	0	0
SiO_2	0.06		75	100	0	40	130	1	130	0	9	120	0.3	123	0	0	0	0	0	60	0	14	0	0
$UO_2(OH)_2$	0.0020		0	12	0	0	0	0	0	0	0	0	0	0	0	0	0	0	0	0	0	0	0	0
$UO_2C_2O_4$	0		0	0	0	10	0	0.2	0	0	0.2	0	0	0	0	0	0	0	15	15	0	1000	0	0
Sum	0.96		18900	5000	410000	410000	1500	5800	1500	80000	82000	760	3000	760	40000	41000	540	2200	590	520000	NA	900000	60000	60000
Unreacted acid			NA	NA	NA	26000	NA	NA	NA	NA	4200	NA	NA	NA	NA	2400	NA	1200	NA	30000	NA	NA	NA	NA
Cumulative of unreacted acid			NA	NA	NA	29500	NA	NA	NA	NA	31000	NA	NA	NA	NA	33000	NA	2500	NA	33300	NA	NA	NA	NA

Note: All minor mass constituents are not shown.

A2.2.2 Phase II of Model – Washing/Effect of Solubility on Preparing Feed for Vitrification (Based on Using a Simple Sodium Dilution Model)

Based on the HLW system plan (Chew and Hamm, 2010), the following assumptions were used as input into creating the *vitrification feed preparation (washing) tank batch* preparation model. Based on previous cited SRS sludge washing studies, the effect of sludge washing on sodium concentration, the net result can be approximated by using a simple dilution model (Fowler, 1980; Wiley, 1978; Pareizs, 2002).

1) Based on pump-down capability, the *vitrification feed preparation washing tank* will always contain a least 18,900 litres of liquid, with a maximum fill volume of 2,600,000 litres.

2) A representative initial sodium concentration of the *vitrification sludge feed batch* before washing is assumed to be 3.7 M. (HLW Engineering, 2008), with washing performed until the Na concentration is < 1 M (Subosits, 1994). Although, the sodium concentration of the *caustic rich excess process supernatant* is typically much > than 6 M (Ketusky *et al.*, 2011), a representative Na concentration in the supernatant in the Tank Farm is 4.21 M (Pareizs, 2002), with the existing *vitrification sludge feed batch* sodium concentration diluted as a result of mechanical cleaning.

3) About 200,000 kg of *vitrification sludge feed* is considered to be representative of the size of planned future batches. That is, smaller batches require less washing. Since the *feed to vitrification* preparation time is so restrictive (i.e. there is little free time), smaller batches are preferred because they are less likely to result in a feed break (Chew and Hamm, 2010).

Laboratory analysis shows that the *existing vitrification sludge* even before adding the *hydroxide restored slurry* from the *hydroxide restoration tank* is likely saturated with oxalate (Pike *et al.*, 2004). As previously discussed as part of Equation 1-1, much of this oxalate can be attributed radiochemical separations, as well as various other activities. Therefore, even without chemically cleaning the HLW tanks with oxalic acid, each *existing vitrification sludge feed batch* (before adding any *hydroxide restored slurry* from the *hydroxide restoration tank*) can be assumed to initially contain about 10,000 kg of sodium oxalate solids (Pike *et al.*, 2004).

Currently, the maximum solid sodium oxalate loading for a *feed to vitrification* is about 14 wt% (Pike *et al.*, 2004). For comparative reasons the model evaluates both 14 wt% and 20 wt%, with the use of 20 wt% based on assuming some hypothetical future operational improvements will allow an increased solid sodium oxalate loading. In modelling, the *feed to vitrification* is washed until the Na concentration is < 1 M (Subosits, 1994). This maximum Na concentration limit is based on the current frit selection, with other possible frits assumed to be similar. In contrast, the minimum Na concentration limit post washing is Na > 0.25 M. This is based on the fact that a very low sodium concentration also does not support vitrification product quality (Pike *et al.*, 2004). For the modelling, therefore, the sodium concentrations of the *feed to vitrification* are maintained between 0.25 M < Na < 1.0 M.

When considering removing the oxalate from the HLW process as *feed to vitrification,* there are two possible washing strategies. They are:

i. Add the *slurry* to an unwashed *existing vitrification sludge feed batch*, drain *excess liquid* then wash as required, or,

ii. Prewash the *existing vitrification sludge feed batch*, then add the *slurry* and drain the excess liquid, with the goal of minimising the necessary number of wash cycles.

As such, the four cases considered were:

Case #1

The slurry would be combined with an unwashed *vitrification sludge feed.* The combined contents of the *Vitrification Feed Preparation Tank* would then be washed. The maximum sodium oxalate solids loading is set at ≤ 14 wt% of the total sludge solids.

Case #2

The slurry would be combined with a pre-washed *vitrification sludge feed batch.* The contents of the *Vitrification Feed Preparation Tank* would then be washed. The maximum sodium oxalate solids loading is set at ≤ 14 wt% of the total sludge.

Case #3

The slurry would be combined with an unwashed *vitrification sludge feed batch.* The contents of the *Vitrification Feed Preparation Tank* would then be washed. The maximum sodium oxalate solids loading is set at ≤ 20 wt% of the total sludge solids.

Case #4

The slurry would be combined with a pre-washed *vitrification sludge feed.* The contents of the *Vitrification Feed Preparation Tank* would then be washed. The maximum sodium oxalate solids loading is set at ≤ 20 wt% of the total sludge solids.

Table 26 summarizes these cases.

Table 26. Bases for the four vitrification feed preparation washing tank cases.

Case	Wash strategy	Explanation	Sodium oxalate loading
#1	Unwashed	No up-front washing before adding slurry	14 wt% of total solid's mass
#2	Pre-washed	Maximised up-front washing before slurry	14 wt% of total solid's mass
#3	Unwashed	No up-front washing before adding slurry	20 wt% of total solid's mass
#4	Pre-washed	Maximised up-front washing before slurry	20 wt% of total solid's mass

Table 26 shows the inputs and assumptions for Case #1 through Case #4.

Table 28 shows the Case #1 impact from chemically cleaning two HLW tanks, while Table 29 through Table 35 show the remaining results of the different cases.

Table 27. Inputs/assumptions for Dilution Model

Feed to vitrification		**Bases/references**
Mass of *existing vitrification sludge feed batch*	200,000 kg	(Chew and Hamm, 2010)
Initial Na concentration in *existing vitrification sludge feed batch* before adding slurry	3.70 M	(HLW Engineering, 2008)
Pumped-down minimum volume of vitrification *feed preporation tank*	1,890,000 litres	(HLW Engineering, 2008)
Mass of sodium oxalate solids in *existing vitrification sludge feed batch*	10,000 kg	(Pike *et al.*, 2004)
Na from $Na_2C_2O_4$ in *existing vitrification sludge feed batch*	3,433 kg	Calculated from mass of sodium oxalate solids in *existing vitrification sludge feed batch*
Volume of wash water added in a typical *Vitrification Feed Preparation Tank wash cycle*	661,500 litres	Calculated from pump down capacity and maximum operating volume of the *Vitrification Feed Preparation Tank*
Additions from *hydroxide restored slurry*		
Solid $Na_2C_2O_4$ in *hydroxide restored slurry*	51,000 kg	Solid $Na_2C_2O_4$ from *hydroxide restored slurry*, Column O, solids (kg) from Table 24 and 25.
Na calculated from solid $Na_2C_2O_4$ in *hydroxide restored slurry*	17,507 kg	Calculated from solid $Na_2C_2O_4$ in *hydroxide restored slurry,* immediately above.
Aqueous Na_2O in *hydroxide restored slurry*	46,000 kg	*Aqueous* Na_2O from *hydroxide restored slurry*, Column O, aqueous (kg) from Table 24 and 25.
Na calculated from aqueous Na_2O in *hydroxide restored slurry*	12,917 kg	Calculated from aqueous Na_2O in *pH restored slurry,* immediately above.
Mass of water available in *hydroxide restored slurry*	803,000 kg for F-Area 807,000 kg for H-Area	Aqueous O from *hydroxide restored slurry,* Column O, aqueous (kg) of Table 24 and 25.
Mass of slurry transferred to V*itrification Feed Batch Preparation Tank*	306,000 litres	Slurry transferring slurry calculated by multiplying *hydroxide restored slurry immediately above* used to transfer solids based on the assumed supernatant to solid's mass ratio (~8/3) used for transferring slurries.
Maximum operating volume of *Vitrification Feed Preparation Tank*	2,551,500 litres	(Pike *et al.,* 2004)

Table 28. Results for Case #1 with two tanks - add *slurry* to an unwashed *vitrification sludge feed batch,* then wash to [Na] ≤ 1 M with a solid sodium oxalate loading of ≤ 14 wt% (Based on Simple Sodium Dilution Model).

Washing type steps	Actions	Initial feed volume in Prep Tank (litre)	Initial Na in the feed [M]	Initial $Na_2C_2O_4$ in the feed (kg)	Add Wash Water to Prep Tank (litre)	Combined Volume in Prep Tank (litre)	Final Na [M]	aq. $Na_2C_2O_4$ [M]	Remove excess liquid from Prep Tank (litre)	$Na_2C_2O_4$ Removed (kg)	$Na_2C_2O_4$ Remaining in the feed (wt%)	Volume remaining in prep tank when drained (litre)
		Initial slurry/feed properties			Action-add water	Property			Action - drain		Property	
	None - existing vitrification sludge feed batch already in Prep Tank	1.89E+6	3.70	1.00E+4								
	Add slurry from cleaning one tank (Column P of Tables 24 and 25, plus an 8/3 mass ratio of Column O aq. to solids)	3.06E+5	4.32	5.10E+4								
1	Drain Prep Tank to minimum volume to maximise washing efficiency	2.20E+6	3.79	6.10E+4	0	2.20E+6	3.79	0.02	3.06E+5	7.79E+2	30	1.89E+6
	Repeat slurry addition above	3.06E+5	4.32	5.10E+4								
2	wash and drain	2.20E+6	3.86	1.11E+5	3.56E+5	2.55E+6	3.32	0.02	6.62E+5	1.95E+3	55	1.89E+6
3	wash and drain	1.89E+6	3.32	1.09E+5	6.62E+5	2.55E+6	2.46	0.03	6.62E+5	2.66E+3	53	1.89E+6
4	wash and drain	1.89E+6	2.46	1.07E+5	6.62E+5	2.55E+6	1.82	0.04	6.62E+5	3.90E+3	51	1.89E+6
5	wash and drain	1.89E+6	1.82	1.03E+5	6.62E+5	2.55E+6	1.35	0.07	6.62E+5	6.20E+3	48	1.89E+6
6	wash and drain	1.89E+6	1.35	9.65E+4	6.62E+5	2.55E+6	1.00	0.10	6.62E+5	8.86E+3	44	1.89E+6
7	wash and drain	1.89E+6	1.00	8.76E+4	6.62E+5	2.55E+6	0.74	0.12	6.62E+5	3.90E+3	42	1.89E+6
8	wash and drain	1.89E+6	0.74	8.37E+4	6.62E+5	2.55E+6	0.55	0.13	6.62E+5	1.15E+4	36	1.89E+6
9	wash and drain	1.89E+6	**0.55**	7.22E+4	6.62E+5	2.55E+6	0.41	0.50	6.62E+5	4.43E+4	**14**	1.89E+6

Wash Step 9 above shows the [Na] =0.55 M and the $Na_2C_2O_4$ solids loading at 14 wt%, and therefore after the 9th wash batch, the feed would be acceptable for vitrification.

Table 29. Results for Case #1 with three tanks - add *slurry* to an unwashed *vitrification sludge feed batch,* then wash to [Na] ≤ 1 M with a solid sodium oxalate loading of ≤ 14 wt% (Based on Simple Sodium Dilution Model).

Washing type steps	Actions	Initial feed volume in Prep Tank (litre)	Initial Na in the feed [M]	Initial $Na_2C_2O_4$ in the feed (kg)	Add wash water to Prep Tank (litre)	Combined volume in Prep Tank (litre)	Final Na [M]	aq. $Na_2C_2O_4$ [M]	Remove excess liquid from Prep Tank (litre)	$Na_2C_2O_4$ removed (kg)	$Na_2C_2O_4$ remaining (wt%)	Volume in Prep Tank when drained (litre)
		Initial slurry/feed properties			Action - add water	Property			Action - drain		Property	
	None - existing vitrification sludge feed batch already in Prep Tank	1.89E+6	3.70	1.00E+4								
	Add slurry from cleaning one tank (Column P of Tables 24 and 25, plus an 8/3 mass ratio of Column O aq. to solids)	3.06E+5	4.32	5.10E+4								
1`	Drain Prep Tank to minimum drain-down volume to maximise efficiency	2.20E+6	3.79	4.55E+5	0	2.20E+6	3.79	0.019	3.06E+5	7.79E+2	30	1.89E+6
	Repeat slurry addition above	1.89E+6	3.70	1.00E+4								
2	Drain Prep Tank to minimum volume to maximise efficiency	2.20E+6	3.86	8.30E+5	0	2.20E+6	3.86	0.019	3.06E+5	7.79E+2	55	1.89E+6
	Repeat slurry addition above	1.89E+6	3.70	1.00E+4								
3	Drain Prep Tank to minimum volume to maximise efficiency	2.20E+6	3.93	1.20E+6	0	2.20E+6	3.93	0.02	3.06E+5	7.38E+2	80	1.89E+6
4	wash and drain	1.89E+6	3.93	1.20E+6	6.62E+5	2.55E+6	2.91	0.03	6.62E+5	2.22E+3	79	1.89E+6
5	wash and drain	1.89E+6	2.91	1.18E+6	6.62E+5	2.55E+6	2.15	0.04	6.62E+5	3.10E+3	78	1.89E+6
6	wash and drain	1.89E+6	2.15	1.16E+6	6.62E+5	2.55E+6	1.60	0.06	6.62E+5	4.88E+3	75	1.89E+6
7	wash and drain	1.89E+6	1.60	1.12E+6	6.62E+5	2.55E+6	1.18	0.07	6.62E+5	6.20E+3	72	1.89E+6
8	wash and drain	1.89E+6	1.18	1.08E+6	6.62E+5	2.55E+6	0.88	0.12	6.62E+5	1.06E+3	72	1.89E+6
9	wash and drain	1.89E+6	1.00	1.07E+6	6.62E+5	2.55E+6	0.65	0.25	6.62E+5	2.22E+4	61	1.89E+6
10	wash and drain	1.89E+6	0.75	9.04E+5	6.62E+5	2.55E+6	0.48	0.34	6.62E+5	3.01E+4	45	1.89E+6
11	wash and drain	1.89E+6	0.48	6.79E+5	6.62E+5	2.55E+6	0.36	0.50	6.62E+5	4.43E+4	23	1.89E+6
12	wash and drain	1.89E+6	**0.36**	3.48E+5	6.62E+5	2.55E+6	0.26	0.45	3.00E+5	1.81E+4	**14**	1.89E+6

Wash Step 12 shows above shows the [Na] = 0.36 M and the $Na_2C_2O_4$ solids loading at 14 wt%, and therefore after the 12th wash batch, the feed would be acceptable for vitrification.

Table 30. Results for Case #2 with two tanks - prewash *vitrification sludge feed batch*, then add the *slurry* with the goal of minimal additional washing; wash to [Na] ≤ 1 M with a solid sodium oxalate weight loading of ≤ 14 wt% (Based on Simple Sodium Dilution Model).

Washing type steps	Actions	Initial feed volume (litre)	Initial Na in the feed [M]	Initial $Na_2C_2O_4$ in the feed (kg)	Add wash water to Prep Tank (litre)	Combined volume in Prep Tank (litre)	Final Na [M]	aq. $Na_2C_2O_4$ [M]	Remove excess liquid from Prep Tank (litre)	$Na_2C_2O_4$ removed (kg)	$Na_2C_2O_4$ remaining (wt%)	Volume in Prep Tank when drained (litre)
		Initial slurry / feed properties			Action- add water	Property			Action - drain		Property	
	None - existing vitrification sludge feed batch already in Prep Tank	1.89E+6	3.70									
1	wash and drain	1.89E+6	3.70		6.62E+5	2.55E+6	2.74					1.89E+6
2	wash and drain	1.89E+6	2.74		6.62E+5	2.55E+6	2.03					1.89E+6
3	wash and drain	1.89E+6	2.03		6.62E+5	2.55E+6	1.50					1.89E+6
4	wash and drain	1.89E+6	1.50		6.62E+5	2.55E+6	1.11					1.89E+6
5	wash and drain	1.89E+6	1.11		6.62E+5	2.55E+6	0.83					1.89E+6
6	wash and drain	1.89E+6	0.83		6.62E+5	2.55E+6	0.61					1.89E+6
7	wash and drain	1.89E+6	0.61		6.62E+5	2.55E+6	0.45					1.89E+6
8	wash and drain	1.89E+6	0.45		6.62E+5	2.55E+6	0.34					1.89E+6
9	wash and drain	1.89E+6	0.34		6.62E+5	2.55E+6	0.25					1.89E+6
	Sludge Remaining in Prep Tank	1.89E+6	0.25									
	Add slurry from cleaning two tanks after OH restoration = 2× (Column P of Table 24 and 25, plus an 8/3 mass ratio of Column O aq. to solids)	6.12E+5	4.32									
10	wash and drain	2.50E+6	1.25	1.12E+5	6.62E+5		1.24	0.08	6.12E+5	1.06E+5	53	1.89E+6
11	wash and drain	1.89E+6	1.25	1.06E+5	6.62E+5		0.92	0.11	6.62E+5	9.75E+3	48	1.89E+6
12	wash and drain	1.89E+6	1.00	9.61E+4	6.62E+5		0.68	0.23	6.62E+5	2.04E+4	38	1.89E+6
13	wash and drain	1.89E+6	0.68	7.57E+4	6.62E+5		0.51	0.35	6.62E+5	3.10E+4	22	1.89E+6
14	wash and drain	1.89E+6	**0.51**	4.47E+4	2.90E+5		0.44	0.43	2.90E+5	1.67E+4	**14**	1.89E+6

Wash Step 14 above shows the [Na] = 0.51 M and the $Na_2C_2O_4$ solids loading at 14 wt%, and therefore after the 14th wash batch, the feed would be acceptable for vitrification.

Table 31. Results for Case #2 with three tanks - prewash *vitrification sludge feed batch*, then add the *slurry* with the goal of minimal additional washing; wash to [Na] ≤ 1 M with a solid sodium oxalate loading of ≤ 14 wt% (Based on Simple Sodium Dilution Model).

Washing type steps	Actions	Initial feed volume in Prep Tank (litre)	Initial Na in the feed [M]	Initial $Na_2C_2O_4$ in the feed (kg)	Add wash water (litre)	Combined volume in Prep Tank (litre)	Final Na [M]	aq. $Na_2C_2O_4$ [M]	Remove excess liquid from Prep Tank (litre)	$Na_2C_2O_4$ removed (kg)	$Na_2C_2O_4$ remaining (wt%)	Volume in Prep Tank when drained (litre)
		Initial slurry/ feed properties			Action- add water	Property			Action - drain		Property	
	None - existing vitrification sludge feed batch already in Prep Tank	1.89E+6	3.70									
1	wash and drain	1.89E+6	3.70		6.62E+5	2.55E+6	2.74					1.89E+6
2	wash and drain	1.89E+6	2.74		6.62E+5	2.55E+6	2.03					1.89E+6
3	wash and drain	1.89E+6	2.03		6.62E+5	2.55E+6	1.50					1.89E+6
4	wash and drain	1.89E+6	1.50		6.62E+5	2.55E+6	1.11					1.89E+6
5	wash and drain	1.89E+6	1.11		6.62E+5	2.55E+6	0.83					1.89E+6
6	wash and drain	1.89E+6	0.83		6.62E+5	2.55E+6	0.61					1.89E+6
7	wash and drain	1.89E+6	0.61		6.62E+5	2.55E+6	0.45					1.89E+6
8	wash and drain	1.89E+6	0.45		6.62E+5	2.55E+6	0.34					1.89E+6
9	wash and drain	1.89E+6	0.34		6.62E+5	2.55E+6	0.25					1.89E+6
	remaining in Prep tank	1.89E+6	0.25									
	Add – resultant slurry from cleaning three tanks after restoring OH concentration. (Column P of Tables 24 or 25, plus an 8/3 mass ratio of Column O aq. to solids ratio to support transfer).	9.18E+5	4.32									
10	wash and drain	2.81E+6	1.58	1.63E+5	6.62E+5	2.55E+6	2.34	0.06	9.18+5	6.98E+3	78	1.89E+6
11	wash and drain	1.89E+6	1.58	1.56E+5	6.62E+5	2.55E+6	1.17	0.08	6.62E+5	7.09E+3	74	1.89E+6
12	wash and drain	1.89E+6	1.17	1.49E+5	6.62E+5	2.55E+6	0.87	0.11	6.62E+5	9.75E+3	69	1.89E+6
13	wash and drain	1.89E+6	1.00	1.39E+5	6.62E+5	2.55E+6	0.64	0.20	6.62E+5	1.77E+4	61	1.89E+6
14	wash and drain	1.89E+6	0.64	1.21E+5	6.62E+5	2.55E+6	0.48	0.35	6.62E+5	3.10E+4	45	1.89E+6
15	wash and drain	1.89E+6	0.48	9.00E+4	6.62E+5	2.55E+6	0.35	0.45	6.62E+5	2.98E+5	25	1.89E+6
16	wash and drain	1.89E+6	0.35	5.01E+4	3.00E+5	2.55E+6	**0.30**	0.54	3.00E+5	1.62E+5	**14**	1.89E+6

Wash Step 16 above shows the [Na] = 0.30 M and the $Na_2C_2O_4$ solids loading at 14 wt%, and therefore after the 16th wash batch, the feed would be acceptable for vitrification.

Table 32. Results for Case #3 with two tanks - add *slurry* to an unwashed *vitrification sludge feed batch*, then wash to [Na] ≤ 1 M with a solid sodium oxalate loading of ≤ 20 wt% (Based on Simple Sodium Dilution Model).

Washing type steps	Actions	Initial feed volume in Prep Tank (litre)	Initial Na in the feed [M]	Initial $Na_2C_2O_4$ in the feed (kg)	Add wash water (litre)	Combined volume in Prep Tank (litre)	Final Na [M]	aq. $Na_2C_2O_4$ [M]	Remove excess liquid from Prep Tank (litre)	$Na_2C_2O_4$ removed (kg)	$Na_2C_2O_4$ remaining (wt%)	Volume in Prep Tank when drained (litre)
		Initial slurry/Feed properties			Action-add water	Property			Action - drain		Property	
	None - existing vitrification sludge feed batch already in *Vitrification Feed Preparation Tank*	1.89E+6	3.70	1.00E+4								
	Add slurry from cleaning one tank (Column P of Tables 24 or 25, plus an 8/3 mass ratio of Column O aq. to solids)	3.06E+5	4.32	5.10E+4								
1	Drain tank to minimum drain-down volume to maximise efficiency	2.2E+6	3.79	6.10E+4	0	2.20E+6	3.79	0.019	3.06E+5	7.79E+2	0.30	1.89E+6
	Repeat slurry addition above	3.06E+5	4.32	5.10E+4								
2	Drain tank to minimum drain-down volume to maximise efficiency	2.2E+6	3.86	1.11E+5	3.56E+5	2.55E+6	3.32	0.022	6.62E+5	1.95E+3	0.55	1.89E+6
3	wash and drain	1.89E+6	3.32	1.09E+5	6.62E+5	2.55E+6	2.46	0.03	6.62E+5	2.66E+3	0.53	1.89E+6
4	wash and drain	1.89E+6	2.46	1.07E+5	6.62E+5	2.55E+6	1.82	0.044	6.62E+5	3.90E+3	0.51	1.89E+6
5	wash and drain	1.89E+6	1.82	1.03E+5	6.62E+5	2.55E+6	1.35	0.07	6.62E+5	6.20E+3	0.48	1.89E+6
6	wash and drain	1.89E+6	1.35	9.65E+4	6.62E+5	2.55E+6	1.00	0.1	6.62E+5	8.86E+3	0.44	1.89E+6
7	wash and drain	1.89E+6	1.00	8.76E+4	6.62E+5	2.55E+6	0.74	0.044	6.62E+5	3.90E+3	0.42	1.89E+6
8	wash and drain	1.89E+6	0.74	8.37E+4	6.62E+5	2.55E+6	0.55	0.13	6.62E+5	1.15E+4	0.36	1.89E+6
9	wash and drain	1.89E+6	0.55	7.22E+4	4.91E+5	2.38E+6	**0.44**	0.5	4.91E+5	3.29E+4	**0.20**	1.89E+6

Wash Step 9 shows above shows the [Na] = 0.44 M and the $Na_2C_2O_4$ solids loading at 20 wt%, and therefore after the 9th wash batch, the feed would be acceptable for vitrification.

Table 33. Results for Case #3 with three tanks - add *slurry* to an unwashed *vitrification sludge feed batch*, then wash [Na] ≤ 1 M with a solids sodium oxalate loading of ≤ 20 wt% (Based on Simple Sodium Dilution Model).

Washing type steps	Actions	Initial feed volume in Prep Tank (litre)	Initial Na in the feed [M])	Initial $Na_2C_2O_4$ in the feed (kg)	Add wash water (litre)	Combined volume in Prep Tank (litre)	Final Na [M]	aq. $Na_2C_2O_4$ [M]	Remove excess liquid from Prep Tank (litre)	$Na_2C_2O_4$ removed (kg)	$Na_2C_2O_4$ remaining (wt%)	Volume in Prep Tank when drained (litre)
		Initial slurry/ feed properties			Action- add water	Property			Action - drain		Property	
	None - existing vitrification sludge feed batch already in Prep Tank	1.89E+6	3.70	1.00E+4								
	Add slurry from cleaning one tank (Column P of Tables 24 or 25, plus an 8/3 mass ratio of Column O aq. to solids)	3.06E+5	4.32	5.10E+4								
1	Drain tank to minimum drain-down volume to maximise efficiency	2.20E+6	3.79	6.10E+4	0	2.20E+6	3.79	0.019	3.06E+5	7.79E+2	0.30	1.89E+6
	Repeat slurry addition above	3.06E+5	4.32	5.10E+4								
2	Drain tank to minimum drain-down volume to maximise efficiency	2.20E+6	3.86	1.11E+5	0	2.20E+6	3.86	0.019	3.06E+5	7.79E+2	0.55	1.89E+6
	Repeat slurry addition above	3.06E+5	4.32	5.10E+4								
3	Drain tank to minimum drain-down volume to maximise efficiency	2.20E+6	3.93	1.61E+5	0	2.20E+6	3.93	0.018	3.06E+5	7.38E+2	0.80	1.89E+6
4	wash and drain	1.89E+6	3.93	1.61E+5	6.62E+5	2.55E+6	2.91	0.025	6.62E+5	2.22E+3	0.79	1.89E+6
5	wash and drain	1.89E+6	2.91	1.58E+5	6.62E+5	2.55E+6	2.15	0.035	6.62E+5	3.10E+3	0.78	1.89E+6
6	wash and drain	1.89E+6	2.15	1.55E+5	6.62E+5	2.55E+6	1.60	0.055	6.62E+5	4.88E+3	0.75	1.89E+6
7	wash and drain	1.89E+6	1.60	1.51E+5	6.62E+5	2.55E+6	1.18	0.070	6.62E+5	6.20E+3	0.72	1.89E+6
8	wash and drain	1.89E+6	1.18	1.44E+5	6.62E+5	2.55E+6	0.88	0.012	6.62E+5	1.06E+3	0.72	1.89E+6
9	wash and drain	1.89E+6	1.00	1.43E+5	6.62E+5	2.55E+6	0.65	0.250	6.62E+5	2.22E+4	0.61	1.89E+6
10	was and drain	1.89E+6	0.65	1.21E+5	6.62E+5	2.55E+6	0.48	0.340	6.62E+5	3.01E+4	0.45	1.89E+6
11	wash and drain	1.89E+6	0.48	9.09E+4	6.62E+5	2.55E+6	0.36	0.500	6.62E+5	4.43E+4	0.23	1.89E+6
12	wash and drain	1.89E+6	0.36	4.66E+4	4.50E+4	1.89E+6	**0.36**	0.450	1.00E+5	6.03E+3	**0.20**	1.89E+6

Wash Step 12 shows above shows the [Na] = 0.36 M and the $Na_2C_2O_4$ solids loading at 20 wt%, and therefore after the 12th wash batch, the feed would be acceptable for vitrification.

Table 34. Results for Case #4 with two tanks - prewash *vitrification sludge feed batch*, then add *slurry* with a goal of minimal additional washing; wash to [Na] ≤ 1 M with a solids sodium oxalate loading of ≤ 20 wt% (Based on Simple Sodium Dilution Model).

Washing type steps	Actions	Feed volume in Prep Tank or add (litre)	Initial Na in the feed [M]	Add wash water (litre)	Combined volume in Prep tank (litre)	Final Na [M]	aq. $Na_2C_2O_4$ {(M]	Remove excess liquid from Prep Tank (litre)	$Na_2C_2O_4$ removed (kg)	$Na_2C_2O_4$ remaining (wt%)	Volume in Prep Tank when drained (litre)
		Initial slurry/ feed properties		Action- add water	Property			Action - drain		Property	
1	wash and drain	1.89E+6	3.70	6.62E+5	2.55E+6	2.74					1.89E+6
2	wash and drain	1.89E+6	2.74	6.62E+5	2.55E+6	2.03					1.89E+6
3	wash and drain	1.89E+6	2.03	6.62E+5	2.55E+6	1.50					1.89E+6
4	wash and drain	1.89E+6	1.50	6.62E+5	2.55E+6	1.11					1.89E+6
5	wash and drain	1.89E+6	1.11	6.62E+5	2.55E+6	0.83					1.89E+6
6	wash and drain	1.89E+6	0.83	6.62E+5	2.55E+6	0.61					1.89E+6
7	wash and drain	1.89E+6	0.61	6.62E+5	2.55E+6	0.45					1.89E+6
8	wash and drain	1.89E+6	0.45	6.62E+5	2.55E+6	0.34					1.89E+6
9	wash and drain	1.89E+6	0.34	6.62E+5	2.55E+6	0.25					1.89E+6
	Add slurry from cleaning two tanks after OH restoration = 2× (Column P of Tables 24 and 25, plus an 8/3 mass ratio of Column O aq. to solids)	6.12E+5	4.32								
10	wash and drain	2.50E+6	1.25	1.12E+5	2.55E+6	8.36E+5	0.075	6.12E+5	4.59E+4	53	1.89E+6
11	wash and drain	1.89E+6	1.25	6.62E+5	2.55E+6	0.92	0.110	6.62E+5	9.75E+3	48	1.89E+6
12	wash and drain	1.89E+6	1.00	6.62E+5	2.55E+6	0.68	0.230	6.62E+5	2.04E+4	38	1.89E+6
13	wash and drain	1.89E+6	0.68	6.62E+5	2.55E+6	0.51	0.350	6.62E+5	2.32E+5	22	1.89E+6
14	wash and drain	1.89E+6	0.51	9.00E+4	2.55E+6	**0.48**	0.430	9.00E+4	3.87E+4	**20**	1.89E+6

Wash Step 14 shows above shows the [Na] = 0.48 M and the $Na_2C_2O_4$ solids loading at 20 wt%, and therefore after the 14th wash batch, the feed would be acceptable for vitrification.

Table 35. Results for Case #4 with three tanks - prewash *vitrification sludge feed batch*, then add *slurry*, with the goal of minimal additional washing; wash to [Na] ≤ 1 M with a solids sodium oxalate loading of ≤ 20 wt% (Based on Simple Sodium Dilution Model).

Washing type steps	Actions	Feed volume in Prep Tank or add (litre)	Initial Na in the feed [M]	Initial $Na_2C_2O_4$ in the feed (kg)	Add wash water (litre)	Combined volume in Prep tank (litre)	Final Na [M]	Remove excess liquid from Prep Tank (litre)	$Na_2C_2O_4$ removed (kg)	$Na_2C_2O_4$ remaining (wt%)	Volume in Prep Tank when drained (litre)
		Initial slurry/ feed properties			Action- <u>add</u> water	Property		Action - <u>drain</u>		Property	
1	wash and drain	1.89E+6	3.70		6.62E+5	2.55E+6	2.74	6.62E+5			1.89E+6
2	wash and drain	1.89E+6	2.74		6.62E+5	2.55E+6	2.03	6.62E+5			1.89E+6
3	wash and drain	1.89E+6	2.03		6.62E+5	2.55E+6	1.50	6.62E+5			1.89E+6
4	wash and drain	1.89E+6	1.50		6.62E+5	2.55E+6	1.11	6.62E+5			1.89E+6
5	wash and drain	1.89E+6	1.11		6.62E+5	2.55E+6	0.83	6.62E+5			1.89E+6
6	wash and drain	1.89E+6	0.83		6.62E+5	2.55E+6	0.61	6.62E+5			1.89E+6
7	wash and drain	1.89E+6	0.61		6.62E+5	2.55E+6	0.45	6.62E+5			1.89E+6
8	wash and drain	1.89E+6	0.45		6.62E+5	2.55E+6	0.34	6.62E+5			1.89E+6
9	wash and drain	1.89E+6	0.34		6.62E+5	2.55E+6	0.25	6.62E+5			1.89E+6
	Add slurry from cleaning three tanks after OH restoration = 3× (Column P of Tables 24 and 25, plus an 8/3 mass ratio of Column O aq. to solids)	1.89E+6	0.25								
		9.18E+5	4.32								
10	10th wash	2.81E+6	1.58	1.63E+5	6.62E+5	2.55E+6	0.06	9.18E+5	5.51E+4	78	
11	11th wash	1.89E+6	1.58	1.56E+5	6.62E+5	2.55E+6	1.17	6.62E+5	5.29E+4	74	1.89E+6
12	12th wash	1.89E+6	1.17	1.49E+5	6.62E+5	2.55E+6	0.87	6.62E+5	7.28E+4	69	1.89E+6
13	13th wash	1.89E+6	1.00	1.39E+5	6.62E+5	2.55E+6	0.64	6.62E+5	1.32E+5	61	1.89E+6
14	14th wash	1.89E+6	0.64	1.21E+5	6.62E+5	2.55E+6	0.48	6.62E+5	2.32E+5	45	1.89E+6
15	15th wash	1.89E+6	0.48	9.00E+4	6.62E+5	2.55E+6	0.45	6.62E+5	2.98E+5	25	1.89E+6
16	16th wash	1.89E+6	0.35	5.01E+4	1.60E+5	2.55E+6	**0.32**	1.60E+5	7.20E+4	**20**	1.89E+6

Wash Step 16 shows above shows the [Na] = 0.32 M and the $Na_2C_2O_4$ solids loading at 20 wt%, and therefore after the 16th wash batch, the feed would be acceptable for vitrification.

A1.3 Observations and Discussion

A1.3.1 Impact on Vitrification

Section A1.2 details the input, the model, and the results for the impacts associated with Case #1, Case #2, Case #3, and Case #4, with Table 36 below summarising the vitrification type impacts from the *Historical Baseline Chemical Cleaning Process*.

Table 36. Estimated vitrification type impacts from the *Historical Baseline Chemical Cleaning Process*.

Case	Number of HLW tanks cleaned	Total sodium oxalate added (kg)	Washing strategy	Solid NaC_2O_4 max. in the feed (wt%)	Impacts to vitrification	
					Number of wash cycles needed	Fraction of total sodium oxalate as *feed to vitrification*
#1	2	102,000	Add to unwashed	14	9	0.25
	3	153,000			12	0.18
#2	2	102,000	Add to pre-washed	14	9 pre + 5 post =14	0.25
	3	153,000			9 pre + 7 post =16	0.17
#3	2	102,000	Add to unwashed	20	8	0.29
	3	153,000			12	0.25
#4	2	102,000	Add to pre-washed	20	9 pre + 5 post =14	0.35
	3	153,000			9 pre + 7 post =16	0.25

As seen in Table 36, the impact from increasing the sodium oxalate from two to three heels results in an increased number of vitrification feed wash cycles required, with a corresponding decrease in the fraction of total oxalate in the *feed to vitrification*. This is largely because of the additional

wash cycles and the desire to keep the vitrification feed loading of solid sodium oxalate to either 14 or 20 wt%, as shown in the column entitled "Solid NaC_2O_4 max. in the feed." Decreasing the fraction of total oxalate in the *feed to vitrification* logically results in an increase in the impacts to salt processing. By looking at the columns entitled, "Impacts to vitrification-Number of wash cycles needed" in Table 36 it is seen that regardless of the amount of pre-washing done on an existing vitrification feed batch (i.e. a feed batch generated from other than chemical cleaning, such as from mechanical heel removal), after combining the existing vitrification feed with the resultant sodium oxalate solids generated as the result of chemical cleaning (Column O in Table 24 and 25), significant additional washing will be required. Based on Table 36, if nine pre-washes are performed on the existing vitrification feed, and then the additional sodium oxalate solids are added to the feed, at least five to seven additional washes of the combined vitrification feed will then be required. This number of additional washes is substantial since if no pre-washing of the existing feed batch is performed, only eight to 12 washes of the combined feed are required.

A2.3.2 Impact on Salt Processing

The impacts of the *Historical Baseline Chemical Cleaning Process* on salt processing can be equated to of the future additional *feed for salt processing*. The assumptions/input used to estimate the impacts are as follows:

- Conservatively, based on processing history, the feed to grout ratio for saltstone was 10 vol% (Chew and Hamm, 2010).

- The capacity of the vaults (based on using the most current design) is about 20,000,000 litres (Chew and Hamm, 2010).

As previously stated based on Pike *et al.*, 2004, if all of the additional $Na_2C_2O_4$ from cleaning a single tank were sent directly to the *evaporator concentrate receipt tank*, 1,890,000 litres of water would be required to dissolve the additional *salt heel* volume. The basic assumptions used to convert gallons of sparingly-soluble salt into future *feed for salt processing* are as follows:

- Transfer of the resultant $Na_2C_2O_4$ solids from the cleaning of one tank to the *evaporator concentrate receipt tan*k requires 1,890,000 litres of water to solubilise it, resulting in an additional approximate 1,890,000 litres of feed for salt processing

Based on the results in Table 36, along with Equations 1-1 and A-1, the impacts to salt processing can be summarised as Table 37.

Table 37. Impacts to Vitrification and Additional Feed for salt Processing.

Case	Tanks cleaned	Resultant $Na_2C_2O_4$ (kg)	Vitrification feed preparation handling		Impacts to vitrification		*Feed for salt processing*	
			Blending / washing	$Na_2C_2O_4$ max (wt%)	Additional wash cycles	Fraction of total $Na_2C_2O_4$ to vitrification	Fraction of $Na_2C_2O_4$ to salt processing	Future *feed for salt* processing (litres)
#1	2	102,000	Add to Unwashed	14	9	0.25	0.75	2,900,000
	3	153,000			12	0.18	0.82	4,800,000
#2	2	102,000	Add to Pre-washed	14	9 pre, 5 post	0.25	0.75	2,900,000
	3	153,000			9 pre, 7 post	0.17	0.83	4,800,000
#3	2	102,000	Add to Unwashed	20	8	0.29	0.61	2,400,000
	3	153,000			12	0.25	0.75	4,300,000
#4	2	102,000	Add to Pre-washed	20	9 pre, 5 post	0.35	0.65	2,500,000
	3	153,000			9 pre, 7 post	0.25	0.75	4,300,000

With the quantity of feed for salt processing shown in Table 37, the number of additional current-design vaults required was calculated using Equation A-2, shown below:

$$\begin{array}{ccccccc} \textit{feed for salt processing} & \times & \textit{saltstone grout-to-feed ratio} & / & \textit{capacity of each new vault} & = & \textit{additional number of vaults required} \end{array} \quad \text{(eq A-2)}$$

Where:

- Feed for salt processing volumes are shown in Table 1.
- The saltstone grout-to-feed ratio (vol/vol) is 100 litres of grout to 10 litres of feed (Ketusky, 2010).
- As previously stated, the capacity of the current design vault is 20,000,000 litres (Ketusky, 2010).

Table 38 summarises the relationship between the number of tanks cleaned using the *Historical Baseline Chemical Cleaning Process*, washing strategy, wt% solids processed, additional feed for salt processing, and the additional vault space required per tank cleaned.

Table 38. Additional salt processing feed and vault space required, per two or three tanks cleaned.

Case	Tanks cleaned	Vitrification feed preparation handling		Impacts to salt processing	
		Washing	$Na_2C_2O_4$ max (wt%)	Add. salt processing feed (kl)	Additional vaults (based on current design)
#1	2	Add to unwashed vitrification feed batch, then wash	14	2,900	1.44
	3			4,740	2.37
#2	2	Add to pre-washed vitrification feed batch, minimised additional washing	14	2,900	1.44
	3			4,800	2.40
#3	2	Add to unwashed vitrification feed batch, then wash	20	2,354	1.18
	3			4,350	2.16
#4	2	Add to pre-washed vitrification feed batch, minimised additional. washing	20	2,520	1.26
	3			4,350	2.16

A1.4 Summary of Model Determined Impacts

The estimated impacts on the tank farm from the *Historical Baseline Chemical Cleaning Process* on the SRS HLW tanks are summarised in Table 39.

Table 39. Estimated *Historical Baseline Chemical Cleaning Process* impacts.

Case	Number of tanks cleaned	NaC_2O_4 added to HLW system (kg)	Washing strategy (add to washed or unwashed)	Solid NaC_2O_4 max. in the feed (wt%)	Impacts to vitrification	Impacts to salt processing	
					Number of wash cycles needed	Feed for salt processing (litres)	Additional vaults (based on current design)
#1	2	1.02×10^5	Unwashed	14	9	2.90×10^6	1.44
	3	1.53×10^5			12	4.74×10^6	2.37
#2	2	1.02×10^5	Pre-washed	14	14	2.90×10^6	1.44
	3	1.53×10^5			16	4.80×10^6	2.40
#3	2	1.02×10^5	Unwashed	20	8	2.36×10^6	1.18
	3	1.53×10^5			12	4.35×10^6	2.16
#4	2	1.02×10^5	Pre-washed	20	12	2.50×10^6	1.26
	3	1.53×10^5			14	4.35×10^6	1.2

By looking at the column entitled, "impacts to vitrification," it is seen that see that even with pre-washing, additional wash cycles will be required. This can be largely explained by the fact that even during the pre-washing the soluble sodium concentration will remain > 0.25 M. Based on Section A2.3, washing will be required after adding the slurry, to reduce the solid sodium oxalate mass concentration to $\leq$ 14 wt% or 20 wt%. Adding the sodium oxalate from cleaning two tanks vs three to a feed batch results in a lower "Additional vaults needed" per "total oxalate added," because that for processability there is a maximum solid sodium oxalate loading. Going beyond this maximum loading results in a significant increase in the processing time within the vitrification process which decreases the throughput. As expected, if the maximum solid sodium oxalate loading in the vitrification feed can be increased from 14 wt% to 20 wt%, fewer additional vaults will be needed.

APPENDIX 2. SLURRY AND TRANSFER PUMPS DETAILS

A picture of the submersible mixer pumps being installed into an SRS HLW tank is shown in Figure 48, with Figure 49 showing a diagram of a Typical Standard Slurry Pump at SRS. Figure 50 shows an example of a submersible mixing pump in a test tank, while Figure 51 shows an example of an SRS submersible transfer pump. Table 40 provides pump attributes and operability details of those used in the SRS HLW tanks.

Figure 48. Submersible Mixer Pumps being installed into an SRS HLW tank.

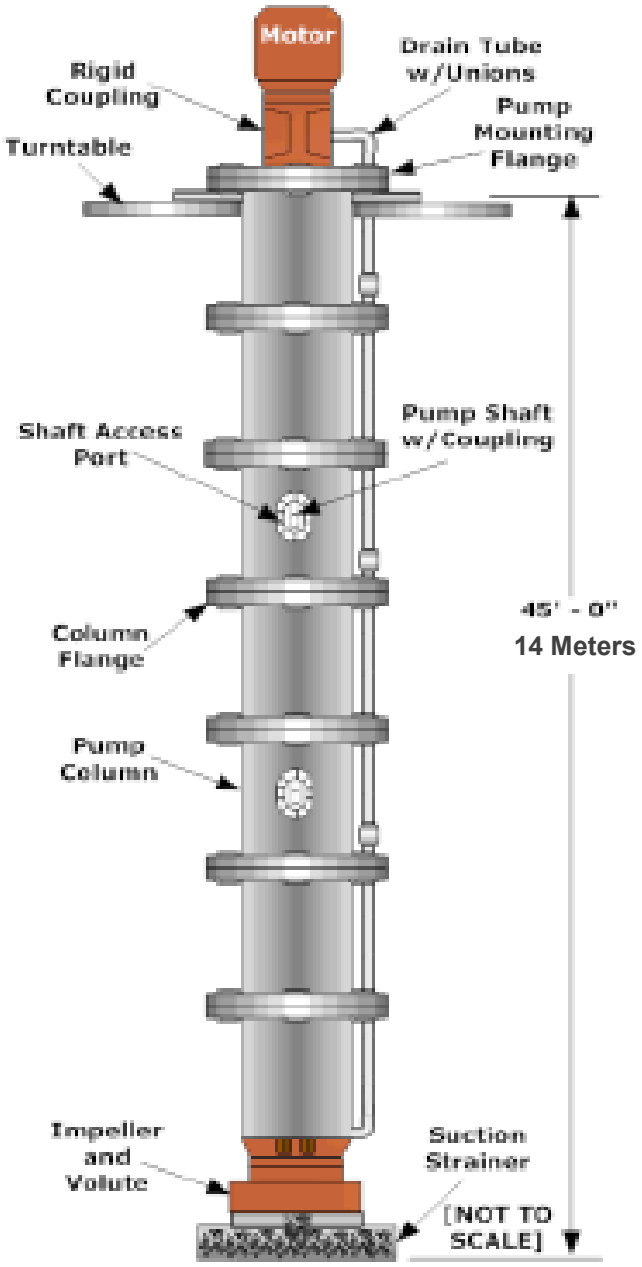

Figure 49. Typical Standard Slurry Pump at SRS (U.S. DOE-SR, 2014).

Figure 50. Example of an SRS submersible mixing pump in a test tank (U.S. DOE-SR, 2014).

Figure 51. Example of an SRS submersible transfer pump (U.S. DOE-SR, 2014).

Both the mixer and transfer pumps are pumps are long-shafted, with system attributes of the pumps currently used in the SRS HLW identified in Table 40 (Saldivar, 2002; Davis and Dickert, 2011).

Table 40. Pumps, attributes, and operability of those used in the SRS HLW tanks (1 of 2).

Pump Type	System Attributes	System Operability	Comments
Standard Slurry Pumps: There are approximately 38 slurry pumps in HLW, with four general specification types. The specifications include: 1) 150 hp/7.6-metre Effective Cleaning Radius (ECR), 1,750 rpm, 4,500 litres/minute with 2 nozzles. 2) 300 hp, 12 metre ECR, 2,200 rpm, 15,000 litres/minute with 4 nozzles. 3) 75 hp, 900 rpm, 6-metre ECR, 3,400 litres/minute with 2 nozzles. 4) 300 hp, 15 metre ECR, 1,100 rpm with 2 nozzles, 20,000 litres/minute per nozzle.	An approximate 14 metre long-shaft centrifugal pump, journal bearings with a lower product lube bearing, mechanical seals used to reject contamination in 2.1×10^5 Pa bearing water column, at approximately 4500 litres/minute , with 2 radial /tangential 3.8 cm nozzles, with a nitronic 15 metre shaft with tungsten carbide product lube bearing shaft coating, a 36 cm 304L ss column, 1780 rpm, 150 hp, 480 v, 165 amp, variable frequency drive control, 360º rotation utilising a 1/3 rpm rotek bearing and electrical motor slip ring, with 25 cm spacer cans used to raise and lower the pumps.	Slurry pumps are installed in 61 cm risers only after concentricity checks are performed. They must be submerged at a minimum of 41 cm of fluid above the bottom of the pump screen (25 cm above centre line of pump discharge nozzles) required to prevent vortexing. Rotations are 1,600 rpm to protect against resonant frequency and excessive vibration.	Due to the obstructions in select tanks, the slurry pumps meet the fundamental deployment requirements that other technologies cannot. For this reason, the long-shafted centrifugal pump will certainly be considered for future waste removal.
Submersible Mixer - Flynt Mixer: SRS has deployed six mixers since 1997. They range in power from the following: • one is 15 hp • two are 4 hp • three are 50 hp	The 50 hp motor in one design turns a shrouded propeller at speeds up to 860 rpm. The mixer delivers approximately 34,000 litres/minute, less than vendor published value of approximately 76,000 litres/minute due to the introduction of a shroud on mixer discharge while providing a velocity of 30.5 cm/second at a 15-metres' distance, with an ECR of only 6.4 metres.	The mixers require a 91 cm liquid level for operation to prevent excessive vortexing. The mass of the approximate 4500 kg mixer mast assembly rests on the tank floor, while the rotek bearing is supported by structural steel that prevents tank top loading.	Mixers are challenged by a stationary single-point transfer location due to their limited suspension ECR.

Table 40 Continued. Pumps, attributes, and operability of those used in the SRS HLW tanks (2 of 2).

Pump type	System attributes	System operability	Comments
Advanced Design Mixer Pumps: At SRS considered state of the art, with two recently installed in a HLW tank	They have an approximate 10,000-hour service life. The ECR is 15-metres. It can be installed through a 61-cm diameter riser. The pump can be supported by the tank floor or a tank-top platform. The new approach and advanced pump design was produce the highest performance pump ever deployed in an SRS tank allowing the tanks to be cleaned using two pumps instead of the customary four.		
Air Driven Transfer Pumps: Numerous air driven transfer pumps are used throughout SRS to pump heavy slurries/ materials from tanks.	They are double diaphragm pumps. Pumping 454 litres/minute with 12 metres of head capacity used. Required 1.8×10^6 Pa dry but lubricated air supply. Most recent, air driven transfer pump was installed with a flushing system, a set of nibbler dams to assist with pushing material to the pump suction and an anti-cavitation plate to support HLW tank pump downs to low levels.	The pumps transferred a total of 29,000 litres of sludge from a HLW tank. The ratio of water to sludge ranged from 9:1 to 19:1. System performance was monitored by measuring the gamma rates on the above grade transfer line.	Materials of construction, flushing, dry but lubricated air are all very significant design attributes that need to be considered for successful deployments.
Submersible Centrifugal Pumps: One pump is currently installed in Tank 19 and has successfully operated for over 400 hours.	Centrifugal pump, 13 hp to 20 hp, submersible, 681 litres/minute at 38 metres of head, capable of pumping down to 3.81 cm. Used to transfer waste from Tank 19 to Tank 18.	The pumps are stationary in the Tank 18 and 19. They can only be elevated or lowered with great difficulty because that they are in fixed positions.	Proven system that would be considered disposable as long as the space that the pump system occupied in the tank riser was not needed for isolation and closure activities.
Telescoping Transfer Pump (TTP): Approx. 20 in SRS HLW System.	Long-shafted centrifugal pump, telescoping, 303 to 378 litres/minute, 75 hp, 4,800 kg without bearing water in column, 3600 rpm, 460 volts, 14-metre-long, 63.5-metre dia. discharge nozzle, nitronic 50 shaft, 6.35 cm dia. shaft, 304L ss column.	The TTP requires a 60 cm riser to accommodate the 58.4 cm dia. Pump casing. Bearing water for contamination control in pump column. The pump can be telescoped to different elevations.	The Tank 8 TTP worked flawlessly once the impeller clearance caused by a cold set was resolved. The system is effective for emptying a HLW tank down to a depth of approximately 7.6 cm.

From the beginning of early waste removal, long-shaft slurry pumps have proven to be a very effective system for imparting significant jet velocities to mobilise and suspend waste. However numerous failures have been associated with this design that has resulted in modifications and improvements in testing at SRS that has produced a much-improved design for future use.

APPENDIX 3. SIMULANT BASED SLURRY OXALATE *DECOMPOSITION TEST APPARATUS* EQUIPMENT LIST AND PERFORMANCE DETAILS

For completeness previously discussed Figure 9 is shown below, with the detailed equipment list and model numbers following.

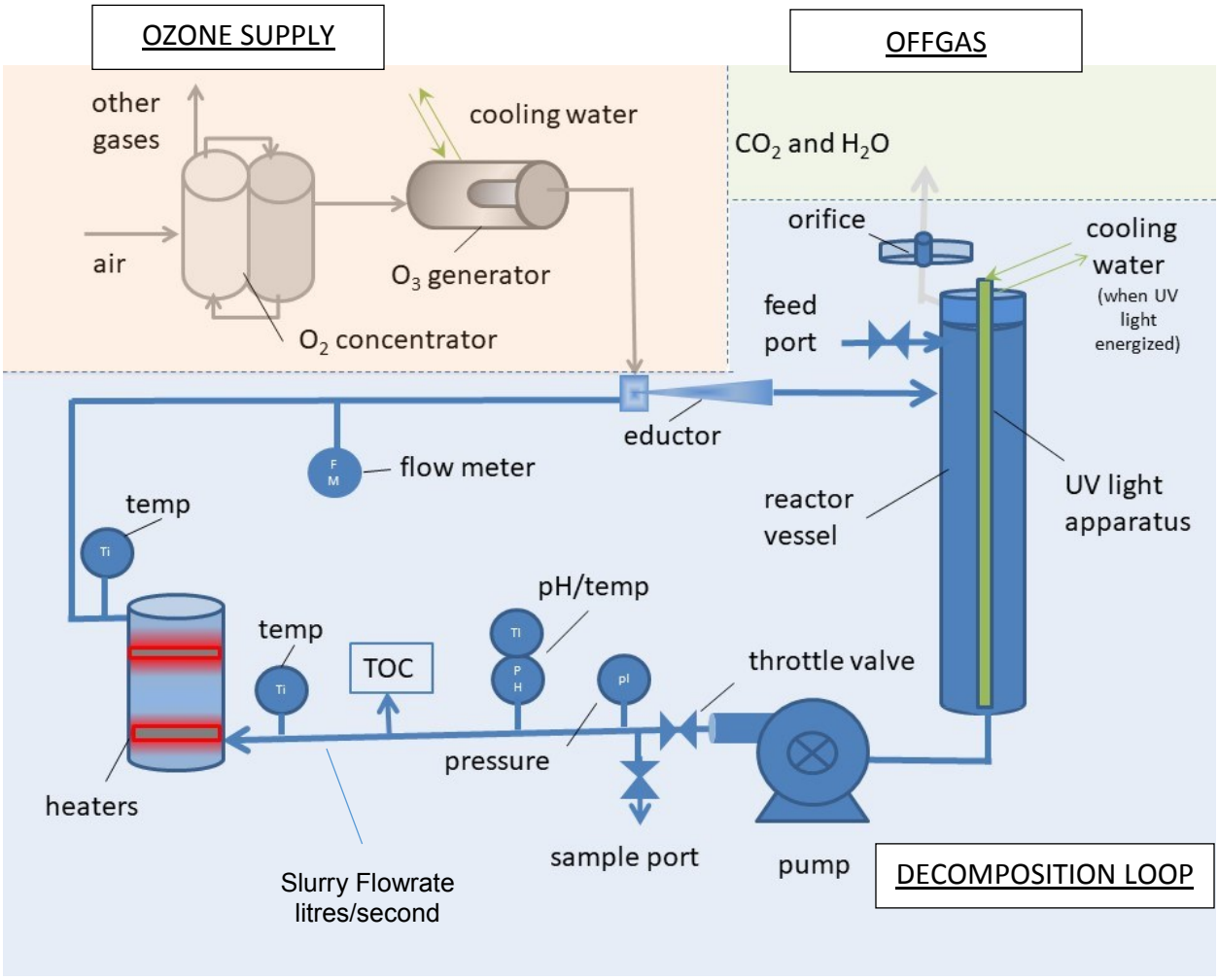

Previously shown Figure 9. Diagram of the oxalate *decomposition test apparatus*.

SIMULANT TEST APPARATUS EQUIPMENT LIST AND MANUFACTURER PROVIDED DETAILS

- All components/piping in contact with ozone and decomposition slurries are made of 304 or 316 stainless steel.

Ozone Supply

- *Oxygen Concentrator* - (model OG-25 by Oxygen Generating Systems International (OGSI), North Tonawanda, New York, USA) with *Integrated Flow Meter*.
- *Ozone Generator* - (Ozat model CFS-1, by Ozonia Ltd.) with *Integrated Ozone Monitor*.
- *Piping* – ozone generator connected to eductor by approximately 8 metres of ½ inch, 316 ss tubing.

Decomposition Loop

- *Eductor* - ½" × 2" (model 2081 by Mazzei Injector Company, Bakersfield, California, USA).
- *Feed Port* - containing 2-inch Swagelok Ball Valve (model SS-68TS-32 by Swagelok, Solon, Ohio, USA).
- *Reactor Vessel* - approximately 15 cm (i.d.) × 76 cm (height) self-made from 6" inch Schedule 80, 316 stainless steel pipe, containing UV Lamp Apparatus listed below:
  - *UV Lamp Sheath* - 72 cm long, made from 25 mm (dia i.d.), 27 mm (dia. o.d.) fused quartz tubing (supplied by Technical Glass Products, Painesville, Ohio, USA).
  - *UV Lamp* - synthetic quartz medium pressure 1.5 kW UV lamp, having a 70 mm arc length (supplied by Helios, Milano, Italy), powered by a 1.5 kW Luxon driver.
- *Recirculation pump* - centrifugal pump, 3500 rpm motor, (model 2ST1G9C4 by Goulds Pump, Seneca Falls, New York, USA).
- *Throttle Valve* - used for controlling flow and back pressure (model GC11.5, by Dole Control Valves, Batavia, Illinois, USA).
- *Sample Port* – used for taking grab samples, containing Swagelok Ball Valve (model SS-68ts-32 Swagelok, Solon, Ohio, USA). .
- *Pressure Gage* (model 35-1009-SW-04L-3000 by Ashcroft, Stratford, Connecticut, USA).
- *pH meter* - (Orion model 250-A, Thermo Fischer Scientific, Waltham, Massachusetts, USA).
- *Thermocouples* - (model KQXL-18E-12 by OMEGA Engineering, Norwalk, Connecticut, USA).
- *TOC Analyser* - Total Organic Carbon Analyser (Model TOC L with 680°C combustion catalytic oxidation method by Shimadzu Ltd., Tokyo, Japan).
- *Heater Vessel* - approx. 20 cm dia×10 cm, self-made from schedule 80, 316 ss, 8-inch pipe, containing
  - *Band Heater*s - two 3000 W attached mica band heaters (model 14099 by IMS Company, Chagrin Falls, Ohio, USA).
- *Flow Meter* - (model 142-SG-50-0000-00 by Midwest Instruments, Heights, Michigan, USA).

- *Orifice* - back pressure regulator (model BP-3 by Circle Seal Controls, Corona, California, USA).
- *Piping* – decomposition components connected by approximately 22.9 metres (total) of 2-inch Schedule 80 stainless steel (316).

ANALYTICAL EQUIPMENT

- Total Organic Carbon (TOC) Analyser (Model TOC-L by Shimadzu Ltd., Tokyo). Equipped with a 680°C combustion catalytic oxidation system. The TOC Analyser can be used on slurries containing significant amounts of mineral salts (Shimazdu, 2013). TOC Limit of Detection is 3.28×10^{-4} M.

- Atomic Absorption (AA) Spectrometer (Varian Model 220FS & software version 5.0 by Agilent Ltd., Santa Clara, California) A Varian model SpectraAA 220 FS (Mulgrave, Victoria, Australia) flame atomic absorption spectrometer equipped with a deuterium background corrector and an automatic hollow cathode lamp switch was used for absorbance measurements. Fe – 248.3 nm; Mn – 279.5 nm; Ni – 232 nm. The burner height was 13.5 mm. The nebuliser flow rate was 5 mL/ min, and the flame was composed of acetylene (flow rate 1.5 litres/ minute) and air (flow rate 13.5 litres/ minute).

PROCESS CONDITIONS DURING DECOMPOSITION

- *Simulant decomposition test slurry* recirculated at approx. 40 litres/minute, 1.7×10^5 Pa, with temperature maintained at 70$\pm$5ºC.
- Ozone fed at approx. 60 g/hr., with a calculated solubility of 6.3×10^{-4} M based on Henry's Law.
- *Oxygen Concentrator is* supplying 9.4 litres/minute gas at 97 wt% O_2.
- Pressure in the *decomposition loop is maintained* at approx. 1.7×10^5 Pa by *Orifice*, Recirculation Pump, and Throttle valve.
- Tap water at ambient supplied as cooling water to *UV Light Apparatus* at approximately 1 litre/minute, and also supplied to *Ozone Generator* at approx. 1.5 litres/minute.

APPENDIX 4. REAL HLW BASED SLURRY TEST APPARATUS EQUIPMENT LIST AND PERFORMANCE DETAILS

To aid in understanding, the real HLW *decomposition test apparatus* previously shown Figure 52, is shown below, with an equipment list, and model numbers following.

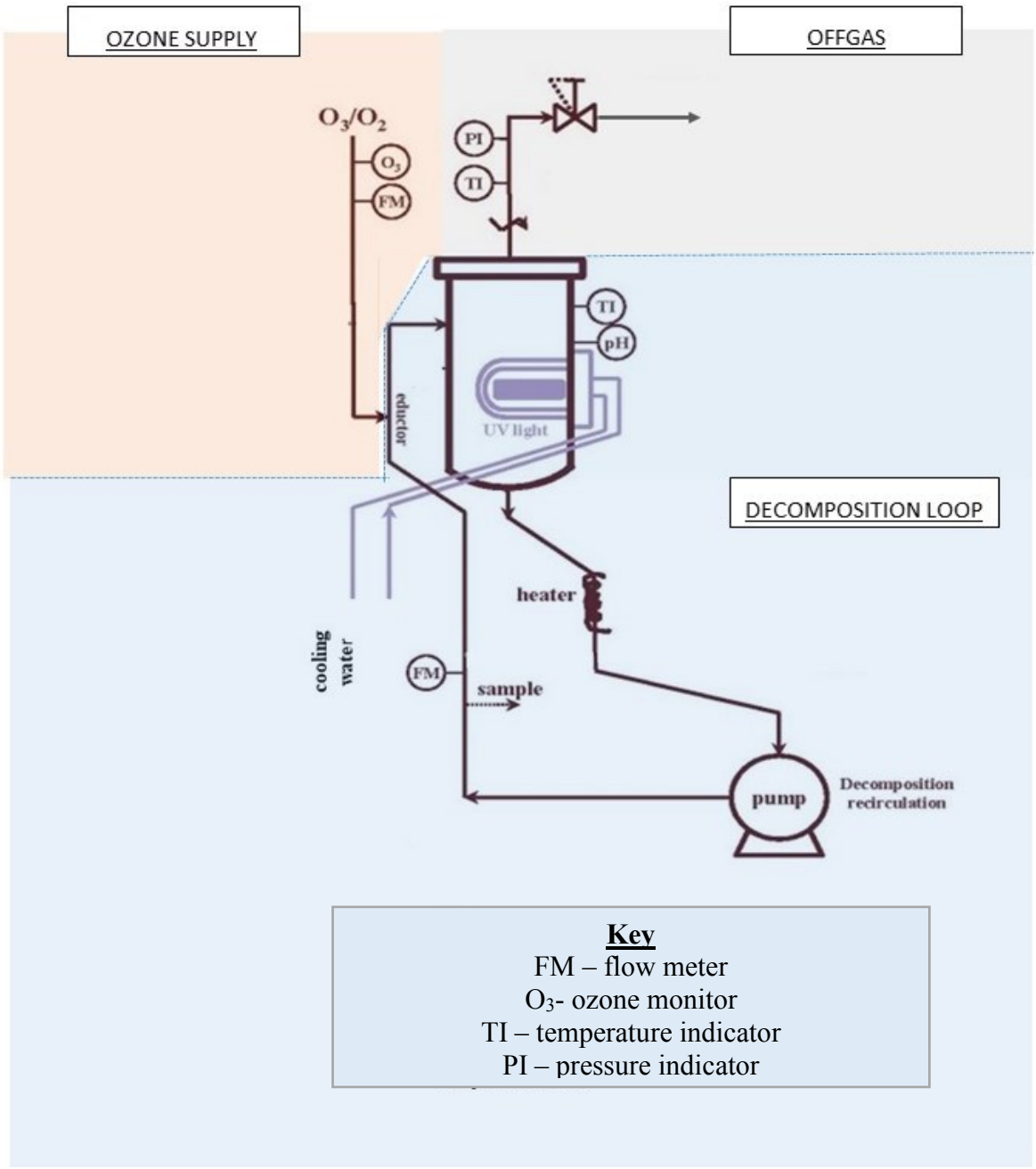

Figure 52. Simplified Schematic of the HLW based slurry *Decomposition Test Apparatus*.

EQUIPMENT AND PIPING

Ozone Supply

- *Ozone Generator* (model TOGC13X by Ozonia Ltd.) capable of supplying 13 gram/hour ozone, air cooled, containing an *Integrated Oxygen Concentrator*.
- *Flow meter* - Smart Trak Thermal Mass Flow Meter (model S100 by Sierra Instruments, Monterey, California, USA).
- *Ozone Monitor* - High Concentration Ozone Monitor (model Mini-HiCon by InUSA, Norwood, Massachusetts, USA).

Decomposition Unit

- *Feed Port* containing Swagelok Ball Valve (model SS-62PF4JK-5229 by Swagelok, Solon, Ohio, USA).
- *Eductor* - ½ inch by ¾ inch (model 484 by Mazzei Injector Company, Bakersfield, California, USA).
- *Decomposition Vessel,* self-made from 6-inch schedule 80 ss pipe, volume approx. 14.6 cm i.d. × 21.6 cm high, approximately 3.6 litres, with 0.6 litres occupied by UV lamp apparatus, and 1 litre as an expansion volume. Vessel Contains:
  - *pH Probe* - (model 871PH-3G1A-Q-E by Foxboro, a division of Invensys, Plano, Texas, USA).
  - *Thermocouple* - K-type (model K20-2-513 by Watlow Semiconductor, San Jose, California, USA).
  - *UV Lamp Sheaths* - o.d. 3.9 cm (i.d. 3.5 cm) × approximately 17.7 cm (supplied by Technical Glass Products, Painesville, Ohio, USA).
  - *Cooling Water* supplied to UV quartz sheaths at 10ºC, leaving at approximately 69ºC flowing at approx. 4.90 litres/minutes.
  - *UV Light* - 400 W Mercury Metal Halide UV Lamp (model RQ410E by Heraeus Noblelight, Banbury, UK) with NEDAP 400 W Luxon Lamp driver (model 99559906, by Nedap Light Controls Europe, Groenlo, Netherlands).
  - *Ceramic Rectangle Heaters* - two (2) by 1455 W band heaters. Approximate size 75 mm × 5 mm × 2.5 mm by Watlow Semiconductor, San Jose, California, USA).
  - *Recirculation Pump* - pump and motor assembly operates at 3500 rpm, with the flow at approximately 5.7 litres/minute (model MMP11-R25x6N by Magnatex Pump, Plano, Texas, USA).

- *Flow meter* - (model710l053005A, King Instruments, Garden Grove, California, USA).

Offgas

- 2.54 cm *Back Pressure Regulator* - (model 152SS by Watts, North Andover, Massachusetts, USA).

APPENDIX 5. DECOMPOSITION TEST DATA

Table 41. Decomposition test data for 1 wt% oxalic acid Fe-rich sludge simulant based *decomposition test slurries*

de-comp test slurry	time (hr)	pH	Ox (M)	Fe (M)	Mn (M)	Ni (M)	*de-comp test slurry*	time (hr)	pH	Oxalate (M)	Fe (M)	Mn (M)	Ni (M)	*de-comp test slurry*	time (hr)	pH	Oxalate (M)	Fe (M)	Mn (M)	Ni (M)
1-Fe-1.no	0	1.7	9.3E-2	1.3E-2	3.8E-3	5.6E-	1-Fe-1.clean	0	2.0	7.7E-2	7.0E-3	4.9E-3	6.2E-4	1-Fe-1.fouled	0	1.7	1.0E-1	5.6E-3	3.6E-3	5.4E-
	1.0	3.2	6.8E-2	2.3E-3	3.8E-3	5.9E-4		1.0	4.7	5.1E-2	2.2E-3	2.6E-3	4.8E-4		1.0	1.6	9.8E-2	5.9E-3	3.5E-3	4.9E-4
	2.0	3.8	4.6E-2	1.3E-2	3.7E-3	5.5E-4		2.0	5.4	3.2E-2	1.9E-4	9.1E-6	4.7E-4		2.0	2.0	6.8E-2	6.3E-3	3.5E-3	3.9E-4
	4.0	5.5	2.3E-2	2.5E-4	4.2E-5	3.5E-4		4.0	7.2	2.7E-3	1.0E-4	9.1E-6	3.6E-4		3.0	4.7	3.4E-2	1.5E-3	2.0E-3	4.0E-4
	6.0	7.4	2.6E-4	1.8E-5	1.8E-5	6.8E-5		5.0	8.3	2.7E-3	7.3E-5	9.1E-6	4.8E-5		4.0	6.6	2.3E-3	7.5E-5	9.1E-6	2.6E-4
	7.3	8.2	1.1E-4	1.8E-5	1.8E-5	3.4E-5		5.3	8.6	1.1E-3	5.0E-5	9.1E-6	3.6E-5		4.7	7.2	1.1E-3	3.7E-5	9.1E-6	9.7E-5
	9.4	8.8	1.6E-4	1.8E-5	1.8E-5	1.7E-5		5.5	8.7	2.6E-4	3.6E-5	9.1E-6	2.9E-5		5.0	7.5	5.7E-4	1.8E-5	9.1E-6	1.7E-5
															6.3	8.5	2.6E-4	1.8E-5	9.1E-6	1.7E-5
1-Fe-2.no	0	1.8	1.1E-1	1.3E-2	2.4E-3	3.0E-4	1-Fe-2.clean	0	1.8	9.0E-2	6.9E-3	3.6E-3	4.3E-4	1-Fe-2.fouled	0	1.7	1.0E-1	7.0E-3	4.1E-3	8.0E-4
	1.0	2.0	6.8E-2	2.4E-2	2.7E-3	3.6E-4		1.0	2.4	6.7E-2	7.9E-3	3.8E-3	3.7E-4		1.0	2.1	6.8E-2	7.2E-3	4.0E-3	2. 9E-
	1.9	2.3	4.5E-2	2. 7E-2	2.7E-3	3.9E-4		2.0	4.3	4.4E-2	6.0E-4	2.6E-3	3.5E-4		2.1	4.4	3.4E-2	6. 5E-4	2.4E-3	6.3E-4
	3.9	3.5	1.1E-2	7.2E-3	2.5E-3	2.8E-4		4.0	6.0	2.0E-2	3.2E-5	9.1E-6	3.7E-4		4.0	6.1	2.3E-3	2.0E-5	9.1-6	4.6E-4
	7.2	6.3	7.6E-3	3.2E-5	1.8E-5	3.1E-4		5.4	7.8	1.1E-3	1.9E-5	9.1E-6	3.6E-5		4.8	7.0	1.1E-3	1.9E-5	9.1E-6	2.1E-4
	8.5	7.6	2.2E-4	2.0E-5	1.8E-5	1.7E-4		5.5	7.9	4.19E-4	1.8E-5	9.1E-6	2.2E-5		5.5	7.7	2.6E-4	1.8E-5	9.1E-6	1.7E-5
															6.0	8.1	2.0E-4	1.8E-5	9.1E-6	1.7E-5
1-Fe-3.no	0	1.9	1.1E-1	1.6E-2	1.6E-3	2.6E-4	1-Fe-3.clean	0.0	1.5	1.0E-1	6.5E-3	2.9E-3	7.1E-4	1-Fe-3.fouled	0	1.7	1.0E-1	8.1E-3	3.5E-3	6.8E-4
	1.0	1.9	9.7E-2	2.0E-2	1.6E-3	2.7E-4		1.0	2.0	6.2E-2	8.1E-3	2.9E-3	2.4E-4		1.0	1.8	9.1E-2	8.1E-3	3.5E-3	5.7E-4
	2.0	2.1	8.2E-2	2.1E-2	1.6E-3	2.6E-4		2.4	4.1	3.5E-2	1.7E-3	2.5E-3	4.6E-4		2.0	4.1	6.8E-2	2.5E-3	3.3E-3	5.0E-4
	4.0	3.5	4.0E-2	1.2E-2	1.5E-3	2.8E-4		4.0	5.3	4.2E-3	1.8E-5	9.1E-6	3.8E-4		4.0	5.8	2.3E-3	1.8E-5	9.1E-6	4.5E-4
	6.0	5.6	1.2E-2	3.6E-5	1.3E-5	2.5E-4		5.5	6.8	1.1E-3	1.8E-5	9.1E-6	1.0E-4		4.8	6.7	1.1E-3	1.8E-5	9.1E-6	2.2E-4
	7.7	6.7	1.1E-3	1.9E-5	1.8E-5	3.1E-5		6.0	7.2	2.0E-4	1.8E-5	9.1E-6	1.7E-5		5.5	7.5	1.6E-4	1.8E-5	9.1E-6	1.7E-5
	7.8	6.7	4.1E-4	1.8E-5	1.8E-5	1.7E-5		6.2	7.3	1.5E-4	1.8E-5	9.1E-6	1.7E-5		6.0	7.9	2.0E-4	1.8E-5	9.1E-6	1.7E-5
	8.1	7.6	1.0E-4	1.8E-5	1.8E-5	1.7E-5														

Note: Limit of Detection (LOD) values: C_2O_4=3.28×10^{-4} M; Fe=1.8×10^{-6} M; Mn=6.4×10^{-6} M; and Ni=1.2×10^{-6} M.

Table 42. Decomposition test data for 1 wt% oxalic acid Al/Mn-rich sludge simulant based *decomposition test slurries*.

de-comp test slurry	time (hr)	pH	Ox (M)	Fe (M)	Mn (M)	Ni (M)	*de-comp test slurry*	time (hr)	pH	Oxalate (M)	Fe (M)	Mn (M)	Ni (M)	*de-comp test slurry*	time (hr)	pH	Oxalate (M)	Fe (M)	Mn (M)	Ni (M)
1-Al/Mn-1.no	0	2.5	6.8E-2	6.1E-4	6.6E-3	1.5E-4	1-Al/Mn-1.clean	0	2.4	7.5E-2	7.1E-4	8.4E-3	2.2E-4	1-Al/Mn-1.fouled	0	2.2	7.7E-2	7.0E-4	9.8E-3	1.8E-4
	1.1	5.4	5.1E-2	4.3E-4	2.3E-3	3.1E-5		1.1	5.7	3.5E-2	2.2E-4	1.2E-4	1.3E-4		1.0	5.5	5.7E-2	2.1E-4	2.6E-3	1.1E-4
	2.1	5.4	3.1E-2	5.2E-5	9.1E-6	1.7E-5		2.1	6.8	1.1E-2	2.5E-5	9.1E-6	5. 5E-5		2.0	6.6	3.4E-2	2.2E-5	2.6E-5	5.0E-5
	4.1	5.5	3.8E-3	1.8E-5	9.1E-6	1.7E-5		4.1	8.2	3.6E-3	1.8E-5	9.1E-6	1.7E-5		4.0	8.2	7.8E-3	1.8E-5	9.1E-6	1.E-5
	5.6	7.0	1.1E-3	1.8E-5	9.1E-6	1.7E-5		4.8	8.4	1.1E-3	1.8E-5	1.1E-5	1.7E-5		4.9	8.4	1.1E-3	1.8E-5	1.5E-5	1.7E-5
	6.1	7.4	3.1E-4	1.8E-5	9.1E-6	1.7E-5		5.1	8.5	2.0E-4	1.8E-5	1.1E-5	1.7E-5		5.0	8.5	2.0E-4	1.8E-5	1.5E-5	1.7E-5
	6.4	8.5	1.6E-4	1.8E-5	9.1E-6	1.7E-5		5.4	8.6	2.0E-4	1.8E-5	9.1E-6	1.7E-5		5.3	8.6	1.9E-4	1.8E-5	1.3E-5	1.7E-5
1-Al/Mn-2.no	0	1.7	1.1E-1	2.1E-3	1.1E-2	2.8E-4	1-Al/Mn-2.clean	0	2.2	8.2E-2	1.1E-3	1.2E-2	2.6E-4	1-Al/Mn-2.fouled	0	1.9	9.2E-2	1.1E-3	1.1E-2	3.1E-4
	1.1	2.3	7.6E-2	2.7E-3	8.6E-3	1.7E-4		1.0	5.3	6.8E-2	2.7E-4	5.3E-3	1.9E-4		1.1	5.0	6.8E-2	3.6E-4	7.0E-3	2.5E-4
	2.1	4.9	4.6E-2	1.8E-3	7.0E-3	2.1E-4		2.1	5.7	4.5E-2	4.6E-5	3.8E-4	1.4E-4		2.1	5.4	2.4E-2	4.8E-5	1.6E-3	2.0E-4
	4.1	6.5	1.9E-2	6.6E-5	1.8E-5	2.1E-5		4.1	8.0	7.5E-3	1.8E-5	9.1E-6	1.7E-5		4.1	7.4	9.2E-3	1.8E-5	9.1E-6	1.7E-5
	6.0	8.3	1.1E-3	2.0E-5	9.5E-6	2.6E-5		5.0	8.0	1.1E-3	1.8E-5	1.1E-5	1.7E-5		5.0	8.0	1.1E-3	1.8E-5	9.1E-6	1.7E-5
	6.1	8.3	2.0E-4	1.8E-5	9.1E-6	1.7E-5		5.1	8.0	2.0E-4	1.8E-5	1.1E-5	1.7E-5		5.1	8.1	3.1E-4	1.8E-5	9.1E-6	1.7E-5
	6.4	8.4	2.0E-4	1.8E-5	9.1E-6	1.7E-5		5.6	8.4	1.6E-4	1.8E-5	1.1E-5	1.7E-5		5.4	8.2	2.0E-4	1.8E-5	9.10E-6	1.7E-5
1-Al/Mn-3.no	0	1.5	1.1E-1	2.6E-3	7.3E-3	2.3E-4	1-Al/Mn-3.clean	0	2.0	8.6E-2	1.2E-3	1.3E-2	2.5E-4	1-Al/Mn-3.fouled	0	2.7	8.2E-2	9.4E-4	1.3E-2	3.2E-4
	1.0	1.9	7.1E-2	4.4E-3	7.5E-3	1.3E-4		1.0	5.1	4.5E-2	2.1E-4	7.2E-3	2.0E-4		1.1	5.0	5.7E-2	1.9E-4	6.7E-3	2.6E-4
	2.0	4.5	5.9E-2	5.9E-3	7.6E-3	1.6E-4		2.4	5.5	4.0E-2	3.6E-5	1.6E-3	1.5E-4		2.1	5.4	4.5E-2	3.6E-5	1.35E-3	2.0E-4
	4.0	5.5	1.2E-2	1.8E-5	6.0E-5	8.9E-5		4.0	7.3	1.1E-2	1.8E-5	9.1E-6	1.7E-5		4.1	7.3	1.2E-2	1.8E-5	9.1E-6	9.1E-6
	5.9	8.0	1.1E-3	1.8E-5	1.3E-5	2.2E-5		4.9	7.9	1.1E-3	1.8E-5	9.1E-6	1.7E-5		5.1	8.0	2.5E-3	1.8E-5	9.1E-6	1.7E-5
	6.0	8.2	3.1E-4	1.8E-5	9.1E-6	1.7E-5		5.0	7.9	5.7E-4	1.8E-5	9.1E-6	1.7E-5		5.4	8.0	1.1E-3	1.8E-5	9.1E-6	1.7E-5
	6.3	8.5	1.6E-4	1.8E-5	9.1E-6	1.7E-5		5.3	8.2	2.0E-4	1.8E-5	1.6E-5	1.7E-5		5.6	8.0	2.6E-4	1.8E-5	9.1E-6	1.7E-5
															5.8	8.1	2.0E-4	1.8E-5	9.1E-6	1.7E-5

Note: Limit of Detection (LOD) values: C_2O_4=3.28×10^{-4} M; Fe=1.8×10^{-6} M; Mn=6.4×10^{-6} M; and Ni=1.2×10^{-6} M.

Table 43. Decomposition test data for 2.5 wt% oxalic acid Fe-rich and Al/Mn-rich simulant based *decomposition test slurries.*

Fe-rich simulant decomposition test slurry	time (hr)	pH	Ox (M)	Fe (M)	Mn (M)	Ni (M)	*Al/Mn-rich simulant decomposition test slurry*	time (hr)	pH	Ox (M)	Fe (M)	Mn (M)	Ni (M)
2.5-Fe-1.no	0	1.3	2.4E-1	1.1E-2	4.8E-3	7.3E-4	2.5-Al/Mn-1.no	0	1.5	2.5E-1	1.8E-2	4.1E-3	4.5E-4
	1.0	1.5	2.3E-1	1.2E-2	4.9E-3	7.2E-4		1.0	1.5	2.3E-1	2.5E-2	4.3E-3	4.7E-4
	2.0	1.6	2.2E-1	1.3E-2	5.0E-3	7.3E-4		2.0	1.6	1.8E-1	2.9E-2	4.1E-3	4.7E-4
	4.0	1.9	1.0E-1	1.3E-2	5.0E-3	7.3E-4		4.0	1.7	1.5E-1	2.7E-2	3.9E-3	4.3E-4
	8.0	4.0	3.9E-2	5.4E-5	1.3E-5	7.5E-4		8.0	4.9	5.4E-2	1.9E-4	1.4E-4	3.9E-4
	12.0	7.0	1.5E-3	1.8E-5	1.8E-5	5.1E-4		12.0	7.7	3.8E-3	8.9E-7	3.3E-6	5.1E-6
	13.2	8.5	1.0E-3	1.8E-5	6.4E-5	3.1E-4		13.3	8.4	2.0E-4	2.3E-6	7.8E-6	3.4E-7
2.5-Fe-2.no	0	1.3	2.5E-1	1.5E-2	4.6E-3	8.1E-4	2.5-Al/Mn-3.no	0	1.4	2.8E-1	1.1E-2	2.1E-3	2.7E-4
	1.00	1.3	2.3E-1	1.5E-2	4.6E-3	7.9E-4		1.0	1.5	2.7E-1	1.3E-2	2.2E-3	2.8E-4
	2.00	1.4	1.9E-1	1.5E-2	4.6E-3	8.0E-4		2.0	1.6	2.3E-1	1.4E-2	1.9E-3	2.9E-4
	4.00	1.5	4.5E-2	1.5E-2	4.6E-3	7.5E-4		4.0	1.5	1.9E-1	1.6E-2	2.1E-3	3.0E-4
	8.00	4.4	4.2E-2	9.8E-3	4.3E-4	7.0E-4		8.0	1.9	7.5E-2	4.7E-3	1.8E-3	3.3E-4
	12.3	8.2	4.7E-4	1.0E-5	1.1E-5	2.8E-4		12.0	5.0	2.7E-2	1.8E-6	5.1E-6	2.1E-4
								14.7	7.9	8.9E-5	1.8E-6	7.3E-6	2.0E-4
2.5-Fe-3.no	0	1.0	2.6E-1	1.9E-2	3.9E-3	7.1E-4	2.5-Al/Mn-3.no	0	1.3	2.9E-1	6.9E-3	1.2E-3	1.8E-4
	1.0	1.2	2.3E-1	2.0E-2	4.1E-3	6.9E-4		1.0	1.3	2.3E-1	9.1E-3	1.3E-3	1.9E-4
	2.1	1.1	2.0E-1	1.7E-2	3.8E-3	6.7E-4		2.0	1.6	1.9E-1	9.9E-3	1.4E-3	1.7E-4
	4.1	1.3	1.1E-1	1.8E-2	3.9E-3	6.7E-4		6.0	3.0	9.9E-2	1.0E-2	1.4E-3	2.1E-4
	8.1	4.2	4.6E-2	2.6E-3	3.0E-3	6.2E-4		12.0	4.2	5.4E-2	2.3E-4	2.3E-3	1.9E-4
	12.1	7.9	7.2E-4	1.0E-5	1.5E-5	4.3E-4		16.0	4.4	3.4E-2	8.8E-5	1.5E-5	1.7E-4
	12.3	8.0	2.6E-4	1.0E-5	1.8E-5	4.3E-4		20.0	5.0	8.2E-3	2.3E-5	8.0E-6	1.6E-4
								21.3	8.9	8.8E-4	3.6E-7	6.4E-6	2.0E-6

Note: Limit of Detection (LOD) values: C_2O_4=3.28×10^{-4} M; Fe=1.8×10^{-6} M; Mn=6.4×10^{-6} M; and Ni=1.2×10^{-6} M.

Table 44. Decomposition test data for 2 wt% oxalic acid real F-Area HLW based *decomposition test slurries*.

Real HLW *decomposition test slurry*	time (hr)	pH	Oxalate (M)	Fe (M)	Mn (M)	Ni (M)	Real HLW *decomposition test slurry*	time (hr)	pH	Oxalate (M)	Fe (M)	Mn (M)	Ni (M)
2-Fe-1.no	0	2.2	4.26E-2	4.87E-2	1.60E-2	7.45E-4	2-Fe-1.clean	0	1.4	1.59E-1	1.83E-3	5.13E-3	3.87E-5
	2.5	NR	3.56E-3	1.52E-2	1.32E-2	5.64E-4		0.7	2.5	5.15E-2	1.37E-3	4.44E-3	3.60E-5
	5.1	NR	7.40E-4	9.78E-4	3.28E-4	8.08E-5		1.4	4.1	3.18E-2	1.92E-4	6.90E-4	3.66E-5
	9.7	NR	1.01E-3	9.81E-5	8.39E-5	1.22E-5		2.1	6.1	2.26E-2	2.60E-4	6.70E-4	3.88E-5
	10.9	NR	8.88E-4	9.10E-5	7.48E-5	1.29E-5		5.5	8.5	1.27E-3	6.09E-5	3.44E-5	3.88E-5
2-Fe-2.no	0	1.3	1.18E-1	2.54E-2	3.19E-3	2.68E-4	2-Fe-2.clean	0	1.1	1.14E-1	1.20E-3	3.59E-4	3.61E-4
	3.5	3.2	1.02E-2	1.48E-2	5.24E-3	6.30E-4		1.2	3.1	5.34E-3	1.10E-3	2.49E-4	3.73E-5
	5	6.4	4.59E-3	6.45E-5	8.76E-6	2.83E-4		1.6	4.9	2.23E-3	9.78E-5	3.48E-5	3.80E-5
	7.6	8.5	9.32E-4	8.22E-5	3.17E-5	1.34E-5		2.0	6.7	1.07E-3	2.90E-5	4.64E-6	3.66E-5
								4.5	8.4	1.09E-3	4.87E-5	9.03E-6	3.71E-5
2-Fe-3.no	0	1.2	1.83E-1	1.46E-2	1.48E-3	1.74E-4							
	3.3	1.5	1.09E-3	2.60E-2	2.84E-3	3.44E-4							
	5.8	2.7	1.06E-3	1.33E-2	2.86E-3	5.83E-4							
	7.3	6.5	1.08E-3	8.04E-5	4.24E-6	1.17E-4							
	8.6	7.8	9.07E-4	3.1E-5	6.57E-6	1.26E-5							

Note: Limit of Detection (LOD) values: C_2O_4=3.28×10^{-4} M; Fe=1.8×10^{-6} M; Mn=6.4×10^{-6} M; and Ni=1.2×10^{-6} M.

Table 45. Decomposition test data for 2 wt% oxalic acid real H-Area HLW based *decomposition test slurries.*

Real HLW decomposition test slurry	time (hr)	pH	Ox (M)	Fe (M)	Mn (M)	Ni (M)	Real HLW *decomposition test slurry*	time (hr)	pH	Oxalate (M)	Fe (M)	Mn (M)	Ni (M)
2-Al/Mn-1.no	0	2.5	6.81E-2	6.07E-4	6.62E-3	1.53E-4	2-Al/Mn-1.clean	0	1.7	3.22E-1	6.54E-3	4.57E-3	2.78E-4
	1.1	5.4	5.12E-2	4.30E-4	2.18E-3	3.07E-5		1.2	3.1	8.68E-2	5.51E-3	4.33E-2	2.59E-4
	2.1	5.4	3.12E-2	5.19E-5	9.10E-6	1.70E-5		2.5	4.0	6.86E-2	1.70E-4	3.91E-5	2.02E-4
	4.1	5.5	3.78E-3	1.79E-5	9.10E-6	1.70E-5		5.0	6.0	1.61E-2	8.67E-5	1.30E-5	1.58E-4
	5.6	7.0	1.14E-3	1.79E-5	9.10E-6	1.70E-5		7.9	8.0	1.51E-3	8.83E-6	3.69E-5	1.31E-5
	6.1	7.4	3.07E-4	1.79E-5	9.10E-6	1.70E-5							
	6.4	8.5	1.59E-4	1.79E-5	9.10E-6	1.70E-5							
2-Al/Mn-2.no	0	1.7	1.09E-1	2.13E-3	1.07E-2	2.81E-4	2-Al/Mn-2.clean	0	1.1	9.70E-2	2.45E-3	7.97E-4	3.50E-5
	1.1	2.3	7.55E-2	2.65E-3	8.55E-3	1.65E-4		1.3	1.3	3.07E-2	2.35E-3	7.70E-4	3.10E-5
	2.1	4.9	4.59E-2	1.77E-3	7.03E-3	2.08E-4		3.4	2.7	4.07E-2	8.95E-5	3.11E-5	1.82E-5
	4.1	6.5	1.92E-2	6.62E-5	1.82E-5	2.06E-5		4.4	4.2	1.02E-3	7.70E-6	4.40E-6	1.88E-7
	6.0	8.3	1.14E-3	2.04E-5	9.51E-6	2.61E-5		6.4	6.3	1.14E-3	1.16E-5	4.93E-6	2.11E-7
	6.1	8.3	2.04E-4	1.79E-5	9.10E-6	1.70E-5							
	6.4	8.4	2.03E-4	1.79E-5	9.10E-6	1.70E-5							
2-Al/Mn-3.no	0	1.5	1.14E-1	2.57E-3	7.28E-3	2.33E-4							
	1.0	1.9	7.08E-2	4.44E-3	7.47E-3	1.26E-4							
	2.0	4.5	5.94E-2	5.85E-3	7.64E-3	1.62E-4							
	4.0	5.5	1.19E-2	1.79E-5	6.01E-5	8.86E-5							
	5.9	8.0	1.14E-3	1.79E-5	1.27E-5	2.22E-5							
	6.0	8.2	3.07E-4	1.79E-5	9.10E-6	1.70E-5							
	6.3	8.5	1.59E-4	1.79E-5	9.10E-6	1.70E-5							

Note: Limit of Detection (LOD) values: C_2O_4=3.28×10^{-4} M; Fe=1.8×10^{-6} M; Mn=6.4×10^{-6} M; and Ni=1.2×10^{-6} M.

Table 46. pH vs time for decomposition of real HLW based slurries and pure 2 wt% oxalic acid solution without UV light.

time (hr)	pure 2 wt% OA	2-Al/Mn-1.no	2-Al/Mn-2.no	2-Al/Mn-3.no	2-Fe-1.no	2-Fe-1.no	2-Fe-1.no
	pH						
0.00	1.12	2.34	2.01	1.90	2.49	1.27	1.20
0.25	1.13	2.58	2.02	1.90	2.37	1.31	1.22
0.50	1.13	3.28	2.03	1.93	2.33	1.37	1.24
0.75	1.13	3.39	2.04	1.93	2.36	1.40	1.26
1.00	1.14	3.60	2.06	1.94	2.38	1.45	1.27
1.25	1.15	3.48	2.07	1.95	2.07	1.48	1.29
1.50	1.16	3.63	2.09	1.96	1.92	1.52	1.31
1.75	1.17	3.51	2.11	1.97	2.15	1.56	1.33
2.00	1.18	3.71	2.12	1.98	2.50	1.61	1.36
2.25	1.19	3.97	2.14	1.99	2.84	1.70	1.38
2.50	1.20	5.08	2.16	1.99	3.19	1.87	1.40
2.75	1.21	5.73	2.18	1.99	3.38	2.56	1.41
3.00	1.22	6.30	2.20	2.01	3.64	2.74	1.43
3.25	1.23	6.54	2.22	2.02	3.81	2.94	1.46
3.50	1.23	6.65	2.25	2.03	3.85	3.20	1.48
3.75	1.24	6.68	2.28	2.04	3.99	3.56	1.52
4.00	1.25	6.93	2.32	2.05	4.06	3.97	1.55
4.25	1.26	7.07	2.37	2.07	4.17	4.13	1.59
4.50	1.27	7.47	2.44	2.08	4.25	4.61	1.66
4.75	1.28	7.38	2.52	2.09	4.33	5.62	1.81
5.00	1.29	7.79	2.68	2.11	4.28	6.38	2.13
5.25	1.31	8.09	3.14	2.12	4.35	6.85	2.33
5.50	1.32	7.85	4.28	2.14	4.25	7.31	2.44
5.75	1.33	8.31	4.36	2.26	4.07	7.78	2.62
6.00	1.34	7.94	4.34	2.18	4.16	8.02	2.88
6.25	1.35	8.52	4.63	2.20	4.00	8.15	3.29
6.50	1.36	NR	5.46	2.23	4.10	8.24	3.64
6.75	1.37	7.99	5.98	2.26	4.21	8.30	4.05
7.00	1.38	NR	6.55	2.30	4.30	8.35	5.36
7.25	1.39	8.13	7.11	2.34	4.42	8.42	6.45
7.50	1.40	NR	7.56	2.40	4.50	8.49	6.97
7.75	1.41	8.39	7.68	2.50	4.54		7.33
8.00	1.44		7.91	2.71	4.59		7.52
8.25	1.45		8.19	3.47	NR		7.72
8.50	1.47		8.37	4.01	4.60		7.84
8.75	1.49		8.46	4.12	4.54		7.90
9.00	1.51		8.52	4.43	NR		

Note: NR refers to data Not Recorded

Tank 46 Continued. Decomposition test data for real HLW based slurries and pure 2 wt% oxalic acid without UV light.

time (hr)	pure 2 wt% OA	2-Al/Mn-1.no	2-Al/Mn-2.no	2-Al/Mn-3.no	2-Fe-1.no	2-Fe-1.no	2-Fe-1.no
	pH						
9.25	1.53		8.55	4.55	4.47	NR	
9.50	1.58			8.58	4.67	4.39	
9.75	1.60			8.60	4.95	4.34	
10.00	1.63			8.66	5.20	4.33	
10.25	1.67			8.68	5.89	4.33	
10.50	1.78			8.69	6.97	4.34	
10.75	1.82			8.70	7.18	NR	
11.00	1.89				7.46	4.27	
11.25	2.00				7.76	4.19	
11.50	2.07				7.86		
11.75	2.25				7.98		
12.00	2.93				8.06		
12.25	3.69				8.09		
12.50	4.39				8.11		
12.75	7.26				8.15		
13.00	7.69						
13.25	7.79						
13.50	7.88						
13.75	7.94						
14.00	7.97						

Note: NR refers to data Not Recorded.